Oxidative Medicine and Cellular Longevity

Oxidative Stress, Chronic Inflammation, and Amyloidoses

Lead Guest Editor: Arkadiusz Orzechowski
Guest Editors: Anna Cywińska, Agueda A. Rostagno, and Federica M. Rizzi

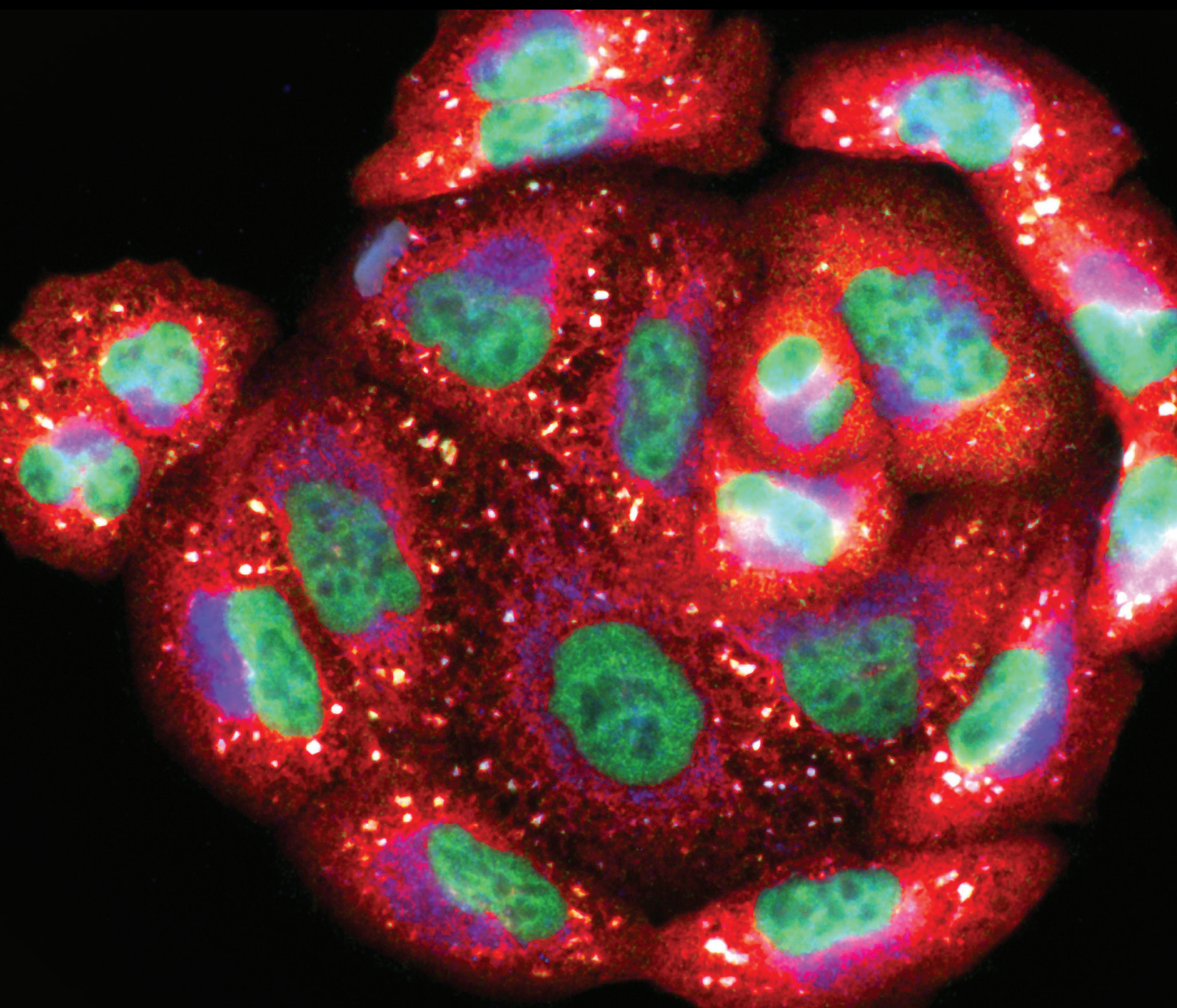

Oxidative Stress, Chronic Inflammation, and Amyloidoses

Oxidative Medicine and Cellular Longevity

Oxidative Stress, Chronic Inflammation, and Amyloidoses

Lead Guest Editor: Arkadiusz Orzechowski
Guest Editors: Anna Cywinska, Agueda A. Rostagno, and Federica Rizzi

Editorial Board

Contents

Hindawi
Oxidative Medicine and Cellular Longevity
Volume 2019, Article ID 6024975, 2 pages
https://doi.org/10.1155/2019/6024975

Editorial

Oxidative Stress, Chronic Inflammation, and Amyloidoses

Arkadiusz Orzechowski[1], **Anna Cywińska**[2], **Agueda A. Rostagno**[3] and **Federica M. Rizzi**[4]

[1]*Department of Physiological Sciences, Warsaw University of Life Sciences (SGGW), Nowoursynowska 159, 02-776 Warsaw, Poland*
[2]*Department of Pathology and Veterinary Diagnostics, Warsaw University of Life Sciences (SGGW), Nowoursynowska 159, 02-776 Warsaw, Poland*
[3]*Department of Pathology, New York University School of Medicine, 550 First Avenue, MSB 556, New York, NY 10016, USA*
[4]*Dipartmento di Medicina a Chirurgia, Universita degli Studi di Parma, Via Volturno 39/E, Parma, Italy*

Correspondence should be addressed to Arkadiusz Orzechowski; orzechowski_arkadiusz@wp.pl

Received 25 July 2019; Accepted 29 July 2019; Published 8 September 2019

Amyloid diseases are part of an emerging complex group of chronic and progressive entities collectively known as disorders of protein folding. For reasons still under active investigation, soluble proteins normally found in interstitial or biological fluids change their conformation and form poorly soluble molecular assemblies that accumulate as extracellular fibrillar aggregates within the parenchyma and blood vessels of different organs. Once formed, these amyloid fibrils that typically exhibit a β-sheet-rich secondary structure are highly resistant to proteolytic degradation, a characteristic that impairs their effective physiologic removal and leads to their tissue accumulation inducing local hypoxia and cellular damage with overall organ dysfunction and, eventually, death.

The molecular pathogenic mechanisms associated with amyloid diseases are complex and involve cross-talk among different cell populations and cellular pathways. Mounting evidence points out to inflammation-related mechanisms and oxidative stress as associated burden for amyloidosis. In spite of multiple studies, it still remains to be elucidated whether oxidative stress is a key contributor to the disease pathogenesis and progression or whether—on the contrary—it is a mere consequence of the cellular responses elicited by the presence of amyloid deposits and the concomitant inflammatory processes affecting injured tissue. This special issue provides an updated view on the role of oxidative stress and inflammation-related cellular pathways to the etiopathogenesis, progression, and treatment strategies of amyloid diseases.

One of the papers of this special issue, "Hypoxia and Inflammation as a Consequence of β-fibril Accumulation: A Perspective View for New Potential Therapeutic Targets," addresses the link between local hypoxia and the induction of chronic long-lasting inflammation in the context of the tissue accumulation of the β-sheet-rich amyloid deposits. The authors propose that the induction of cell death mechanisms in conjunction with local tissue hypoxia associated with the amyloid accumulation constitutes important events for the pathogenesis and progression of amyloidosis. The authors hypothesize that molecules released by necrotic cells activate inflammatory responses through Damage-Associated Molecular Patterns (DAMPs) and evoke activation of HIF-1α/NF-κB-dependent pathways suggesting that modulation of these cellular paths may constitute new therapeutic strategies. Another manuscript of the special issue focuses on the role of oxidative stress for the process of amyloid formation. The authors of "Suppression of Mouse AApoAII Amyloidosis Progression by Daily Supplementation with Oxidative Stress Inhibitors" examined the effect of the nonspecific reactive oxygen species (ROS) scavenger tempol and the NADPH oxidase inhibitor apocynin on the process of amyloidogenesis using a mouse model of AApoAII amyloidosis. Their results provide evidence that oxidative stress is involved in the progression of systemic amyloidosis but indicate that, although oxidative stress inhibitors ameliorated amyloid deposition, their use was unable to completely block the progression of amyloidosis. The paper entitled

"High levels of β-Amyloid, Tau, and Phospho-Tau in Red Blood Cells as Biomarkers of Neuropathology in Senescence-Accelerated Mouse" describes a study conducted on the Senescence-Accelerated Mouse-Prone, SAMP8, a validated model of Alzheimer's disease (AD) with the aim of establishing novel sensitive disease biomarkers. The study illustrates the increasing brain accumulation of amyloid-beta (Aβ) as well as total and phosphorylated tau concomitant with the elevated levels of the inflammatory marker interleukin-1β. The brain accumulation kinetics parallels findings in red blood cells suggesting these proteins as putative peripheral AD biomarkers. The authors of the original manuscript "Syk and Hrs Regulate TLR3-Mediated Antiviral Response in Murine Astrocytes" examined the regulation of the innate immune response-related Toll-like receptor 3 (TLR3) signaling in the astrocytic cell line C8-D1A following stimulation with a viral dsRNA mimetic (Pathogen-Associated Molecular Patterns (PAMPs)). The study uncovers a relationship between TLR3 and the endosomal sorting complex required for transportation-0 (ESCRT-0), pointing out to the spleen tyrosine kinase (Syk) as a dsRNA-activated kinase mediating TLR3 signaling and the concomitant induction of IFNs and proinflammatory gene expression. The paper "Nitric Oxide Influences HSV-1-Induced Neuroinflammation," aimed to elucidate the role of NO in neuroinflammation and neurodegeneration based on the use of *in vitro* models of herpes simplex virus (HSV-1) infection of neuronal and glial cell cultures as well as intranasal viral infection of BALB/c mice. The authors describe a differential response to NO and HSV-1 infection for neuronal, microglial, and astrocytic cells as well as in the concomitant production of IFN-alpha (IFN-α) and proinflammatory cytokines CXCL9 and CXCL10. Presented results help elucidate the molecular roles of NO and NO-related signaling during HSV-1-induced neuroinflammation and neurodegeneration and indicate for the first time the existence of a link between Fas signaling due to neuroinflammation and nitrosative stress during HSV-1 infection.

Overall, the special issue highlights the contribution of oxidative stress and chronic inflammation to the pathobiology of amyloid-associated diseases. The papers compiled in this special issue widen the current knowledge of the molecular mechanisms involved in the etiology, progression, and accumulation of β-sheet-enriched deposits in infectious and noninfectious forms of amyloidosis.

Conflicts of Interest

The editors declare that there is no conflict of interest.

Arkadiusz Orzechowski
Anna Cywińska
Agueda A. Rostagno
Federica M. Rizzi

Hindawi
Oxidative Medicine and Cellular Longevity
Volume 2019, Article ID 7935310, 10 pages
https://doi.org/10.1155/2019/7935310

Review Article

Hypoxia and Inflammation as a Consequence of β-Fibril Accumulation: A Perspective View for New Potential Therapeutic Targets

Matteo A. Russo,[1,2] **Carlo Tomino**,[3] **Enza Vernucci**,[1,4] **Federica Limana**,[1,2,5] **Luigi Sansone**,[1,2] **Andrea Frustaci**,[4,6] **and Marco Tafani**[7]

[1]*MEBIC Consortium, San Raffaele Rome Open University, Via val Cannuta 247, 00166 Rome, Italy*
[2]*Department of Cellular and Molecular Pathology, IRCCS San Raffaele, Via val Cannuta 247, 00166 Rome, Italy*
[3]*IRCCS San Raffaele, Scientific Direction, Via Val Cannuta 247, 00166 Rome, Italy*
[4]*Department of Cardiovascular, Nephrologic, Anesthesiologic and Geriatric Sciences, Sapienza University of Rome, Viale Regina Elena 324, 00161 Rome, Italy*
[5]*Laboratory of Cellular and Molecular Pathology, IRCCS San Raffaele Pisana, San Raffaele Open University, Via Val Cannuta 247, 00166 Rome, Italy*
[6]*Laboratory of Cellular and Molecular Cardiology, IRCCS "L. Spallanzani", Via Portuense 292, 00149 Rome, Italy*
[7]*Department of Experimental Medicine, Sapienza University of Rome, Viale Regina Elena 324, 00161 Rome, Italy*

Correspondence should be addressed to Carlo Tomino; carlo.tomino@sanraffaele.it and Marco Tafani; marco.tafani@uniroma1.it

Received 14 March 2019; Accepted 22 May 2019; Published 26 June 2019

Guest Editor: Arkadiusz Orzechowski

Amyloidoses are heterogeneous diseases that result from the deposition of toxic insoluble β-sheet fibrillar protein aggregates in different tissues. The cascade of molecular events leading to amyloidoses and to the related clinical manifestations is not completely understood. Nevertheless, it is known that tissue damage associated to this disease involves alteration of tissue architecture, interaction with cell surface receptors, inflammation elicited by the amyloid protein deposition, oxidative stress, and apoptosis. However, another important aspect to consider is that systemic protein massive deposition not only subverts tissue architecture but also determines a progressive cellular hypertrophy and dilation of the extracellular space enlarging the volume of the organ. Such an alteration increases the distance between cells and vessels with a drop in pO_2 that, in turn, causes both necrotic cell death and activation of the hypoxia transcription factor HIF-1α. Herewith, we propose the hypothesis that both cell death and hypoxia represent two important events for the pathogenesis of damage and progression of amyloidoses. In fact, molecules released by necrotic cells activate inflammatory cells from one side while binding to HIF-1α-dependent membrane receptors expressed on hypoxic parenchymal cells on the other side. This latter event generates a signaling cascade triggering NFκB activation and chronic inflammation. Finally, we also suggest that this scenario, once proved and detailed, might suggest important targets for new therapeutic interventions.

1. Introduction

Amyloidoses are a group of heterogeneous diseases presenting many common molecular, cellular, and clinical features strictly associated to a shared pathogenetic mechanism of the tissue/organ damage [1].

Although the available clinical descriptions and studies of different amyloidoses are numerous and several studies have detailed the molecular characteristics of the proteins and their aggregates in the disease, the precise molecular pathogenetic mechanism that leads to the tissue damage is still incomplete and debated [2].

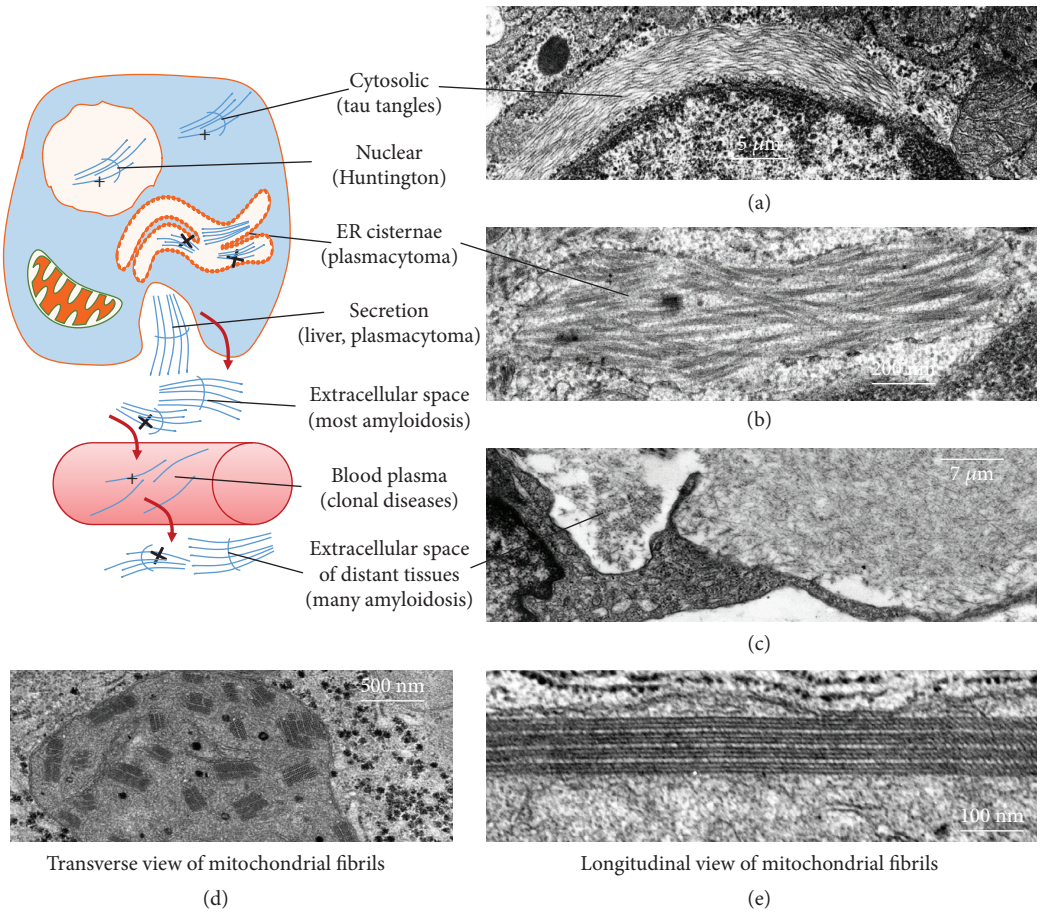

Figure 1: Production and localization of β-fibrils. The drawing shows the intracellular and the extracellular localization of β-fibrils of amyloidosic substance as observed at the electron microscope in different β-fibrilloses. Transmission electron micrographs of β-fibril localization in the cytosol (tau tangles of Alzheimer's disease) (a), in the cisternae of the endoplasmic reticulum (light chain polymers in a transformed B-lymphocyte/plasma cell) (b), and in the extracellular space (c) in close contact with a macrophage in the process of phagocytizing the fibrillar amyloid substance. Occasionally, β-fibrils have been observed in the mitochondrial matrix, being frequently organized as paracrystals (d, e). The nature of fibrillar protein is usually unknown. Mitochondria bearing fibril accumulation usually increase their volume, suggesting that accumulated misfolded fibrillar protein can be either imported from the cytosol or endogenously synthesized by mitochondrial machinery.

Recently, a number of authors have suggested an important role for inflammation, both as a trigger of amyloidoses and as a consequence of the β-fibril formation and accumulation [3, 4]. In addition, inflammation has been identified as an independent negative prognostic factor for clinical progression and severity [5–7]. However, very few studies have considered and explored the hypothesis that hypoxia, due to β-fibril accumulation, might represent an important pathogenetic factor by favoring the inflammatory-reparative response (IRR) and the consequent cellular damage [3, 4, 8].

The main focus of this short perspective review is to highlight the early and substantial role of hypoxia and hypoxia-triggered inflammation in producing tissue damage observed in the progressive advanced amyloidoses.

2. Molecular Features of Amyloidoses

A constant feature of amyloidoses is the progressive accumulation of β-fibrils in the intra- and extracellular space of involved tissues and organs as reported in Figure 1.

In particular, β-fibrils can also accumulate in the blood plasma. We have termed such an accumulation as "clonal diseases." In fact, "clonal diseases" are pathologic human conditions characterized by proliferation of a single cell lineage, mostly referred to disorders of the immunohematologic diseases, such as plasmocytoma/multiple myeloma [9–11]. In this case, patients typically present with bone marrow infiltration of *clonal* plasma cells and *monoclonal protein* in the serum and/or urine. Occasionally, when polymers are more than one, "clonal peaks" may be more than one. Clinical pathologists refer to clonal diseases (maybe inexactly) when abnormal "clonal" peaks are evidenced in serum protein electrophoretic trace, for instance, when abnormal production of a single protein occurs (liver, kidney, producing adenomas, etc.). In the case of β-fibrilloses, the "abnormal clonal peak" may be evidenced in the serum and/or urine not only in the case of plasma cell disorders but also in other conditions in which abnormal production of a single protein can give rise to β-fibrils [11].

Table 1: Common molecular features of amyloidosis.

Molecular features	Description and mechanisms	References
Misfolded proteins	Misfolding of β-sheet-rich proteins, such as amyloid β-protein tau, tau, α-synuclein, and prion protein (PrP^{sc})	[1, 24]
Polymers/protofibrils	Formation of intra/extracellular polymers with antiparallel β-sheet-rich proteins or protofibrils	[69]
β-Fibrils at optical microscopy (OM)	β-Fibrils show green birefringence at polarized OM after red Congo staining	[2]
β-Fibrils at TEM	β-Fibrils are linear, 8-12 nm in diameter, and interact with EM extracellular matrix molecules	[1, 2, 12]
β-Fibril physicochemistry	Linear, rigid, nonbranching, and protease-resistant polymers, probably interacting with extracellular matrix proteins	[12, 70]
β-Fibril protein composition	β-Fibril proteins are heterogeneous in their origin and composition, depending on the cell type involved	[12]
β-Fibril passing in the blood	β-Fibrils associate with SAP (serum amyloid protein)	[1, 2]
Large aggregates and deposits of β-fibrils	Formations of aggregates and deposits of rigid, stable, and protease-resistant β-fibrils, containing 15% of SAP, localized in the extracellular space, mostly around the vessel	[71]

Nevertheless, β-fibrils can also accumulate intracellularly in various cell compartments (Figure 1) [1].

β-Fibrils are polymers of β-sheet-rich proteins, which in normal conditions and conformation accomplish specific cell functions. Upon mutations or abnormal posttranslational modifications, they undergo misfolding, polymerization, loss of function, and possibly, acquisition of toxicity [12].

Initial protofibrils are small polymers of antiparallel β-sheet-rich misfolded proteins. Larger polymers are linear, rigid, and nonbranching, with an 8-12 nm diameter, easily detectable under a transmission electron microscope (TEM) (Figure 1) [1, 2, 12]. β-Fibrils exhibit a green birefringence at polarized light under an optical microscope after red Congo staining and more importantly a strong resistance to proteases that normally provide to their turnover in order to avoid accumulation in cells and tissues [2].

β-Fibrils are heterogeneous in their origin, localization, and composition, depending on the involved proteins (Table 1).

Fibrillar aggregates can be found in different subcellular compartments (Figure 1) or in extracellular space (Figure 2), where they can be easily detected because of their birefringence. Intracellular β-fibrils are also detectable by TEM as *cytosolic* bundles or aggregates in Alzheimer's disease (such as tau protein tangles) (Figure 1(a)), Parkinson's disease frontotemporal dementia, and dementia with Lewy bodies (α-synuclein and tau protein) and as *nuclear* aggregates, in Huntington's disease and other polyglutamine expansion diseases [1, 13]. Occasionally, β-fibrils can be observed in other subcellular compartments such as mitochondria, autophagosomes, and *cisternae of the endoplasmic reticulum* (Figure 1(b)) [14, 15]. The localization in the cisternae of the endoplasmic reticulum is more frequent in systemic amyloidosis where misfolded and polymerized proteins accumulate in producing cell, such as B lymphocyte/plasma cell (antibody light chain), pancreatic islet β-cell (insulin), and atrial myocardiocyte (ANF or atrial natriuretic factor) (Figure 3) [16].

Interestingly, sometimes, secretion of β-fibrils can be observed at the secretory pole of the cell producing the involved protein. Intracellular β-fibrils are able to activate various pathways of oxidative metabolism with production of ROS which contribute substantially to the cell damage.

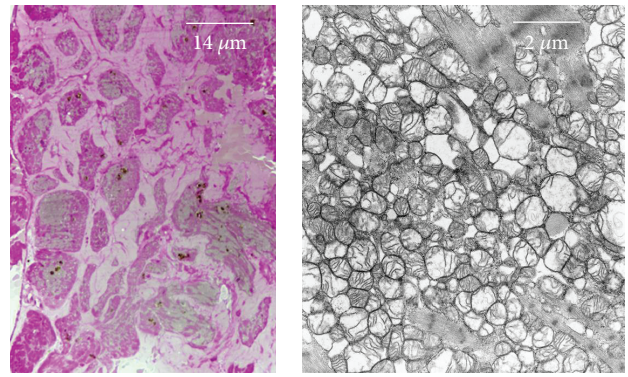

(a) (b)

Figure 2: Aspects of cardiac amyloidosis with accumulation of mutated transthyretin amyloid (a). The extracellular space (ES) is constantly enlarged increasing the distance between myocardiocytes and vessels (not visible). (b) At TEM, myocardiocytes display mitochondria with various degree of swelling and alteration of cristae; both are early cell reactions to ATP depletion and hypoxia. Sarcomere ultrastructure is still intact.

The misfolded proteins, once accumulated outside the cell, can become *resident* in the extracellular space (Figure 1(c)), probably fixed by some interaction with common domains of various components of the extracellular matrix. In particular, this interaction may involve glycosaminoglycan- (GAG-) rich components, such as fibrillar (collagens, elastin, laminins, and fibronectins) and nonfibrillar glycoproteins (proteoglycans, hyaluronans) [17]. In alternative, misfolded proteins or their polymers can reach the *circulation* by entering the vessel lumen. This latter situation has two consequences: (a) the protein can be evidenced as clonal peak in serum protein electrophoretic trace and (b) it can infiltrate and deposit in the extracellular space in distant organs and tissues.

Interestingly, in the first case, proteins and their polymers can be appropriately measured for diagnosis and disease

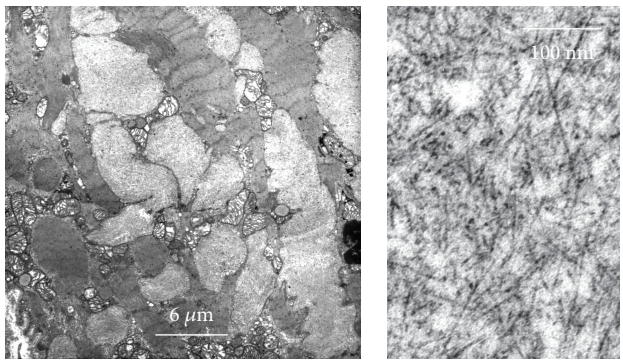

(a) (b)

Figure 3: Aspects of myocardial atrial amyloidosis with intracellular accumulation of β-fibrils constituted of polymerized ANP (atrial natriuretic factor) peptides. (a) An advanced disorganization of the cytoplasm is evident due to the displacement of the various cytoplasmic components. (b) High-magnification detail of 10 nm β-fibril aggregate.

monitoring [18]. Moreover, in systemic amyloidoses, 15% of amyloidosic substance is constituted by SAP or *serum amyloid protein*, a member of the major acute-phase protein family, i.e., pentraxins, which strongly interacts with β-fibrils, probably through chemical patterns usually recognized by pentraxins. This interaction may protect β-aggregates from proteolysis on one side and stimulate their phagocytosis by macrophages on the other side (Figure 1) [19, 20].

3. Clinical Features of Amyloidoses

Amyloidosis can be *familial* or *acquired*. In the first case, numerous mutations of the involved proteins have been described, strictly influencing the misfolding, the instability, and the propensity to form β-fibrils [2]. *Acquired* amyloidosis is generally secondary to conditions presenting abnormal/prolonged production and secondary misfolding of involved protein. Typical examples are represented by the excessive production of Ig light chain (lambda or kappa) by a transformed clone of lymphocyte/plasma cell and by the abnormal production of acute-phase proteins such as Serum amyloid A (SAA) or transthyretin in chronic inflammatory diseases and ageing [1, 2, 21].

β-Fibrillosis can be *localized* or *systemic*. *Localized or organ-limited amyloidoses* accumulate, both intracellularly and in the extracellular space, polymers of specific proteins such as β-amyloid (neurons in Alzheimer's disease), atrial natriuretic factor (in atrial myocardiocytes), procalcitonin (transformed medullary thyroid cells), and amylin (in pancreatic islet cells). *Systemic* amyloidoses are characterized by the deposition of culprit proteins such as immunoglobulin light chains (intact or fragments) and many acute-phase proteins (SAA, transthyretin, fibrinogen α-chain, β_2-macroglobulin, lysozyme, and gelsolin) [1, 21]. Upon entering the vessels, culprit proteins and their polymers may be evidenced in the electrophoretic diagram of blood plasma as a narrow high peak or by different bands when polymers of different MW are present. After leaving the blood, β-fibrils accumulate in the extracellular space of distant organs (liver, kidney, myocardium, lungs, brain, etc.), such as primary systemic amyloidosis (Ig light chains monomers and polymers or macroglobulins) and senile systemic amyloidosis (nonmutated transthyretin monomers), triggering the variable clinical features, typical of systemic amyloidoses [22].

β-Fibrilloses are *progressive* diseases in relation to the rate of accumulation of β-aggregates and to the severity of specific organ dysfunctions, as it occurs in Alzheimer's or Parkinson's disease, in myocardial amyloidosis by transthyretin and in kidney amyloidosis in the course of primary systemic amyloidosis [13, 23–25].

"False hypertrophy" of the involved organ/tissue, as evaluated by imaging, may be the first clinical sign for a diagnosis of amyloidosis [23]. β-Fibrils accumulate in the parenchyma of large organs, including the liver, kidneys, lungs, myocardium, skeletal muscle, intestine, and brain, progressively subverting their architecture and function [26, 27]. Typically, tissues show enlarged extracellular spaces, occupied by the amyloid substance (apparently amorphous and similar to the starch) (Figure 2(a)), which, as said, under optical microscope (OM) exhibits a green birefringence at polarized light after red Congo staining while under TEM appears composed of β-fibrils, 8-12 nm in diameter (Figure 3(b)) (Tables 1 and 2).

3.1. Hypoxic Microenvironment Generation. In tissues accumulating β-aggregates, the distance between vessels and parenchymal cells progressively increases above 200 μm representing the physical limit for an efficient gas diffusion and exchange (oxygen from blood and carbon dioxide from cells) [3]. As a consequence, in this area, a hypoxic environment is generated, leading to HIF-1α activation that is accompanied by NFκB activation. Importantly, both HIF-1α and NFκB trigger and amplify the inflammatory-reparative response and cellular damage [28].

3.2. Consequences of HIF-1α/NFκB Axis Activation

3.2.1. Hypoxic Cell Damage and Cell Adaptation to Hypoxia. *Acute* hypoxia causes cell death. O_2 shortage causes inhibition of ATP production, rapid fall of the energy charge, and loss of ionic gradients with the alteration of cytosolic calcium homeostasis [29]. The increase of cytosolic Ca^{++} concentration above 10^{-6} M dramatically activates the peroxidative metabolism, an irreversible contraction and degradation of the cytoskeleton and the activation of Ca^{++}-dependent cytosolic proteases (calpains) and DNAases, leading to an irreversible and rapid cell degradation [30]. Upon plasma membrane rupture, there is a release of intracellularly segregated molecules, many of which are called *alarmins* for their ability to signal the cell damage to specific receptors on adjacent cells [31]. Obviously, n*ecrosis* is more evident in the regions more distant from tissue vessels, where pO_2 reaches the lowest levels.

In *chronic* mild hypoxia, most cells (especially less differentiated cells and stem cells) are able to survive adapting their phenotype to the low pO_2 [3]. This *adaptation* to hypoxia

Table 2: Common clinical features of amyloidosic diseases.

Clinical features	Description and mechanisms	References
Familial	Mutations of the involved protein, strictly influencing misfolding and conformational instability, such as transthyretin in familial amyloidosic polyneuropathy	[72]
Acquired	Conditions presenting abnormal/toxic production and posttransductional misfolding of culprit proteins, such as plasmocytoma (light chains) or chronic inflammatory diseases (SAA) or haemodialysis-related amyloidosis (β_2-microglobulin)	[1, 73]
Localized	Organ-limited amyloidosis in which β-fibrils and polymers may became resident, almost stably, in the extracellular space around the cells producing the misfolded protein (see text)	[1]
Systemic	Bulk production and secretion of culprit protein in the extracellular space; protein entering the vessel lumen may be evidenced in blood plasma by a typical electrophoretic peak; accumulation in the extracellular space of distant tissues around the organism (liver, kidney, myocardium, lungs, brain, etc.), such as primary systemic amyloidosis (Ig light chains) and senile systemic amyloidosis (nonmutated transthyretin)	[1]
Progressive	The rate of amyloid accumulation depends not only on the rate of synthesis and on insensitivity to the extracellular proteases but also on the early start and duration length of disease.	[13, 23–25]
False hypertrophy	Both producing cells and accumulating tissues/organs increase their volume at various sizes, depending on the degree of progression.	[23, 74]
Systemic inflammation	A low-degree inflammation is constantly present in a patient bearing amyloidosis. Its intensity level is determined by the strength of the activation mechanisms (see text) and by the nature of the involved protein.	[5, 23, 75]
Hypoxia	There are a few specific studies demonstrating that the space accumulating the amyloid substance is actually hypoxic. However, an accurate evaluation of the distance between the vessels and the peripheral parenchymal cells shows that frequently this is larger than 200 μm, which is the diffusion limit of gas such as oxygen and carbon dioxide.	[3, 76]

occurs through the activation of hypoxic inducible factors (HIFs) [32] and the expression of a number of HIF-1α-dependent genes, involved in vital pathways, such as angiogenesis (vascular endothelial growth factors or VEGFs), metabolism (glucose transporter 1 or Glut1, hexokinase II or HKII, and glycolysis) [33], inflammation (Toll-like receptors or TLRs and other receptors for alarmins, cytokines, and matrix metalloproteinases or MMPs), and repair (autophagocytosis for disposal of damaged cell components, telomerase reverse transcriptase (TERT), and stemness genes to increase the stem cell compartment to substitute death cells) [34], transforming growth factor β (TGF-β) and fibrosis pathways [33].

3.2.2. Amplification and Maintenance of a Chronic IRR in Amyloidosic/Hypoxic Microenvironment. The importance of the unconventional expression of receptors for alarmins must be underlined, directly in parenchymal cells (probably *less differentiated and resident stem cells*) [35] which allows the acquisition of the proinflammatory phenotype in nonleukocytic (CD45-) cells, such as neurons, astrocytes, neuroglia, epithelial cells, and muscle cells [7]. Unconventionally, these cells express receptor for advanced glycation end products (RAGE), purinergic type 2 X7 (P2X7), Toll-like receptors, nucleotide oligomerization domain-like (NOD-like) receptors, inflammasomes, etc. [5], normally abundantly observed in activated leukocytes and endothelial cells.

As a consequence, alarmins released by necrotic cells (β-fibrils, high-mobility group box 1 or HMGB1, ATP/ADP, membrane debris, nucleic acids, etc.) bind to these newly expressed receptors producing an additional activation of transcription factors (NFκB, STAT3, AP1, etc.) driving IRR gene transcription not only in resident inflammatory cells but also in remodeled parenchymal cells [26, 27]. The latter further activate oxidative metabolism, produce mediators and other proinflammatory cytokines, and maintain a chronic inflammatory status in the affected tissue. Unfortunately, clinical consequences of this prolonged IRR activation include cell/tissue damage, continuous repair and fibrosis with progressive deterioration of the function leading to organ insufficiency, and neuronal damages, the typical final outcome of amyloidoses [5, 7, 36].

4. Mechanism of Tissue Damage

A number of different mechanisms contribute to the damage of affected tissue. However, they can all be included in three categories: (a) direct toxicity of β-fibrils, (b) structural damage and phenotype remodeling produced by the progressive growth of β-aggregates, and (c) activation of natural immunity or inflammatory response, ROS production, cell damage, chronic repair, fibrosis, and functional insufficiency.

Although a general consensus on these categories is present, a number of questions are still unresolved.

(a) Direct Toxicity of β-Fibrils. The chemical patterns of β-fibrils share many characteristics with exogenous pathogen-associated molecular patterns (PAMPs) or endogenous damage-associated molecular patterns (DAMPs). Therefore, extracellular β-fibrils may be recognized by alarmin receptors (Toll-like receptors, RAGE, and P2X7) [37, 38] and pentraxin family members such as SAP [39]. Extracellular β-fibril-alarmin receptor binding can then activate NFκB pathways for oxidative metabolism and apoptosis [40, 41]

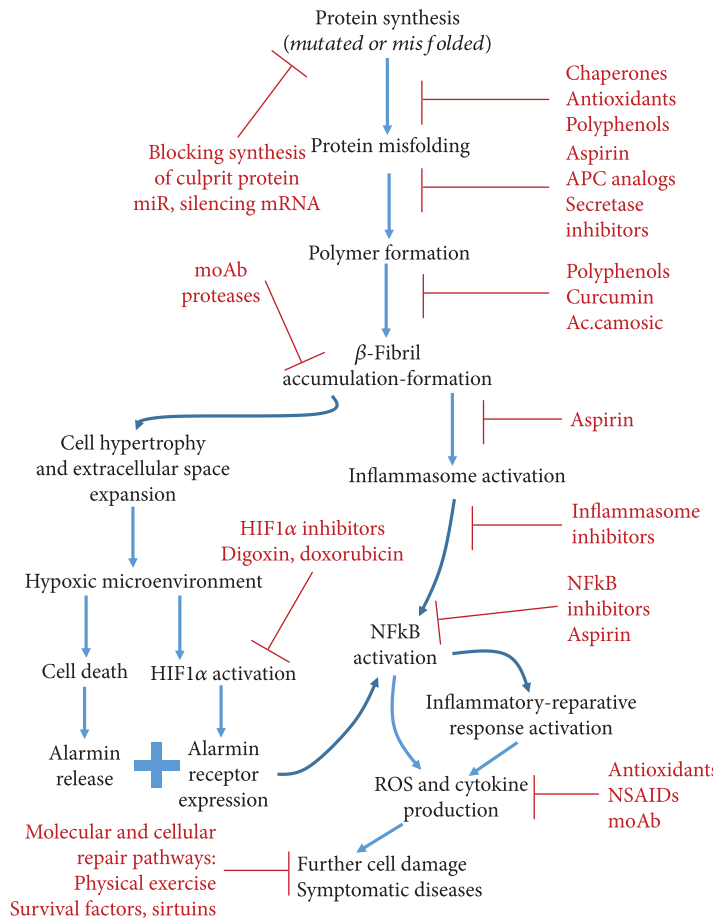

FIGURE 4: β-Aggregate formation and sequence of the tissue/organ damage. The possible therapeutic targets and the potential pharmacological agents are indicated in red color (see also text).

as well as phagocytic activity of macrophages (Figure 1(c)). On the other hand, intracellular β-fibrils are able to activate inflammasomes [42, 43]. Through these mechanisms, inflammation and ROS contribute substantially to the cell/tissue damage and severity of the disease.

(b) Structural Damage and Phenotype Remodeling Associated by the Progressive Growth of β-Aggregates. The progressive accumulation of β-fibrils is mainly due to their insensitivity to proteases that usually dispose of misfolded/aged proteins and their polymers [44, 45]. Although intracellular β-fibrils may undergo autophagocytosis, they still display a clear insensitivity to the intralysosomal acidic proteases, leading to lipofuscin accumulation that can be observed in aged and amyloidosic tissues [46]. An obvious consequence of β-fibril accumulation is the progressive architectural alteration of both cells and tissues with functional loss.

(c) Activation of Inflammatory-Reparative Response. In conclusion, as it has been underlined previously, progressive accumulation of amyloid fibrils is responsible for a local hypoxia and of a chronic long lasting inflammation, which in turn produces tissue damage leading to continuous repair, fibrosis, and organ insufficiency.

4.1. Putative Therapeutic Targets. Amyloidoses have an urgent need for new and effective therapeutic strategies. A better definition of the pathogenetic scenario here presented might suggest more precise and rational targets, changing the present disappointing and malignant outcomes of these diseases.

Three main approaches can be pursued: (a) control the synthesis of misfolded β-sheet-rich proteins and prevent/correct their misfolding; (b) inhibit polymer/fibril formation and accumulation and/or favor their clearance; and (c) inhibit and modulate HIF-1α/NFκB axis activation, limiting or repairing the damage associated to the β-fibrils. Figure 4 summarizes these approaches.

(a) The use of specific microRNA [47, 48] and RNA silencing [49] blocks/reduces the synthesis of the culprit protein and ameliorates mitochondrial respiration, synaptic function, and clinical symptoms. Recently, it has been shown [50] that recombinant APC (activated protein C, a plasma protease) or its analogs, inhibiting the neuronal β-secretase, may strongly slow or block the generation of β-amyloid protein protecting from Alzheimer's disease or slowing its progression [51, 52]

(b) Using chaperones [53, 54], small molecules [54], and aspirin [55] slows or inhibits polymer formation [50, 55, 56]

and β-fibril aggregation and accumulation, preventing the disease and attenuating its progression and symptoms. In cellular and animal models, *aspirin* has been shown to be highly effective in inhibiting polymer formation and β-fibril aggregation with *in vivo* reduction of the incidence of Alzheimer's and Parkinson's diseases. Although the mechanism(s) is still unclear, it has been demonstrated that aspirin is able to donate its acetyl group to the culprit proteins, increasing their acetylation and reducing the tendency of phosphorylation. This appears to be a common mechanism for inhibiting polymer and β-fibril formation in all different β-fibrillosis [55]. Aspirin may, as well, contribute with other beneficial mechanisms, such as inhibition of NFκB and cyclooxygenase, reducing the damaging impact of the inflammatory-reparative response (see below)

(c) Modulating HIF-1α and hypoxia adaptation [3, 4, 53] can represent a new strategy to block or limit the damage in tissues accumulating β-fibrils. A long list of potential HIF-1α inhibitors is now available, such as digoxin, acriflavine, doxorubicin, and chetomin [57–59]

(d) The utilization of NFκB inhibitors, anti-inflammatory drugs, and anti-inflammasome agents is aimed at modulating and inhibiting chronic inflammation and ROS production responsible for continuous cell damage, repair, and fibrosis [31, 60]

(e) Microbiota and nutrients may be in many ways involved in the pathogenesis of β-fibrillosis, including neurodegenerative diseases such as Alzheimer's and Parkinson's disease. Surprisingly, an intense gut-brain cross-talk has been evidenced, suggesting an important therapeutic role of the maintenance of intestinal microbiome equilibrium in preventing neurodegenerative diseases [61–63]. As a consequence, natural nutrients [64] such as curcumin and in particular vanillin, a degradation product of curcumin, have been shown to reduce the formation of advanced glycation end products (AGEs) [65]. Therefore, it is conceivable that they may also be used to modify microbiota with the goal to prevent, slow, and ameliorate beta-fibrillosis [64]

(f) Recently, *physical exercise* has been shown to be able to prevent Alzheimer's disease and substantially slow its progression. Mechanisms are unclear and controversial, but it seems that endocrine and metabolic effects associated with physical activity may be responsible for these beneficial effects. In particular, the release of survival factors, such as BDGF (neurons), IGF-1 (systemic or organ-specific release), and testosterone, and the activation of survival/repairing pathways, such as sirtuin-dependent transcription factors, are able to reduce apoptosis and to repair abnormal cell components, rescuing sublethally damaged postmitotic cells, such as neurons [66], myocardiocytes, skeletal muscle, and hepatocytes [67]

5. Conclusions

Clinically, amyloidoses are chronic progressive degenerative diseases leading to severe and irreversible insufficiency/failure of the involved organ/tissue. Even if genetic or acquired protein misfolding represents the primary trigger of the disease, during the pathogenetic sequence and progression, other pathophysiological responses are activated that strongly contribute to the damage production [68]. In particular, activation of the HIF-1α/NFκB axis by local hypoxia produces a proinflammatory remodeling of the affected tissue, explaining the final fibrosis and organ/tissue failure. Therefore, hypoxia and inflammation must be taken into consideration as potential targets for more rational and effective therapies aimed not only at preventing the formation and accumulation of β-fibrils and/or at increasing their clearance from deposits but more importantly at blocking/reducing the damage associated with the chronic inflammatory-reparative response.

Conflicts of Interest

No conflicts of interest, financial or otherwise, are declared by the authors.

Acknowledgments

This work was supported by funding of the Italian Ministry of Health (Ricerca corrente) given to IRCCS Spallanzani and IRCCS San Raffaele Pisana. This work was also supported in part by funding from Fondazione Roma given to MEBIC (grants 2016 and 2019).

References

[1] D. J. Selkoe, "Folding proteins in fatal ways," *Nature*, vol. 426, no. 6968, pp. 900–904, 2003.

[2] G. Merlini and V. Bellotti, "Molecular mechanisms of amyloidosis," *The New England Journal of Medicine*, vol. 349, no. 6, pp. 583–596, 2003.

[3] N. K. Jha, S. K. Jha, R. Sharma, D. Kumar, R. K. Ambasta, and P. Kumar, "Hypoxia-induced signaling activation in neurodegenerative diseases: targets for new therapeutic strategies," *Journal of Alzheimer's Disease*, vol. 62, no. 1, pp. 15–38, 2018.

[4] A. Merelli, J. C. G. Rodríguez, J. Folch, M. R. Regueiro, A. Camins, and A. Lazarowski, "Understanding the role of hypoxia inducible factor during neurodegeneration for new therapeutics opportunities," *Current Neuropharmacology*, vol. 16, no. 10, pp. 1484–1498, 2018.

[5] C. Matrone, M. Djelloul, G. Taglialatela, and L. Perrone, "Inflammatory risk factors and pathologies promoting Alzheimer's disease progression: is RAGE the key?," *Histology and Histopathology*, vol. 30, no. 2, pp. 125–139, 2015.

[6] L. Pontano Vaites and J. W. Harper, "Protein aggregates caught stalling," *Nature*, vol. 555, no. 7697, pp. 449–451, 2018.

[7] E. E. Tuppo and H. R. Arias, "The role of inflammation in Alzheimer's disease," *The International Journal of Biochemistry & Cell Biology*, vol. 37, no. 2, pp. 289–305, 2005.

[8] O. Weinreb, T. Amit, S. Mandel, and M. B. H. Youdim, "Novel therapeutic approach for neurodegenerative pathologies: multitarget iron-chelating drugs regulating hypoxia-inducible factor 1 signal transduction pathway," *Neurodegenerative Diseases*, vol. 10, no. 1-4, pp. 112–115, 2012.

[9] S. K. Kumar, V. Rajkumar, R. A. Kyle et al., "Multiple myeloma," *Nature Reviews Disease Primers*, vol. 3, no. 1, article 17046, 2017.

[10] C. R. McCudden, R. A. Booth, D. C. C. Lin, A. McCurdy, N. Rupani, and A. Kew, "Synoptic reporting for protein

electrophoresis and immunofixation," *Clinical Biochemistry*, vol. 51, pp. 21–28, 2018.

[11] P. C. Chana, Y. Chen, E. W. Randell, Monoclonal Gammopathy Interest Group (MGIG), and Canadian Society of Clinical Chemists, "On the path to evidence-based reporting of serum protein electrophoresis patterns in the absence of a discernible monoclonal protein – a critical review of literature and practice suggestions," *Clinical Biochemistry*, vol. 51, pp. 29–37, 2018.

[12] C. M. Dobson, "Protein folding and misfolding," *Nature*, vol. 426, no. 6968, pp. 884–890, 2003.

[13] M. Kujawska and J. Jodynis-Liebert, "What is the evidence that Parkinson's disease is a prion disorder, which originates in the gut?," *International Journal of Molecular Sciences*, vol. 19, no. 11, p. 3573, 2018.

[14] E. Area-Gomez, A. de Groof, E. Bonilla et al., "A key role for MAM in mediating mitochondrial dysfunction in Alzheimer disease," *Cell Death & Disease*, vol. 9, no. 3, p. 335, 2018.

[15] P. Gómez-Suaga, J. M. Bravo-San Pedro, R. A. González-Polo, J. M. Fuentes, and M. Niso-Santano, "ER-mitochondria signaling in Parkinson's disease," *Cell Death & Disease*, vol. 9, no. 3, p. 337, 2018.

[16] R. Sitia and I. Braakman, "Quality control in the endoplasmic reticulum protein factory," *Nature*, vol. 426, no. 6968, pp. 891–894, 2003.

[17] A. D. Theocharis, D. Manou, and N. K. Karamanos, "The extracellular matrix as a multitasking player in disease," *The FEBS Journal*, 2019.

[18] T. Scheidt, U. Łapińska, J. R. Kumita et al., "Secondary nucleation and elongation occur at different sites on Alzheimer's amyloid-β aggregates," *Science Advances*, vol. 5, no. 4, article eaau3112, 2019.

[19] L. Rojanathammanee, A. M. Floden, G. D. Manocha, and C. K. Combs, "Attenuation of microglial activation in a mouse model of Alzheimer's disease via NFAT inhibition," *Journal of Neuroinflammation*, vol. 12, no. 1, p. 42, 2015.

[20] K. K. Kopec and R. T. Carroll, "Alzheimer's beta-amyloid peptide 1-42 induces a phagocytic response in murine microglia," *Journal of Neurochemistry*, vol. 71, no. 5, pp. 2123–2131, 1998.

[21] C. C. Quarta, S. D. Solomon, I. Uraizee et al., "Left ventricular structure and function in transthyretin-related versus light-chain cardiac amyloidosis," *Circulation*, vol. 129, no. 18, pp. 1840–1849, 2014.

[22] I. G. Halatchev, J. Zheng, and J. Ou, "Wild-type transthyretin cardiac amyloidosis (ATTRwt-CA), previously known as senile cardiac amyloidosis: clinical presentation, diagnosis, management and emerging therapies," *Journal of Thoracic Disease*, vol. 10, no. 3, pp. 2034–2045, 2018.

[23] A. K. Mankad and K. B. Shah, "Transthyretin cardiac amyloidosis," *Current Cardiology Reports*, vol. 19, no. 10, 2017.

[24] C. Cerami, L. Iaccarino, and D. Perani, "Molecular imaging of neuroinflammation in neurodegenerative dementias: the role of in vivo PET imaging," *International Journal of Molecular Sciences*, vol. 18, no. 5, p. 993, 2017.

[25] F. E. Cohen and J. W. Kelly, "Therapeutic approaches to protein-misfolding diseases," *Nature*, vol. 426, no. 6968, pp. 905–909, 2003.

[26] L. F. Lue, D. G. Walker, L. Brachova et al., "Involvement of microglial receptor for advanced glycation endproducts (RAGE) in Alzheimer's disease: identification of a cellular activation mechanism," *Experimental Neurology*, vol. 171, no. 1, pp. 29–45, 2001.

[27] L. L. Man, F. Liu, Y. J. Wang et al., "The HMGB1 signaling pathway activates the inflammatory response in Schwann cells," *Neural Regeneration Research*, vol. 10, no. 10, pp. 1706–1712, 2015.

[28] M. Tafani, L. Schito, L. Pellegrini et al., "Hypoxia-increased RAGE and P2X7R expression regulates tumor cell invasion through phosphorylation of Erk1/2 and Akt and nuclear translocation of NF-κB," *Carcinogenesis*, vol. 32, no. 8, pp. 1167–1175, 2011.

[29] T. Kristián, "Metabolic stages, mitochondria and calcium in hypoxic/ischemic brain damage," *Cell Calcium*, vol. 36, no. 3-4, pp. 221–233, 2004.

[30] M. Tafani, L. Sansone, F. Limana et al., "The interplay of reactive oxygen species, hypoxia, inflammation, and sirtuins in cancer initiation and progression," *Oxidative Medicine and Cellular Longevity*, vol. 2016, Article ID 3907147, 18 pages, 2016.

[31] M. Tafani, B. Pucci, A. Russo et al., "Modulators of HIF1α and NFkB in cancer treatment: is it a rational approach for controlling malignant progression?," *Frontiers in Pharmacology*, vol. 4, p. 13, 2013.

[32] M. C. Brahimi-Horn and J. Pouysségur, "Hypoxia in cancer cell metabolism and pH regulation," *Essays in Biochemistry*, vol. 43, pp. 165–178, 2007.

[33] G. N. Masoud and W. Li, "HIF-1α pathway: role, regulation and intervention for cancer therapy," *Acta Pharmaceutica Sinica B*, vol. 5, no. 5, pp. 378–389, 2015.

[34] M. Tafani, A. Russo, M. di Vito et al., "Up-regulation of pro-inflammatory genes as adaptation to hypoxia in MCF-7 cells and in human mammary invasive carcinoma microenvironment," *Cancer Science*, vol. 101, no. 4, pp. 1014–1023, 2010.

[35] S. R. Mulay, A. Linkermann, and H. J. Anders, "Necroinflammation in kidney disease," *Journal of the American Society of Nephrology*, vol. 27, no. 1, pp. 27–39, 2016.

[36] J. W. Kinney, S. M. Bemiller, A. S. Murtishaw, A. M. Leisgang, A. M. Salazar, and B. T. Lamb, "Inflammation as a central mechanism in Alzheimer's disease," *Alzheimer's & Dementia: Translational Research & Clinical Interventions*, vol. 4, pp. 575–590, 2018.

[37] L. J. Sparvero, D. Asafu-Adjei, R. Kang et al., "RAGE (receptor for advanced glycation endproducts), RAGE ligands, and their role in cancer and inflammation," *Journal of Translational Medicine*, vol. 7, no. 1, p. 17, 2009.

[38] F. Di Virgilio, A. L. Giuliani, V. Vultaggio-Poma, S. Falzoni, and A. C. Sarti, "Non-nucleotide agonists triggering P2X7 receptor activation and pore formation," *Frontiers in Pharmacology*, vol. 9, p. 39, 2018.

[39] A. Agrawal, P. P. Singh, B. Bottazzi, C. Garlanda, and A. Mantovani, "Pattern recognition by pentraxins," *Advances in Experimental Medicine and Biology*, vol. 653, p. 98, 2009.

[40] D. G. Smith, R. Cappai, and K. J. Barnham, "The redox chemistry of the Alzheimer's disease amyloid β peptide," *Biochimica et Biophysica Acta (BBA) - Biomembranes*, vol. 1768, no. 8, pp. 1976–1990, 2007.

[41] X. J. Han, Y. Y. Hu, Z. J. Yang et al., "Amyloid β-42 induces neuronal apoptosis by targeting mitochondria," *Molecular Medicine Reports*, vol. 16, no. 4, pp. 4521–4528, 2017.

[42] A. Halle, V. Hornung, G. C. Petzold et al., "The NALP3 inflammasome is involved in the innate immune response to amyloid-β," *Nature Immunology*, vol. 9, no. 8, pp. 857–865, 2008.

[43] Z. Wu, L. Sun, S. Hashioka et al., "Differential pathways for interleukin-1β production activated by chromogranin A and amyloid β in microglia," *Neurobiology of Aging*, vol. 34, no. 12, pp. 2715–2725, 2013.

[44] T. Saido and M. A. Leissring, "Proteolytic degradation of amyloid β-protein," *Cold Spring Harbor Perspectives in Medicine*, vol. 2, no. 6, article a006379, 2012.

[45] S. Thellung, A. Corsaro, M. Nizzari, F. Barbieri, and T. Florio, "Autophagy activator drugs: a new opportunity in neuroprotection from misfolded protein toxicity," *International Journal of Molecular Sciences*, vol. 20, no. 4, p. 901, 2019.

[46] Y. Kakimoto, C. Okada, N. Kawabe et al., "Myocardial lipofuscin accumulation in ageing and sudden cardiac death," *Scientific Reports*, vol. 9, no. 1, p. 3304, 2019.

[47] Y. Zhao, V. R. Jaber, A. LeBeauf, N. M. Sharfman, and W. J. Lukiw, "microRNA-34a (miRNA-34a) mediated down-regulation of the post-synaptic cytoskeletal element SHANK3 in sporadic Alzheimer's disease (AD)," *Frontiers in Neurology*, vol. 10, p. 28, 2019.

[48] S. Ramakrishna and R. S. Muddashetty, "Emerging role of microRNAs in dementia," *Journal of Molecular Biology*, vol. 431, no. 9, pp. 1743–1762, 2019.

[49] M. Manczak and P. H. Reddy, "RNA silencing of genes involved in Alzheimer's disease enhances mitochondrial function and synaptic activity," *Biochimica et Biophysica Acta (BBA) - Molecular Basis of Disease*, vol. 1832, no. 12, pp. 2368–2378, 2013.

[50] D. Lazic, A. P. Sagare, A. M. Nikolakopoulou, J. H. Griffin, R. Vassar, and B. V. Zlokovic, "3K3A-activated protein C blocks amyloidogenic BACE1 pathway and improves functional outcome in mice," *Journal of Experimental Medicine*, vol. 216, no. 2, 2019.

[51] J. M. Long, B. Ray, and D. K. Lahiri, "MicroRNA-339-5p down-regulates protein expression of β-site amyloid precursor protein-cleaving enzyme 1 (BACE1) in human primary brain cultures and is reduced in brain tissue specimens of Alzheimer disease subjects," *The Journal of Biological Chemistry*, vol. 289, no. 8, pp. 5184–5198, 2014.

[52] S. Higaki, M. Muramatsu, A. Matsuda et al., "Defensive effect of microRNA-200b/c against amyloid-beta peptide-induced toxicity in Alzheimer's disease models," *PLoS One*, vol. 13, no. 5, article e0196929, 2018.

[53] A. J. L. Macario and E. C. de Macario, "Sick chaperones, cellular stress, and disease," *The New England Journal of Medicine*, vol. 353, no. 14, pp. 1489–1501, 2005.

[54] P. Hammarström, R. L. Wiseman, E. T. Powers, and J. W. Kelly, "Prevention of transthyretin amyloid disease by changing protein misfolding energetics," *Science*, vol. 299, no. 5607, pp. 713–716, 2003.

[55] S. Ayyadevara, M. Balasubramaniam, S. Kakraba, R. Alla, J. L. Mehta, and R. J. Shmookler Reis, "Aspirin-mediated acetylation protects against multiple neurodegenerative pathologies by impeding protein aggregation," *Antioxidants & Redox Signaling*, vol. 27, no. 17, pp. 1383–1396, 2017.

[56] N. Azad, H. Rasoolijazi, M. T. Joghataie, and S. Soleimani, "Neuroprotective effects of carnosic acid in an experimental model of alzheimer's disease in rats," *Cell Journal*, vol. 13, no. 1, pp. 39–44, 2011.

[57] G. L. Semenza, "Pharmacologic targeting of hypoxia-inducible factors," *Annual Review of Pharmacology and Toxicology*, vol. 59, no. 1, pp. 379–403, 2019.

[58] J. Fallah and B. I. Rini, "HIF inhibitors: status of current clinical development," *Current Oncology Reports*, vol. 21, no. 1, 2019.

[59] S. Ouyang, Y. H. Yao, Z. M. Zhang, J. S. Liu, and H. Xiang, "Curcumin inhibits hypoxia inducible factor-1α-induced inflammation and apoptosis in macrophages through an ERK dependent pathway," *European Review for Medical and Pharmacological Sciences*, vol. 23, no. 4, pp. 1816–1825, 2019.

[60] M. A. Russo, L. Sansone, I. Carnevale et al., "One special question to start with: can HIF/NFkB be a target in inflammation?," *Endocrine, Metabolic & Immune Disorders Drug Targets*, vol. 15, no. 3, pp. 171–185, 2015.

[61] E. M. M. Quigley, "Microbiota-brain-gut axis and neurodegenerative diseases," *Current Neurology and Neuroscience Reports*, vol. 17, no. 12, 2017.

[62] T. G. Dinan and J. F. Cryan, "The microbiome-gut-brain axis in health and disease," *Gastroenterology Clinics of North America*, vol. 46, no. 1, pp. 77–89, 2017.

[63] K. Kowalski and A. Mulak, "Brain-gut-microbiota axis in Alzheimer's disease," *Journal of Neurogastroenterology and Motility*, vol. 25, no. 1, pp. 48–60, 2019.

[64] N. Apetz, G. Munch, S. Govindaraghavan, and E. Gyengesi, "Natural compounds and plant extracts as therapeutics against chronic inflammation in Alzheimer's disease - a translational perspective," *CNS & Neurological Disorders Drug Targets*, vol. 13, no. 7, pp. 1175–1191, 2014.

[65] C. Iannuzzi, M. Borriello, G. Irace, M. Cammarota, A. Di Maro, and I. Sirangelo, "Vanillin affects amyloid aggregation and non-enzymatic glycation in human insulin," *Scientific Reports*, vol. 7, no. 1, article 15086, 2017.

[66] B. Pucci, F. Bertani, M. Indelicato et al., "Insulin-like growth factor-1 inhibits STS-induced cell death and increases functional recovery of in vitro differentiated neurons," *Cell Cycle*, vol. 7, no. 24, pp. 3869–3877, 2008.

[67] C. Ridler, "Exercise wards off Alzheimer disease by boosting neurogenesis and neuroprotective factors," *Nature Reviews Neurology*, vol. 14, no. 11, p. 632, 2018.

[68] R. Papa and H. J. Lachmann, "Secondary, AA, Amyloidosis," *Rheumatic Diseases Clinics of North America*, vol. 44, no. 4, pp. 585–603, 2018.

[69] P. T. Lansbury and H. A. Lashuel, "A century-old debate on protein aggregation and neurodegeneration enters the clinic," *Nature*, vol. 443, no. 7113, pp. 774–779, 2006.

[70] G. A. Tennent, L. B. Lovat, and M. B. Pepys, "Serum amyloid P component prevents proteolysis of the amyloid fibrils of Alzheimer disease and systemic amyloidosis," *Proceedings of the National Academy of Sciences of the United States of America*, vol. 92, no. 10, pp. 4299–4303, 1995.

[71] G. G. Glenner, "Amyloid deposits and amyloidosis. The beta-fibrilloses (first of two parts)," *The New England Journal of Medicine*, vol. 302, no. 23, pp. 1283–1292, 1980.

[72] M. Vieira and M. J. Saraiva, "Transthyretin: a multifaceted protein," *Biomolecular Concepts*, vol. 5, no. 1, pp. 45–54, 2014.

[73] B. Frost and M. I. Diamond, "Prion-like mechanisms in neurodegenerative diseases," *Nature Reviews Neuroscience*, vol. 11, no. 3, pp. 155–159, 2010.

[74] S. Mörner, U. Hellman, O. B. Suhr, E. Kazzam, and A. Waldenström, "Amyloid heart disease mimicking hypertrophic cardiomyopathy," *Journal of Internal Medicine*, vol. 258, no. 3, pp. 225–230, 2005.

[75] C. J. G. de Almeida, L. B. Chiarini, J. P. da Silva, P. M. R. e Silva, M. A. Martins, and R. Linden, "The cellular prion protein modulates phagocytosis and inflammatory response," *Journal of Leukocyte Biology*, vol. 77, no. 2, pp. 238–246, 2005.

[76] D. T. Stephenson, K. Rash, and J. A. Clemens, "Amyloid precursor protein accumulates in regions of neurodegeneration following focal cerebral ischemia in the rat," *Brain Research*, vol. 593, no. 1, pp. 128–135, 1992.

Hindawi
Oxidative Medicine and Cellular Longevity
Volume 2019, Article ID 5030475, 16 pages
https://doi.org/10.1155/2019/5030475

Research Article

High Levels of β-Amyloid, Tau, and Phospho-Tau in Red Blood Cells as Biomarkers of Neuropathology in Senescence-Accelerated Mouse

Rebecca Piccarducci,[1] **Deborah Pietrobono**,[1] **Carolina Pellegrini**,[1] **Simona Daniele**,[1] **Matteo Fornai**,[2] **Luca Antonioli**,[2] **Maria Letizia Trincavelli**,[1] **Corrado Blandizzi**,[2] **and Claudia Martini**[1]

[1]*Department of Pharmacy, University of Pisa, Pisa, Italy*
[2]*Department of Clinical and Experimental Medicine, University of Pisa, Pisa, Italy*

Correspondence should be addressed to Simona Daniele; simona.daniele@unipi.it
and Maria Letizia Trincavelli; maria.trincavelli@unipi.it

Received 18 December 2018; Revised 25 March 2019; Accepted 6 May 2019; Published 9 June 2019

Guest Editor: Anna Cywińska

Alzheimer's Disease (AD) is the most common Neurodegenerative Disease (ND), primarily characterised by neuroinflammation, neuronal plaques of β-amyloid (Aβ), and neurofibrillary tangles of hyperphosphorylated tau. α-Synuclein (α-syn) and its heteroaggregates with Aβ and tau have been recently included among the neuropathological elements of NDs. These pathological traits are not restricted to the brain, but they reach peripheral fluids as well. In this sense, Red Blood Cells (RBCs) are emerging as a good model to investigate the biochemical alterations of aging and NDs. Herein, the levels of homo- and heteroaggregates of ND-related proteins were analysed at different stages of disease progression. In particular, a validated animal model of AD, the SAMP8 (Senescence-Accelerated Mouse-Prone) and its control strain SAMR1 (Senescence-Accelerated Mouse-Resistant) were used in parallel experiments. The levels of the aforementioned proteins and of the inflammatory marker interleukin-1β (IL-1β) were examined in both brain and RBCs of SAMP8 and SAMR1 at 6 and 8 months. Brain Aβ, tau, and phospho-tau (p-tau) were higher in SAMP8 mice than in control mice and increased with AD progression. Similar accumulation kinetics were found in RBCs, even if slower. By contrast, α-syn and its heterocomplexes (α-syn-Aβ and α-syn-tau) displayed different accumulation kinetics between brain tissue and RBCs. Both brain and peripheral IL-1β levels were higher in SAMP8 mice, but increased sooner in RBCs, suggesting that inflammation might initiate at a peripheral level before affecting the brain. In conclusion, these results confirm RBCs as a valuable model for monitoring neurodegeneration, suggesting peripheral Aβ, tau, and p-tau as potential early biomarkers of AD.

1. Introduction

Alzheimer's Disease (AD) is the most common form of Neurodegenerative Disease (ND) and the leading cause of dementia in the elderly population. The molecular hallmarks associated with AD are primarily represented by misfolding and brain deposition of β-amyloid protein 1-42 (Aβ), which generates the amyloid plaques, and by neurofibrillary tangles (NTs) of hyperphosphorylated tau protein. According to the "amyloid hypothesis," Aβ promotes a glycogen synthase kinase-mediated tau phosphorylation, resulting in amyloid plaques and NTs, which damage the blood-brain barrier and produce neuronal apoptosis, inflammation, and oxidative stress [1]. In particular, it has been suggested that neuroinflammation in AD, particularly at its earlier stages, reflects a vicious cycle of microglial activation, release of proinflammatory factors, and neuronal damage [2, 3].

At present, a mixed pattern of protein aggregates in AD and other NDs has been identified [4, 5]. For instance, besides amyloid plaques and NTs, the disease has been

associated with intracellular accumulation of α-synuclein (α-syn) [6], which represents the major component of Lewy bodies and Lewy neuritis, and may play a role in amyloid aggregation in senile plaques [7]. Interestingly, α-syn has been shown to physically interact with tau [8, 9] or Aβ [8] giving rise to the formation of hybrid proteins ("heteroaggregates") in brains of patients affected by NDs [4, 5, 10].

Brain amyloid accumulation and aggregation have been shown to kick off even decades before the onset of clinical disease symptoms, and to reach the biological compartments. In this context, cerebrospinal fluid (CSF) has proven the most explored medium, as it is deemed to reproduce brain pathological processes [5, 11]. Consistently, AD diagnosis is nowadays based on the identification of misfolded-aggregated proteins in the brain (where amyloid plaques are visualised through imaging techniques) and CSF [12, 13]. However, considering the disadvantages that limit the clinical use of CSF, several efforts have been devoted to explore fluids other than CSF as a source of neurodegeneration biomarkers. In this respect, it has been suggested that pathological alterations of blood proteins reflect the changes in CSF due to the simple diffusion or barrier impairment that characterises neurodegeneration [11, 14].

Red Blood Cells (RBCs) are emerging as a good model to investigate the biochemical alterations related to aging and neurodegeneration, including oxidative stress and inflammation [15, 16]. Indeed, RBCs are highly susceptible to oxidative damage, due to the high concentration of oxygen and haemoglobin [17, 18]. Moreover, recent findings have shown an accumulation of ND-related proteins in these cells and its relationship with NDs [11, 19–21]. In particular, the presence of misfolded proteins (α-syn, Aβ, and tau) and their aggregates (α-syn-Aβ and α-syn-tau) has been recently proved in RBCs from healthy subjects and patients with NDs [5, 10, 11, 22]. At present, putative correlation between the accumulation of the aforementioned proteins in the brain and RBCs and inflammation has never been investigated.

To this end, we used here an animal model of AD, SAMP8 (Senescence-Accelerated Mouse-Prone), which is characterised by an early beginning of irreversible and severe learning and memory deficits. At a molecular level, this animal model displays an increase in Aβ proteins in hippocampal granules, hyperphosphorylation of tau protein, increase in α-synuclein, and increase in oxidative damage [23]. SAMR1 (Senescence-Accelerated Mouse-Resistant), which does not develop the disease [23], was used as control.

Herein, misfolded proteins were quantified in both the brain and RBCs of SAMP8 and SAMR1 mice, in order to establish a correlation between brain and peripheral fluids, as well as to ascertain the putative use of misfolded proteins in RBCs as AD biomarkers. Finally, to establish the link between brain/peripheral inflammation and accumulation of ND-related proteins, interleukin-1β (IL-1β) was quantified as one representative marker [14]. Indeed, neuroinflammatory cytokines, including IL-1β, have been involved in the formation of AD neuritic plaques [24–26] and were found in higher quantities in AD with respect to controls in both humans and animals [27–29].

2. Materials and Methods

2.1. Animals. SAMP8 mice (2 months old, 20-25 g body weight), employed as a spontaneous genetic model of AD [30], and their control strain SAMR1 (2 months old, 20-25 g body weight) were purchased from Envigo SRL (San Pietro al Natisone UD, Italy).

Animal care and handling were in accordance with the provisions of the European Community Council Directive 210-63-EU, recognised and adopted by the Italian Government. The experiments were approved by the Ethical Committee for Animal Experimentation of the University of Pisa and by the Italian Ministry of Health (authorization no. 198-2016-PR). One day after the end of cognitive tests (see the following discussion), the animals were euthanized by cervical dislocation and the cerebral cortex was carefully isolated by microscopic forceps. Blood samples were collected by cardiac puncture.

In the acquisition training, animals are subjected to sessions of four trials every day for 2 days. In the hidden-platform training, performed by submerging the platform 1.5 cm below the surface of the water, animals are subjected to sessions of four trials every day for 5 days. Finally, in the probe trial on the eighth day, the platform is removed and the number of target crossings, number of entries into the target quadrant, and the time spent in the target quadrant are assessed as measures for 60 s.

2.2. Evaluation of Cognitive Functions: Morris Water Maze Test and Behavioural Test. The behavioural test consists of visible-platform acquisition training, hidden-platform training, and probe trial (Figure 1). The platform was in the same location for both visible-platform training and hidden-platform training. In the acquisition training, the escape latency was assessed for each animal (time required to reach the platform). Mice were placed on the platform for 10 s before being released into the water. Mice were allowed to swim and find the visible platform within 60 s. Each animal was subjected to sessions of four trials every day for 2 days. After the daily trial, mice were returned to their home cages for resting. In the hidden-platform training, performed by submerging the platform 1.5 cm below the surface of the water, escape latency was evaluated over the next 5 days (Figure 1). Each animal was subjected to sessions of four trials every day. Finally, on the eighth day, the platform was removed from the tank for the probe trial (Figure 1). The number of target crossings, number of entries into the target quadrant, the time spent in the target quadrant where the platform was placed, the swimming speed, swim distance, and swim distance in the target quadrant were assessed as measures for 60 s. Data are expressed as raw values, while the data regarding the time spent in the target quadrant are expressed as the percent time spent in the quadrant with the platform in comparison to each of the other quadrants.

2.3. Collection of Brain Tissues and RBCs. Brains were dissected from mice. The samples were suspended in phosphate-buffered saline (PBS) and then sonicated. The blood was sampled from mice, and it was preserved into an

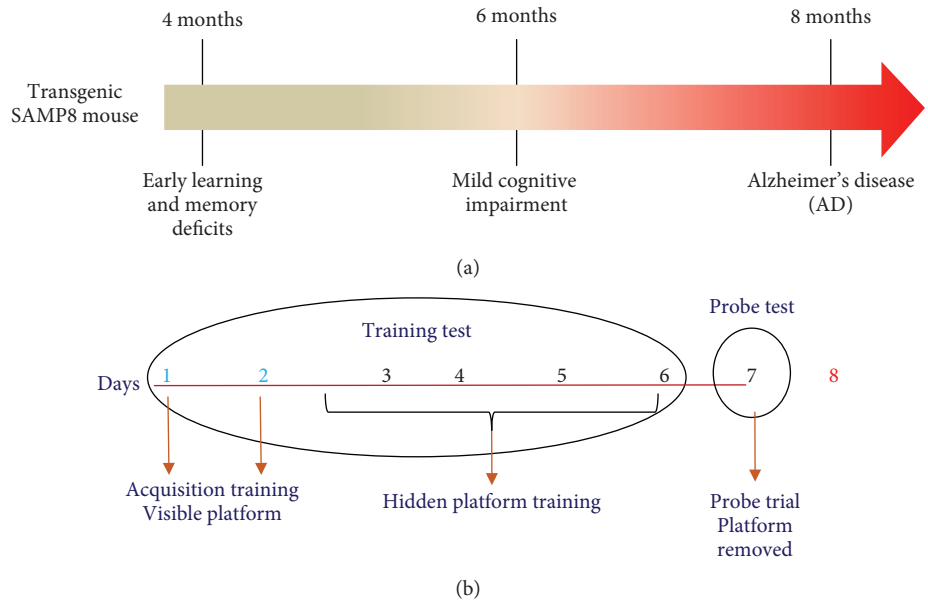

FIGURE 1: (a) Diagram showing the timing of cognitive impairment and AD progression in SAMP8 mice. (b) Diagram showing the different phases of the behavioural test.

EDTA tube. A centrifugation at 200 × g at 4°C for 10 min was required to isolate RBCs from plasma. The RBC pellet was suspended in 3 ml of PBS and subjected to centrifugation at 1000 × g for 10 min and washed thrice with PBS. Finally, RBCs were centrifuged at 1500 × g for 10 min and frozen at -20°C until use.

2.4. Coimmunoprecipitation-Western Blotting. RBC (1 mg) and brain (30 μg) samples were lysed in RIPA buffer and later resolved by SDS-PAGE (8.5%) to assess the expression of Aβ, α-syn, and tau. Samples were transferred to PVDF membranes and probed overnight at 4°C with primary antibodies to Aβ (β-amyloid H-43, sc-9129, Santa Cruz Biotechnology Inc.), α-syn (α-β synuclein N-19, sc-7012, Santa Cruz Biotechnology Inc.), or tau (H-150, sc-5587, Santa Cruz Biotechnology Inc.) [11, 22]. Then, the primary antibodies were revealed through peroxidase-conjugated secondary antibodies and a chemiluminescent substrate (ECL, PerkinElmer).

A coimmunoprecipitation assay was used to prove the presence of α-syn heterocomplexes with Aβ or tau [11, 22]. Briefly, lysates (1 mg) recovered from RBCs or the brain were suspended in RIPA buffer; they were probed with an anti-α-syn antibody (5 μg sample), maintained under constant rotation overnight, and successively immunoprecipitated with protein A-Sepharose. The immunocomplexes were suspended in Laemmli solution following an extensive washing; thereafter, the immunocomplexes were determined by SDS-PAGE and probed overnight with primary antibodies to α-syn (input), Aβ, or tau as described previously [11, 22].

2.5. Preparation of Aged Solutions of α-Syn and of the α-Syn-Biotinylated Antibody. The incubation of recombinant α-syn took place in parafilm-sealed tubes at 37°C for 4 days in an Eppendorf ThermoMixer under continuous mixing (1000 rpm) [31]. The α-syn-biotinylated antibody was prepared through a reaction among Sulfo-NHS-LC-Biotin (Pierce, Rockford, IL, USA) (200 mg) and the 211 mouse monoclonal antibody (mAb) (Santa Cruz Biotechnology Inc., Santa Cruz, CA, USA) [32]. To remove excess uncoupled biotin, the mixture was desalted on Bio-Spin-6 Columns (Bio-Rad, UK) [11, 22].

2.6. Immunoassay Methods. The presence and quantification of total Aβ, tau, and α-syn and its heterocomplexes (α-syn-Aβ and α-syn-tau) in RBCs and in brain tissues were assessed by a "homemade" sandwich enzyme-linked immunosorbent assay (ELISA) system [11, 33, 34]. The plate was precoated overnight with 60 μl-well of a specific antibody directed to the protein in analysis. Following an extensive washing with PBS-T (PBS, containing 0.01% Tween 20), BSA 1% (200 μl-well) was added to block nonspecific sites and the plate was incubated. After additional washes with PBS-T, RBCs and brain tissues were added to each well (100 μl-well) and incubated. Following an extensive washing, an antibody (75 μl-well) directed to a specific amino-acidic sequence of the protein was employed for capturing, followed by an incubation. For antigen detection, an HRP antibody (100 μl-well) was used and it was incubated [11]. The wells were then washed with PBS-T before the addition of 100 μl-well of 3,3′,5,5′-tetramethylbenzidine (TMB) (Thermo Fisher Scientific). The absorbance was evaluated at 450 nm after the addition of the Stop Solution (0.4 N HCl, 100 μl-well). All measurements were performed in duplicate to reduce interassay variability. The standard curve for the ELISA assay was constructed using a recombinant human protein solution at different concentrations diluted in PBS [11, 22, 34]. The concentration of ND-related proteins in the brain and RBCs was expressed as the nanogram or picogram of protein and normalised to the quantity of total proteins present in the analysed samples.

2.6.1. Detection of Total α-Synuclein. The plate was coated with full-length polyclonal antibody to α-syn (sc-10717, Santa Cruz Biotechnology Inc.) overnight at 4°C. After the incubation with BSA 1% and three washes with PBS-T, RBCs (0.1 mg-100 μl) and brain tissues (10 μg-100 μl) were added to each well and incubated at 25°C for 2 h. Then, mouse monoclonal antibody to α-syn (sc-12767, Santa Cruz Biotechnology Inc.) was employed and incubated at 37°C for 2 h. An anti-mouse-HRP antibody was used, and it was incubated at 37°C for 1.5 h [11, 21, 22, 35].

2.6.2. Detection of Total Aβ. A precoating with a specific antibody to Aβ (sc-9129, Santa Cruz Biotechnology Inc.) was prepared (60 μl-well) and maintained overnight at 4°C. BSA 1% was added and the plate was incubated for 2 h at 37°C. RBCs (0.05 mg-100 μl) and brain tissues (0.25 μg-100 μl) were added to each well and incubated at 25°C for 1 h. Samples were probed with polyclonal antibody to Aβ (sc-5399, Santa Cruz Biotechnology Inc.) (75 μl-well) for 1.5 h at 25°C. For antigen detection, a donkey anti-goat-HRP antibody was incubated at 37°C for 1 h [11, 32, 36].

2.6.3. Detection of Total Tau. The plate was precoated with a specific antibody to tau (sc-32274, Santa Cruz Biotechnology Inc.) and left overnight at 4°C. BSA 1% was added and the plate was incubated for 1 h at 37°C. RBCs (0.4 mg-100 μl) and brain tissues (2 μg-100 μl) in each well were incubated at 25°C for 2 h. Samples were probed with polyclonal antibody to tau (sc-5587, Santa Cruz Biotechnology Inc.) and incubated at 37°C for 2 h. A goat anti-rabbit-HRP antibody (Invitrogen) was incubated for 1.5 h [11, 32, 36].

2.6.4. Detection of Phospho-Tau. The plate was precoated with a specific antibody to tau (sc-32274, Santa Cruz Biotechnology Inc.) and left overnight at 4°C. BSA 1% (200 μl-well) was added, and the plate was incubated for 2 h at 37°C. RBCs (0.2 mg-100 μl) and brain tissues (1 μg-100 μl) in each well were incubated at 25°C for 2 h. Samples were probed with polyclonal antibody to tau (70R-32555, Fitzgerald Industries International) and incubated at 37°C for 1.5 h. For antigen detection, goat anti-rabbit-HRP antibody (Invitrogen) was incubated for 1.5 h [11, 32].

2.6.5. Immunoassay Detection of α-Syn-Tau Heterocomplexes. The ELISA plate was coated with α-β-syn N-19 antibody (sc-7012, Santa Cruz Biotechnology Inc.) overnight at room temperature. RBCs (400 μg-100 μl) and brain tissues (1 μg-100 μl) were added to each well and incubated at 25°C for 2 h. BSA 1% was added to each well for 20 min at 37°C. Rabbit polyclonal anti-tau H-150 antibody (sc-5587, Santa Cruz Biotechnology Inc., 37°C for 2 h) was employed for capturing. A goat anti-rabbit-HRP antibody was used at 37°C for 1.5 h [11]. The concentration of α-syn-tau interaction in the samples was quantified according to a standard curve [11], which was constituted using a solution of recombinant human α-syn and recombinant human tau at different concentrations in SDS 2 mM. The solution was prepared by incubating 1 mg of each protein, diluted in 2 mM SDS, in parafilm-sealed tubes at 37°C for 1 h in an Eppendorf ThermoMixer with continuous mixing (500 rpm) [11, 22].

2.6.6. Immunoassay Detection of α-Syn-Aβ Heterocomplexes. The ELISA plate was coated with β-amyloid H-43 antibody (sc-9129, Santa Cruz Biotechnology Inc.) overnight at room temperature. RBCs (0.2 mg-100 μl) and brain tissues (1 μg-100 μl) were added to each well and incubated at 25°C for 2 h. BSA 1% was incubated for 20 minutes at 37°C. A mouse monoclonal anti-α-synuclein 211 antibody (sc-12767, Santa Cruz Biotechnology Inc.) was employed for capturing and was incubated at 37°C for 2 h. Goat anti-mouse-HRP antibody was incubated at 37°C for 1.5 h [11]. The concentration of α-syn-Aβ interaction in the samples was quantified according to a standard curve [11], which was constituted using a solution of recombinant human α-syn and recombinant human Aβ at different concentrations in SDS 2 mM. The solution was prepared by incubating 1 mg of each protein, diluted in 2 mM SDS, in parafilm-sealed tubes at 37°C for 16 h in an Eppendorf ThermoMixer with continuous mixing (500 rpm) [11, 37].

2.7. Evaluation of IL-1β Levels in Brain Tissues and in RBCs. IL-1β levels in the cerebral cortex and RBCs were measured by a commercial enzyme-linked immunosorbent assay kit (Abcam, Cambridge, UK), as previously described. Briefly, 20 mg of cerebral cortex, stored previously at -80°C, were homogenised in 400 μl of PBS, pH 7.2, at 4°C and centrifuged at 10000 × g for 5 min. Aliquots (50 μl) of the supernatants were then used for the assay. In parallel, 0.2 mg-50 μl of RBCs, homogenised in PBS, were used for the assay. IL-1β levels were expressed as picogram per milligram of total proteins present in the analysed samples.

2.8. Statistical Analysis. The results are presented as the mean ± S.E.M. unless otherwise stated. The significance of differences was evaluated by a two-way analysis of variance followed by post hoc analysis with the Fisher LSD test or a one-way analysis of variance followed by post hoc analysis with the Student-Newman-Keuls test where appropriate. P values <0.05 were deemed significantly different. All statistical procedures were performed by commercial software (GraphPad Prism, version 7.0; GraphPad Software Inc., San Diego, CA).

3. Results

3.1. Evaluation of Cognitive Functions (Morris Water Maze Test). As a first step, mice cognitive functions, i.e., spatial learning and memory ability, were evaluated by the Morris water maze test. SAMR1 mice rapidly learned the location of the platform (Figure 2(a)). SAMP8 mice at 4, 6, and 8 months displayed a significant increase in escape latency time at every test day compared with SAMR1 mice (Figure 2(a)).

These findings are in line with other studies showing that SAMP8 mice displayed a significant increase in escape latency time since the first day of training as compared with SAMR1 mice, while no significant difference was observed among training days [38, 39].

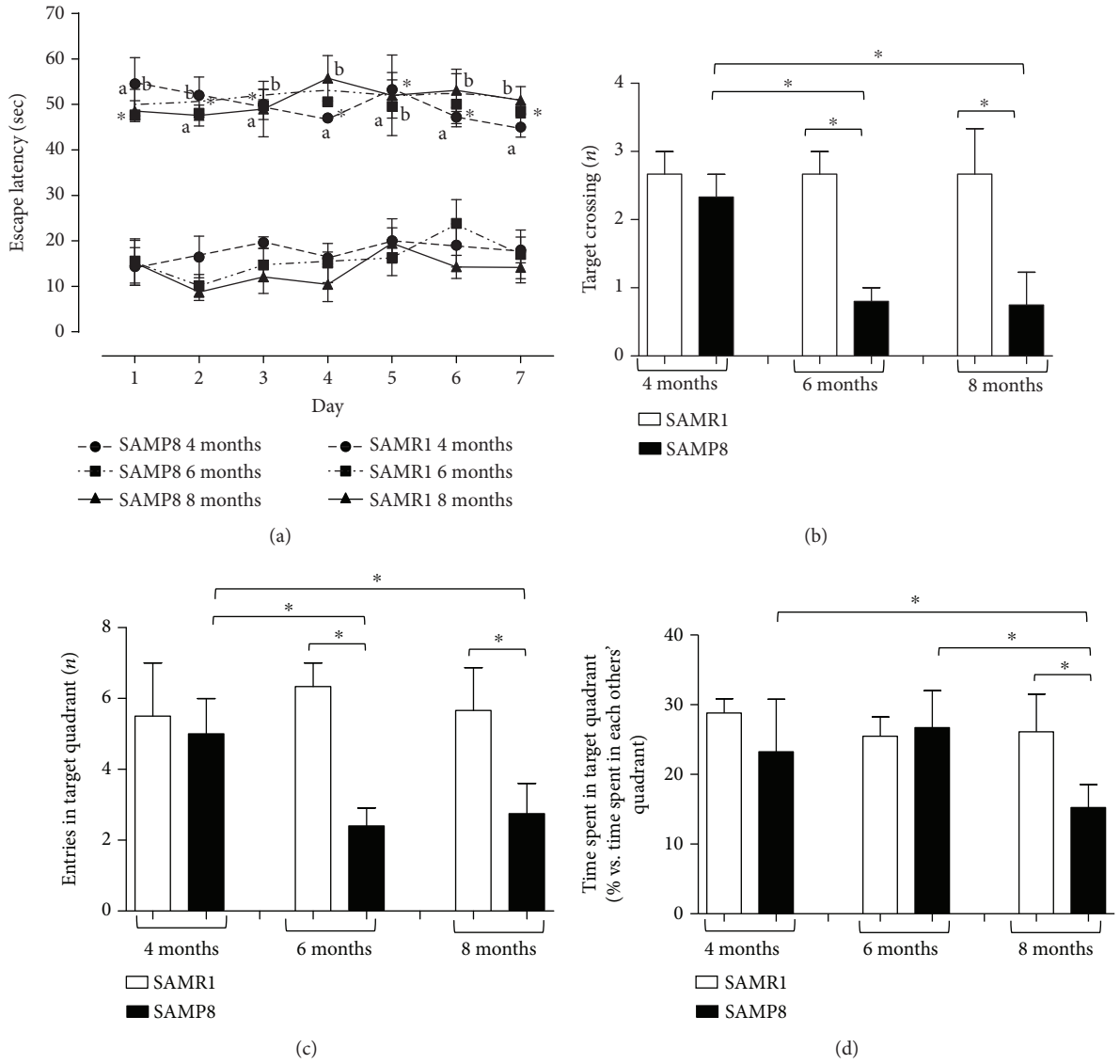

Figure 2: Cognitive performance of SAM. (a) Escape latency in SAMR1 and SAMP8 mice at 4, 6, and 8 months of age, during seven consecutive days of Morris water maze test training. Cognitive performance of SAMR1 and SAMP8 mice at 4, 6, and 8 months of age, during the probe trial session of the Morris water maze test; (b) number of target crossings; (c) entries into the target quadrant; (d) time spent within the target quadrant. Data are expressed as mean ± S.E.M. obtained from 8 animals. Differences among groups were evaluated by two-way analysis of variance followed by post hoc analysis with the Fisher LSD test or a one-way analysis of variance followed by post hoc analysis with the Student-Newman-Keuls test where appropriate. $^{*}P < 0.05$ between the indicated subgroups.

During the probe trial, the number of target crossings as well as the entries into the target quadrant were significantly decreased in SAMP8 mice at 6 and 8 months, compared with respective controls (SAMR1) and SAMP8 animals at 4 months (Figures 2(b) and 2(c)). The time spent within the target quadrant was significantly decreased in SAMP8 mice at 8 months, compared with respective SAMR1 animals and SAMP8 mice at 4 and 6 months (Figure 2(d)). Considering the swimming speed, the swim distance, and the swim distance in the target quadrant, our results show that SAMP8 animals displayed a decrease in swimming speeds and distance traveled, as compared with age-matched SAMR1 (Figures 3(a)–3(c)). Of note, our results point out that SAMP8 animals did not float in the quadrant where the platform was located, but they reached it slowly, thus excluding despair or depression signs. In addition, the number of target crossings and the entries into the target quadrant were significantly decreased in SAMP8 mice starting from 6 months of age as compared with age-matched SAMR1, while the time spent in the target quadrant decreased significantly in SAMP8 animals at 8 months of age. This discrepancy could be ascribed to a learning and memory deficit in looking for the platform and to a decrease in swimming speed, as well as to a reduced motivation to escape from the water of SAMP8 mice not being in an aversive situation [40].

Altogether, these data confirm that SAMP8 mice develop a deficit in spatial learning and memory performance

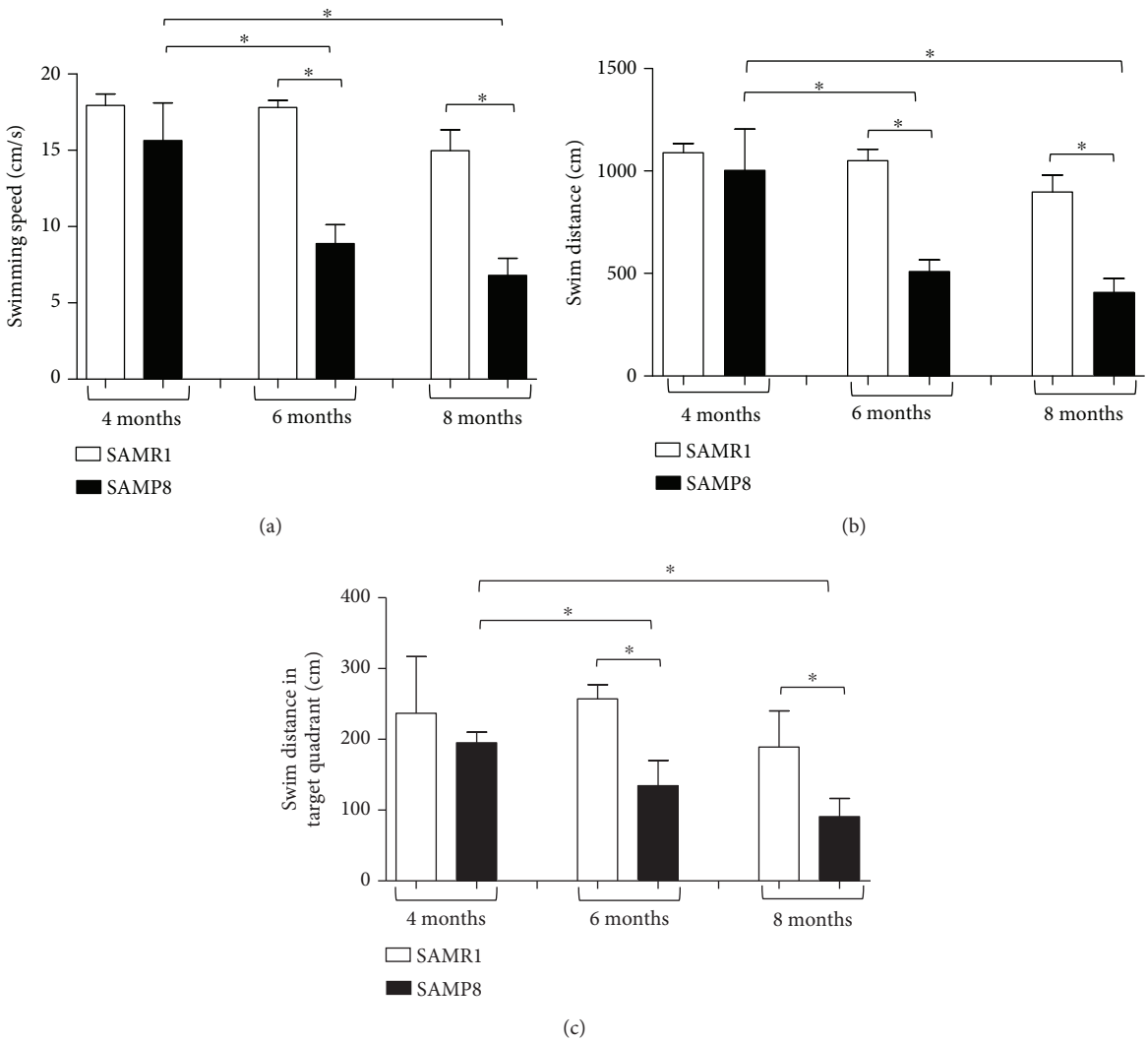

Figure 3: Cognitive performance of SAM. Cognitive performance of SAMR1 and SAMP8 mice at 4, 6, and 8 months of age, during the probe trial session of the Morris water maze test: (a) swimming speed; (b) swim distance; (c) swim distance in the target quadrant. Data are expressed as mean ± S.E.M. obtained from 8 animals. Differences among groups were evaluated by two-way analysis of variance followed by post hoc analysis with the Fisher LSD test or a one-way analysis of variance followed by post hoc analysis with the Student-Newman-Keuls test where appropriate. $^*P < 0.05$ between the indicated subgroups.

compared with control SAMR1 mice. Moreover, such deficits become clearer as AD develops in SAMP8 mice.

3.2. Expression of α-Syn, Tau, and Aβ in Brain Tissues and RBCs: Immunoblotting Analysis. The presence of AD-related misfolded proteins (i.e., α-syn, tau, and Aβ) was assessed by western blotting analysis in brain and RBC samples obtained from SAM mice. The quantitative comparison between pathological and control animals was subsequently performed by immunoenzymatic assays. Considering the timing of ageing, the demonstrated cognitive impairment, and the onset of the pathological processes, samples obtained from 4-month animals were excluded from further investigations, focusing on the brain tissues and RBCs obtained from animals at 6 and 8 months.

The anti-Aβ antibody recognised 5 and 15 kDa proteins (Figure 4(a)) corresponding to Aβ monomeric and oligomer forms, respectively [41], in both brain tissues and RBCs. Bands with a molecular weight higher than 25 kDa (Figure 4(a)) were especially revealed in brain tissues, presumably indicating elevated oligomeric forms of the protein [42].

In brain tissues, the anti-tau antibody revealed the characteristic bands (Figure 4(b)) ranging from 55 to 74 kDa [11, 43, 44]. Worth noting, a band lower than 50 kDa, which was particularly evident in RBCs (Figure 4(b)), has been related to truncated or cleaved forms of tau containing the C-terminal region [11, 43, 44]. These data demonstrate that the antibody is able to recognise both truncated and uncleaved forms of the protein and that the triplet bands do not refer to oligomeric tau.

Finally, the anti-α-syn antibody-labelled proteins of 15 kDa and 30 kDa proteins correspond to α-syn [43] in both brain tissues and RBCs (Figure 4(d)).

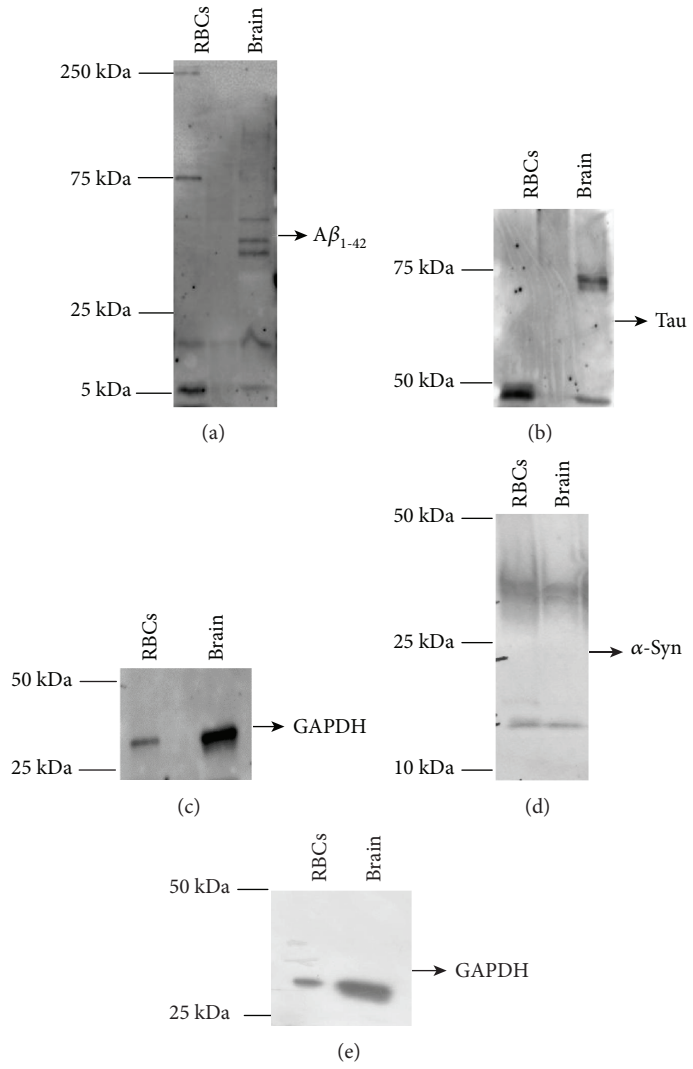

Figure 4: Detection of misfolded proteins in cell lysates of RBCs and brain tissues by western blot analysis. Cell lysates of RBCs and brain tissues from SAMs were immunoblotted with antibodies to Aβ (a), tau (b), and α-syn (d). (c, e) GAPDH was used as a loading control for Aβ and tau (c) or for α-syn (e) normalisation. A representative image for each protein is shown ($n = 3$).

3.3. Expression of α-Syn Heterocomplexes with Tau or Aβ in Brain Tissues and RBCs of SAM Mice. A coimmunoprecipitation-western blotting assay was employed to explore the presence of α-syn heterocomplexes in brain and RBC samples of SAM mice (Figure 5). To this purpose, lysates obtained from brain tissues or RBCs were immunoprecipitated using an anti-α-syn antibody and then immunoblotted with a specific antibody for α-syn (i.e., input), tau, or anti-Aβ [11]. In α-syn immunoprecipitates (Figure 5(a)), two major bands of 15 kDa and 30 kDa, corresponding to α-syn protein [11, 45], were noticed in both brain tissues and RBCs.

The Aβ immunoblotting on α-syn immunoprecipitates obtained from brain tissues and RBCs produced two main immunoreactive bands of 5 and 30 kDa (Figure 5(b)), mainly associated to monomeric and oligomeric Aβ forms [11]. Moreover, probing α-syn immunoprecipitates with an anti-tau antibody showed an immunoreactive band of 55 kDa, ascribable to the tau protein (Figure 5(c)). Altogether, the results demonstrated that α-syn forms heterocomplexes with Aβ and tau in brain tissues and in RBCs of SAM mice, similarly to previous data reported in human samples [5, 11, 22].

3.4. Concentrations of α-Syn, Tau, and Aβ in Brain Tissues and RBCs of SAM Mice. Specific and quantitative immunoenzymatic assays were employed to measure α-syn, tau, and Aβ levels in brain tissues and RBCs of SAMP8 mice at different stages of AD progression and their age-matched SAMR1 controls. The values are set out in Table 1.

3.4.1. Aβ. The amount of Aβ in the brain did not change with age either in SAMR1 or in SAMP8 (Figure 6(a)), although an incremental trend was noticed. By contrast, SAMP8 animals showed significantly higher Aβ concentrations than age-matched SAMR1 mice (6 months: $P = 0.0193$; 8 months: $P = 0.0104$), consistent with previous data. These results confirm that Aβ accumulated early in the brain of AD animals.

As observed in the brain, the levels of Aβ in RBCs of SAMR1 did not change with age (Figure 6(b)). By contrast,

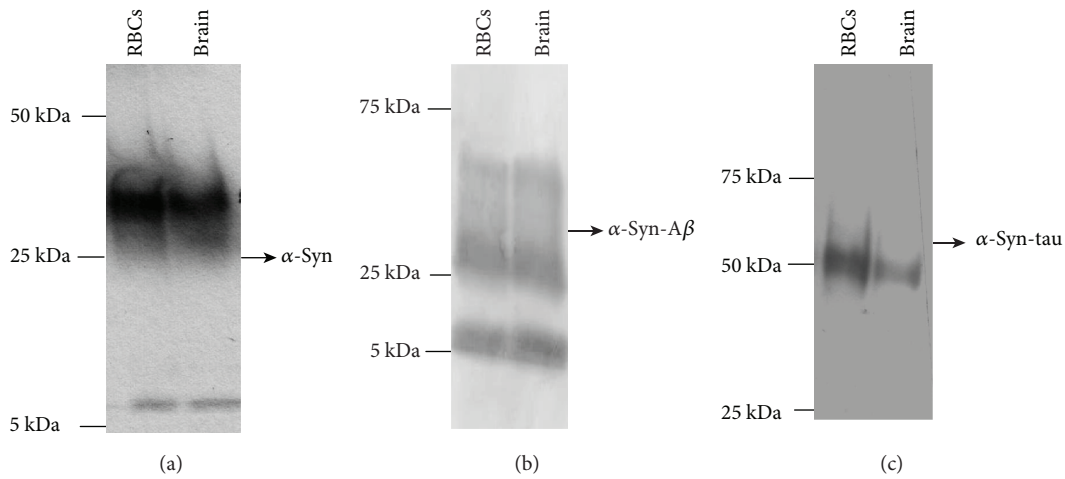

Figure 5: Detection of α-syn heterocomplexes with tau and Aβ in RBCs and brain samples. From SAMs, cell lysates of RBCs and brain tissues were immunoprecipitated with an anti-α-syn antibody and then immunoblotted with antibodies to α-syn ((a), i.e., input), Aβ (b), or tau (c). A representative image for each protein is shown.

Table 1: Concentrations of Aβ, α-syn, tau, p-tau, α-syn-Aβ, and α-syn-tau in brain tissues and RBCs of SAMP8 and SAMR1 at different ages.

Brain	Aβ (ng/μg)	α-Syn (ng/μg)	Tau (ng/μg)	p-Tau (pg/μg)	α-Syn-Aβ (ng/μg)	α-Syn-tau (ng/μg)
SAMR1 6 m	7.63 ± 3.06	6.22 ± 4.59	7.51 ± 3.10	158 ± 92.2	1.35 ± 1.36	2.08 ± 1.58
SAMP8 6 m	13.5 ± 4.75*	15.5 ± 7.73*	7.28 ± 2.77	327 ± 118*	2.70 ± 1.77	8.74 ± 3.12**
SAMR1 8 m	8.81 ± 3.72	8.54 ± 5.94	13.0 ± 3.6$^{\#}$	123 ± 105	2.81 ± 1.68	1.54 ± 1.04
SAMP8 8 m	15.5 ± 4.8*	0.69 ± 0.42$^{**\#\#}$	22.1 ± 6.0$^{*\#\#}$	397 ± 152***	0.53 ± 0.50$^{*\#}$	1.17 ± 1.49$^{\#\#\#}$
RBCs	Aβ (ng/mg)	α-Syn (ng/mg)	Tau (ng/mg)	p-Tau (ng/mg)	α-Syn-Aβ (ng/mg)	α-Syn-tau (ng/mg)
SAMR1 6 m	147 ± 48.1	37.5 ± 25.2	14.7 ± 1.59	0.36 ± 0.09	19.7 ± 13.6	3.56 ± 2.77
SAMP8 6 m	121 ± 68.6	279 ± 242***	12.1 ± 6.95	0.36 ± 0.09	39.9 ± 23.8*	4.78 ± 6.04
SAMR1 8 m	123 ± 13.5	39.1 ± 47.4	14.0 ± 6.38	0.92 ± 0.74$^{\#\#}$	40.7 ± 50.7$^{\#}$	3.70 ± 3.57
SAMP8 8 m	213 ± 120$^{*\#}$	204 ± 186**	34.4 ± 23.9$^{*\#}$	1.21 ± 1.33$^{\#\#}$	103 ± 99.4$^{\#}$	8.67 ± 5.45$^{*\#\#}$

Values are expressed as mean ± SD. Differences among the groups were evaluated by a nonparametric analysis (Kruskal-Wallis). $^{*}P < 0.05$, $^{**}P < 0.01$, and $^{***}P < 0.001$ indicate significant differences of SAMR1 versus the age-matched SAMP8. $^{\#}P < 0.05$, $^{\#\#}P < 0.01$, and $^{\#\#\#}P < 0.001$ indicate significant differences between SAMR1 6 m and SAMR1 8 m or between SAMP8 6 m and SAMP8 8 m.

Aβ significantly accumulated with age in RBCs from SAMP8 ($P = 0.0270$, Figure 6(b)). Moreover, SAMP8 animals at 8 months displayed significantly higher Aβ RBC levels than the age-matched SAMR1 ($P = 0.0279$), consistent with the data obtained in the brain. By contrast, comparable levels were noticed in SAMP8 and SAMR1 at 6 months ($P = 0.3029$, Figure 6(b)). These data suggest that Aβ accumulated in RBCs with AD progression, albeit with a slower accumulation kinetics than that observed in the brain.

3.4.2. Tau. Brain levels of total tau (Figure 6(c)) were proven to increase significantly with age either in SAMR1 ($P = 0.0293$) or in SAMP8 mice ($P = 0.0095$). Moreover, SAMP8 animals at 8 months displayed significantly higher brain concentrations of total tau compared to their age-matched controls ($P = 0.0350$). These data confirm that tau accumulated in the brain along with AD progression in the SAM experimental model.

Tau concentrations in RBCs increased with age in SAMP8 only ($P = 0.0019$; SAMR1: $P = 0.7430$, Figure 6(d)). Consistent with the data obtained in the brain, total tau significantly accumulated in RBCs of SAMP8 mice at 8 months compared to control mice ($P = 0.00019$, Figure 6(d)). These results suggest that tau accumulation in RBCs in pathological mice may reflect the increase of this protein in the brain.

3.4.3. Phospho-Tau. The levels of p-tau in the brain (Figure 6(e)) did not differ with mice ages, either in SAMP8 or in SAMR1 ($P = 0.4140$ and $P = 0.5737$, respectively, Figure 6(e)). By contrast, pathological mice displayed significantly higher levels of brain p-tau compared to the age-matched controls, either at 6 months or at 8 months ($P = 0.0485$ and $P = 0.0010$, respectively, Figure 6(e)). These data confirm that tau is hyperphosphorylated in the brain of the AD animal model.

Interestingly, an age-dependent p-tau accumulation was observed in RBCs, both in control ($P = 0.0011$, Figure 6(f)) and SAMP8 mice ($P = 0.0015$, Figure 6(f)). Nevertheless, no significant changes in p-tau levels in RBCs were observed comparing SAMP8 and SAMR1 (6

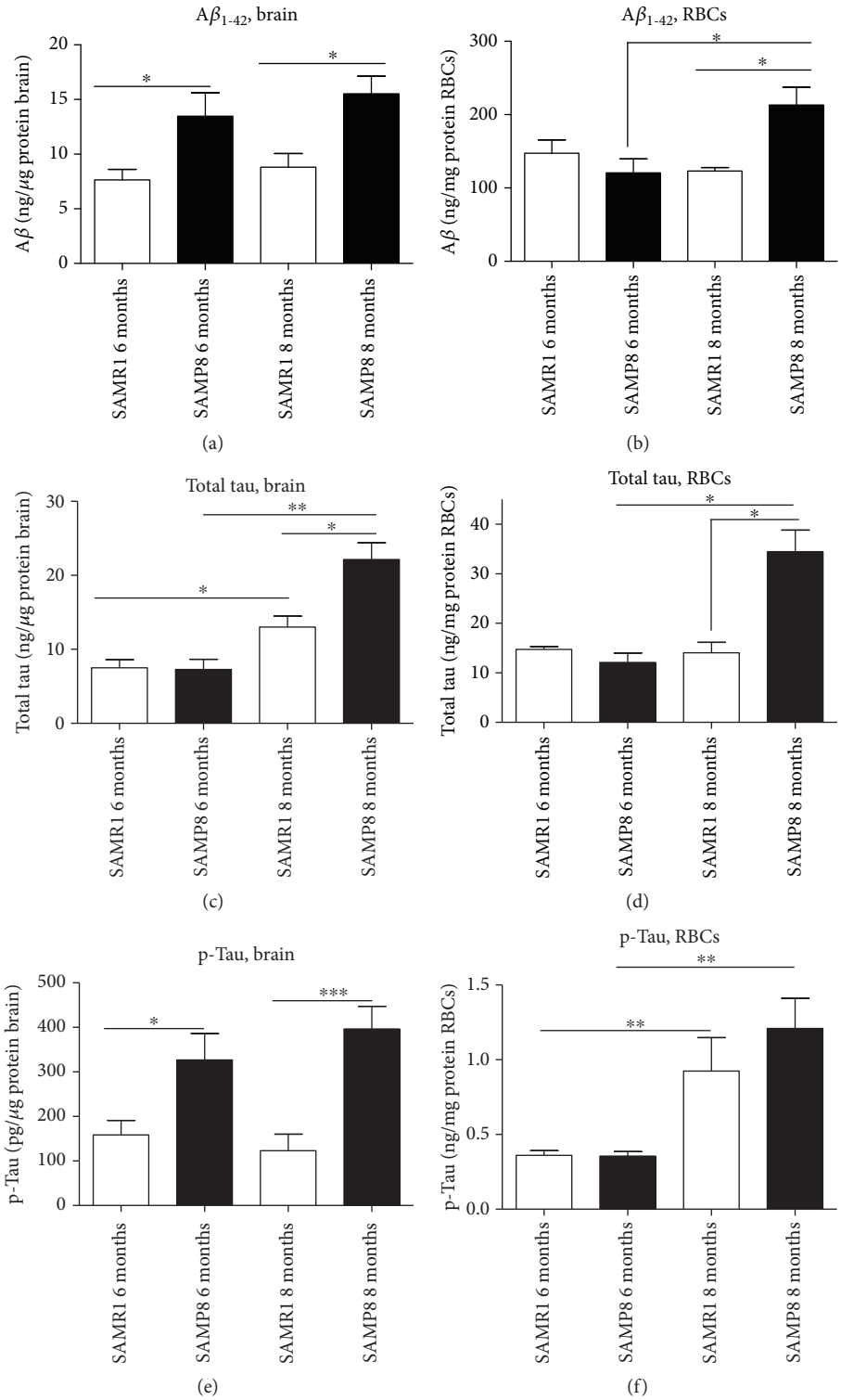

Figure 6: Quantitative assay of misfolded protein Aβ, tau, and p-tau in RBCs and brain tissues. The levels of Aβ, tau, and p-tau in brain tissues (a, c, and e) and RBCs (b, d, and f) from SAMP8 and SAMR1 mice at 6 and 8 months were assessed by specific immunoenzymatic assays. Differences among groups were evaluated by one-way ANOVA. P values were adjusted with Sidak's multiple comparison test: $^{*}P < 0.05$, $^{**}P < 0.01$, and $^{***}P < 0.001$ between the indicated subgroups.

months: $P = 0.6965$; 8 months: $P = 0.09401$, Figure 6(f)). These results suggest that phosphorylated tau accumulated in RBCs both under physiological ageing and AD progression.

3.4.4. α-Syn. The brain concentrations of total α-syn significantly decreased with animals' age in SAMP8 ($P = 0.0095$, Figure 7(a)), but not in control animals ($P = 0.5622$, Figure 7(a)), suggesting that total α-syn decreases as the

disease progresses. Consistent with these data, SAMP8 mice at 8 months presented significantly lower brain concentrations of total α-syn compared to age-matched controls ($P = 0.0022$, Figure 7(a)). Surprisingly, the opposite condition was found when comparing animals at 6 months ($P = 0.0240$, Figure 7(a)).

Total α-syn in RBCs did not show significant variations with age (SAMR1: $P = 0.2643$, Figure 7(b)) or AD progression (SAMP8: $P = 0.8968$, Figure 7(b)). Differently from the brain, RBCs from SAMP8 animals showed significantly higher total α-syn concentrations compared to the age-matched controls (6 months: $P < 0.0001$; 8 months: $P = 0.0097$, Figure 7(b)). Globally, these data suggest a different kinetics of α-syn in peripheral fluids compared to the brain.

3.5. Concentrations of α-Syn Heterocomplexes in Brain Tissues and RBCs. α-Syn heterocomplexes with Aβ or tau were measured both in brain tissues and RBCs through a "homemade" immunoenzymatic assay [11, 22].

3.5.1. α-Syn-Aβ. The levels of α-syn-Aβ in SAMP brains (Figure 7(c)) showed an interesting trend depending on ageing and progression of the disease. Indeed, the brain concentrations decreased along with age-AD progression in SAMP8 mice ($P = 0.0303$, Figure 7(c)). Moreover, α-syn-Aβ levels in the brain decreased in SAMP8 at 8 months compared to age-matched controls ($P = 0.0101$, Figure 7(c)). These data suggest that brain α-syn-Aβ levels may follow the accumulation kinetics of total α-syn.

Surprisingly, α-syn-Aβ levels in RBCs increased with age-AD progression in SAMR1 ($P = 0.0017$, Figure 7(d)) and SAMP8 mice ($P = 0.0308$). Moreover, such levels in RBCs were higher in SAMP8 compared to age-matched controls, even if a statistical significance was reached at 6 months only (6 months: $P = 0.0168$; 8 months. $P = 0.1797$, Figure 7(d)). These data suggest that the α-syn-Aβ level in RBCs has an opposite trend compared to that in the brain.

3.5.2. α-Syn-Tau. The levels of α-syn-tau heterocomplexes in the brain decreased with the pathological progression in SAMP8 mice ($P = 0.0002$, Figure 7(e)). Nevertheless, such concentrations were significantly elevated in SAMP8 compared to SAMR1 at 6 months ($P = 0.0012$, Figure 7(e)). Taken together, these data suggest that the α-syn-tau trend in the brain reflects what is elicited by α-syn.

The levels of α-syn-tau heterocomplexes in RBCs did not significantly differ in SAMR1 at different ages ($P = 1.000$, Figure 7(f)) or between SAMR1 and SAMP8 at 6 months ($P = 0.8907$, Figure 7(f)). By contrast, α-syn-tau concentrations increased in SAMP8 mice at 8 months compared to the age-matched controls ($P = 0.0155$, Figure 7(f)) or to SAMP8 at 6 months ($P = 0.0025$, Figure 7(f)). These data suggest that the α-syn-tau level in RBCs has an opposite trend compared to that in the brain.

3.6. Assessment of IL-1β Levels in Brain Tissues and RBCs. In order to monitor the progress of inflammation in the animal model of AD, IL-1β was chosen as a representative inflammatory factor [14] and measured in brain tissues of SAMP8 mice and in their age-matched SAMR1 controls.

In the cerebral cortex from SAMR1 mice at 6 and 8 months, IL-1β levels accounted for 1.3 ± 0.5 and 3.3 ± 0.4 pg – mg, respectively (Figure 8(a)), suggesting an increase in interleukin levels with physiological ageing. At 6 months, SAMP8 mice showed IL-1β levels of 1.8 ± 0.7 pg – mg in the cerebral cortex (Figure 8(a)), which were comparable to those detected in the respective age-matched control (SAMR1) mice. By contrast, IL-1β levels in the cerebral cortex from SAMP8 mice at 8 months were significantly increased (29.6 ± 5.4 pg – mg) compared to the age-matched controls (SAMR1) and to SAMP8 mice at 6 months (Figure 8(a)). These data suggest that brain IL-1β concentrations increased in the AD animal model and that such an increase became more prominent with age (i.e., with AD progression) in SAMP8 mice compared with aged SAMR1 mice.

In order to check whether brain inflammation was associated with an enhancement in peripheral inflammatory factors, IL-1β concentration was monitored in RBCs, which are able to produce cytokines, too [46]. The interleukin significantly accumulated with ageing (6 months vs. 8 months) in RBCs of SAMR1 mice (Figure 8(b)). Surprisingly, an opposite trend was observed in SAMP8 mice (Figure 8(b)), which displayed the highest IL-1β concentrations at 6 months (839.7 ± 398.1 pg – mg, Figure 8(b)). The IL-1β concentration in RBCs was significantly higher in SAMP8 mice at 6 months compared to the age-matched control (i.e., SAMR1, 6 months, 384.4 ± 72.98 pg – mg); by contrast, comparable values were obtained in SAMP8 and SAMR1 at 8 months (538.8 ± 421.2 and 460.9 ± 42.12 pg – mg, Figure 8(b)). Overall, these data show that the inflammatory cytokine is released maximally in RBCs during the initial phases of AD development. Moreover, the cytokine accumulation in RBCs seems to follow a faster accumulation kinetics compared to that elicited in the cerebral cortex.

4. Discussion

In the present study, the brain accumulation of neurodegeneration-related proteins such as homo- and heteroaggregates was analysed and compared to the levels of the same proteins in RBCs, using a validated animal model of AD at different stages of disease progression. Moreover, the amounts of IL-1β, chosen as a marker of AD-associated inflammation, were analysed both in brain tissues and RBCs. The main conclusions of this work are as follows: (a) brain Aβ, tau, and p-tau were elevated in SAMP8 mice compared to control and increased with AD progression; similar, although slower, accumulation kinetics were found in RBCs; (b) α-syn and its heterocomplexes, α-syn-Aβ and α-syn-tau, showed different accumulation kinetics in brain tissues and RBCs; and (c) both brain and peripheral IL-1β levels were elevated in SAMP8 mice, but increased earlier in RBCs. Overall, these results support RBCs as a valuable model to monitor neurodegeneration, suggesting Aβ, tau, and p-tau levels as suitable AD biomarkers in peripheral cells, both for diagnosis and follow-up.

Recent findings have suggested that each ND is not associated with the misfolding of a single specific protein, but rather with a mixed pattern of proteinopathies [4, 5], which

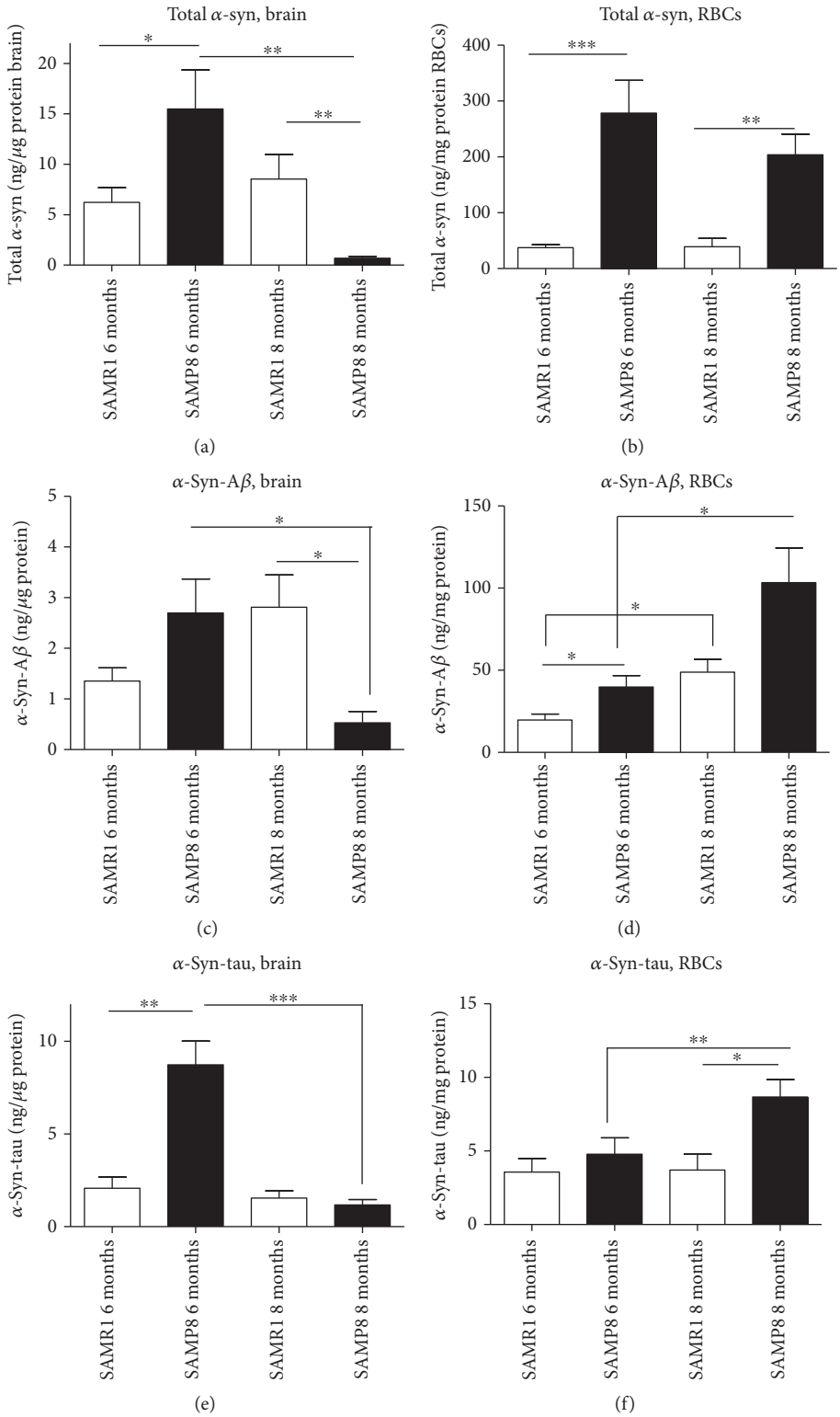

Figure 7: Quantitative assay of α-syn and misfolded protein's heterocomplex in both RBCs and in brain tissues. Levels of α-syn, α-syn-Aβ, and α-syn-tau in brain tissues (a, c, and e) and in RBCs (b, d, and f) from SAMP8 and SAMR1 mice at 6 and 8 months were assessed by specific immunoenzymatic assays. Difference among groups were evaluated by one-way ANOVA. P values were adjusted with Sidak's multiple comparison test: $^{*}P < 0.05$, $^{**}P < 0.01$, and $^{***}P < 0.001$ between the indicated subgroups.

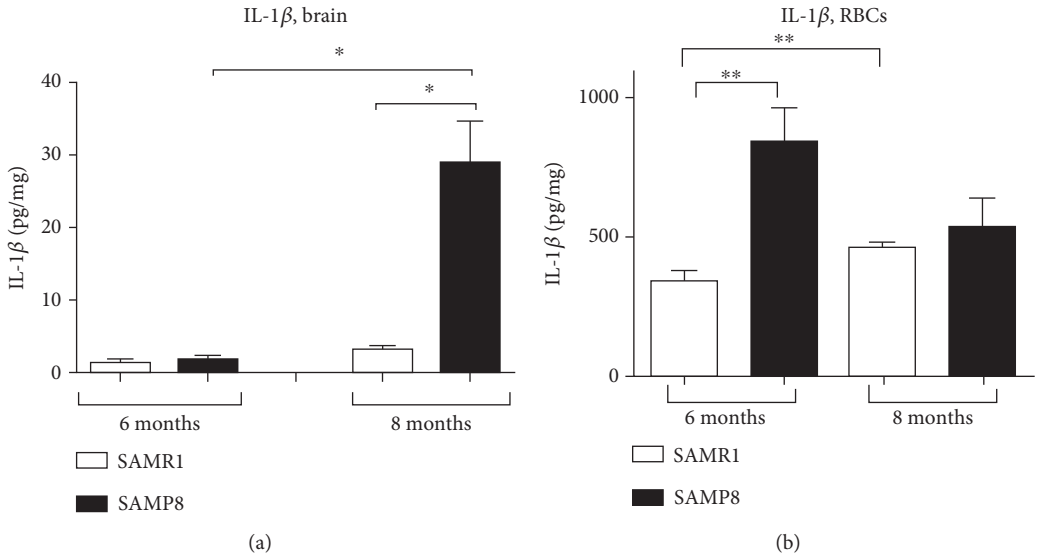

Figure 8: Quantitative detection of IL-1β. IL-1β levels were assessed in brain (a) and RBC (b) tissues from control animals (SAMR1) and SAMP8 mice at 6 and 8 months of age. Each column represents the mean ± S.E.M. value ($n = 8$). Differences among groups were evaluated by one-way ANOVA. P values were adjusted with Sidak's multiple comparison test: $^{*}P < 0.05$ and $^{**}P < 0.01$ between the indicated subgroups.

reach peripheral compartments even years before the onset of clinical symptoms. Herein, a validated animal model of AD, i.e., SAMP8, and its control strain SAMR1 were used to quantify the accumulation of Aβ, tau, α-syn in brain tissues and RBCs and to compare them at different stages of progress of the disease.

Behavioural tests showed that SAMP8 mice develop an age-dependent deficit in spatial learning and memory performance, as compared with control SAMR1 mice, endorsing the validity of this animal model.

Consistent with previous data [1], Aβ was found to accumulate in the brain of AD animals. Similarly, Aβ levels were augmented in RBCs along with AD progression. This observation is of interest since Aβ levels in RBCs have been shown to increase with ageing in humans and to decrease upon providing an antioxidant supplement [15]. A noteworthy aspect we observed is a slower Aβ accumulation kinetics in RBCs compared to that detected in the brain. In this respect, Aβ increase in the brain and the onset of NDs have been linked to blood-derived Aβ, which can enter the brain [47], even preceding the neuronal and glial pathological alterations of AD brains [48]. Nevertheless, this "peripheral sink hypothesis" is still a bone of contention because inhibiting the Aβ-producing enzyme in the periphery does not alter Aβ accumulation in the CNS [49].

Similarly to what was observed for Aβ, tau and its phosphorylated form accumulated in the brain with ageing and/or AD progression in the SAM model, as previously reported by others [50, 51]. In particular, our data are consistent with evidences that tau hyperphosphorylation is an integral part of ageing and represents an early event in AD animal models [30, 52]. A similar, albeit quite slower, accumulation kinetics of tau and p-tau was found in the RBCs of SAMs, suggesting this protein as a valuable RBC marker reflecting brain neuropathology. Consistent with this hypothesis, significantly elevated concentrations of p-tau have been shown in the RBCs of PD patients [11].

Overall, our data allow hypothesising that the increase in the levels of Aβ, tau, and p-tau in the brain is due to an enhanced production in neurons associated with the progression of AD. In this respect, the increase of the same proteins in RBCs might result from an alteration of the blood-brain barrier (BBB), leading to the subsequent leakage of proteins from the brain to the blood. Therefore, further investigations are needed to elucidate the degree of production of these proteins in blood cells and the efficiency of proteasome systems deputed to the degradation of misfolded proteins.

Altered levels of α-syn, a protein commonly associated with PD, have recently been detected in the brain and CSF of AD patients [53]. In the present study, α-syn levels in the brain were found to be higher than those of age-matched controls in the early analysed phase of AD progression, consistent with the increase in the expression of α-syn found in 5-month SAMP8 [52]. Nevertheless, total α-syn was found to decrease with AD progression and comparatively with controls when 8-month-old mice were examined. The latter results are consistent with several findings reporting a significant decrease in the total concentration of brain α-syn in PD [54] and PD with dementia [55]. This partial controversy in α-syn levels in the early phase of AD suggests that SAMP8 does not fully reflect the human brain pathology associated with α-syn. Of note, a different trend was found for α-syn in RBCs: indeed, RBCs from SAMP8 showed significantly higher total α-syn concentrations than age-matched controls. These results are at odds with the data obtained in human RBCs from PD patients presenting lower levels than HC [11, 20] and highlight the need for further investigations to elucidate putative differences in posttranslational α-syn modifications, degradation pathways, and passage through the BBB [56, 57].

In addition to homoaggregates, the presence of heterocomplexes of α-syn (α-syn-tau and α-syn-Aβ) has been documented both in cellular models and patients' brains [5, 8, 9, 11, 58]. On this basis, α-syn heterocomplexes were measured for the first time in this experimental model through "homemade" immunoenzymatic assays. Interestingly, α-syn was shown to form heterocomplexes with Aβ and tau both in brain tissues and RBCs of SAM mice, similarly to previous data reported in human samples [5, 11, 22].

Both α-syn-Aβ and α-syn-tau concentrations in SAM brains followed the same accumulation kinetics shown for total α-syn. Indeed, the initial increment was followed by a decrement in the second phase of AD compared to controls and AD progression. Interestingly, α-syn-Aβ and α-syn-tau levels in RBCs displayed a similar trend, presenting a significant increase in AD mice compared to controls and along with AD progression. As observed for brain samples, α-syn heterocomplexes showed the same temporal kinetics of accumulation of total α-syn in RBCs, too. Consistent with these data, α-syn-Aβ concentrations in human RBCs were elevated in PD patients and correlated with the progress of the disease [11]. Surprisingly, our recent findings have probed a significant decrease of α-syn heterocomplexes in RBCs from AD patients [10]. These findings point out the need for further investigations in relation to the specific neurodegenerative disease and the fluid compartment in which these proteins are analysed.

With these data at our disposal, the accumulation of α-syn and its heterocomplexes in RBCs does not seem to reflect the brain trend. The discrepancy could be ascribed to the trafficking across the BBB or to the difficulty of measuring appropriately the α-syn oligomeric form [5].

In the present study, the possible relationship between AD progression and inflammation was investigated by assessing IL-1β levels, as one of the most important inflammatory mediators, both in brain tissues and RBCs from SAMP8 and SAMR1. In this sense, it has to be underlined that peripheral and central cytokines are released upon inflammation [59] and not strictly related to AD. Nevertheless, IL-1β has been demonstrated to be significantly higher in AD with respect to controls in both humans and animals [27–29] and can be considered as a good marker of inflammation in an animal model of this disease. In our hands, brain IL-1β levels increased in an AD animal model at 8 months and in age-matched control, as previously reported by others in the hippocampus [26]. Interestingly, IL-1β concentrations were higher in RBCs than in the brain. However, not surprisingly, RBCs have been identified recently as a reservoir for cytokines, with a median concentration 12-fold higher than plasma [18]. RBC IL-1β levels were significantly elevated in the pathological animals, consistent with the greater level of oxidative stress found in RBCs from SAMP8 [60]. These changes were particularly evident at 6 months, suggesting that the cytokine accumulation in RBCs seems to follow a faster kinetics compared to the cerebral cortex, and thus it could represent an early diagnostic for its early stage. In this respect, recent findings have highlighted a close link between peripheral inflammation and accumulation of misfolded proteins [11, 61]. For instance, inflammation has been shown to augment Aβ levels through an increased production in the brain, an increased influx, and a decreased efflux, due to alterations of the BBB [62]. Recently, peripheral inflammation has been shown to modulate the amyloid phenotype in mice by regulating blood-derived and local brain inflammatory cell populations involved in Aβ clearance [63]. On the other side, in animal models, in AD and in aged brains, accumulation of Aβ seems to trigger inflammatory responses with an enhanced production of inflammatory factors, which have been localised in brain plaques [64]. Besides the inflammasome pathway, amyloid fibrils have been proven to induce the secretion of proinflammatory cytokines through the activation of the Toll-like receptor 2 [65]. Future studies will investigate the involvement of this innate immune receptor in immune responses associated to amyloidosis in an AD animal model. Among the limitations of our study, it should be underlined that the available immunoenzymatic assays cannot distinguish the oligomeric or monomeric nature of ND-related proteins, both in brain tissues and blood. Further studies will confirm the multiaggregation status of these proteins.

In conclusion, we proved in the present study that Aβ, tau, and p-tau kinetics of accumulation in RBCs from SAMP8 followed similar patterns to those in the brain, suggesting these proteins as putative peripheral biomarkers of AD. Future studies will be needed to confirm our preliminary data.

Abbreviations

AD: Alzheimer's disease
ND: Neurodegenerative disease
Aβ: β-Amyloid
p-tau: Phospho-tau
α-syn: α-Synuclein
NTs: Neurofibrillary tangles
RBCs: Red blood cells
SAMP8: Senescence-accelerated mouse-prone
SAMR1: Senescence-accelerated mouse-resistant
IL-1β: Interleukin-1β.

Data Availability

The data used to support the findings of this study are available from the corresponding author upon request.

Conflicts of Interest

The authors declare no conflict of interest.

Acknowledgments

This work was supported by a grant from PRA to SD and MF (grant number: PRA-2018-31).

References

[1] J. E. Morley, H. J. Armbrecht, S. A. Farr, and V. B. Kumar, "The senescence accelerated mouse (SAMP8) as a model for oxidative stress and Alzheimer's disease," *Biochimica et Biophysica Acta (BBA) – Molecular Basis of Disease*, vol. 1822, no. 5, pp. 650–656, 2012.

[2] V. Calsolaro and P. Edison, "Neuroinflammation in Alzheimer's disease: current evidence and future directions," *Alzheimer's & Dementia*, vol. 12, no. 6, pp. 719–732, 2016.

[3] S. Daniele, C. Giacomelli, and C. Martini, "Brain ageing and neurodegenerative disease: the role of cellular waste management," *Biochemical Pharmacology*, vol. 158, pp. 207–216, 2018.

[4] F. Baldacci, S. Lista, F. Garaci, U. Bonuccelli, N. Toschi, and H. Hampel, "Biomarker-guided classification scheme of neurodegenerative diseases," *Journal of Sport and Health Science*, vol. 5, no. 4, pp. 383–387, 2016.

[5] C. Giacomelli, S. Daniele, and C. Martini, "Potential biomarkers and novel pharmacological targets in protein aggregation-related neurodegenerative diseases," *Biochemical Pharmacology*, vol. 131, pp. 1–15, 2017.

[6] M. E. Larson, M. A. Sherman, S. Greimel et al., "Soluble α-synuclein is a novel modulator of Alzheimer's disease pathophysiology," *The Journal of Neuroscience*, vol. 32, no. 30, pp. 10253–10266, 2012.

[7] L. Crews, I. Tsigelny, M. Hashimoto, and E. Masliah, "Role of synucleins in Alzheimer's disease," *Neurotoxicity Research*, vol. 16, no. 3, pp. 306–317, 2009.

[8] A. D. Andersen, M. Binzer, E. Stenager, and J. B. Gramsbergen, "Cerebrospinal fluid biomarkers for Parkinson's disease – a systematic review," *Acta Neurologica Scandinavica*, vol. 135, no. 1, pp. 34–56, 2017.

[9] U. Sengupta, M. J. Guerrero-Muñoz, D. L. Castillo-Carranza et al., "Pathological interface between oligomeric alpha-synuclein and tau in synucleinopathies," *Biological Psychiatry*, vol. 78, no. 10, pp. 672–683, 2015.

[10] F. Baldacci, S. Daniele, R. Piccarducci et al., "Potential diagnostic value of red blood cells α-synuclein heteroaggregates in Alzheimer's disease," *Molecular Neurobiology*, 2019.

[11] S. Daniele, D. Frosini, D. Pietrobono et al., "α-Synuclein heterocomplexes with β-amyloid are increased in red blood cells of Parkinson's disease patients and correlate with disease severity," *Frontiers in Molecular Neuroscience*, vol. 11, p. 53, 2018.

[12] L. Koric, E. Guedj, M. O. Habert et al., "Molecular imaging in the diagnosis of Alzheimer's disease and related disorders," *Revue Neurologique*, vol. 172, no. 12, pp. 725–734, 2016.

[13] J. Marksteiner, H. Hinterhuber, and C. Hinterhuber, "Cerebrospinal fluid biomarkers for diagnosis of Alzheimer's disease: beta-amyloid(1-42), tau, phospho-tau-181 and total protein," *Drugs Today*, vol. 43, no. 6, pp. 423–431, 2007.

[14] H. B. Stolp and K. M. Dziegielewska, "Review: Role of developmental inflammation and blood–brain barrier dysfunction in neurodevelopmental and neurodegenerative diseases," *Neuropathology and Applied Neurobiology*, vol. 35, no. 2, pp. 132–146, 2009.

[15] T. Kiko, K. Nakagawa, A. Satoh et al., "Amyloid β levels in human red blood cells," *PLoS One*, vol. 7, no. 11, article e49620, 2012.

[16] S. Singh, "Antioxidants as a preventive therapeutic option for age related neurodegenerative diseases," *Therapeutic Targets for Neurological Diseases*, vol. 2, 2015.

[17] K. A. Arbos, L. M. Claro, L. Borges, C. A. M. Santos, and A. M. Weffort-Santos, "Human erythrocytes as a system for evaluating the antioxidant capacity of vegetable extracts," *Nutrition Research*, vol. 28, no. 7, pp. 457–463, 2008.

[18] E. Karsten, E. Breen, and B. R. Herbert, "Red blood cells are dynamic reservoirs of cytokines," *Scientific Reports*, vol. 8, no. 1, p. 3101, 2018.

[19] Y. S. Eisele, U. Obermüller, G. Heilbronner et al., "Peripherally applied Aβ-containing inoculates induce cerebral β-amyloidosis," *Science*, vol. 330, no. 6006, pp. 980–982, 2010.

[20] X. Wang, S. Yu, F. Li, and T. Feng, "Detection of α-synuclein oligomers in red blood cells as a potential biomarker of Parkinson's disease," *Neuroscience Letters*, vol. 599, pp. 115–119, 2015.

[21] S. Daniele, B. Costa, D. Pietrobono et al., "Epigenetic modifications of theα-synuclein gene and relative protein content are affected by ageing and physical exercise in blood from healthy subjects," *Oxidative Medicine and Cellular Longevity*, vol. 2018, Article ID 3740345, 16 pages, 2018.

[22] S. Daniele, D. Pietrobono, J. Fusi et al., "α-Synuclein aggregates with β-amyloid or tau in human red blood cells: correlation with antioxidant capability and physical exercise in human healthy subjects," *Molecular Neurobiology*, vol. 55, no. 3, pp. 2653–2675, 2018.

[23] D. A. Butterfield and H. F. Poon, "The senescence-accelerated prone mouse (SAMP8): a model of age-related cognitive decline with relevance to alterations of the gene expression and protein abnormalities in Alzheimer's disease," *Experimental Gerontology*, vol. 40, no. 10, pp. 774–783, 2005.

[24] W. S. T. Griffin, J. G. Sheng, G. W. Roberts, and R. E. Mrak, "Interleukin-1 expression in different plaque types in Alzheimer's disease: significance in plaque evolution," *Journal of Neuropathology & Experimental Neurology*, vol. 54, no. 2, pp. 276–281, 1995.

[25] P. H. Patterson, "Cytokines in Alzheimer's disease and multiple sclerosis," *Current Opinion in Neurobiology*, vol. 5, no. 5, pp. 642–646, 1995.

[26] K. K. Tha, Y. Okuma, H. Miyazaki et al., "Changes in expressions of proinflammatory cytokines IL-1β, TNF-α and IL-6 in the brain of senescence accelerated mouse (SAM) P8," *Brain Research*, vol. 885, no. 1, pp. 25–31, 2000.

[27] K. S. P. Lai, C. S. Liu, A. Rau et al., "Peripheral inflammatory markers in Alzheimer's disease: a systematic review and meta-analysis of 175 studies," *Journal of Neurology, Neurosurgery & Psychiatry*, vol. 88, no. 10, pp. 876–882, 2017.

[28] A. A. Gomaa, R. M. Makboul, M. A. el-Mokhtar, E. A. Abdel-Rahman, I. A. Ahmed, and M. A. Nicola, "Terpenoid-rich *Elettaria cardamomum* extract prevents Alzheimer-like alterations induced in diabetic rats via inhibition of GSK3β activity, oxidative stress and pro-inflammatory cytokines," *Cytokine*, vol. 113, pp. 405–416, 2019.

[29] I. S. Ebenezer and R. Tite, "Sex difference in the feeding responses of non-deprived rats to the 5-HT1A agonists 8-OH-DPAT and gepirone," *Methods and Findings in Experimental and Clinical Pharmacology*, vol. 16, no. 2, pp. 91–96, 1994.

[30] A. M. Canudas, J. Gutierrez-Cuesta, M. I. Rodríguez et al., "Hyperphosphorylation of microtubule-associated protein tau in senescence-accelerated mouse (SAM)," *Mechanisms of Ageing and Development*, vol. 126, no. 12, pp. 1300–1304, 2005.

[31] O. M. A. El-Agnaf, S. A. Salem, K. E. Paleologou et al., "Detection of oligomeric forms of α-synuclein protein in human plasma as a potential biomarker for Parkinson's disease," *The FASEB Journal*, vol. 20, no. 3, pp. 419–425, 2006.

[32] P. Pesini, V. Pérez-Grijalba, I. Monleón et al., "Reliable measurements of the β-amyloid pool in blood could help in the early diagnosis of AD," *International Journal of Alzheimer's Disease*, vol. 2012, article 604141, 10 pages, 2012.

[33] E. Zappelli, S. Daniele, M. Abbracchio, C. Martini, and M. Trincavelli, "A rapid and efficient immunoenzymatic assay to detect receptor protein interactions: G protein-coupled receptors," *International Journal of Molecular Sciences*, vol. 15, no. 4, pp. 6252–6264, 2014.

[34] M. Fumagalli, E. Bonfanti, S. Daniele et al., "The ubiquitin ligase Mdm2 controls oligodendrocyte maturation by intertwining mTOR with G protein-coupled receptor kinase 2 in the regulation of GPR17 receptor desensitization," *Glia*, vol. 63, no. 12, pp. 2327–2339, 2015.

[35] E. Emmanouilidou, D. Elenis, T. Papasilekas et al., "Assessment of α-synuclein secretion in mouse and human brain parenchyma," *PLoS One*, vol. 6, no. 7, article e22225, 2011.

[36] A. F. Teich, M. Patel, and O. Arancio, "A reliable way to detect endogenous murine β-amyloid," *PLoS One*, vol. 8, no. 2, article e55647, 2013.

[37] P. K. Mandal, J. W. Pettegrew, E. Masliah, R. L. Hamilton, and R. Mandal, "Interaction between Aβ peptide and α synuclein: molecular mechanisms in overlapping pathology of Alzheimer's and Parkinson's in dementia with Lewy body disease," *Neurochemical Research*, vol. 31, no. 9, pp. 1153–1162, 2006.

[38] X. Q. Hou, H. P. Song, Y. B. Chen et al., "Effects of Bushen-Yizhi formula on age-related inflammation and oxidative stress in senescence-accelerated mice," *Molecular Medicine Reports*, vol. 17, no. 5, pp. 6947–6960, 2018.

[39] P. Xu, S. P. Xu, K. Z. Wang et al., "Cognitive-enhancing effects of hydrolysate of polygalasaponin in SAMP8 mice," *Journal of Zhejiang University-Science B*, vol. 17, no. 7, pp. 503–514, 2016.

[40] L. Kang, S. Li, Z. Xing et al., "Dihydrotestosterone treatment delays the conversion from mild cognitive impairment to Alzheimer's disease in SAMP8 mice," *Hormones and Behavior*, vol. 65, no. 5, pp. 505–515, 2014.

[41] E. Cerf, R. Sarroukh, S. Tamamizu-Kato et al., "Antiparallel β-sheet: a signature structure of the oligomeric amyloid β-peptide," *Biochemical Journal*, vol. 421, no. 3, pp. 415–423, 2009.

[42] M. A. Kostylev, A. C. Kaufman, H. B. Nygaard et al., "Prion-protein-interacting amyloid-β oligomers of high molecular weight are tightly correlated with memory impairment in multiple Alzheimer mouse models," *The Journal of Biological Chemistry*, vol. 290, no. 28, pp. 17415–17438, 2015.

[43] L. Buée, T. Bussière, V. Buée-Scherrer, A. Delacourte, and P. R. Hof, "Tau protein isoforms, phosphorylation and role in neurodegenerative disorders," *Brain Research Reviews*, vol. 33, no. 1, pp. 95–130, 2000.

[44] G. Santpere, B. Puig, and I. Ferrer, "Low molecular weight species of tau in Alzheimer's disease are dependent on tau phosphorylation sites but not on delayed post-mortem delay in tissue processing," *Neuroscience Letters*, vol. 399, no. 1-2, pp. 106–110, 2006.

[45] T. Bartels, J. Choi, N. Kim, and D. Selkoe, "Non-denaturing purification of alpha-synuclein from erythrocytes," *Protocol Exchange*, 2011.

[46] K. E. Jacobi, C. Wanke, A. Jacobi, V. Weisbach, and T. M. Hemmerling, "Determination of eicosanoid and cytokine production in salvaged blood, stored red blood cell concentrates, and whole blood," *Journal of Clinical Anesthesia*, vol. 12, no. 2, pp. 94–99, 2000.

[47] X. L. Bu, Y. Xiang, W. S. Jin et al., "Blood-derived amyloid-β protein induces Alzheimer's disease pathologies," *Molecular Psychiatry*, vol. 23, no. 9, pp. 1948–1956, 2018.

[48] M. Citron, C. Vigo-Pelfrey, D. B. Teplow et al., "Excessive production of amyloid beta-protein by peripheral cells of symptomatic and presymptomatic patients carrying the Swedish familial Alzheimer disease mutation," *Proceedings of the National Academy of Sciences of the United States of America*, vol. 91, no. 25, pp. 11993–11997, 1994.

[49] B. Georgievska, S. Gustavsson, J. Lundkvist et al., "Revisiting the peripheral sink hypothesis: inhibiting BACE1 activity in the periphery does not alter β-amyloid levels in the CNS," *Journal of Neurochemistry*, vol. 132, no. 4, pp. 477–486, 2015.

[50] K. Blennow, "A review of fluid biomarkers for Alzheimer's disease: moving from CSF to blood," *Neurology and Therapy*, vol. 6, Supplement 1, pp. 15–24, 2017.

[51] M. Pallàs, "Senescence-accelerated mice P8: a tool to study brain aging and Alzheimer's disease in a mouse model," *ISRN Cell Biology*, vol. 2012, Article ID 917167, 12 pages, 2012.

[52] Ó. Álvarez-García, I. Vega-Naredo, V. Sierra et al., "Elevated oxidative stress in the brain of senescence-accelerated mice at 5 months of age," *Biogerontology*, vol. 7, no. 1, pp. 43–52, 2006.

[53] M. Shi, L. Tang, J. B. Toledo et al., "Cerebrospinal fluid α-synuclein contributes to the differential diagnosis of Alzheimer's disease," *Alzheimer's & Dementia*, vol. 14, no. 8, pp. 1052–1062, 2018.

[54] T. Tokuda, S. A. Salem, D. Allsop et al., "Decreased alpha-synuclein in cerebrospinal fluid of aged individuals and subjects with Parkinson's disease," *Biochemical and Biophysical Research Communications*, vol. 349, no. 1, pp. 162–166, 2006.

[55] Y. Y. Fathy, A. J. Jonker, E. Oudejans et al., "Differential insular cortex subregional vulnerability to α-synuclein pathology in Parkinson's disease and dementia with Lewy bodies," *Neuropathology and Applied Neurobiology*, vol. 45, no. 3, pp. 262–277, 2018.

[56] C. A. Bates and W. Zheng, "Brain disposition of α-Synuclein: roles of brain barrier systems and implications for Parkinson's disease," *Fluids and Barriers of the CNS*, vol. 11, no. 1, p. 17, 2014.

[57] H. V. Miranda, R. Cássio, L. Correia-Guedes et al., "Posttranslational modifications of blood-derived alpha-synuclein as biochemical markers for Parkinson's disease," *Scientific Reports*, vol. 7, no. 1, article 13713, 2017.

[58] C. Iofrida, S. Daniele, D. Pietrobono et al., "Influence of physical exercise on β-amyloid, α-synuclein and tau accumulation: an in vitro model of oxidative stress in human red blood cells," *Archives Italiennes de Biologie*, vol. 155, no. 1-2, pp. 33–42, 2017.

[59] K. Ren and R. Torres, "Role of interleukin-1beta during pain and inflammation," *Brain Research Reviews*, vol. 60, no. 1, pp. 57–64, 2009.

[60] M. R. Nogués, M. Giralt, M. Romeu et al., "Melatonin reduces oxidative stress in erythrocytes and plasma of senescence-accelerated mice," *Journal of Pineal Research*, vol. 41, no. 2, pp. 142–149, 2006.

[61] U. Träger and S. J. Tabrizi, "Peripheral inflammation in neurodegeneration," *Journal of Molecular Medicine*, vol. 91, no. 6, pp. 673–681, 2013.

[62] D. Kempuraj, R. Thangavel, G. P. Selvakumar et al., "Brain and peripheral atypical inflammatory mediators potentiate neuroinflammation and neurodegeneration," *Frontiers in Cellular Neuroscience*, vol. 11, p. 216, 2017.

[63] E. Paouri, O. Tzara, G. I. Kartalou, S. Zenelak, and S. Georgopoulos, "Peripheral tumor necrosis factor-alpha (TNF-α) modulates amyloid pathology by regulating blood-derived immune cells and glial response in the brain of AD/TNF transgenic mice," *The Journal of Neuroscience*, vol. 37, no. 20, pp. 5155–5171, 2017.

[64] D. Doens and P. L. Fernández, "Microglia receptors and their implications in the response to amyloid β for Alzheimer's disease pathogenesis," *Journal of Neuroinflammation*, vol. 11, no. 1, p. 48, 2014.

[65] A. Gustot, V. Raussens, M. Dehousse et al., "Activation of innate immunity by lysozyme fibrils is critically dependent on cross-β sheet structure," *Cellular and Molecular Life Sciences*, vol. 70, no. 16, pp. 2999–3012, 2013.

Hindawi
Oxidative Medicine and Cellular Longevity
Volume 2019, Article ID 1263274, 14 pages
https://doi.org/10.1155/2019/1263274

Research Article

Suppression of Mouse AApoAII Amyloidosis Progression by Daily Supplementation with Oxidative Stress Inhibitors

Jian Dai[1], **Xin Ding**[1], **Hiroki Miyahara**[1,2], **Zhe Xu**[1,3], **Xiaoran Cui**[1], **Yuichi Igarashi**[1], **Jinko Sawashita**[4], **Masayuki Mori**[1,5] and **Keiichi Higuchi**[1,2]

[1]*Department of Aging Biology, Institute of Pathogenesis and Disease Prevention, Shinshu University Graduate School of Medicine, Matsumoto 390-8621, Japan*
[2]*Department of Biological Sciences for Intractable Neurological Diseases, Institute for Biomedical Sciences, Interdisciplinary Cluster for Cutting Edge Research, Shinshu University, Matsumoto 390-8621, Japan*
[3]*The First Hospital of Hebei Medical University, Shijiazhuang 050030, China*
[4]*Supplemental Nutrition Division, Pharma & Supplemental Nutrition Solutions Vehicle, Kaneka Corporation, Osaka 530-8288, Japan*
[5]*Department of Advanced Medicine for Health Promotion, Institute for Biomedical Sciences, Interdisciplinary Cluster for Cutting Edge Research, Shinshu University, Matsumoto 390-8621, Japan*

Correspondence should be addressed to Keiichi Higuchi; keiichih@shinshu-u.ac.jp

Received 12 March 2019; Accepted 22 April 2019; Published 4 June 2019

Guest Editor: Federica Rizzi

Amyloidosis is a group of diseases characterized by protein misfolding and aggregation to form amyloid fibrils and subsequent deposition within various tissues. Previous studies have indicated that amyloidosis is often associated with oxidative stress. However, it is not clear whether oxidative stress is involved in the progression of amyloidosis. We administered the oxidative stress inhibitors tempol and apocynin via drinking water to the R1.P1-*Apoa2*^{c} mouse strain induced to develop mouse apolipoprotein A-II (AApoAII) amyloidosis and found that treatment with oxidative stress inhibitors led to reduction in AApoAII amyloidosis progression compared to an untreated group after 12 weeks, especially in the skin, stomach, and liver. There was no effect on ApoA-II plasma levels or expression of *Apoa2* mRNA. Detection of the lipid peroxidation markers 4-hydroxynonenal (4-HNE) and malondialdehyde (MDA) revealed that the antioxidative effects of the treatments were most obvious in the skin, stomach, and liver, which contained higher levels of basal oxidative stress. Moreover, the unfolded protein response was reduced in the liver and was associated with a decrease in oxidative stress and amyloid deposition. These results suggest that antioxidants can suppress the progression of AApoAII amyloid deposition in the improved microenvironment of tissues and that the effect may be related to the levels of oxidative stress in local tissues. This finding provides insights for antioxidative stress treatment strategies for amyloidosis.

1. Introduction

Amyloidosis is a group of diseases in which abnormal protein aggregates, known as amyloid fibrils, build up in the brains of patients with Alzheimer's disease (AD), as well as in various organs in cases of amyloid light-chain (AL) amyloidosis, transthyretin (ATTR) amyloidosis, and mouse apolipoprotein A-II (AApoAII) amyloidosis [1–3]. Amyloidosis is a serious health problem that can lead to life-threatening organ failure. Aggregation of amyloid proteins proceeds via structurally unstable amyloid proteins or precursor proteins under certain conditions, such as overproduction of amyloid proteins, mutation, enzymatic cleavage of precursor proteins, low pH, and aging, resulting in a transition to an unstable protein state [2, 4–7]. Recent evidence suggests that oxidative modification of amyloid proteins may also be one of these factors that may lead to an increase in aggregation propensity [8–10]. Amyloid fibril formation is a gradual process that involves conformationally modified monomers, oligomers, and protofibrils. Most of the intermediates have been shown

to be cytotoxic and stimulate stress and immune responses in the cells around the areas of deposition [11–13]. Increased levels of oxidative stress around the amyloid deposits have been detected in a variety of amyloid diseases [12–16].

Apolipoprotein A-II (ApoA-II) is the second most abundant protein in high-density lipoprotein (HDL) particles and is involved in lipid metabolism [17]. However, the exact functions of ApoA-II protein remain unclear. Some studies have found that ApoA-II protein is related to lipid transport from peripheral organs to the liver and binding of plasma proteins with HDL [17–19]. In a previous study, we found that ApoA-II modifies the binding of the plasma acute phase inflammatory response protein serum amyloid A (SAA) with plasma lipoproteins and plays a role in regulating the inflammatory response and AA amyloid fibril formation [20]. We found that ApoA-II proteins form amyloid fibrils (AApoAII) and deposit extracellularly in a number of organs (except the brain) and are associated with aging in senescence-accelerated mouse prone-1 (SAMP1) strains of mice. We later identified AApoAII deposits in various strains of mice [3, 21]. We demonstrated that there are seven ApoA-II alleles among various strains of mice. Among them, amyloidogenic C-type ApoA-II protein (APOA2C) was found to form AApoAII amyloid fibrils in mice associated with earlier aging than the other types of ApoA-II [22]. A congenic strain of mice with the amyloidogenic *Apoa2*^{c} allele on the genetic background of the senescence-accelerated resistant mouse 1 (SAMR1) strain was developed and named R1.P1-*Apoa2*^{c} mice [3]. Our previous research revealed that AApoAII amyloidosis is transmitted in a prion-like manner and is induced by the intake of amyloid fibrils through feces, saliva, breast milk, and blood [23–25]. R1.P1-*Apoa2*^{c} mice rarely exhibit spontaneous AApoAII amyloidosis under specific pathogen-free (SPF) conditions, but intravenous injection of a small amount of AApoAII amyloid fibrils induces AApoAII amyloidosis at high reproducibility [3].

In amyloidosis studies, amyloid deposition induced rising oxidative stress in surrounding cells and tissues and led to subsequent cell dysfunction and elevation of apoptosis markers [12–15], which is considered to be a major aspect of organ impairment associated with amyloidosis. There is sufficient experimental evidence from Alzheimer's disease research suggesting that nerve cell degeneration is mainly due to damage caused by oxidative stress, both in animals and in humans [26, 27]. Our previous studies also found that AApoAII amyloid deposition induced both unfolded protein response (UPR) and endoplasmic reticulum (ER) stress in the liver and kidney, leading to an increase of apoptotic cells [28]. On the other hand, studies of localized amyloidosis found that increases in oxidative stress preceded Aβ deposition, which may promote subsequent protein aggregation [29, 30]. In other studies, it was hypothesized that oxidative stress induces protein aggregation [7–9]. It was reported that TTR protein treated with oxynitride exhibited higher aggregation activity *in vitro*, which may be caused by structural instability of the modified amyloid protein [9]. However, satisfactory evidence does not exist to prove the role that oxidative stress plays in the process of amyloid deposition, especially in systemic amyloidosis.

Aging is a strong common feature of amyloidosis, except for early-onset amyloidosis caused by genetic mutations or overproduction of amyloid protein by acute phase immune reaction and cancer [31, 32]. Considering the important role of oxidative stress in various age-related diseases, we hypothesized that age-associated oxidative stress is also involved in the pathogenesis of AApoAII amyloidosis. Our recent study found that following caloric restriction, the degree of amyloid deposition in mice decreased significantly and was accompanied by downregulation of expression of genes associated with both oxidative stress and aging in the liver [33]. It is not clear whether the decline in oxidative stress levels caused the suppression in AApoAII amyloidosis.

Although the importance of oxidative stress during the progression of amyloidosis has been recognized, it needs to be determined whether oxidative stress is the cause or the consequence of amyloid deposition. To address this critical knowledge gap, we examined the effect of the nonspecific reactive oxygen species (ROS) scavenger tempol and the NADPH oxidase inhibitor apocynin on the process of systemic amyloidosis using our unique amyloid analyzing system of mouse AApoAII amyloidosis.

2. Materials and Methods

2.1. Animals. We used female R1.P1-*Apoa2c* congenic mice, which carry the amyloidogenic type c allele (*Apoa2c*) from the AApoAII amyloidosis-susceptible SAMP1 strain on a genetic background of the SAMR1 strain. R1.P1-*Apoa2*^{c} mice exhibit normal aging and do not develop AApoAII amyloidosis under specific pathogen-free (SPF) conditions, whereas they develop accelerated AApoAII amyloidosis by oral or intravenous administration of AApoAII fibrils [3]. R1.P1-*Apoa2*^{c} mice were maintained in our laboratory.

Mice were raised under SPF conditions at 24 ± 2°C with a light-controlled regimen (12-hour light/dark cycle, lights on at 9:00 and off at 21:00) in the Division of Animal Research, Research Center for Supports to Advanced Science, Shinshu University. Mice were raised on a commercial diet (MF, Oriental Yeast, Tokyo, Japan) and tap water. Three to 6 female mice housed in a single cage were used for experiments to avoid the anticipated adverse impacts due to fighting among male mice housed in the same cage.

Mice were sacrificed by cardiac puncture under deep sevoflurane anesthesia. For biochemical analysis, plasma and a portion of the organs were snap-frozen by liquid nitrogen and stored at -80°C. For histochemical analysis, the remaining organs were fixed in 10% neutral buffered formalin followed by embedding in paraffin. All experiments were performed with the approval of the Committee for Animal Experiments of Shinshu University (Approval No. 280086).

2.2. Experimental Design

2.2.1. Drug Administration. Two-month-old female R1.P1-*Apoa2*^{c} mice were divided into 4 groups: control (Con), no treatment (A-NT), tempol (Tem), and apocynin (Apo). AApoAII amyloidosis was induced in mice in the A-NT, Tem, and Apo groups by injection with 1 μg AApoAII fibrils

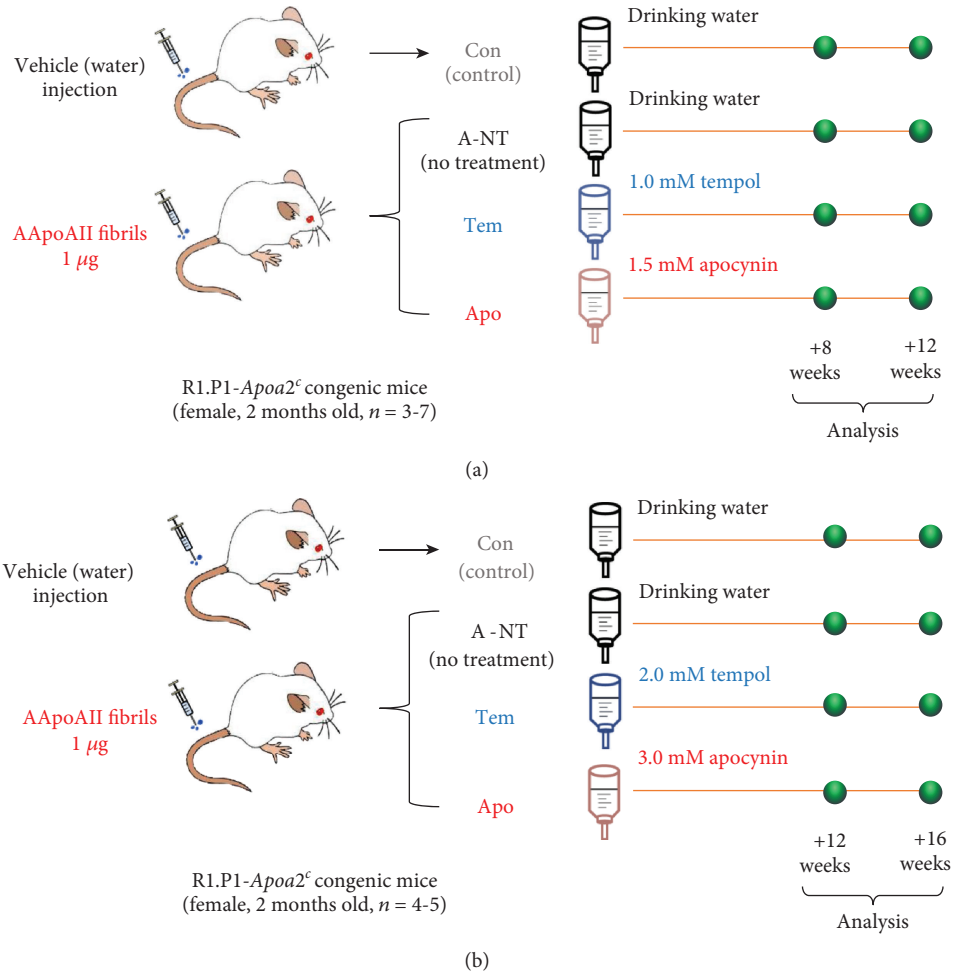

Figure 1: Experimental design. (a) Two-month-old female R1.P1-*Apoa2c* mice were divided into 4 groups: control (Con), no treatment (A-NT), tempol (Tem), and apocynin (Apo). AApoAII amyloidosis was induced in the mice in the A-NT, Tem, and Apo groups by injection with 1 μg AApoAII fibrils in the tail vein; the Con group was injected with distilled water instead of AApoAII fibrils. Concomitantly, the Tem and Apo group mice were treated with either tempol (1 mM) or apocynin (1.5 mM) in drinking water for 8 or 12 weeks ($N = 3$–7 per group). (b) In the high-dose series, the experiment was repeated with double doses of tempol (2 mM) or apocynin (3 mM) and the experimental period was 12 and 16 weeks ($N = 4$ or 5 per group).

in the tail vein; the Con group was injected with distilled water (DW) instead of AApoAII fibrils (Figure 1(a)). Concomitantly, the Tem and Apo group mice were treated with either the free radical scavenger tempol (1 mM) or the NADPH oxidase inhibitor apocynin (1.5 mM) in drinking water for 8 or 12 weeks ($N = 3$-7 mice per group). For the high-dose experimental series, R1.P1-*Apoa2*^{c} mice were treated with 2 mM tempol or 3 mM apocynin in drinking water for 12 or 16 weeks ($N = 4$ or 5 mice per group) (Figure 1(b)). Doses of apocynin and tempol were chosen in accordance with previous reports [34–36]. The drug solution was prepared prior to use. Tempol (Cat No. 176141) and apocynin (Cat No. w508454) were purchased from Sigma-Aldrich (Tokyo, Japan).

2.2.2. Induction of AApoAII Amyloidosis. We isolated AApoAII amyloid fibrils using Pras' method [37] from the liver of a 14-month-old R1.P1-*Apoa2*^{c} mouse having heavy amyloid deposits and injected 1 μg amyloid fibrils in each mouse to induce AApoAII amyloidosis followed the protocols of Li et al. [33]. Before injection, the fibril samples were sonicated (Fig. S1) and used immediately as described previously [20].

2.3. Histology

2.3.1. Amyloid Fibril Detection. Amyloid deposits were detected as apple-green birefringence in organ sections stained with a saturated solution of 1% Congo red dye under polarizing light microscopy (LM) (Axioskop 2, Carl Zeiss, Tokyo, Japan). An amyloid score (from 0 to 4) in each organ was determined semiquantitatively as described previously [21]. Two observers having no information of the tissue evaluated the grade of amyloid deposition in Congo red stained tissue. The degree of amyloid deposition in each mouse was represented by an amyloid index (AI) which is the average of the amyloid scores in seven organs (heart, liver, spleen, stomach, small intestine, tongue, and skin) [21, 33, 38].

2.3.2. Immunohistochemistry. AApoAII and AA fibrils were also detected by immunohistochemistry (IHC) with specific rabbit antiserum against mouse ApoA-II or mouse AA, which were produced against guanidine hydrochloride-denatured AApoAII or AA fibrils in our laboratory [20, 21, 33, 38]. Four-micron (4 μm) thick sections of fixed organs were treated with 3% H_2O_2 in methanol for 30 minutes (min) to inactivate endogenous peroxidase and were blocked with 5% bovine serum albumin in PBS. The sections were incubated overnight at 4°C with rabbit antisera against mouse ApoA-II (1 : 3000) and AA (1 : 3000) prepared in our laboratory [39] or 4-hydroxynonenal (4-HNE) (1 : 300, Abcam plc, Cambridge, UK), followed by incubation with the biotinylated secondary antibody (Abcam plc). Target proteins were identified by the horseradish peroxidase-labeled streptavidin-biotin method (DAKO, Glostrup, Denmark). In a negative control section, the first antibody was omitted to confirm the specificity of staining. To analyze the positive area in each organ quantitatively, the ratios of the positively stained area to a whole organ in randomly captured 5 areas under ×200 or ×400 magnification were measured using image processing program (NIH ImageJ software, version 1.61) [33].

2.3.3. Semiquantification of Oxidative Stress. Two blinded observers, who had no information regarding the tissue, observed 4-HNE stain intensity in tissue specimens of IHC. We evaluated the stain intensity in every organ. The stain intensity was scored as follows: 0 (absent), 1 (few), 2 (mild), 3 (middle), and 4 (severe). The average of these scores by two observers represented the final 4-HNE evaluations for statistical analyses by the Steel-Dwass test.

2.4. Biochemical Analysis

2.4.1. Malondialdehyde (MDA). Lipid peroxidation was analyzed using a Lipid Peroxidation Colorimetric/Fluorometric Assay Kit (BioVision, San Francisco CA, USA) by means of malondialdehyde (MDA) content in accordance with the instructions provided by the manufacturer. The 10 mg liver stored at -80°C was homogenized to detect the MDA concentration followed by the methods as described previously [40]. Three technical replicates were conducted for each sample. The MDA content is calculated by comparing the measured values to a calibration curve prepared using an MDA standard (BioVision). The coefficient of variation (r^2) for the calibration curve was 0.99.

2.4.2. High-Density Lipoprotein (HDL). We determined the HDL-cholesterol levels in the plasma using quantitative assay kits (HDL-cholesterol E test, Wako, Osaka, Japan) [33, 38, 41].

2.5. Immunoblot Analysis. We followed the methods as described previously [33, 42, 43] to determine the level of plasma apolipoproteins. Plasma samples were separated on Tris-Tricine/SDS–16.5% polyacrylamide gels electrophoresis (PAGE) as follows: 0.5 μL plasma for ApoA-I or ApoE and 1 μL plasma for ApoA-II. After electrophoresis, proteins were transferred to a polyvinylidene difluoride membrane (Immobilon, 0.2 μm pore, Millipore Corp., MA, USA). The membrane was incubated with primary antibody solution, polyclonal rabbit anti-mouse ApoA-I antiserum produced in our laboratory [41, 42] (diluted 1 : 4000), or the ApoA-II antiserum (diluted 1 : 3000) or ApoE antibody (1 : 500, Santa Cruz, San Francisco, CA, USA) for 1 hour at room temperature and then overnight at 4°C. Next, the horseradish peroxidase-conjugated anti-rabbit IgG (Code #7074, Cell Signaling Technology Inc., Danvers MA, USA) (1 : 3000) was used for 1-hour incubation at room temperature. ApoA-I, ApoA-II, and ApoE were detected with the enhanced chemiluminescence (ECL) method, and the target protein levels were analyzed using the NIH ImageJ software.

2.6. Gene Expression Analysis. We followed a previously described method to analyze the mRNA expression [33, 44]. Quantitative real-time PCR analysis was carried out using an ABI PRISM 7500 Sequence Detection system (Applied Biosystems) with SYBR Green (TaKaRa Bio, Tokyo, Japan). The β-actin gene was used to normalize gene expression. The forward and reverse primer sequences for real-time PCR are listed in Table S1. Chemical reagents in the experiments, unless otherwise specified, were obtained from Wako Pure Chemical Industries Ltd. (Osaka, Japan).

2.7. Statistical Analyses. All data are presented as the mean ± S.D. For the comparison of the parametrical data, one-way analysis of variance (ANOVA) with key's test was performed using the SPSS 25.0 software package (Abacus Concepts, Berkley, CA USA). For the comparison of the nonparametrical data, the Kruskal-Wallis test with the Steel-Dwass test was performed. p values less than 0.05 were considered to be statistically significant.

3. Results

3.1. AApoAII Amyloidosis Significantly Declined in the 12-Week Intake Groups, Especially in the Stomach, Skin, and Liver. To examine whether oxidative stress contributes to the process of AApoAII amyloidosis, R1.P1-*Apoa2*^{c} mice were administered the ROS scavenger tempol (1 mM) or the NADPH oxidase inhibitor apocynin (1.5 mM) in drinking water for 8 or 12 weeks beginning at 8 weeks of age. At 7 weeks old, we measured the body weight, food intake, and water consumption of the mice and monitored abnormal conditions of the mice for one week. At 8 weeks old, we divided the mice into 4 groups and confirmed that these data were not different among the 4 groups and that no obvious abnormal performance was observed in any of the mice. The Con group, which had no induction of AApoAII amyloidosis, nor drug intervention, was used as a control group to provide baseline data. The A-NT, Tem, and Apo groups were injected with 1 μg of AApoAII amyloid fibrils through the tail vein at 8 weeks of age to induce AApoAII amyloidosis. Concomitantly, the Tem and Apo groups were administered the respective drugs in drinking water (Figure 1(a)). There was no difference in body weight, food intake, and water consumption among the 4 groups during the

experiments (Fig. S2). To observe the effect of drug dose on the experimental results, a high-dose (twice the initial dose) experiment was repeated, and the time points were determined at 12 weeks and 16 weeks (Figure 1(b)).

After 8 weeks, we collected several organs (heart, liver, spleen, stomach, small intestine, tongue, skin, lung, and kidney) for the evaluation of amyloid deposits. First, the amyloid deposits were graded by the presence of apple-green color birefringence in Congo red-stained tissue under polarized LM. Small green birefringence signals were observed in the heart, small intestine, tongue, stomach, and lung, but not in the liver, spleen, skin, or kidney (Fig. S3a). However, the degree of amyloid deposition was not significantly different among the 3 induced groups (Fig. S3b). At 12 weeks postinjection, amyloid protein deposition was found in all seven organs, except the spleen (Fig. S4), and the amyloid indices (AIs) were significantly lower in the Tem and Apo groups than in the A-NT group (Figure 2(a)). We then analyzed the degree of amyloid deposition in each organ and found that the effect of oxidative stress inhibitors was inconsistent among the different organs and that significant inhibitory effects appeared in the stomach and skin compared with the A-NT group (Figures 2(b)–2(f)), with apocynin exhibiting a stronger inhibitory effect than tempol. IHC was used to confirm the type of amyloid protein with anti-ApoA-II and anti-AA antiserum (Figure 2(e) and Fig. S5) and for quantitative analysis of AApoAII amyloid load in the skin using an image processing program (Figure 2(f)). Results showed a significant suppression of AApoAII amyloid deposition in the skin following 12-week supplementation with oxidative stress inhibitors. Although the amyloid scores of the livers in the 3 induced groups were nearly identical, we found that the oxidative stress inhibitors showed significant inhibitory effects in amyloid deposition in the liver by calculating the ApoA-II positive area (Figures 2(g) and 2(h)).

3.2. Decrease in Oxidative Stress Levels following Supplementation with Oxidative Stress Inhibitors. To verify whether tempol or apocynin suppressed oxidative stress levels *in vivo*, we detected lipid peroxidation marker 4-HNE in various organs using IHC. The results showed that 4-HNE was slightly increased in the A-NT group compared with the Con group and that intake of oxidative stress inhibitors reduced oxidative stress in the liver, stomach, and skin, in which higher basal values of 4-HNE were observed (Figures 3(a) and 3(b)). Based on the grading of the staining intensity, the effects of oxidative stress inhibitors showed a trend towards a decline in the liver and a significant decline in the skin (Fig. S6). Moreover, we found that another oxidative stress marker in the liver, namely, MDA, increased in the A-NT group, but not in the Tem and Apo groups. These results suggest that oxidative stress levels may have increased more in the A-NT group than in the Con group in the liver, stomach, and skin and that this change was inhibited upon intake of oxidative stress inhibitors (Figure 3(c)). To confirm the rise in oxidative stress at the gene level, we also determined expression levels of the oxidative stress-related genes *Ncf1* and *Ncf2*, which code for the subunit of NADPH oxidase [45] and *SOD2*, respectively, in the liver. Figure 3(d) shows that *Sod2* expression was suppressed by supplementation with apocynin but that there was no change in *Ncf1* and *Ncf2*.

3.3. Effects on Plasma ApoA-II Protein and HDL Concentrations and Liver Apoa2 mRNA Expression following Intake of Oxidative Stress Inhibitors. To investigate whether oxidative stress inhibitors directly decrease plasma concentrations of precursor ApoA-II protein or HDL and result in suppression of AApoAII amyloid deposition, we used immunoblotting of the plasma to detect levels of ApoA-II, ApoA-I, and ApoE (Figures 4(a)–4(c)). Results showed that tempol and apocynin had no effect on plasma concentrations of ApoA-II and ApoA-I. However, we found that ApoE levels increased significantly in the induced groups. Moreover, plasma HDL levels were similar across groups (Figure 4(d)). As both ApoA-I and ApoA-II are produced in the liver, we also detected the expression of *Apoa2* and *Apoa1* mRNA levels in the liver by real-time PCR and found that *Apoa1* expression was upregulated in the induced group (Apo) compared with the Con group, but no difference was observed between the induced groups. The *Apoa2* gene did not differ significantly among all groups (Figure 4(e)).

3.4. Antioxidative Treatment Downregulates Gene Expression of ER Stress in the Liver and May Improve the Microenvironment. To further investigate the effects of oxidative stress inhibitors on the microenvironment of tissues, we determined the mRNA levels of genes involved in ER stress (*Hspa5* and *Atf4*) in the liver (Figure 5). The mRNA levels of *Hspa5* were increased in the A-NT group, but were suppressed in the Apo group; levels of *Atf4* were significantly decreased in the Tem and Apo groups compared with the Con and A-NT groups. We also determined the expression levels of the mitochondrial function-related factors *Ppargc1α* and *Idh2*, macrophage marker *Adgre1* (F4/80), and autophagy-related factor *Atg5*. The levels of these genes were not different among any of the groups, except for upregulated levels of *Ppargc1a* in the Tem group.

3.5. The High-Dose Series Exhibited a Consistent Preventive Effect on Amyloid Deposition. To determine the effect of different drug doses of oxidative stress inhibitors on amyloidosis progression, the drug dose was doubled and the experiment was repeated with modified incubation times (i.e., 12 and 16 weeks after induction of amyloidosis). Consistent with the initial-dose series, a significant suppression of amyloid deposition also occurred after 12-week intake of oxidative stress inhibitors, based on both AI and skin amyloid scores (Figure 6(a) and Fig. S7a). ApoA-II IHC was subsequently performed, and decreased levels were observed in the liver and skin of treated animals compared to the A-NT group, in both the 12-week and 16-week groups (Figures 6(b)–6(d) and Fig. S8b-d). However, following the increase in the degree of deposition, we did not observe significant decreases in AI among the induced groups after 16-week intake (Fig. S7b and Fig. S8a).

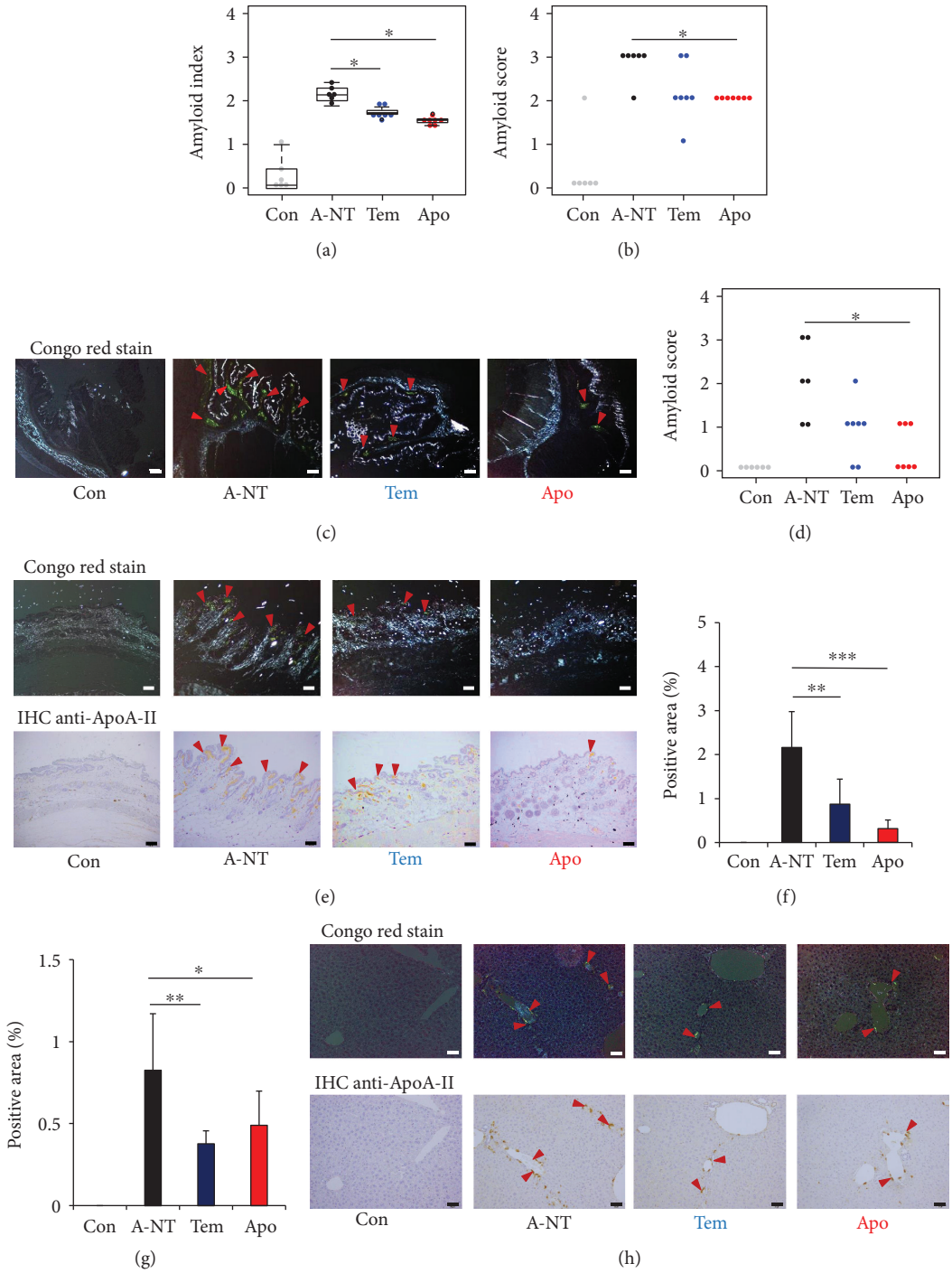

Figure 2: AApoAII amyloidosis significantly declined in the 12-week-intake groups. (a) Amyloid index (AI) of the 12-week groups. (b) Amyloid score of the 12-week groups in the stomach. (c) Representative LM images of AApoAII deposits in the stomach in induced mice. Amyloid deposits (red arrows) were identified by green birefringence in Congo red-stained sections using polarized LM. Each scale bar indicates 100 μm. (d) Amyloid score of the 12-week groups in the skin. (e) Representative LM and IHC images of AApoAII deposits in the skin in induced mice. AApoAII deposits were confirmed by IHC with anti-ApoA-II antiserum. Amyloid deposits are indicated by red arrows. Each scale bar indicates 100 μm. Comparisons of positive areas of amyloid deposits in the (f) skin and (g) liver. (h) Representative LM and IHC images of AApoAII deposits in the liver in induced mice. Amyloid deposits are indicated by red arrows. Each scale bar indicates 50 μm. $N = 6$ (Con and A-NT) and 7 (Tem and Apo). Results are shown as box and whisker plots, where a box extends from the 25th to the 75th percentile with the median shown as a line in the middle and whiskers indicate the smallest and largest values (a). Each dot represents an individual mouse (a, b, d). Each symbol and bar represent the mean ± S.D. (f, g). $^{*}p < 0.05$, $^{**}p < 0.01$, and $^{***}p < 0.001$, the Kruskal-Wallis test with the Steel-Dwass test for the amyloid index and amyloid score (a, b, d). The Tukey-Kramer method for the multiple comparison of the IHC-positive area (f, g).

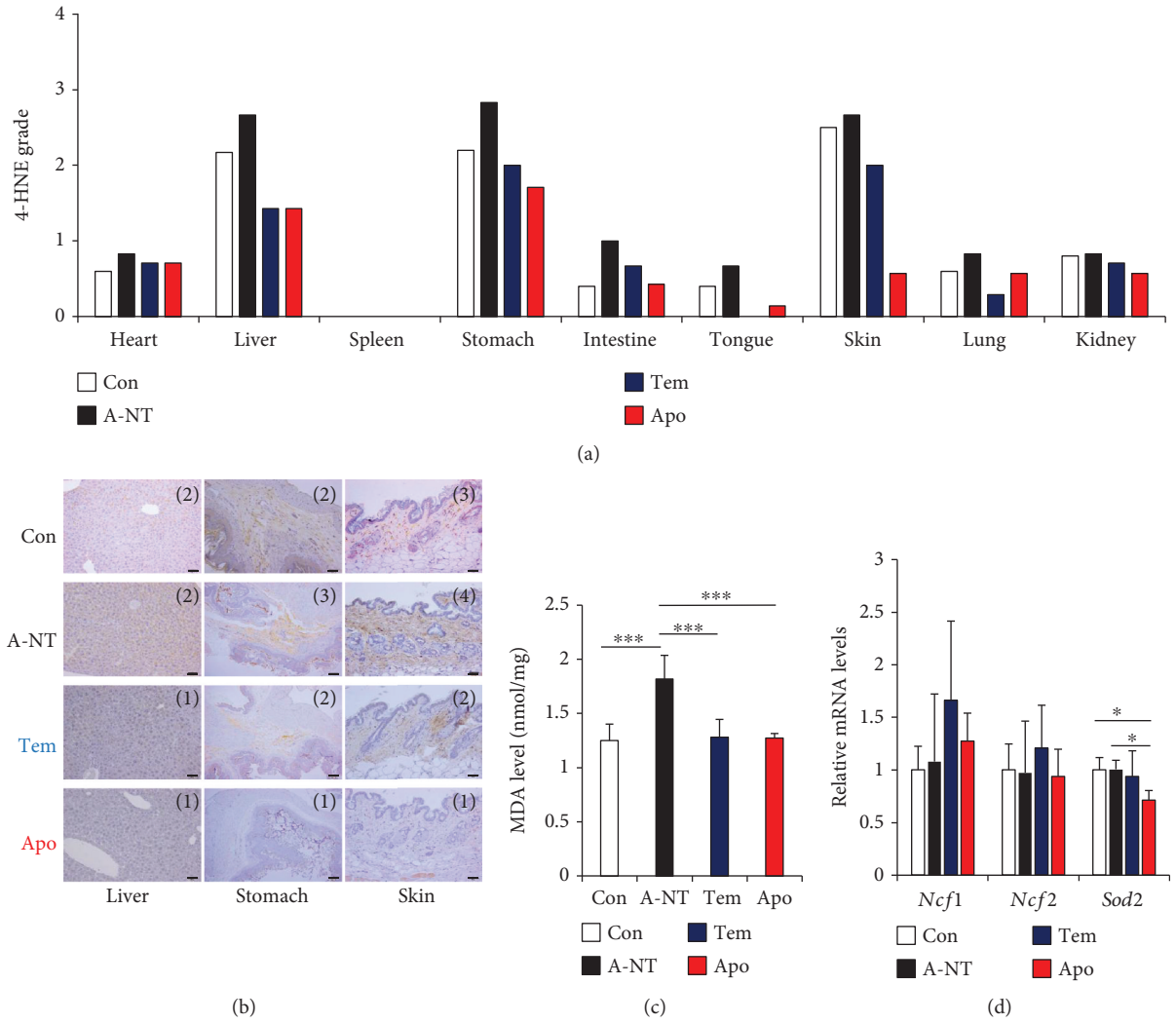

Figure 3: Detection of oxidative stress levels following daily supplementation with oxidative stress inhibitors for 12 weeks. (a) The schema of grades of 4-HNE in every organ following IHC detection. Each column represents the mean of the grade. (b) Representative images of 4-HNE IHC of the liver, stomach, and skin. The grades of each section are shown on the upper-right of the image. Each scale bar indicates 50 μm. (c) MDA levels in the liver. (d) mRNA expression levels of genes related to oxidative stress response in the liver. Histograms show the fold change in mRNA levels relative to the Con group. Each column and bar represent the mean ± S.D. $N = 6$ (Con and A-NT) and 7 (Tem and Apo). $^{*}p < 0.05$ and $^{***}p < 0.001$, the Tukey-Kramer method for multiple comparison.

4. Discussion

4.1. Oxidative Stress Is Involved in AApoAII Amyloid Formation. With aging, the balance between production and removal of ROS is altered and levels of oxidative stress gradually increase to cause oxidative damage to lipids, proteins, and DNA, leading to cellular dysfunction and various age-related diseases [46, 47]. Numerous studies have investigated the relationship between oxidative stress and pathogenesis of amyloidosis, especially on localized brain amyloidosis and amyloid-related neurodegenerative diseases: Alzheimer's disease, cerebral amyloid angiopathy (CAA), amyotrophic lateral sclerosis (ALS), etc. [8, 11, 13, 16, 34, 36, 48–50]. However, a clear understanding of the specific mechanism responsible for the acceleration of amyloidosis and neurodegeneration caused by oxidative stress remains elusive. Unfortunately, there are still insufficient reports supporting the contribution of oxidative stress to the pathogenesis of systemic amyloidosis and related adverse effects on tissues [51].

In this study, supplementation with oxidative stress inhibitors for 12 weeks led to decreases in mouse AApoAII amyloidosis and demonstrated that inhibition of oxidative stress was effective at suppressing systemic amyloid deposition *in vivo*. Meanwhile, our results suggest that the effect of antioxidants varied depending on the specific organs. In the amyloid-induced groups, amyloid scores in the stomach and skin were significantly decreased by supplementation with tempol and apocynin, with the preventive effect being most distinct in the skin (Figure 2). Although the amyloid scores evaluating the grading of amyloid deposition in the liver were not significantly different between groups with

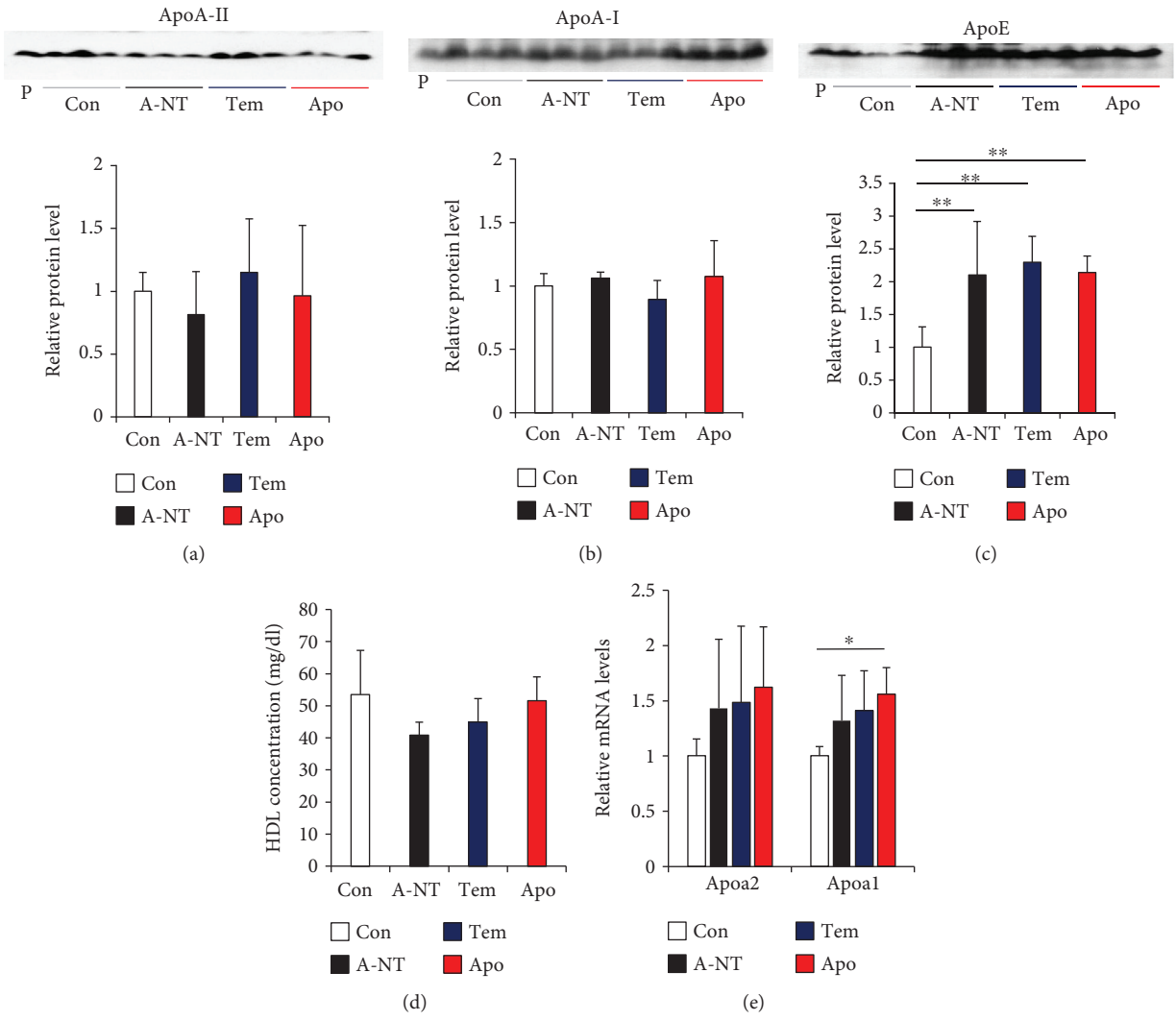

Figure 4: Effects of daily supplementation with oxidative stress inhibitors on plasma lipoproteins. (a–c) Concentrations of ApoA-II, ApoA-I, and ApoE proteins in the plasma were determined by densitometry of Western blot after SDS-PAGE of the plasma. The representative results of Western blot are shown above the figures. There was no difference in ApoA-II or ApoA-I plasma concentrations; however, the concentration of ApoE increased significantly in the 3 amyloidosis-induced groups. Histograms show fold changes relative to the Con group and represent the means ± S.D. P indicates, the pooled plasmas of female R1.P1-Apoa2c mice at 2 months of age ($N = 4$) that did not have AApoAII amyloid deposits, as the positive control of these proteins. (d) HDL plasma concentration was determined using quantitative assay kits. (e) mRNA expression levels of ApoA-II and ApoA-I in the liver were determined by quantitative real-time PCR and shown by fold changes relative to the Con group. $N = 6$ (Con and A-NT) and 7 (Tem and Apo). $^{*}p < 0.05$ and $^{**}p < 0.01$, the Tukey-Kramer method for multiple comparison.

and without oxidative stress inhibitors, quantitatively measuring the positive area of ApoA-II deposition in IHC demonstrated a significant preventive effect of oxidative stress inhibitors against amyloid deposition in the liver. We did not observe this change in other organs, including the heart, spleen, small intestine, tongue, lung, and kidney.

Our recent study found that following caloric restriction, the degree of amyloid deposition in almost all organs (except for the stomach) was significantly decreased [33]. These results suggest that caloric restriction may prevent amyloid deposition, not only via the same pathway as that of oxidative stress inhibitors but also via other mechanisms as well. The two oxidative stress inhibitors investigated in the present study exhibited different degrees of inhibition. Apocynin showed a relatively stronger preventive effect against amyloid deposition in the stomach and skin than tempol (Figures 2(a), 2(b), 2(d), and 2(f)), although the preventive effects of the two inhibitors were nearly identical in the liver (Figure 2(g)). By measuring the degree of oxidative stress using 4-HNE and MDA as markers, we identified relatively high baseline levels of oxidative stress in the liver, stomach, and skin and found that apocynin reduced oxidative stress more strongly in the stomach and skin compared with tempol (Figure 3(a)), but to similar degrees in the liver (Figure 3(c)). These differences may be due to differences in the main sources of oxidative

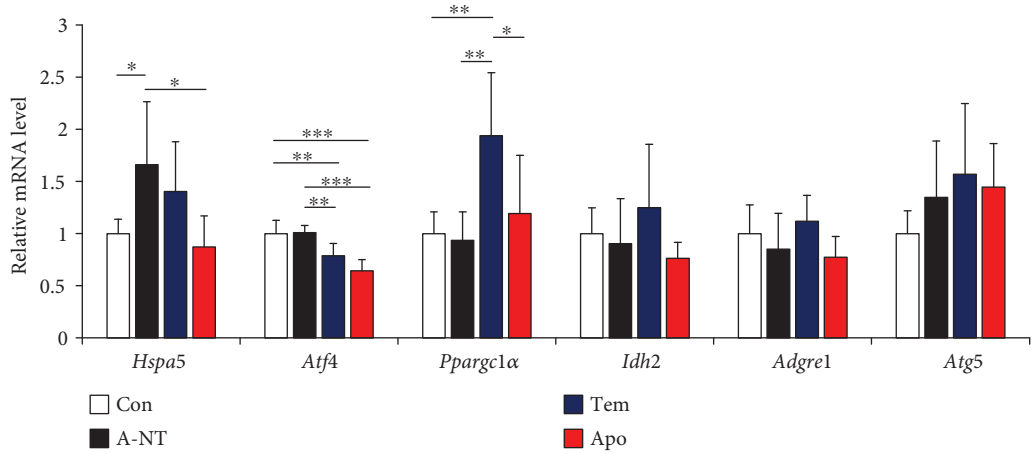

Figure 5: Determination of the effects of antioxidative treatment on mRNA expression levels of the genes related to UPR. Using real-time RT-PCR, we determined mRNA expression levels of the following genes in the liver: UPR sensor gene (*Hspa5* and *Atf4*), mitochondrial function-related gene (*Ppargc1α* and *Idh2*), macrophage marker gene (*Adgre1*), and autophagy-related gene (*Atg5*). Each column represents fold changes relative to the Con group and the mean ± S.D. $N = 6$ (Con and A-NT) and 7 (Tem and Apo). $^{*}p < 0.05$, $^{**}p < 0.01$, and $^{***}p < 0.001$, the Tukey-Kramer method for multiple comparison.

stress within each organ [46, 47, 52–54]. We considered that these organs are susceptible to induction of oxidative stress by external influences depending on their function [52–54] and that relatively high levels of baseline oxidative stress may be related to the antiamyloidogenic effects of the antioxidants. In a study of CAA, antioxidants were found to reduce amyloid deposition, improve vascular conditions, and reduce the occurrence of complications, but the same changes did not appear in the amyloid deposits of the brain parenchyma [36]. Further experiments are needed to confirm our hypothesis that the effect of antioxidant treatments on amyloidosis depends on the oxidative stress state of the target organs and may provide support for the use of antioxidant treatments in the clinic.

We repeated the second experiment with a higher antioxidant dose to confirm the results of the first experiment and to determine dose effects on the inhibition of amyloidosis. Because amyloid deposits were not been observed in the liver and skin in the 8-week groups of the initial dose experiment, we chose a longer incubation time and sacrificed mice at 12 weeks and 16 weeks after induction of amyloidosis in the second high-dose series. Results were similar to those of the initial-dose experiment and suggest that 1.0 mM tempol and 1.5 mM apocynin are sufficient to show significant preventive effects.

4.2. Oxidative Stress May Suppress Amyloid Deposition by Affecting Protein Stability. Considering that various factors affect AApoAII amyloid deposition, we investigated whether oxidative stress inhibitors directly affect levels of precursor ApoA-II protein and HDL. Results showed that neither levels of *Apoa2* mRNA expression in the liver nor plasma levels of ApoA-II protein were significantly changed by supplementation with oxidative stress inhibitors. In our previous study, we showed that one possible mechanism of suppression of amyloid deposition by caloric reduction is a reduction in plasma concentrations of ApoA-II and ApoA-II/ApoA-I ratios [33]. These findings suggest that oxidative stress inhibitors suppress AApoAII amyloid deposition, not by reducing plasma concentrations or synthesis of ApoA-II, but by a pathway distinct from that of caloric reduction.

We considered the second possibility for reducing amyloid deposition by increasing amyloid protein stability. During the pathogenesis of amyloidosis, oxidative modification of amyloid proteins may play a key role. Oxidative conditions could modify the proteins and alter the structure to one with a higher aggregation propensity [8–10, 55–57]. Several experiments confirmed that antioxidants help to maintain protein stability and can reduce amyloid formation *in vivo* [36, 51, 58]. Low pH states cause protein instability and promote amyloid fibril formation of Aβ, TTR, and ApoA-II *in vitro* [29, 38, 59]. Results of these previous studies suggest that increased levels of oxidative stress may induce a change in the local microenvironment to an acidic pH [60]. Reports by Saito et al. have shown that tissues exhibiting TTR amyloid deposition were under oxidative stress and that both the Val30Met mutant and wild-type TTR proteins had higher ratios of S-nitrosylation, with the ability to form amyloid fibrils *in vitro* [9]. Polyphenolic compounds such as curcumin are known to exhibit antioxidative effects and prevent fibril formation by binding to amyloid proteins [61–63]. Thus, preventing the destabilization of amyloid proteins may offer a target of oxidative stress inhibitors, such as tempol and apocynin. Future experiments allowing for the accurate measurement of the oxidation state of AApoAII amyloid protein *in vivo* should provide greater insight into the relationship between amyloidosis and oxidative stress.

4.3. Decreased Oxidative Stress May Improve the Microenvironment Involved in Amyloid Fibril Formation. Real-time PCR results suggest a significant decline in the degree of UPR and ER stress in the liver by supplementation with oxidative stress inhibitors (Figure 5). Our previous studies have shown that ER stress in the liver and kidney

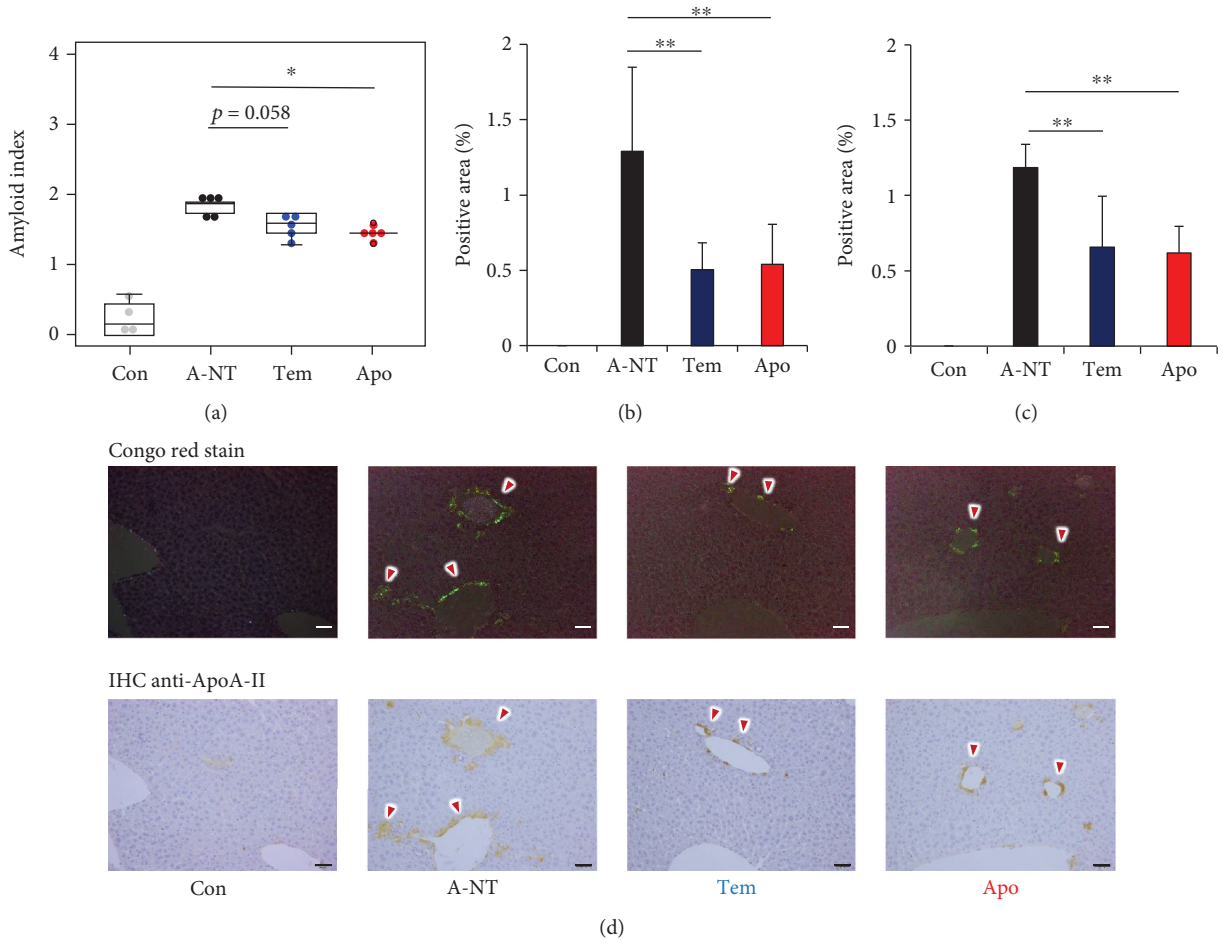

FIGURE 6: High-dose supplementation exhibits a consistent preventive effect against amyloidosis with the initial dose. (a) The amyloid index was significantly lower in the Tem and Apo groups compared with the A-NT group after 12-week-supplementation. Comparison of IHC-positive areas showed decreased amyloid deposition in the Tem and Apo groups in the (b) skin and (c) liver. (d) Representative polarized LM and IHC images of AApoAII deposits (red arrows) in the liver in induced mice. Results are shown as box and whisker plots, where a box extends from the 25th to the 75th percentile with the median shown as a line in the middle and whiskers indicate the smallest and largest values. Each dot represents an individual mouse (a). Each scale bar indicates 50 μm (d). Each column and bar represents the mean ± S.D. (b, c) $N = 4$ (Con) and 5 (A-NT, Tem, and Apo). $^{*}p < 0.05$, the Kruskal-Wallis test with the Steel-Dwass test (a). $^{**}p < 0.01$, the Tukey-Kramer method for multiple comparison (b, c).

increased with the appearance and progression of AApoAII amyloidosis [28]. Thus, the decreased amyloid deposition caused by oxidative stress inhibitors may reduce *Hspa5* expression. Expression levels of *Atf4*, a transcription factor involved in various intracellular stress signaling pathways (e.g., ER stress and mitochondrial stress [64, 65]), were decreased by oxidative stress inhibitors. Mitochondrial dysfunction caused by amyloid deposition is considered to be the most important cause of subsequent cell dysfunction and death. In our previous report, we demonstrated that caloric reduction improved mitochondrial function and reduced AApoAII amyloid deposition [33]. However, in the present study, the expression of *Ppargc1α and Idh2* did not change with amyloid deposition and the presence of oxidative stress inhibitors. Moreover, macrophage (*Adgre1*) and autophagy (*Atg5*) markers also did not change with amyloid deposition and antioxidant treatment. Further studies are needed to clarify the relevant molecular mechanisms by which treatment with antioxidants can improve the microenvironment involved in amyloid fibril deposition.

4.4. Plasma ApoE Is Increased in the Early Stages of ApoA-II Amyloidosis. ApoE is a chaperone protein that is widely found to be associated with various amyloid depositions and is considered a risk factor for the onset of amyloidosis [66–68]. In Alzheimer's disease, different isoforms of ApoE play different roles in the pathogenesis of amyloidosis: ApoE4 has been shown to promote or inhibit the assembly of Aβ protein into filaments in both *in vitro* and *in vivo* mouse models [69, 70]. Our recent studies have shown that AApoAII amyloid fractions isolated from the liver exhibited a large number of codeposited amyloid-associated proteins, which may contribute to the progression of amyloid deposition [71]. Plasma concentrations of ApoE, which is the most abundant amyloid-associated protein, were gradually decreased and associated with an increasing degree of

amyloid deposition [71]. Interestingly, plasma concentrations of ApoE significantly increased in the amyloidosis-induced groups compared with the Con group in the present study. These results suggest that amyloid deposition may stimulate the upregulation of ApoE protein in the early stages of amyloidosis and provide new evidence that ApoE is closely involved in the pathogenesis of amyloidosis. Supplementation with antioxidants did not have an effect on increasing ApoE plasma levels.

5. Conclusion

Taken together, our results provide evidence that oxidative stress is involved in the progression of amyloidosis. The formation and deposition of amyloid fibrils are the result of a combination of various factors. Although the application of oxidative stress inhibitors has a certain inhibitory effect on amyloid deposition, it is not enough to completely block the progression of amyloidosis. Results of the present study suggest that antioxidants mainly reduce the levels of oxidative stress, can help to maintain protein stability, and may improve the cellular microenvironment. Oxidative stress inhibitors offer a therapeutic strategy that should be considered for the future treatment of amyloidosis.

Data Availability

The data used to support the findings of this study are included within the article.

Conflicts of Interest

The authors declare that they have no competing interests.

Authors' Contributions

J.D., J.S., and K.H. conceived and designed the experiments. J.D., X.D., H.M., Z.X., X.C., and Y.I. performed the experiments and were responsible for data acquisition and analysis. J.D., H.M., and K.H. analyzed the data. M.M. interpreted the data and experimental methods. J.D., H.M., and K.H. wrote the manuscript. All authors reviewed the manuscript.

Acknowledgments

This work was supported in part by Grants-in-Aid for Scientific Research (B) 17H04063 and Challenging Exploratory Research 26670152 from the Ministry of Education, Culture, Sports, Science and Technology, Japan, and JSPS Core-to-Core Program, A. Advanced Research Networks. The authors thank Drs. Kiyoshi Matsumoto and Takahiro Yoshizawa, Hiroto Yamanaka, and Ms. Kayo Suzuki (Research Center for Supports to Advanced Science, Shinshu University) for the animal care and technical assistance in the preparation of tissue sections.

Supplementary Materials

Figure S1: detection of AApoAII amyloid fibrils for injection. Abundant AApoAII amyloid fibrils were observed in the injected solution. Scale bar is 50 nm. Figure S2: body weight, food intake, and water consumption were measured weekly. (a) Body weight of 8-week groups and 12-week groups. Each column and bar represent the mean ± S.D. (N = 3-7). (b) Food intake and (c) water consumption of each cage were measured weekly. Data are represented in g/mouse/d (food intake) and mL/mouse/d (water consumption). Figure S3: no significant differences were observed in amyloid deposition among the three induced groups in the 8-week groups. (a) Amyloid scores of the 8-week groups in each organ. Each column represents the mean. (b) Amyloid indices of the 8-week groups. Amyloid indices were not significantly different among the three induced groups. The amyloid index (AI) was calculated as the average of the amyloid scores in seven organs (heart, liver, spleen, tongue, stomach, small intestine, and skin). Results are shown as box and whisker plots, where a box extends from the 25th to the 75th percentile with the median shown as a line in the middle and whiskers indicate the smallest and largest values. Each dot represents an individual mouse. (c) 4-HNE grade in each organ. Each column represents the mean. $N = 3$. The Kruskal-Wallis test with the Steel-Dwass test for the amyloid index and amyloid score. Figure S4: amyloid scores of the 12-week groups in each organ. The amyloid index (AI) was calculated as the average of the amyloid scores in seven organs (heart, liver, spleen, tongue, stomach, small intestine, and skin). Each column represents the mean. $N = 6$ or 7. Figure S5: no AA amyloid deposition was detected in this experiment. Representative IHCs with anti-ApoA-II or AA antisera in the intestine, liver, and tongue of amyloidosis-induced mice. No detectable AA staining was observed in any organ. Each scale bar indicates 100 μm. Figure S6: statistical analysis of 4-HNE grade in 12-week groups. (a) 4-HNE grade in the liver, (b) stomach, and (c) skin. Results are shown as box and whisker plots, where a box extends from the 25th to the 75th percentile with the median shown as a line in the middle and whiskers indicate the smallest and largest values. Each dot represents an individual mouse. $^*p < 0.05$ vs. Con, the Kruskal-Wallis test with the Steel-Dwass test for 4-HNE grade. $N = 6$ (Con and A-NT) or 7 (Tem and Apo). Figure S7: amyloid scores of high-dose 12-week and 16-week groups in each organ. The amyloid index (AI) was calculated as the average of the amyloid scores in seven organs (heart, liver, spleen, tongue, stomach, small intestine, and skin). Each column represents the mean. $N = 4$ or 5. Figure S8: the high-dose oxidative stress inhibitors exhibited the same level of an antiamyloid effect on R1.P1-*Apoa2*^{c} mice for 16 weeks. (a) Amyloid indices of the high-dose 16-week groups. Comparison of positive areas of amyloid deposition in the skin (b) and liver (c). (d) Representative IHC images of AApoAII deposits in the liver of induced mice. Results are shown as box and whisker plots, where a box extends from the 25th to the 75th percentile with the median shown as a line in the middle and whiskers indicate the smallest and largest values. Each dot represents an individual mouse (a). Each column and bar represent the

mean ± S.D. (b, c). Each scale bar indicates 100 μm. $N = 4$ (Con, A-NT, and Tem) and 5 (Apo). $^{*}p < 0.05$, $^{**}p < 0.01$, and $^{***}p < 0.001$, the Tukey-Kramer method for multiple comparison of an IHC-positive area. Table S1: the specific primers for real-time PCR. *(Supplementary Materials)*

References

[1] G. Merlini and V. Bellotti, "Molecular mechanisms of amyloidosis," *New England Journal of Medicine*, vol. 349, no. 6, pp. 583–596, 2003.

[2] T. P. J. Knowles, M. Vendruscolo, and C. M. Dobson, "The amyloid state and its association with protein misfolding diseases," *Nature Reviews Molecular Cell Biology*, vol. 15, no. 6, pp. 384–396, 2014.

[3] K. Higuchi, H. Naiki, K. Kitagawa et al., "Apolipoprotein A-II gene and development of amyloidosis and senescence in a congenic strain of mice carrying amyloidogenic ApoA-II," *Laboratory Investigation*, vol. 72, no. 1, pp. 75–82, 1995.

[4] D. Games, D. Adams, R. Alessandrini et al., "Alzheimer-type neuropathology in transgenic mice overexpressing V717F β-amyloid precursor protein," *Nature*, vol. 373, no. 6514, pp. 523–527, 1995.

[5] M. C. Chartier-Harlin, F. Crawford, H. Houlden et al., "Early-onset Alzheimer's disease caused by mutations at codon 717 of the β-amyloid precursor protein gene," *Nature*, vol. 353, no. 6347, pp. 844–846, 1991.

[6] P. P. Mangione, R. Porcari, J. D. Gillmore et al., "Proteolytic cleavage of Ser52Pro variant transthyretin triggers its amyloid fibrillogenesis," *Proceedings of the National Academy of Sciences of the United States of America*, vol. 111, no. 4, pp. 1539–1544, 2014.

[7] X. Jiang, C. S. Smith, H. M. Petrassi et al., "An engineered transthyretin monomer that is nonamyloidogenic, unless it is partially denatured," *Biochemistry*, vol. 40, no. 38, pp. 11442–11452, 2001.

[8] L. Liu, H. Komatsu, I. V. J. Murray, and P. H. Axelsen, "Promotion of amyloid β protein misfolding and fibrillogenesis by a lipid oxidation product," *Journal of Molecular Biology*, vol. 377, no. 4, pp. 1236–1250, 2008.

[9] S. Saito, Y. Ando, M. Nakamura et al., "Effect of nitric oxide in amyloid fibril formation on transthyretin-related amyloidosis," *Biochemistry*, vol. 44, no. 33, pp. 11122–11129, 2005.

[10] A. Witkowski, G. K. L. Chan, J. C. Boatz et al., "Methionine oxidized apolipoprotein A-I at the crossroads of HDL biogenesis and amyloid formation," *The FASEB Journal*, vol. 32, no. 6, pp. 3149–3165, 2018.

[11] G. Ganguly, S. Chakrabarti, U. Chatterjee, and L. Saso, "Proteinopathy, oxidative stress and mitochondrial dysfunction: cross talk in Alzheimer's disease and Parkinson's disease," *Drug Design, Development and Therapy*, vol. 11, pp. 797–810, 2017.

[12] Y. Ando, N. Nyhlin, O. Suhr et al., "Oxidative stress is found in amyloid deposits in systemic amyloidosis," *Biochemical and Biophysical Research Communications*, vol. 232, no. 2, pp. 497–502, 1997.

[13] E. Alberdi, M. V. Sanchez-Gomez, A. Ruiz et al., "Mangiferin and morin attenuate oxidative stress, mitochondrial dysfunction, and neurocytotoxicity, induced by amyloid beta oligomers," *Oxidative Medicine and Cellular Longevity*, vol. 2018, Article ID 2856063, 13 pages, 2018.

[14] R. Q. Migrino, P. Hari, D. D. Gutterman et al., "Systemic and microvascular oxidative stress induced by light chain amyloidosis," *International Journal of Cardiology*, vol. 145, no. 1, pp. 67-68, 2010.

[15] S. Zraika, R. L. Hull, J. Udayasankar et al., "Oxidative stress is induced by islet amyloid formation and time-dependently mediates amyloid-induced beta cell apoptosis," *Diabetologia*, vol. 52, no. 4, pp. 626–635, 2009.

[16] S. Porcellotti, F. Fanelli, A. Fracassi et al., "Oxidative stress during the progression of β-amyloid pathology in the neocortex of the Tg2576 mouse model of Alzheimer's disease," *Oxidative Medicine and Cellular Longevity*, vol. 2015, Article ID 967203, 18 pages, 2015.

[17] F. Blanco-Vaca, J. C. Escola-Gil, J. M. Martin-Campos, and J. Julve, "Role of apoA-II in lipid metabolism and atherosclerosis: advances in the study of an enigmatic protein," *Journal of Lipid Research*, vol. 42, no. 11, pp. 1727–1739, 2001.

[18] T. M. Forte, J. K. Bielicki, R. Goth-Goldstein, J. Selmek, and M. R. McCall, "Recruitment of cell phospholipids and cholesterol by apolipoproteins A-II and A-I: formation of nascent apolipoprotein-specific HDL that differ in size, phospholipid composition, and reactivity with LCAT," *Journal of Lipid Research*, vol. 36, no. 1, pp. 148–157, 1995.

[19] S. Zhong, I. J. Goldberg, C. Bruce, E. Rubin, J. L. Breslow, and A. Tall, "Human ApoA-II inhibits the hydrolysis of HDL triglyceride and the decrease of HDL size induced by hypertriglyceridemia and cholesteryl ester transfer protein in transgenic mice," *The Journal of Clinical Investigation*, vol. 94, no. 6, pp. 2457–2467, 1994.

[20] M. Yang, Y. Liu, J. Dai et al., "Apolipoprotein A-II induces acute-phase response associated AA amyloidosis in mice through conformational changes of plasma lipoprotein structure," *Scientific Reports*, vol. 8, no. 1, p. 5620, 2018.

[21] Y. Xing, A. Nakamura, T. Korenaga et al., "Induction of protein conformational change in mouse senile amyloidosis," *Journal of Biological Chemistry*, vol. 277, no. 36, pp. 33164–33169, 2002.

[22] K. Kitagawa, J. Wang, T. Mastushita et al., "Polymorphisms of mouse apolipoprotein A-11: seven alleles found among 41 inbred strains of mice," *Amyloid*, vol. 10, no. 4, pp. 207–214, 2003.

[23] Y. Xing, A. Nakamura, T. Chiba et al., "Transmission of mouse senile amyloidosis," *Laboratory Investigation*, vol. 81, no. 4, pp. 493–499, 2001.

[24] T. Korenaga, J. Yan, J. Sawashita et al., "Transmission of amyloidosis in offspring of mice with AApoAII amyloidosis," *The American Journal of Pathology*, vol. 168, no. 3, pp. 898–906, 2006.

[25] X. Ding, Y. Liu, M. Yang et al., "Amyloidosis-inducing activity of blood cells in mouse AApoAII amyloidosis," *Experimental Animals*, vol. 67, no. 2, pp. 105–115, 2018.

[26] D. A. Butterfield, "Amyloid β-peptide (1-42)-induced oxidative stress and neurotoxicity: implications for neurodegeneration in Alzheimer's disease brain. A review," *Free Radical Research*, vol. 36, no. 12, pp. 1307–1313, 2002.

[27] C. Cheignon, M. Tomas, D. Bonnefont-Rousselot, P. Faller, C. Hureau, and F. Collin, "Oxidative stress and the amyloid beta peptide in Alzheimer's disease," *Redox Biology*, vol. 14, pp. 450–464, 2018.

[28] H. Luo, J. Sawashita, G. Tian et al., "Extracellular deposition of mouse senile AApoAII amyloid fibrils induced different

unfolded protein responses in the liver, kidney, and heart," *Laboratory Investigation*, vol. 95, no. 3, pp. 320–333, 2015.

[29] A. Nunomura, G. Perry, M. A. Pappolla et al., "Neuronal oxidative stress precedes amyloid-β deposition in Down syndrome," *Journal of Neuropathology & Experimental Neurology*, vol. 59, no. 11, pp. 1011–1017, 2000.

[30] H. Misonou, M. Morishima-Kawashima, and Y. Ihara, "Oxidative stress induces intracellular accumulation of amyloid β-protein (Aβ) in human neuroblastoma cells," *Biochemistry*, vol. 39, no. 23, pp. 6951–6959, 2000.

[31] H. T. Blumenthal, "Amyloidosis: a universal disease of aging?," *The Journals of Gerontology Series A: Biological Sciences and Medical Sciences*, vol. 59, no. 4, pp. 361–369, 2004.

[32] R. H. Swerdlow, "Is aging part of Alzheimer's disease, or is Alzheimer's disease part of aging?," *Neurobiology of Aging*, vol. 28, no. 10, pp. 1465–1480, 2007.

[33] L. Li, J. Sawashita, X. Ding et al., "Caloric restriction reduces the systemic progression of mouse AApoAII amyloidosis," *PLoS One*, vol. 12, no. 2, article e0172402, 2017.

[34] N. Nicolakakis, T. Aboulkassim, B. Ongali et al., "Complete rescue of cerebrovascular function in aged Alzheimer's disease transgenic mice by antioxidants and pioglitazone, a peroxisome proliferator-activated receptor γ agonist," *Journal of Neuroscience*, vol. 28, no. 37, pp. 9287–9296, 2008.

[35] F. Liu, C. C. Wei, S. J. Wu et al., "Apocynin attenuates tubular apoptosis and tubulointerstitial fibrosis in transgenic mice independent of hypertension," *Kidney International*, vol. 75, no. 2, pp. 156–166, 2009.

[36] B. H. Han, M. L. Zhou, A. W. Johnson et al., "Contribution of reactive oxygen species to cerebral amyloid angiopathy, vasomotor dysfunction, and microhemorrhage in aged Tg2576 mice," *Proceedings of the National Academy of Sciences of the United States of America*, vol. 112, no. 8, pp. E881–E890, 2015.

[37] M. Pras, D. Zucker-Franklin, A. Rimon, and E. C. Franklin, "Physical, chemical, and ultrastructural studies of water-soluble human amyloid fibrils. Comparative analyses of nine amyloid preparations," *Journal of Experimental Medicine*, vol. 130, no. 4, pp. 777–795, 1969.

[38] J. Sawashita, B. Zhang, K. Hasegawa et al., "C-terminal sequence of amyloid-resistant type F apolipoprotein A-II inhibits amyloid fibril formation of apolipoprotein A-II in mice," *Proceedings of the National Academy of Sciences of the United States of America*, vol. 112, no. 8, pp. E836–E845, 2015.

[39] K. Higuchi, A. Matsumura, A. Honma et al., "Systemic senile amyloid in senescence-accelerated mice. A unique fibril protein demonstrated in tissues from various organs by the unlabeled immunoperoxidase method," *Laboratory Investigation*, vol. 48, no. 2, pp. 231–240, 1983.

[40] P. Rzymski, P. Klimaszyk, W. Marszelewski et al., "The chemistry and toxicity of discharge waters from copper mine tailing impoundment in the valley of the Apuseni Mountains in Romania," *Environmental Science and Pollution Research*, vol. 24, no. 26, pp. 21445–21458, 2017.

[41] Y. Wang, J. Sawashita, J. Qian et al., "ApoA-I deficiency in mice is associated with redistribution of apoA-II and aggravated AApoAII amyloidosis," *Journal of Lipid Research*, vol. 52, no. 8, pp. 1461–1470, 2011.

[42] T. Chiba, K. Kogishi, J. Wang et al., "Mouse senile amyloid deposition is suppressed by adenovirus-mediated overexpression of amyloid-resistant apolipoprotein A-II," *The American Journal of Pathology*, vol. 155, no. 4, pp. 1319–1326, 1999.

[43] F. Ge, J. Yao, X. Fu et al., "Amyloidosis in transgenic mice expressing murine amyloidogenic apolipoprotein A-II (Apoa2c)," *Laboratory Investigation*, vol. 87, no. 7, pp. 633–643, 2007.

[44] G. Tian, J. Sawashita, H. Kubo et al., "Ubiquinol-10 supplementation activates mitochondria functions to decelerate senescence in senescence-accelerated mice," *Antioxidants & Redox Signaling*, vol. 20, no. 16, pp. 2606–2620, 2014.

[45] K. A. Gauss, L. K. Nelson-Overton, D. W. Siemsen, Y. Gao, F. R. DeLeo, and M. T. Quinn, "Role of NF-κB in transcriptional regulation of the phagocyte NADPH oxidase by tumor necrosis factor-α," *Journal of Leukocyte Biology*, vol. 82, no. 3, pp. 729–741, 2007.

[46] T. Finkel and N. J. Holbrook, "Oxidants, oxidative stress and the biology of ageing," *Nature*, vol. 408, no. 6809, pp. 239–247, 2000.

[47] E. Birben, U. M. Sahiner, C. Sackesen, S. Erzurum, and O. Kalayci, "Oxidative stress and antioxidant defense," *World Allergy Organization Journal*, vol. 5, no. 1, pp. 9–19, 2012.

[48] J. Bieschke, Q. Zhang, E. T. Powers, R. A. Lerner, and J. W. Kelly, "Oxidative metabolites accelerate Alzheimer's amyloidogenesis by a two-step mechanism, eliminating the requirement for nucleation," *Biochemistry*, vol. 44, no. 13, pp. 4977–4983, 2005.

[49] J. K. Andersen, "Oxidative stress in neurodegeneration: cause or consequence?," *Nature Medicine*, vol. 10, no. S7, pp. S18–S25, 2004.

[50] S. C. Barber and P. J. Shaw, "Oxidative stress in ALS: key role in motor neuron injury and therapeutic target," *Free Radical Biology & Medicine*, vol. 48, no. 5, pp. 629–641, 2010.

[51] B. Macedo, J. Magalhaes, A. R. Batista, and M. J. Saraiva, "Carvedilol treatment reduces transthyretin deposition in a familial amyloidotic polyneuropathy mouse model," *Pharmacological Research*, vol. 62, no. 6, pp. 514–522, 2010.

[52] M. L. Ballesteros, D. A. Wunderlin, and M. A. Bistoni, "Oxidative stress responses in different organs of *Jenynsia multidentata* exposed to endosulfan," *Ecotoxicology and Environmental Safety*, vol. 72, no. 1, pp. 199–205, 2009.

[53] J. Jun, V. Savransky, A. Nanayakkara et al., "Intermittent hypoxia has organ-specific effects on oxidative stress," *American Journal of Physiology-Regulatory, Integrative and Comparative Physiology*, vol. 295, no. 4, pp. R1274–R1281, 2008.

[54] K. Rashid, K. Sinha, and P. C. Sil, "An update on oxidative stress-mediated organ pathophysiology," *Food and Chemical Toxicology*, vol. 62, pp. 584–600, 2013.

[55] L. Zhao, J. N. Buxbaum, and N. Reixach, "Age-related oxidative modifications of transthyretin modulate its amyloidogenicity," *Biochemistry*, vol. 52, no. 11, pp. 1913–1926, 2013.

[56] M. Arimon, S. Takeda, K. L. Post, S. Svirsky, B. T. Hyman, and O. Berezovska, "Oxidative stress and lipid peroxidation are upstream of amyloid pathology," *Neurobiology of Disease*, vol. 84, pp. 109–119, 2015.

[57] D. Praticò, K. Uryu, S. Leight, J. Q. Trojanoswki, and V. M. Y. Lee, "Increased lipid peroxidation precedes amyloid plaque formation in an animal model of Alzheimer amyloidosis," *Journal of Neuroscience*, vol. 21, no. 12, pp. 4183–4187, 2001.

[58] D. R. Howlett, A. R. George, D. E. Owen, R. V. Ward, and R. E. Markwell, "Common structural features determine the effectiveness of carvedilol, daunomycin and rolitetracycline as inhibitors of Alzheimer β-amyloid fibril formation," *Biochemical Journal*, vol. 343, no. 2, pp. 419–423, 1999.

[59] A. R. Hurshman, J. T. White, E. T. Powers, and J. W. Kelly, "Transthyretin aggregation under partially denaturing conditions is a downhill polymerization," *Biochemistry*, vol. 43, no. 23, pp. 7365–7381, 2004.

[60] K. Oorni, K. Rajamaki, S. D. Nguyen et al., "Acidification of the intimal fluid: the perfect storm for atherogenesis," *Journal of Lipid Research*, vol. 56, no. 2, pp. 203–214, 2015.

[61] N. Ferreira, N. P. Goncalves, M. J. Saraiva, and M. R. Almeida, "Curcumin: a multi-target disease-modifying agent for late-stage transthyretin amyloidosis," *Scientific Reports*, vol. 6, no. 1, article 26623, 2016.

[62] E. R. Veldman, Z. Jia, C. Halldin, and M. M. Svedberg, "Amyloid binding properties of curcumin analogues in Alzheimer's disease postmortem brain tissue," *Neuroscience Letters*, vol. 630, pp. 183–188, 2016.

[63] M. Stefani and S. Rigacci, "Protein folding and aggregation into amyloid: the interference by natural phenolic compounds," *International Journal of Molecular Sciences*, vol. 14, no. 6, pp. 12411–12457, 2013.

[64] L. Bouman, A. Schlierf, A. K. Lutz et al., "Parkin is transcriptionally regulated by ATF4: evidence for an interconnection between mitochondrial stress and ER stress," *Cell Death and Differentiation*, vol. 18, no. 5, pp. 769–782, 2011.

[65] D. T. Rutkowski and R. J. Kaufman, "All roads lead to ATF4," *Developmental Cell*, vol. 4, no. 4, pp. 442–444, 2003.

[66] D. M. Holtzman, "Role of apoE/Aβ interactions in the pathogenesis of Alzheimer's disease and cerebral amyloid angiopathy," *Journal of Molecular Neuroscience*, vol. 17, no. 2, pp. 147–155, 2001.

[67] S. B. P. Chargé, M. M. Esiri, C. A. Bethune, B. C. Hansen, and A. Clark, "Apolipoprotein E is associated with islet amyloid and other amyloidoses: implications for Alzheimer's disease," *The Journal of Pathology*, vol. 179, no. 4, pp. 443–447, 1996.

[68] D. M. Holtzman, "In vivo effects of ApoE and clusterin on amyloid-β metabolism and neuropathology," *Journal of Molecular Neuroscience*, vol. 23, no. 3, pp. 247–254, 2004.

[69] J. Ma, A. Yee, H. B. Brewer, S. Das, and H. Potter, "Amyloid-associated proteins α_1-antichymotrypsin and apolipoprotein E promote assembly of Alzheimer β-protein into filaments," *Nature*, vol. 372, no. 6501, pp. 92–94, 1994.

[70] J. Poirier, P. Bertrand, J. Poirier et al., "Apolipoprotein E polymorphism and Alzheimer's disease," *The Lancet*, vol. 342, no. 8873, pp. 697–699, 1993.

[71] H. Miyahara, J. Sawashita, E. Ishikawa et al., "Comprehensive proteomic profiles of mouse AApoAII amyloid fibrils provide insights into the involvement of lipoproteins in the pathology of amyloidosis," *Journal of Proteomics*, vol. 172, pp. 111–121, 2018.

Hindawi
Oxidative Medicine and Cellular Longevity
Volume 2019, Article ID 6927380, 21 pages
https://doi.org/10.1155/2019/6927380

Research Article

Syk and Hrs Regulate TLR3-Mediated Antiviral Response in Murine Astrocytes

Matylda B. Mielcarska,[1] **Magdalena Bossowska-Nowicka**,[1] **Karolina P. Gregorczyk-Zboroch**,[1] **Zbigniew Wyżewski**,[2] **Lidia Szulc-Dąbrowska**,[1] **Małgorzata Gieryńska**,[1] **and Felix N. Toka**[1,3]

[1]*Division of Immunology, Department of Preclinical Sciences, Faculty of Veterinary Medicine, Warsaw University of Life Sciences, Ciszewskiego 8, 02-786 Warsaw, Poland*
[2]*Department of Biochemistry, Faculty of Agriculture and Biology, Warsaw University of Life Sciences, Nowoursynowska 159, 02-776 Warsaw, Poland*
[3]*Center for Integrative Mammalian Research, Department of Biomedical Sciences, Ross University School of Veterinary Medicine, PO Box 334, Basseterre, Saint Kitts and Nevis*

Correspondence should be addressed to Felix N. Toka; ftoka@rossvet.edu.kn

Received 22 October 2018; Revised 22 December 2018; Accepted 13 January 2019; Published 4 April 2019

Guest Editor: Agueda A. Rostagno

Toll-like receptors (TLRs) sense the presence of pathogen-associated molecular patterns. Nevertheless, the mechanisms modulating TLR-triggered innate immune responses are not yet fully understood. Complex regulatory systems exist to appropriately direct immune responses against foreign or self-nucleic acids, and a critical role of hepatocyte growth factor-regulated tyrosine kinase substrate (HRS), endosomal sorting complex required for transportation-0 (ESCRT-0) subunit, has recently been implicated in the endolysosomal transportation of TLR7 and TLR9. We investigated the involvement of Syk, Hrs, and STAM in the regulation of the TLR3 signaling pathway in a murine astrocyte cell line C8-D1A following cell stimulation with a viral dsRNA mimetic. Our data uncover a relationship between TLR3 and ESCRT-0, point out Syk as dsRNA-activated kinase, and suggest the role for Syk in mediating TLR3 signaling in murine astrocytes. We show molecular events that occur shortly after dsRNA stimulation of astrocytes and result in Syk Tyr-342 phosphorylation. Further, TLR3 undergoes proteolytic processing; the resulting TLR3 N-terminal form interacts with Hrs. The knockdown of Syk and Hrs enhances TLR3-mediated antiviral response in the form of IFN-β, IL-6, and CXCL8 secretion. Understanding the role of Syk and Hrs in TLR3 immune responses is of high importance since activation and precise execution of the TLR3 signaling pathway in the brain seem to be particularly significant in mounting an effective antiviral defense. Infection of the brain with herpes simplex type 1 virus may increase the secretion of amyloid-β by neurons and astrocytes and be a causal factor in degenerative diseases such as Alzheimer's disease. Errors in TLR3 signaling, especially related to the precise regulation of the receptor transportation and degradation, need careful observation as they may disclose foundations to identify novel or sustain known therapeutic targets.

1. Introduction

Astrocytes constitute 19-40% of brain glial cells and are the key component responsible for homeostasis and immune and oxidative stress defense in the CNS [1, 2]. By participating in the biogenesis and transport of a wide range of neuroactive substances, they affect neurons and other glial cells and thus regulate many physiological and pathophysiological processes [3]. In neuropathological conditions, immunologically silent astrocytes often undergo reactive reprogramming [4].

Recent reports reveal astrocytes as cells that play a substantial role in the pathogenesis of Alzheimer's disease (AD), the most frequent type of brain amyloidosis and the

most common type of dementia in humans [5]. Amyloid-β (Aβ) plaques, AD's hallmark, activate cerebral glial cells and cause neuroinflammation resulting in neuronal cell death [6]. Such a process is decisive for the progression of AD. An increase in the number of reactive astrocytes that surround and may phagocytose Aβ plaques is observed in the neuronal vicinity [7]. However, following reactive reprogramming, astrocytes exhibit high concentrations of the amyloid precursor protein (APP) and β- and γ-secretase that enable formulation of the Aβ plaques [6]. Interestingly, during reactive gliosis, about 50% of the altered gene expression in astrocytes is significantly dependent on the initiating brain injury [8]. One of the factors leading to neuroinflammation, which may contribute to astrocyte reprogramming and enhanced astrocytic secretion of Aβ, is herpes simplex type 1 virus (HSV-1) infection in the brain. Aβ accumulates in HSV-1-infected cell cultures, while viral particles, as well as viral nucleic acid were found in the vicinity of amyloid plaques in the brains of mice and humans [9]. Toll-like receptor 3 (TLR3) plays an essential role in the innate immune control of cerebral HSV-1 infection. Therefore, it is likely that infected astrocytes detect the virus through TLR3, thus activating them and contributing to production of Aβ.

Substantial expression of TLR3 occurs in neurons and astrocytes, oligodendrocytes, and microglia, of which expression in astrocytes is the most abundant [10, 11]. An increase in the TLR3 expression in CNS-resident cells is usually associated with the development of neuroinflammation [12]. Stimulated glial cells and macrophages are responsible for the removal of microorganisms and injured cells. In addition to the production of various growth factors, chemokines and cytokines such as IL-1β, TNF-α, IL-6, and glial cells secrete oxides that may become neurotoxic during brain injuries or neurological diseases and exacerbate CNS dysfunction [13, 14].

Toll-like receptors (TLRs) are important contributors to activation of the innate immune response in the brain during infection, injury, or degeneration [15–18]. TLR3 is an evolutionarily conserved protein which recognizes double-stranded RNA (dsRNA) in endosomes. Double-stranded RNA may constitute a viral nucleic acid or an intermediate product formed during replication of viruses such as HSV-1 and HSV-2. Patients, especially children with deficiencies in TLR3 or single-gene errors in components of the TLR3 signaling pathway, are more susceptible to HSV-1 and HSV-2 infections, which may be the cause of a devastating human disease—herpes simplex encephalitis (HSE) [19–22]. Being one of the most common viral brain diseases in the world, HSE entails many deleterious outcomes. The accession of external factors into the central nervous system (CNS) and the CNS immune response are precisely controlled; however, due to the neuronal latency of HSV, inflammation in the brain may last for years and have a recurrent character [23]. The length of inflammatory response in CNS and disease progression is affected by the balance between pro- and anti-inflammatory signals in the neuronal environment [24]. Sustainability of the inflammatory process or deficiencies in distribution of suppressive mechanisms may lead to pathological repercussions and influence the outcome of disease.

Prior to launching the signaling cascade, nucleic acid-sensingTLRs such as TLR3, TLR7, and TLR9 enter the UNC93B1-dependent secretory pathway from the endoplasmic reticulum (ER) through the trans-Golgi network (TGN) to endosomes. However, receptors are subject to differential UNC93B1-related sorting mechanisms [25]. Furthermore, the endosomal sorting complex required for transport-0 (ESCRT-0), composed of hepatocyte growth factor-regulated tyrosine kinase substrate (Hrs) and signal transducing adaptor molecule (STAM), was recently implicated in post-Golgi trafficking by sorting ubiquitinated TLR7 and TLR9 to endosomes [26], and silencing of Hrs reduced signaling through TLR7 and TLR9 [27]. Chiang et al. [27] indicated that Hrs binds directly to particular TLRs and that the interaction of Hrs with TLR9 was much stronger than that with cell-surface-expressed TLR2. STAM, similar to Hrs, may demonstrate endosomal localization and display a potent sorting efficiency due to multiple ubiquitin-binding domains (UBDs). Moreover, it was demonstrated that STAM localizes prominently to early endocytic vesicles and decidedly regulates morphology of the Golgi apparatus [28], the site where TLRs are packaged en route to endosomes.

In addition to TLR trafficking aimed at ligand recognition, ESCRT-0-mediated sorting of receptors may direct them for recycling or degradation. Regardless of ligand stimulation, IL-2 receptor β and IL-4 receptor α were consistently internalized and delivered to late endosomes (LE) in an ESCRT-dependent manner by association with Hrs [29]. Following activation, receptors such as EGFR, PDGF, or TLR4 were endocytosed and targeted via the ESCRT pathway for lysosomal degradation [30–32]. The formation of the endosomal sorting machinery and its ability to target EGFR were regulated in this case by modulation of Hrs protein level, phosphorylation, and ubiquitination [33]. Furthermore, deficiencies and overexpression of ESCRT machinery components led to reduced EGFR degradation [34]. Because EGFR is responsible for TLR3 phosphorylation, posttranslational modifications, as well as alterations in the expression of ESCRT-0 subunits could affect TLR3 signaling.

During HSV infection, release of viral dsRNA from the cells at the site of brain injury entails TLR3 activation. Upon phosphorylation by Bruton tyrosine kinase (Btk), c-terminal Src kinase (c-Src), and epidermal growth factor receptor (EGFR), the receptor triggers signaling in a pathway that enrolls transcription factors such as nuclear factor kappa B (NF-κB), interferon regulatory factor 3 (IRF3), and interferon regulatory factor 7 (IRF7), responsible for the development of inflammatory response [35–37] (Figure 1). Compared to other endosomal TLRs, TLR3 engages a different adaptor protein (Toll/interleukin 1 receptor domain-containing adaptor protein inducing IFN-β (TRIF)) for initiation of IRF3 and NF-κB signaling. Spleen tyrosine kinase (Syk) has been shown to phosphorylate tyrosine residues of TRIF, the TLR3 adaptor protein. Such a process leads to the TRIF proteasomal degradation and entails downregulation of the TLR signaling [38]. Furthermore, Syk significantly regulates Hrs phosphorylation and ubiquitination, as well as its membrane/cytosol localization [39]. Syk is known to function at the plasma membrane, but also in cytoplasmic and nuclear

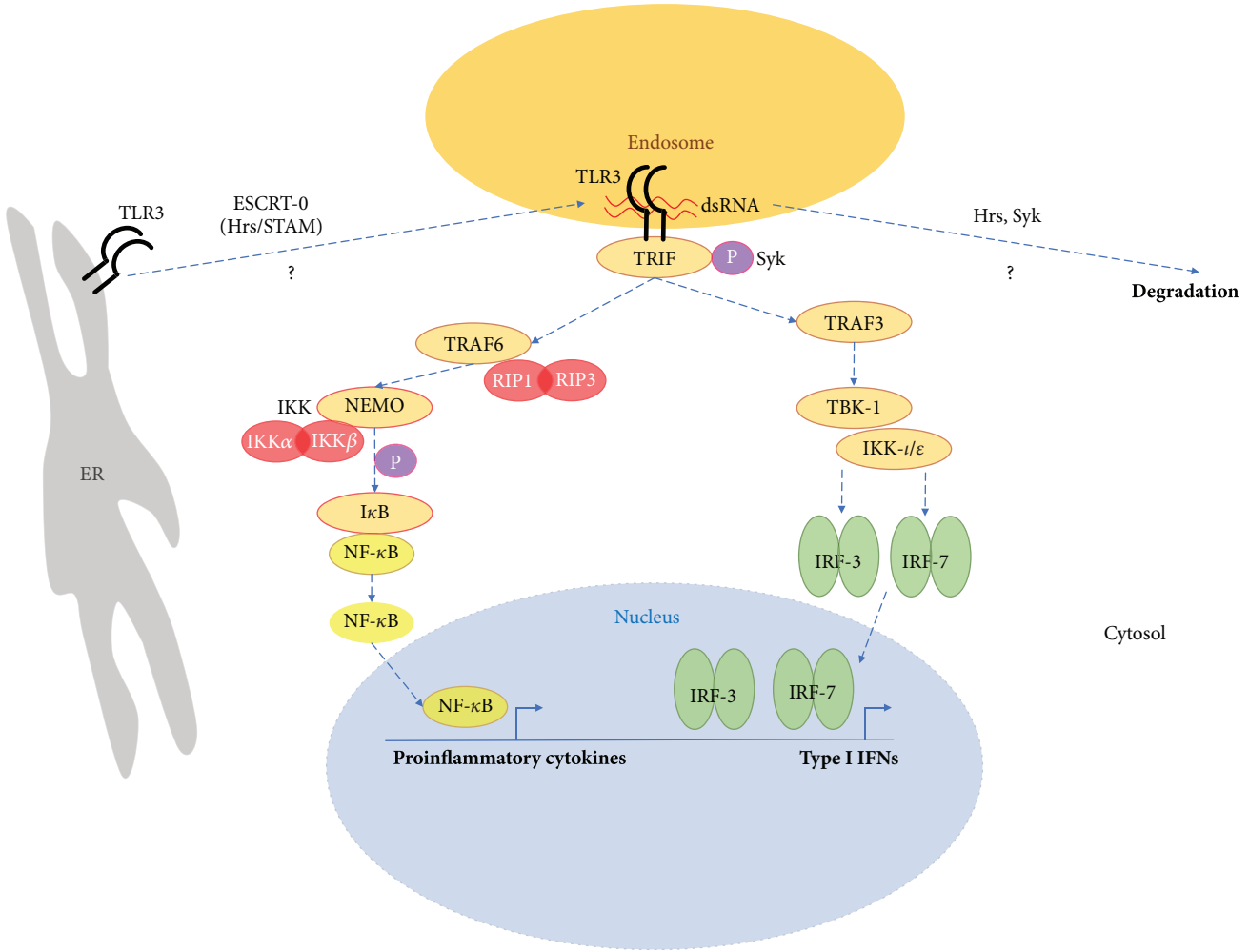

Figure 1: TLR3 signaling in astrocytes. Upon dsRNA recognition in the endosomal compartment, TLR3 undergoes dimerization and interacts with the TRIF adaptor molecule. TRIF activation is followed by TRAF6 and TRAF3 recruitment. TRAF6 conducts the signal *via* RIP-1 and RIP-3 kinases which facilitate NEMO, IKK-α, and IKK-β complex formation, followed by NF-κB phosphorylation and translocation into the nucleus. TRAF3 engages TBK1 and IKK-i/$\mathcal{E}$ for IRF3 and IRF7 activation, followed by their dimerization and translocation into the nucleus. This leads to the induction of type I IFNs and proinflammatory cytokine gene expression. The dotted arrows highlight possible roles of ESCRT-0 in TLR3 transport from the ER to the endosome, as well as the role of Hrs and Syk in TLR3 degradation.

compartments of the cells [40], while Hrs may interact with Golgi proteins or reside in membranes of early endosomes and mediate delivery of protein cargo to multivesicular bodies (MVBs) for the subsequent degradation [41]. Consequently, Hrs serves as an important trafficking regulator and both Syk and Hrs may be critical controllers of protein entry into lysosomes for degradation. However, influence of these proteins on TLR3 signaling in CNS cells remains largely unexplored. The impact of Syk and ESCRT-0 on activation of the immune response may be receptor- and pathway-specific. It may be distinctively regulated in various cellular compartments and types of cells or tissues, as the ESCRT-0 target proteins may fulfill their function in the endosomes or on the cell surface.

Progression of the antiviral defense is guided by increased levels of type I interferons (IFNs) (IFNα, IFNβ), cytokines (IL-1β, IL-6, and TNFα), chemokines (CXCL8, CCL5, and CXCL10), and other molecules, such as $2'5'$OAS. The ground for the clinical signs of HSE is as follows: impaired but not abolished IFNα/β and IFNγ production in response to TLR3 stimulation [42]. Because HSE is manifested in CNS, attention should be paid to discovering and characterizing immunological engagement in HSV-1 and HSV-2 control, particularly related to TLR3 transportation, activation, and degradation in CNS-resident cells.

In this research, we investigated the involvement of Syk, Hrs, and STAM in the regulation of the TLR3 signaling pathway in the C8-D1A cell line. Our studies identify molecular events in murine astrocytes such as phosphorylation of Syk and Hrs and interaction of Syk and Hrs that occur shortly after TLR3 stimulation. We also show that the receptor undergoes ligand-induced proteolytic processing and that the N-terminal form of TLR3 exclusively interacts with Hrs. Finally, we demonstrate that silencing of Syk or Hrs in

Table 1: Primary antibodies used in the western blot assay.

Antibody	Clone/ID	Isotype	Source	Concentration
TLR3	PA5-23105[a]	Polyclonal rabbit	Thermo Fisher Scientific	2 μg/ml
TLR3	MA5-16184[a]	Monoclonal mouse	Thermo Fisher Scientific	2 μg/ml
TLR3	TLR3.7[b]	Monoclonal mouse	OriGene Technologies GmbH	2 μg/ml
Hrs	15087[a]	Monoclonal rabbit	CST	1 : 1000
Hrs	M-79[a]	Polyclonal rabbit	Santa Cruz Biotechnology	1 : 200
Hrs	C-7[a]	Monoclonal mouse	Santa Cruz Biotechnology	1 : 200
STAM	13053[a]	Polyclonal rabbit	CST	1 : 200
STAM	H-175[a]	Polyclonal rabbit	Santa Cruz Biotechnology	1 : 100
STAM	B-2[a]	Monoclonal mouse	Santa Cruz Biotechnology	1 : 200
Syk	N-19[a]	Polyclonal rabbit	Santa Cruz Biotechnology	1 : 200
Syk	4D10[a]	Monoclonal mouse	Santa Cruz Biotechnology	1 : 200
PDI	RL77[b]	Monoclonal mouse	Thermo Fisher Scientific	1 : 100
Phospho-Syk	I120-722[b]	Monoclonal mouse	Becton Dickinson Biosciences	1 : 500
Phosphotyrosine	4G10[a]	Monoclonal mouse	Merck	1 : 1000
Phosphotyrosine	61-5800[a]	Polyclonal rabbit	Thermo Fisher Scientific	1 : 1000
IRF3	4302[a]	Monoclonal rabbit	CST	1 : 1000
NF-κB p65	8242[a]	Monoclonal rabbit	CST	1 : 1000
IRF7	PA1-12810[a]	Polyclonal rabbit	Thermo Fisher Scientific	2 μg/mL
PARP	9532[a]	Monoclonal rabbit	CST	1 : 1000
Ubiquitin	P4D1[a]	Monoclonal mouse	Santa Cruz Biotechnology	1 : 200
Ubiquitin	3933[a]	Polyclonal rabbit	CST	1 : 1000
GAPDH	MA5-15738[a]	Monoclonal mouse	Thermo Fisher Scientific	1 : 1000

[a]Manufacturer's antibody identification. [b]Clone

astrocytes significantly upregulates TLR3-directed signaling, indicating these proteins as targets for modulating TLR3 immune responses.

2. Materials and Methods

2.1. Cell Culture. Murine astrocytes from the C8-D1A cell line (ATCC® CRL-2541, Manassas, VA, USA) were used in all experiments. Cells were cultured in DMEM with high glucose and supplemented with 4.0 mM L-glutamine medium (Sigma-Aldrich, St. Louis, MO, USA), 10% heat-inactivated FBS (Sigma-Aldrich), and 1% solution of penicillin G, streptomycin, and amphotericin B (Sigma-Aldrich), in a humidified 5% CO_2 incubator at 37°C. Astrocytes were subcultured according to the protocol described by Freshney [43]. Trypsin-EDTA solution (0.25%, Sigma-Aldrich) was used to dissociate the C8-D1A cells. Cells from passage 2-15 were used for the experiments.

2.2. Stimulation of Astrocytes with the TLR3 Agonist. Twenty-four-hour cultures of C8-D1A cells were treated with a TLR3 agonist, viral dsRNA substitute—poly(I:C) (InvivoGen, San Diego, CA, USA)—or RIG-I/MDA-5 agonist as a control—poly(I:C)/LyoVec (InvivoGen). At the time of treatment, the culture medium was replaced with fresh medium containing poly(I:C) or poly(I:C)/LyoVec. The 10 μg/ml poly(I:C) and 1 μg/ml poly(I:C)/LyoVec concentrations were determined empirically for further experiments.

2.3. Antibodies and siRNAs. Primary antibodies used in the study are listed in Table 1. Secondary antibodies used in the study were goat anti-mouse HRP-conjugated IgG (1 : 5000, Santa Cruz Biotechnology), goat anti-rabbit HRP-conjugated IgG (1 : 5000, Santa Cruz Biotechnology), donkey anti-goat HRP-conjugated IgG (1 : 5000, Santa Cruz Biotechnology), horse anti-mouse HRP-conjugated IgG (1 : 3000, CST), and goat anti-rabbit HRP-conjugated IgG (1 : 3000, CST). siRNAs against TLR3, Syk, Hrs, and STAM were purchased from Santa Cruz Biotechnology together with their negative control, siRNA-A.

2.4. Western Blot Analysis. At the indicated times or concentrations, astrocytes were processed for protein assays. Cells were lysed with radioimmunoprecipitation assay (RIPA) buffer (Thermo Fisher Scientific, Waltham, MA, USA) supplemented with 1% protease and phosphatase inhibitor cocktail (Thermo Fisher Scientific), and protein concentration was determined with the Pierce BCA Protein Assay Kit (Thermo Fisher Scientific) and spectrophotometry on an Epoch BioTek spectrophotometer. Proteins (20 μg/well) from the cells were separated by SDS-PAGE and electrotransferred onto PVDF membranes using the Bolt® System (Thermo Fisher Scientific). After blocking for 2 h in phosphate-buffered saline with Tween (PBST) containing 5% nonfat milk, the blots were incubated overnight at 4°C with primary antibodies. Subsequently, membranes were washed 3 times after which they were probed with secondary anti-goat or anti-mouse antibodies conjugated to horseradish peroxidase (HRP) (CST,

Boston, MA, USA) for 1 h at room temperature and washed 3 times. The Pierce ECL Western Blotting Substrate (Thermo Fisher Scientific) was used to develop, and autoradiography to visualize the protein bands. The intensity of bands was then analyzed using ImageJ software (NIH, Bethesda, MD, USA) and was normalized to GAPDH.

2.5. siRNA Transfection. Twenty-four hours prior to transfection with TLR3, Syk, Hrs, and STAM siRNA, 2×10^5 astrocytes per well were seeded in a 6-well plate in the antibiotic-free normal growth medium. For each transfection, 40 or 80 pmol of the specific siRNA was added to 8 μl of the Transfection Reagent (Santa Cruz Biotechnology) to obtain Transfection Reagent mixture according to the manufacturer's instructions. Following 45 min incubation of the mixture at room temperature, cells were washed with Transfection Medium (Santa Cruz Biotechnology) and then the Transfection Reagent mixture was overlaid onto the washed cells. After 7 h incubation, a normal growth medium containing 2 times the normal serum was added to the cells without removing the transfection mixture. Astrocytes were cultured for 48 h or 72 h from the beginning of the transfection, and the efficiency of each of the siRNA transfection was affirmed by western blotting (see Figures 2(d), 3(e), and 4(d)).

2.6. Immunostaining and Fluorescence Microscopy. Astrocytes were cultured on 22 mm glass cell culture coverslips in 24-well plates. Untreated or poly(I:C)-treated cells were fixed for 15 min in phosphate-buffered saline (PBS) with 4% paraformaldehyde (Sigma-Aldrich). After washing, cells were permeabilized with 0.5% Triton X-100 (Sigma-Aldrich) in PBS and blocked with 3% bovine serum albumin (Sigma-Aldrich) with 0.1% Triton X-100. Subsequently, cells were incubated for 1 h with anti-TLR3 or anti-STAM or anti-Syk or anti-Hrs antibodies (1 : 50, Thermo Fisher Scientific) and washed with 0.1% Triton X-100 in PBS. Then, astrocytes were incubated with secondary antibodies conjugated with rhodamine Red-X (1 : 100, Jackson ImmunoResearch Laboratories Inc., West Grove, PA, USA) for 1 h. In double immunofluorescence experiments, cells were incubated for 1 h with the mixture of anti-TLR3 and anti-PDI antibodies or anti-STAM and anti-PDI antibodies. Next, after washing, cells were incubated for 1 h with a mixture of secondary antibodies conjugated with rhodamine Red-X or FITC (Jackson ImmunoResearch Laboratories). The cells were then washed and stained with Hoechst 33342 (Sigma-Aldrich) for 10 min. Finally, after washing with PBS, the coverslips were mounted in ProLong Gold Antifade Reagent (Thermo Fisher Scientific). Fluorescence microscopy was performed with an Olympus BX60 fluorescence microscope and analyzed with Cell^F software (Soft Imaging System) (Olympus, Tokyo, Japan).

2.7. Immunoprecipitation. C8-D1A cells were cultured in a 6-well plate to reach 80-100% confluence. Cells were stimulated with poly(I:C) or poly(I:C)/LyoVec at the indicated times. If the transfection with specific siRNA was required, astrocytes were pretransfected and 48 or 72 h posttransfection stimulated with poly(I:C) or poly(I:C)/LyoVec as described in Section 2.2. Subsequently, the cells were lysed with IP lysis buffer (Thermo Fisher Scientific) supplemented with protease and phosphatase inhibitor cocktail (Thermo Fisher Scientific). Syk, Hrs, STAM, and TLR3 were immunoprecipitated using Catch and Release® v2.0 Reversible Immunoprecipitation System (Merck) according to the manufacturer's protocol and subjected for immunoblotting. Normal mouse IgG (Santa Cruz Biotechnology) was used as negative control for immunoprecipitation experiments.

2.8. Enzyme-Linked Immunosorbent Assay (ELISA). For the evaluation of IFNβ, IL-6, and CXCL8 secretion, C8-D1A cells were seeded in a 6-well plate and transfected with specific siRNA (for TLR3, Hrs, STAM, or Syk) or siRNA-A as a negative control. The subsequent concentration of siRNA and duration of the transfection were based on the result, which corresponded to the best knockdown efficiency of the specific protein (see Section 2.4). Following the transfection, cells were detached and seeded in a 24-well plate at a density of 3×10^5 cells per well in a 0.5 ml normal growth medium and treated with polyI:C or poly(I:C)/LyoVec or not treated. After 24 h, the cell supernatants were harvested after centrifugation at 1000 xg for 5 min and stored at -80°C until analysis in ELISA assays. The tested proteins were measured with mouse IFN-beta ELISA Kit (R&D Systems, Minneapolis, MN, USA), mouse IL-6 ELISA Kit (Thermo Fisher Scientific), and mouse CXCL8 ELISA Kit (MyBioSource, San Diego, CA, USA), following the manufacturer's instructions. The measurements of optical densities (OD) were done in a microplate reader (Epoch spectrophotometer, BioTek Instruments Inc., Winooski, VT, USA). Quantification of each cytokine concentration in cell supernatants was determined by reading ODs on a linear calibration curve generated for each protein.

2.9. Cell Fractionation. C8-D1A cells were untreated or treated with poly(I:C) or poly(I:C)/LyoVec for 5, 8, 12, 15, 30, and 60 min. Subsequently, cells were collected and fractionated using NE-PER Nuclear and Cytoplasmic Extraction Reagents (Thermo Fisher Scientific) according to the manufacturer's protocol. Nuclear and cytoplasmic extracts' protein concentration was determined using BCA Protein Assay kit (Thermo Fisher Scientific). Next, nuclear and cytoplasmic extracts were subjected to western blot analysis.

2.10. Statistical Analysis. Quantitative data are presented as mean ± standard deviation (SD) from at least three independent biological experiments (unless otherwise indicated). All data were analyzed in STATISTICA software (StatSoft, Poland). Comparisons were made using Student's t-test. A p value ≤ 0.05 (*) or ≤ 0.01 (**) was considered statistically significant.

3. Results

3.1. TLR3 Undergoes Cleavage upon Poly(I:C) Stimulation of Murine Astrocytes. TLR3 belongs to the subfamily of TLRs that reside in endosomes. Maintaining appropriate conditions in the interior of these structures not only serves for appropriate ligand recognition by TLR3 [44] but also enables

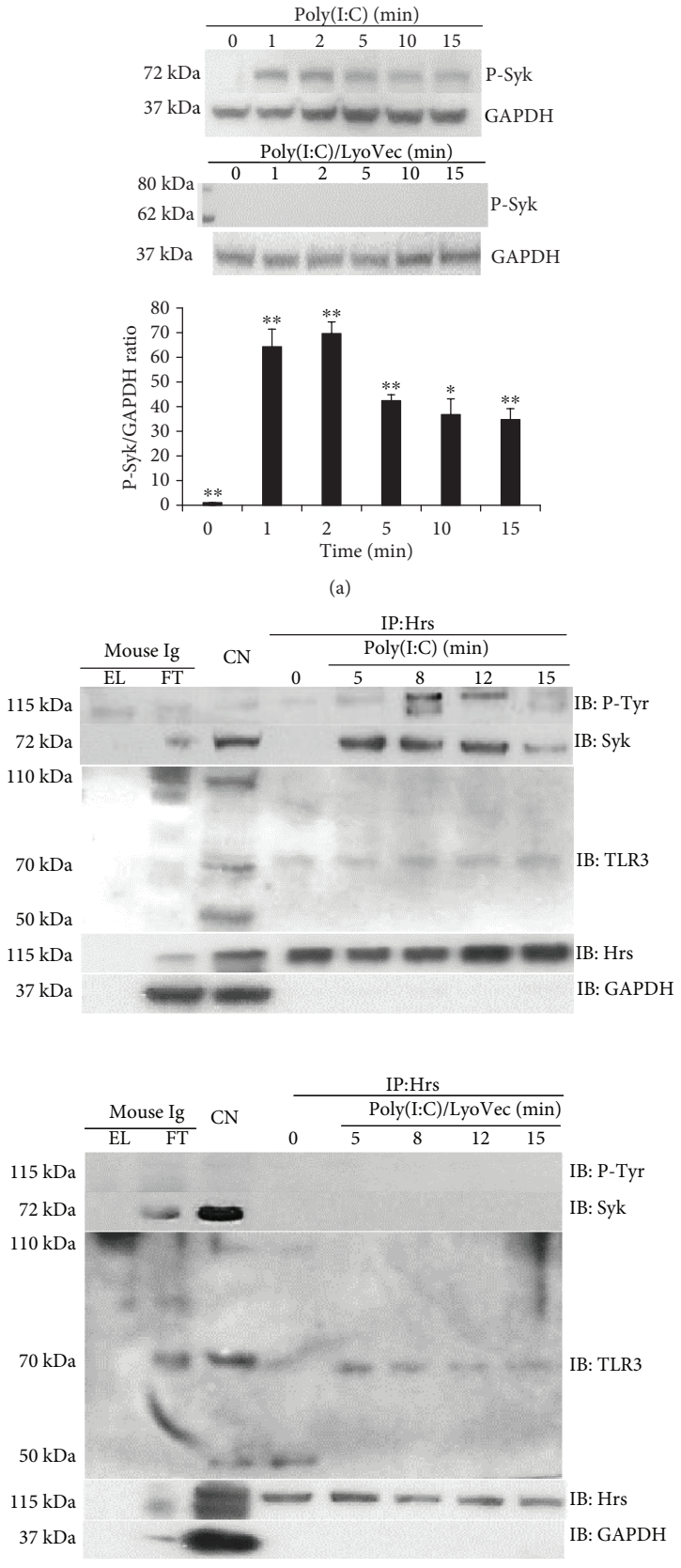

Figure 2: Continued.

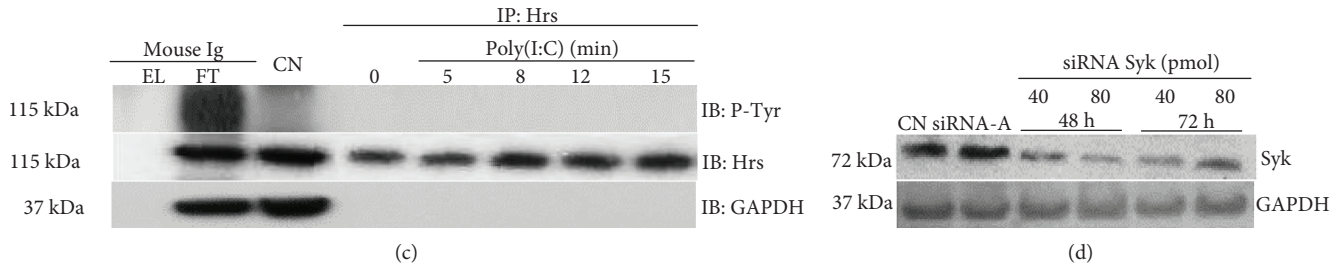

Figure 2: Poly(I:C) treatment of murine astrocytes induces Syk and Hrs phosphorylation and Syk-Hrs interaction. Hrs interacts with the N-terminal cleaved form of TLR3. (a) After poly(I:C) or poly(I:C)/LyoVec stimulation for 1, 2, 5, 10, and 15 min, the phosphorylation of Syk was analyzed by Western blot. The density level of phosphorylated Syk was normalized to GAPDH. Data was obtained from three independent experiments and presented as mean ± SD. $^{*}p \leq 0.05$ and $^{**}p \leq 0.01$. (b) After poly(I:C) or poly(I:C)/LyoVec stimulation for 5, 8, 12, and 15 min, C8-D1A cells were lysed and Hrs was immunoprecipitated using the anti-Hrs antibody. Phosphotyrosine (P-Tyr), Syk, and TLR3 were then detected by Western blot. (c) Following transfection with Syk siRNA, cells were stimulated with poly(I:C) for 5, 8, 12, and 15 min and lysed and Hrs was immunoprecipitated using the anti-Hrs antibody. Phosphotyrosine (P-Tyr) was detected by Western blot. For all immunoprecipitation experiments, 0 min presents untreated cells and mouse IgG were used as a negative control. EL: immunoprecipitation eluate; FT: immunoprecipitation flow-through; CN: control cell lysate. GAPDH was used as protein loading control. (d) Syk silencing efficiency was visualized by immunoblotting with anti-Syk antibodies.

cleavage by pH-dependent cysteine proteases—cathepsins B, H, L, and/or S [45, 46]. To evaluate whether astrocytic TLR3 responds to poly(I:C) treatment and undergoes proteolytic processing, we treated cells with poly(I:C) at different concentrations or with poly(I:C)/LyoVec (10 μg/ml) for various time intervals and performed western blot analysis with the antibodies directed against amino acid fragment localized at the N-terminus of the TLR3 protein. Figures 5(a)–5(d) show that in C8-D1A cells, the receptor occurs in full-length (TLR3 FL) and N-terminal (TLR3 N) progeny form. Demonstration of the TLR3 N was possible due to the use of the monoclonal TLR3 antibody recognizing amino acids 55-70 of the TLR3 protein. Further, the cleavage of TLR3 is dose-dependent (Figure 5(a)) and time-dependent (Figure 5(c)) upon stimulation with poly(I:C). A similar outcome was not observed in the case of astrocytes treated with poly(I:C)/LyoVec, where the dose (Figure 5(b)) and the time of stimulation (Figure 5(d)) did not affect the expression levels of both FL and N forms of TLR3. Western blot data largely agreed with the densitometric data showing statistically significant ($p \leq 0.05$) differences in amounts of cleaved TLR3 depending on dose (Figure 5(a)) and time (Figure 5(c)) of exposure of cells to the TLR3 agonist.

3.2. Expression of Syk and Hrs Is Upregulated upon Stimulation of Murine Astrocytes with Poly(I:C). Recent studies have reported that Syk may be an important controller of the immune receptor transportation and signaling [38, 47, 48] and that Hrs participates in the regulation of responses of multiple TLRs [27, 49]. Importantly, Hrs may contribute to protein cargo sorting as the HRS-STAM heteromer, homotypic hexamer [50], or in combination with subunits from other ESCRT complexes, e.g., with tumor susceptibility gene 101 (TSG101), the ESCRT-I component [51]. Therefore, we investigated if stimulation of astrocytes with the TLR3 ligand entails changes in the level of Syk, Hrs, and STAM expression, which could point to the potential role of these proteins in TLR3 immune modulation. Following TLR3 stimulation, Syk and Hrs expression was upregulated in a time-dependent manner (Figure 6(a)), and densitometric measurements showed highly statistically significant ($p \leq 0.01$) difference for Hrs. Similarly, following poly(I:C)/LyoVec treatment, the Hrs expression level also increased, but not to such a high level as following poly(I:C) treatment (Figure 6(b)). On the contrary, expression of Syk and STAM remained at a similar level throughout all stimulation time intervals with poly(I:C)/LyoVec (Figure 6(b)). We also observed a significant increase in the expression of Syk in response to treatment with increasing concentrations of poly(I:C), in contrast to Hrs (Figure 6(c)). All the studied proteins exhibited reduced expression level when astrocytes were treated with poly(I:C)/LyoVec at concentrations of 2 and 5 μg/ml, which could indicate that these proteins may not participate in MDA5 signaling in murine C8-D1A cells (Figure 6(d)). Interestingly, no significant differences in STAM expression were observed, either after poly(I:C) treatment of astrocytes with various concentrations or at different time courses (Figures 6(a) and 6(c)). Similar results were observed in STAM expression, after stimulation of cells with poly(I:C)/LyoVec (Figures 6(b) and 6(d)).

3.3. Distribution of TLR3 and STAM Is Altered upon Poly(I:C) Stimulation of Murine Astrocytes. To study whether the observed changes have a reflection in protein distribution at the cellular level following stimulation and thus better understand the connection between TLR3, ESCRT-0, and Syk in astrocytes, we examined the localization of TLR3, Syk, Hrs, and STAM in C8-D1A cells stimulated with poly(I:C) (10 μg/ml) for 5 min, 4 h, and 24 h. We chose such a time scale to show that the posttranslational modifications of Syk and Hrs that occur within the first half hour after TLR3 stimulation are not significantly related to the change in their distribution. Consequently, noticeable modification in the arrangement of TLR3 and STAM was found at 4 h and 24 h after the addition of poly(I:C) (Figures 7(a) and 7(b)). Our findings indicate that TLR3, STAM, Syk, and Hrs are highly expressed in murine astrocytes (Figures 7(a)–7(d)). To

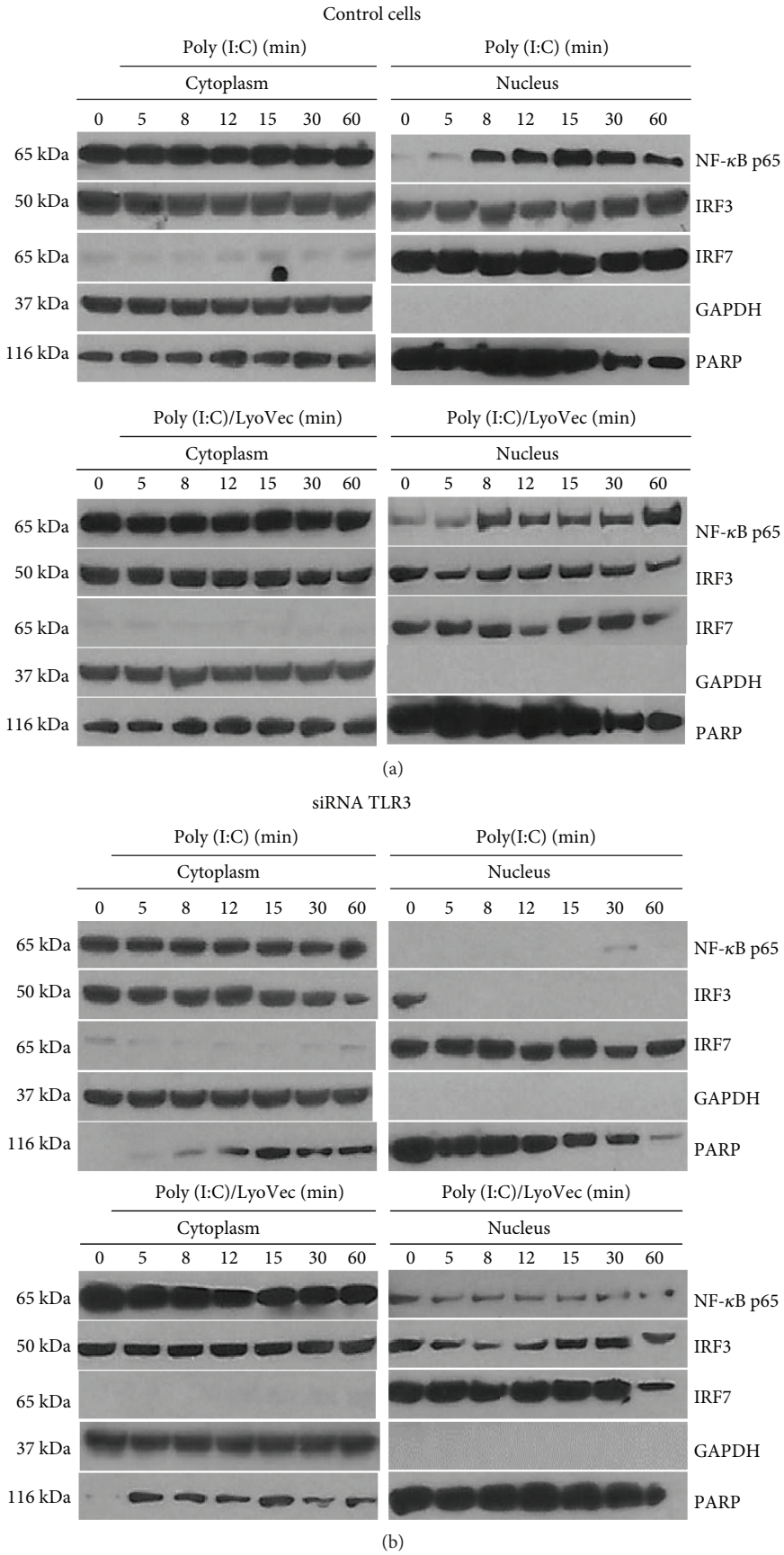

Figure 3: Continued.

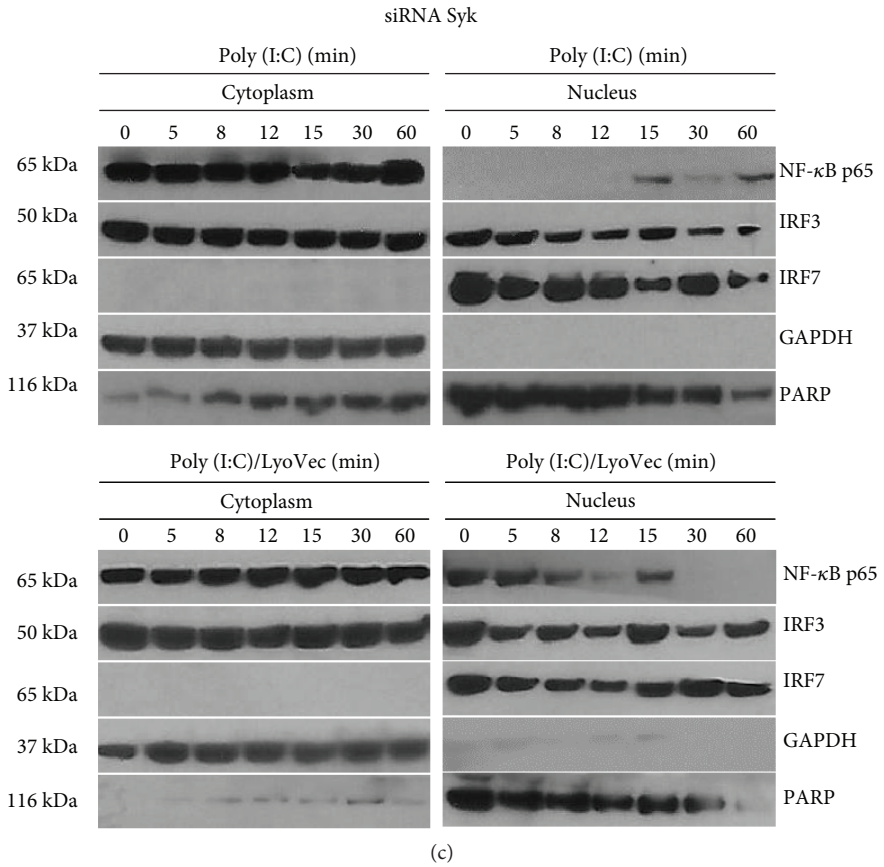

(c)

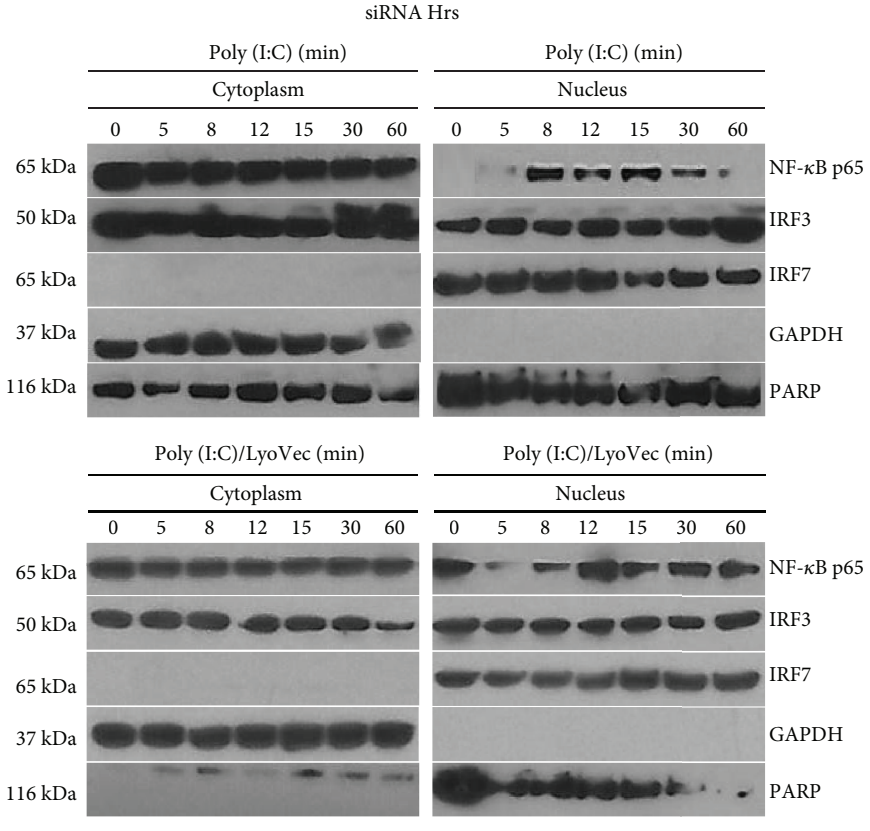

(d)

Figure 3: Continued.

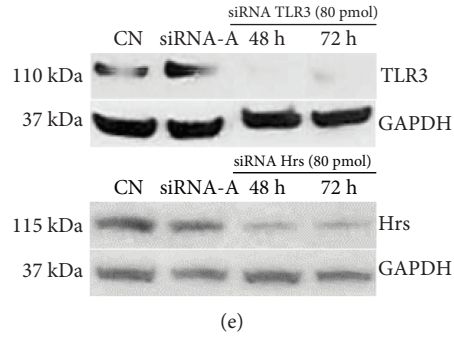

Figure 3: NF-κB nuclear translocation is downregulated in poly(I:C)-treated astrocytes with silenced Syk and Hrs. C8-D1A cells were untreated or treated with poly(I:C) or poly(I:C)/LyoVec for 5 min, 8 min, 12 min, 15 min, 30 min, and 60 min. In advance to the stimulation, astrocytes were not transfected (a) or transfected with siRNA pools for TLR3 (b), Syk (c), and Hrs (d). Following poly(I:C) or poly(I:C)/LyoVec treatment, cytoplasmic and nuclear extracts were immunoblotted with anti-NF-κB p65, -IRF3, -IRF7, -GAPDH, and -PARP antibodies. (e) TLR3 and Hrs silencing efficiency was visualized by immunoblotting with anti-TLR3 and -Hrs antibodies.

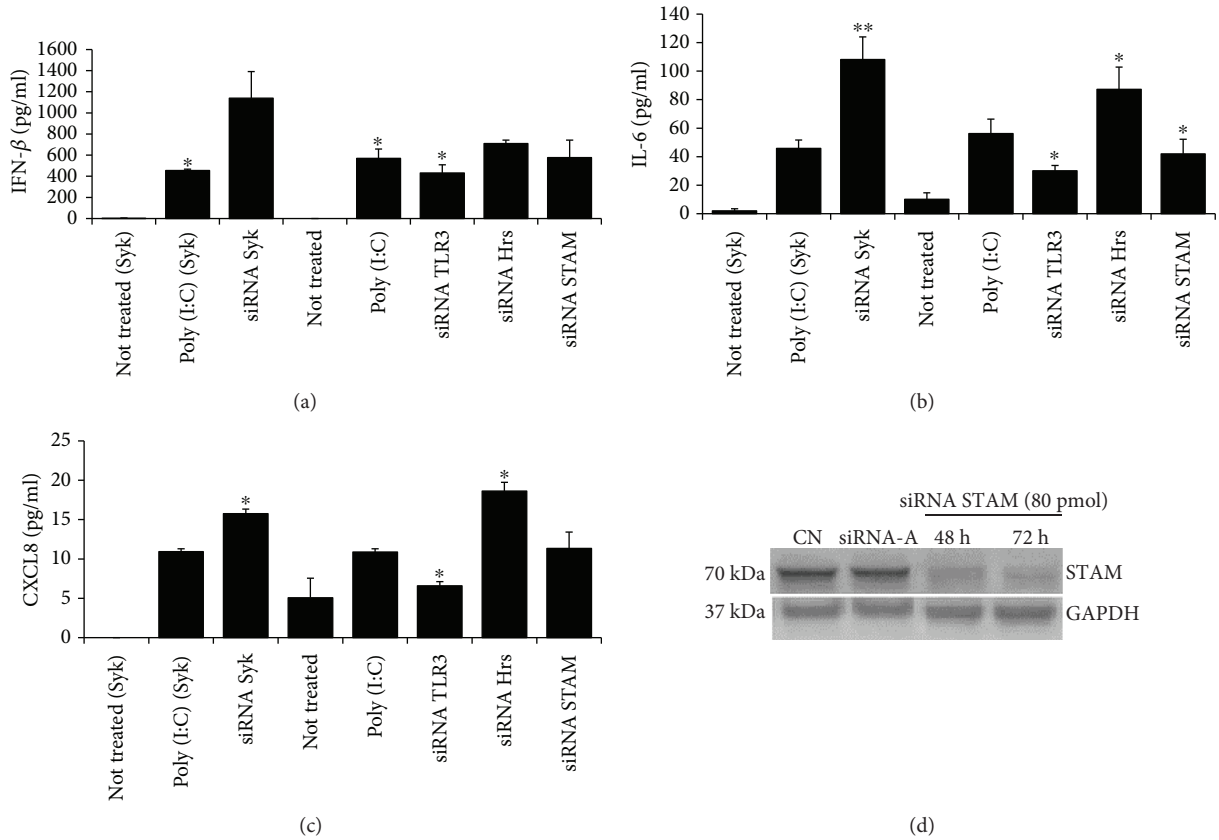

Figure 4: Knockdown of Syk and Hrs expression by siRNA upregulates poly(I:C)-induced IFN-β, IL-6, and CXCL-8 production. C8-D1A cells were transfected with control siRNA-A or siRNA pools for TLR3, Syk, Hrs, and STAM. Following the transfection, astrocytes were treated with poly(I:C) (10 μg/ml) for 24 h. IFN-β (a), IL-6 (b), and CXCL-8 (c) were measured in culture supernatants by ELISA. Because Syk transfection lasted 48 h, in each experiment, supernatants from untreated (not treated (Syk)), poly(I:C)-treated (poly(I:C) (Syk)), and poly(I:C)-treated cells with silenced Syk (siRNA Syk) were tested in the group independent from cells with silenced TLR3, Hrs, and STAM, where transfection lasted 72 h. (d) STAM silencing efficiency was visualized by immunoblotting with anti-STAM antibodies. Data was obtained from three (IFN-β, CXCL-8) or five (IL-6) independent experiments and presented as mean ± SD. $^{*}p \leq 0.05$ and $^{**}p \leq 0.01$.

validate the colocalization of TLR3 and STAM with ER, we performed staining of the ER with the anti-protein disulfide isomerase (anti-PDI) antibody (Figures 7(e) and 7(f)). TLR3 and STAM exhibited distinct distribution patterns in indicated time courses of poly(I:C) stimulation. In nontreated cells (resting cells), TLR3 was localized near the cell nucleus, most likely in the ER, whereas after stimulation it gradually dispersed until it was evenly distributed throughout the cell

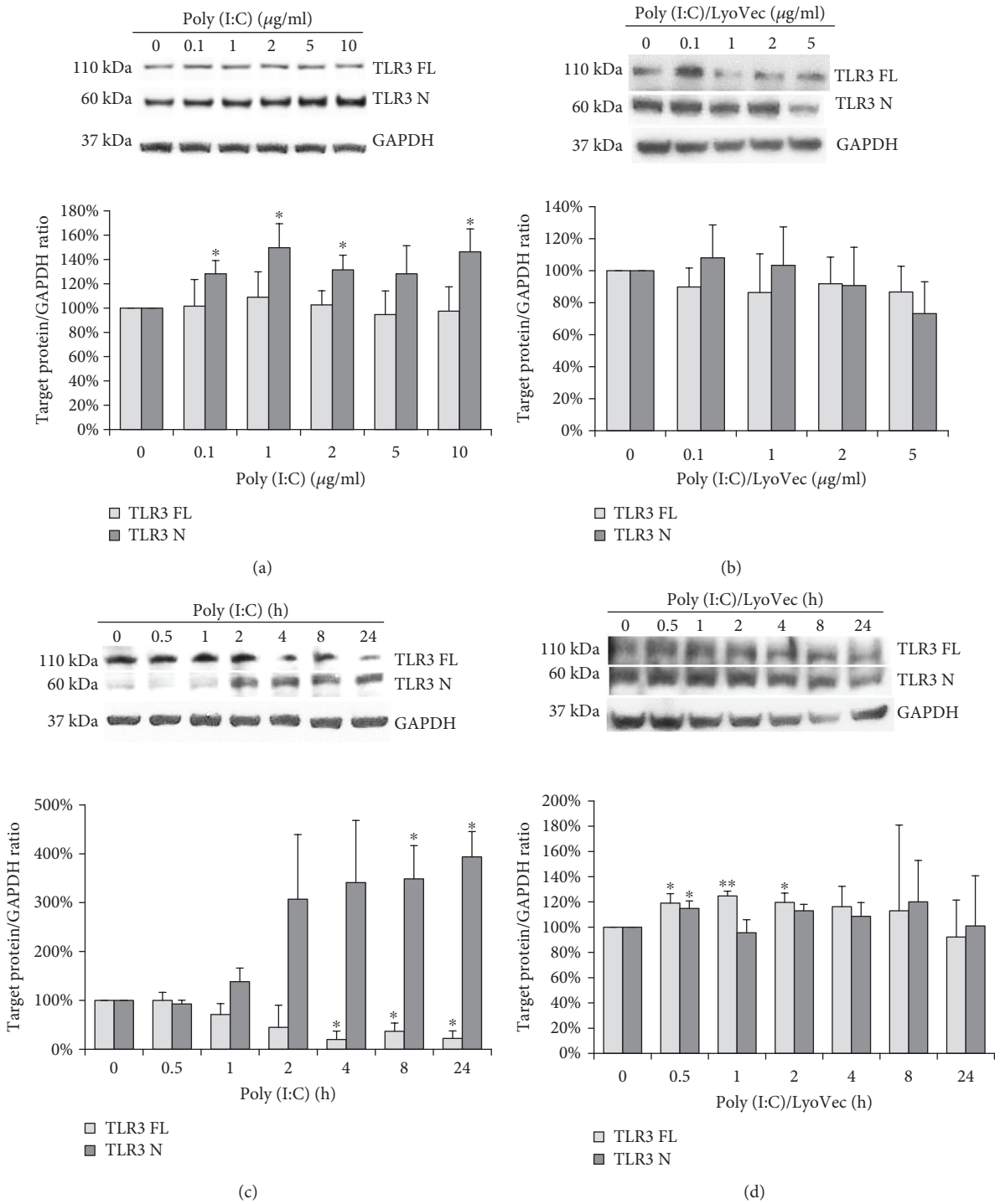

Figure 5: TLR3 of murine astrocytes is cleaved upon stimulation of cells with poly(I:C). Representative western blots of TLR3 expression in C8D1A cells treated with various concentrations of poly(I:C) (0, 0.1, 1, 2, 5, and 10 μg/ml) (a) or poly(I:C)-LyoVec (0, 0.1, 1, 2, and 5 μg/ml) (b) and lysed 24 h after stimulation. TLR3 expression was also analyzed in cells treated with poly(I:C) at concentration 10 μg/ml (c), or with poly(I:C)-LyoVecat concentration 1 μg/ml (d), and lysed at various times of stimulation (0, 30 min, 1 h, 2 h, 4 h, 8 h, and 24 h). TLR3 FL: full-length TLR3; TLR3 N: cleaved N-terminal TLR3 form; GAPDH: protein loading control. Densitometry analysis of TLR3 forms was performed in cells treated with indicated poly(I:C) concentrations for 24 h (a), indicated poly(I:C)/LyoVecconcentrations for 24 h (b), 10 μg/ml poly(I:C) for indicated time points (c), or 1 μg/ml poly(I:C)/LyoVec for indicated time points (d). The density level of each protein was normalized to GAPDH. Data was obtained from three independent experiments and presented as mean ± SD. $^{*}p \leq 0.05$ and $^{**}p \leq 0.01$.

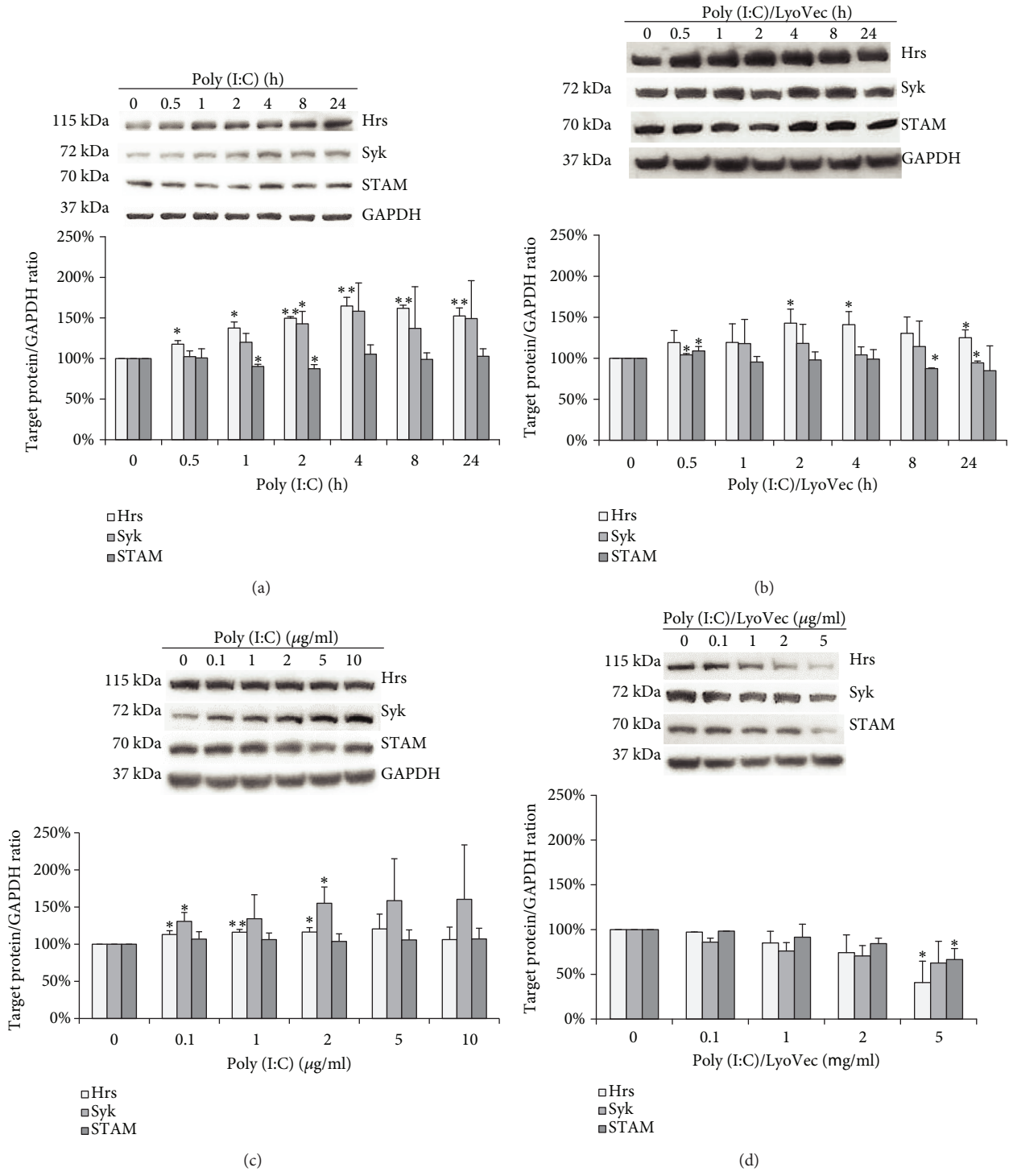

Figure 6: Stimulation of murine astrocytes with poly(I:C) leads to the time-dependent increase in Syk and Hrs expression, while the expression of STAM does not significantly change after stimulation of cells with the TLR3 ligand. Representative western blots of Hrs, Syk, and STAM expression in C8D1A cells treated with various concentrations of poly(I:C) (0, 0.1, 1, 2, 5, and 10 μg/ml) (a), or poly(I:C)-LyoVec (0, 0.1, 1, 2, and 5 μg/ml) (b), and lysed 24 h after stimulation. Hrs, Syk, and STAM expression was also analyzed in cells treated with poly(I:C) at concentration 10 μg/ml (c), or with poly(I:C)-LyoVecat concentration 1 μg/ml (d), and lysed at various times of stimulation (0, 30 min, 1 h, 2 h, 4 h, 8 h, and 24 h). GAPDH was used for evaluating protein loading control. Densitometry analysis of Hrs, Syk, and STAM was performed in cells treated with indicated poly(I:C) concentrations for 24 h (a), indicated poly(I:C)/LyoVecconcentrations for 24 h (b), 10 μg/ml poly(I:C) for indicated time points (c), or 1 μg/ml poly(I:C)/LyoVec for indicated time points (d). The density level of each protein was normalized to GAPDH. Data was obtained from three independent experiments and presented as mean ± SD. $^{*}p \leq 0.05$ and $^{**}p \leq 0.01$.

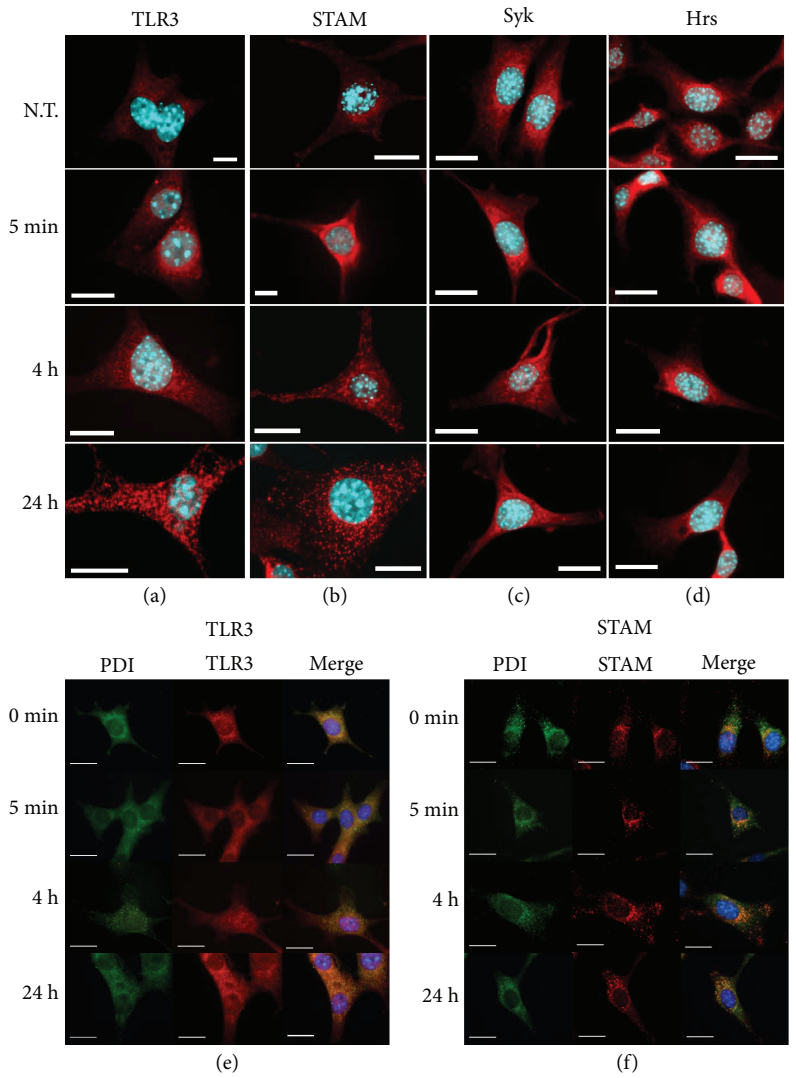

Figure 7: Immunostains of TLR3, Syk, Hrs, and STAM expression and localization in C8D1A cells after treatment with poly(I:C). C8-D1A murine astrocytes were not treated or treated with poly(I:C) (10 μg/ml) for 5 min, 4 h, and 24 h, fixed and immunostained with specific antibodies. Selected images present intracellular distribution of TLR3 (a), Syk (b), Hrs (c), and STAM (d) (red fluorescence). To visualize colocalization of ER with TLR3 or STAM, following poly(I:C) stimulation at the indicated time points, cells were double stained with anti-TLR3 (red) and anti-PDI (green) antibodies (e), or with anti-STAM (red) and anti-PDI (green) antibodies (f). Nuclear DNA was stained with Hoechst 33342 (blue fluorescence). Scale bar = 10 μm, N.T. = no treatment.

following 24 h of poly(I:C) treatment (Figures 7(a) and 7(e)). Similarly, the majority of STAM was present in the perinuclear region in untreated cells, whereas in poly(I:C)-stimulated cells, the longer the duration of stimulation, the larger the dispersion and abundance of the protein vesicles was observed (Figures 7(b) and 7(f)). We observed a similar distribution of Syk and Hrs in untreated cells and cells stimulated with poly(I:C) (Figures 7(c) and 7(d)); most of the proteins were located near the nucleus, while part was dispersed in the cytoplasm.

3.4. Stimulation of Cells with the TLR3 Ligand Promotes Syk Activation and Leads to Syk-Hrs Interaction, Tyrosine Phosphorylation of Hrs, and Hrs Interaction with the N-Terminal Cleaved Form of TLR3. Knowledge regarding factors that contribute to the activation of Syk in TLR signaling still needs to be broadened; however, it has been indicated that TLR ligands are capable of inducing Syk activation [52]. Furthermore, it has been demonstrated that Hrs is the target of Syk activity during high-affinity IgE receptor (FcεRI) endocytosis and that Syk orchestrates Hrs intracellular localization—cytosolic Hrs is ubiquitinated, while Hrs phosphorylation leads to the transfer of Hrs to the membrane compartments [39]. Here, we demonstrate that poly(I:C) stimulation of astrocytes leads to rapid phosphorylation of Syk, which appears at 1 min and peaks at 2-5 min following TLR3 stimulation (Figure 2(a)). Western blot data corresponded with the densitometric analysis where the highest level of Syk phosphorylation was observed 1-2 min after the addition of poly(I:C) (Figure 2(a)). Such a result is consistent with the work of Cao et al. [53], where phosphorylation of the Tyr-346 residue of Syk was detected

at 1 min, and a maximal Syk phosphorylation increase was observed at 5 min poststimulation of FcεRI in MCP5 cells. We have not observed Syk phosphorylation after the addition of poly(I:C)/LyoVec to the cells (Figure 2(a)). To investigate whether Syk could associate with Hrs, lysates from astrocytes stimulated or unstimulated with poly(I:C) for the indicated time points were subjected to immunoprecipitation with anti-Hrs antibody and probed with anti-Syk antibody. In the fifth minute after the addition of the TLR3 ligand, we detected an interaction of Syk and Hrs (Figure 2(b)), which peaked between 5 and 12 min and decreased within 15 min of stimulation, whereas such interaction did not occur after the addition poly(I:C)/LyoVec to the cells (Figure 2(b)). A similar result was observed after FcεRI activation, where the Syk-Hrs interaction was maximal at 5 min and decreased to near-baselinewithin 20 min of stimulation [39]. Next, we evaluated whether Hrs may serve as a substrate for Syk-mediated phosphorylation. Lysates from unstimulated or poly(I:C)-stimulated astrocytes were subjected to immunoprecipitation with anti-Hrs antibody and probed with anti-phosphotyrosine antibody. Stimulation of cells with poly(I:C) resulted in tyrosine phosphorylation of Hrs (Figure 2(b)). Importantly, Hrs phosphorylation peaked at 5-12 min following the addition of poly(I:C), which is consistent with the peak of the Syk-Hrs interaction. Hrs phosphorylation was undetectable in cells stimulated with poly(I:C)/LyoVec (Figure 2(b)). We did not observe phosphorylation of Hrs after the addition of poly(I:C) to the cells treated with siRNA against Syk (Figure 2(c)), indicating that Syk may be the crucial kinase responsible for Hrs modification. Furthermore, following immunoprecipitation of astrocytic lysates with anti-Hrs antibody and immunoblotting with antibody recognizing amino acids at the N-terminal part of TLR3, we observed that the TLR3 N-terminal progeny form interacts in increasing amounts with Hrs following poly(I:C) stimulation (Figure 2(b)).

3.5. Poly(I:C) Treatment of Murine Astrocytes Induces TLR3 Tyrosine Phosphorylation and Promotes Interaction with Hrs. Previous studies have identified Hrs as the protein that directly interacts with TLRs such as TLR2, TLR4, TLR7, and TLR9 [27, 32, 49]. To investigate whether Hrs associates with TLR3, lysates from astrocytes unstimulated or stimulated with poly(I:C) were subjected to immunoprecipitation with anti-TLR3 antibody. Probing of the immunoblot with anti-Hrs antibody showed that Hrs bound to TLR3 in nonstimulated cells. However, an increasing proportion of Hrs associated with TLR3 in a time-dependent manner (Figure 8(a)) in poly(I:C) stimulated cells. A similar result was observed in the case of TLR4, the receptor constitutively associated with Hrs, and the interaction increased after TLR4 stimulation [32]. Following poly(I:C)/LyoVec cell stimulation, only a small amount of Hrs was associated with TLR3 (Figure 8(a)). Similarly, following TLR3 immunoprecipitation, we probed immunoblots with anti-STAM antibody and determined whether the second ESCRT-0 subunit interacts with TLR3. Interestingly, we did not observe any interaction between TLR3 and STAM, either following poly(I:C) or poly(I:C)/LyoVec stimulation of astrocytes (Figure 8(a)). Furthermore, we wanted to address if poly(I:C) induces TLR3 ubiquitination. By probing western blots of immunoprecipitated TLR3 with anti-ubiquitin antibody, we showed that TLR3 is similarly ubiquitinated in C8-D1A cells treated with poly(I:C) or poly(I:C)/LyoVec (Figure 8(b)). Such modification of TLR3 may condition the interaction with ubiquitin-binding molecules, e.g., Hrs. Because ubiquitin ligases are known to interact with tyrosine-phosphorylated proteins, we examined the level of TLR3 phosphorylation in nonstimulated and poly(I:C)-stimulated cells. Phosphorylation of the receptor was observed 8 min after the addition of poly(I:C) and later (Figure 8(a)), which may indicate that TLR3 modification such as ubiquitination is not fully dependent on the receptor's phosphorylation. Finally, we investigated whether Hrs-STAM interaction may be promoted by stimulation of cells with poly(I:C). While the majority of the Hrs cellular pool remained unassociated with STAM, the greater part of STAM interacted with Hrs in a time-dependent manner following TLR3 stimulation (Figure 8(c)). Such a result indicates that Hrs may not reside in the same cellular localization as STAM; however, the addition of poly(I:C) may foster interaction between these proteins.

3.6. Changes in the Intracellular Localization of NF-κB, IRF3, and IRF7 in TLR3-, Syk-, and Hrs-Depleted Astrocytes following TLR3 Stimulation. After describing molecular interactions between Syk and Hrs, as well as TLR3, Syk, and Hrs posttranslational modifications following poly(I:C) stimulation of C8-D1A cells, we investigated the role of Syk and Hrs in poly(I:C)-induced NF-κB, IRF3, and IRF7 nuclear translocation. Following the addition of poly(I:C) to the control cells, we observed translocation of NF-κB and IRF3 to the nucleus (Figure 3(a)). In contrast, NF-κB and IRF3 did not accumulate in the nucleus of TLR3-depleted cells stimulated with poly(I:C) (Figure 3(b)). Furthermore, NF-κB nuclear translocation was downregulated in poly(I:C)-treated astrocytes with knocked-down Syk, and shortage of Syk also appeared to minimally affect nuclear translocation of IRF3 in C8-D1A cells (Figure 3(c)). In Hrs-depleted cells NF-κB activation was reduced to a certain extent after stimulation with poly(I:C), whereas translocation of IRF3 to the nucleus remained intact in comparison to the control cells (Figure 3(d)). Interestingly, the amount of IRF7 localized in the nucleus was similar throughout the duration of poly(I:C) or poly(I:C)/LyoVec stimulation, and its physiological level was also observed in the nontreated cells (0 min time point, Figures 3(a)–3(d)).

3.7. A Role for Syk, Hrs, and STAM in the Regulation of TLR3 Signaling. To verify the influence of Syk, Hrs, and STAM knockdown on the response of C8-D1A cells to TLR3 ligand stimulation, we transfected astrocytes with the specific siRNAs and subsequently activated the cells with poly(I:C). Following cell stimulation, secreted IFNβ, IL-6, and CXCL8 were quantified by ELISA. In Syk-knockdown cells, poly(I:C) significantly increased secretion of IFNβ ($p \leq 0.05$), IL-6 ($p \leq 0.01$), and CXCL8 ($p \leq 0.05$) compared to poly(I:C)-stimulated cells without Syk depletion (Figures 4(a)–4(c)).

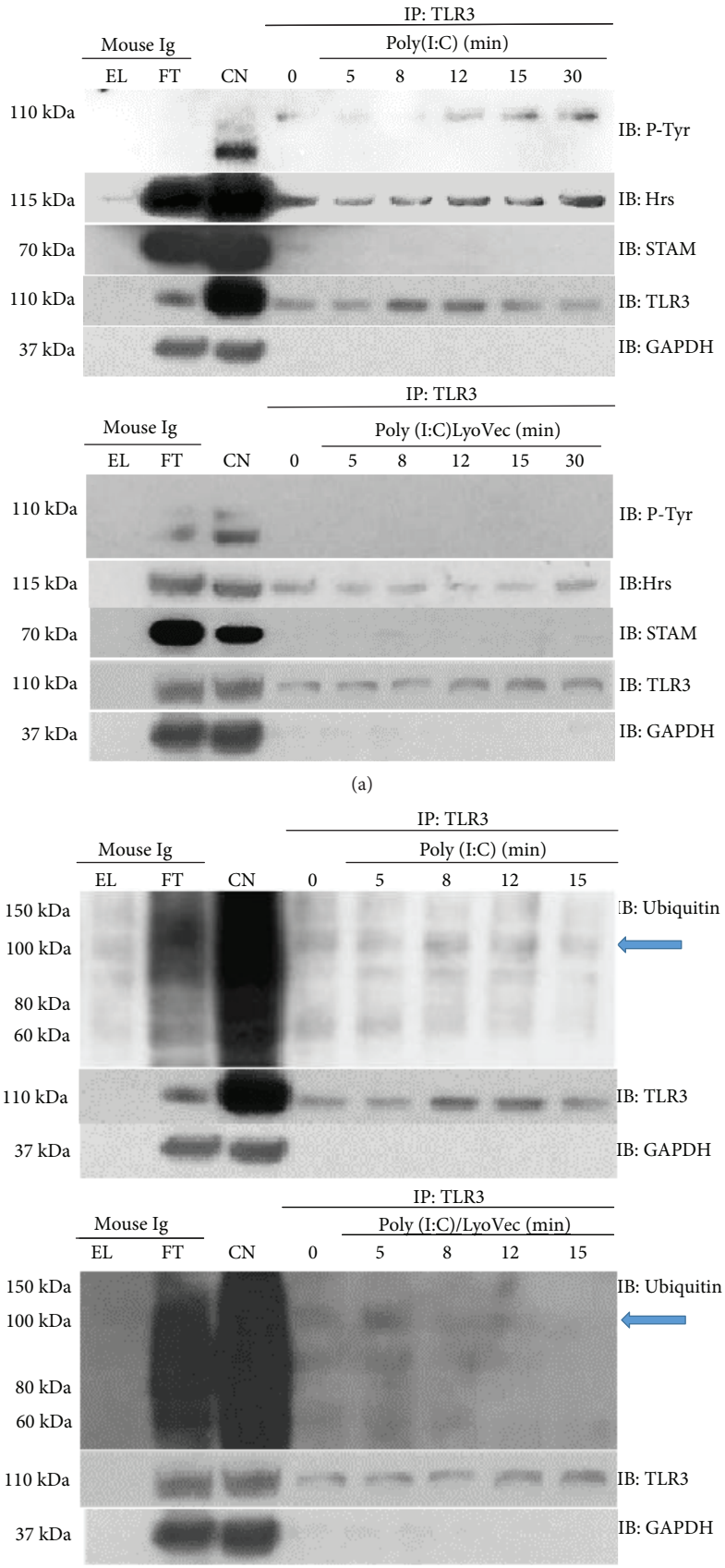

Figure 8: Continued.

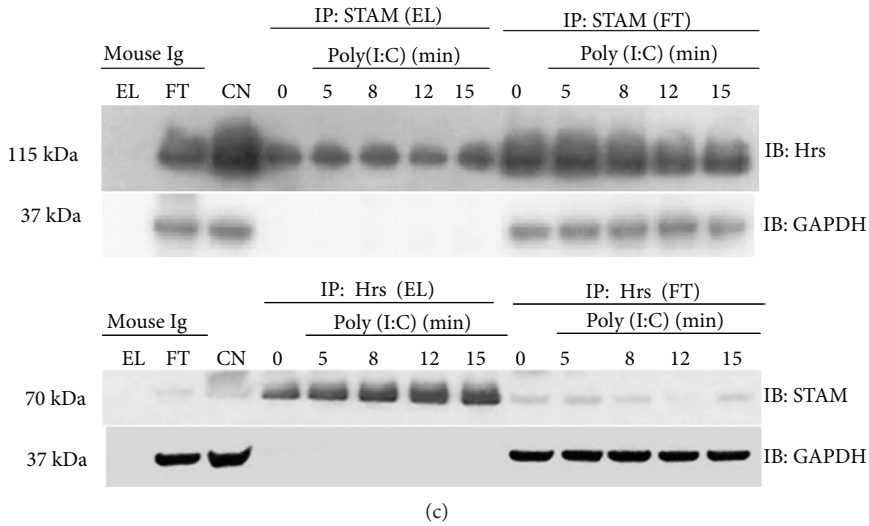

(c)

Figure 8: Poly(I:C) treatment of murine astrocytes induces TLR3 tyrosine phosphorylation and promotes interaction with Hrs. (a) After poly(I:C) or poly(I:C)/LyoVec stimulation for 5, 8, 12, 15, and 30 min, C8-D1A cells were lysed and TLR3 was immunoprecipitated using the anti-TLR3 antibody. Phosphotyrosine (P-Tyr), Hrs, and STAM were then detected by Western blot. (b) Following poly(I:C) or poly(I:C)/LyoVec stimulation for 5, 8, 12, andn 15 min, C8-D1A cells were lysed and TLR3 was immunoprecipitated using the anti-TLR3 antibody. Ubiquitin was detected by Western blot. Blue arrows indicate ubiquitinated TLR3. (c) Following poly(I:C) stimulation for 5, 8, 12, and 15 min, murine astrocytes were lysed and STAM and Hrs were immunoprecipitated using anti-STAM and anti-Hrs antibodies, respectively. Hrs and STAM were detected by Western blot. For all immunoprecipitation experiments, 0 min presents untreated cells and mouse IgG were used as a negative control. EL: immunoprecipitation eluate; FT: immunoprecipitation flow through; CN: control cell lysate. GAPDH was used as protein loading control.

Knockdown of Hrs in C8-D1A cells significantly enhanced poly(I:C)-dependent induction of IFN-β, IL-6, and CXCL8 secretion ($p \leq 0.05$), while levels of IFNβ and CXCL8 in STAM-depleted cells stimulated with poly(I:C) were not significantly different from those in poly(I:C)-treated controls, apart from IL-6 ($p \leq 0.05$) (Figures 4(a)–4(c)). Collectively, these results indicate that Syk and Hrs are involved in TLR3-mediated signaling events. Because Syk and Hrs knockdown results in the increase of IFN-β, IL-6, and CXCL8 secretion, Syk and Hrs may serve to regulate TLR3-mediated immune response in intact astrocytes.

4. Discussion

In our study, we reveal that astrocytic TLR3 undergoes proteolytic processing and that the expression of TLR3 N increases in proportion to the poly(I:C) dose and length of exposure. Presentation of TLR3 in such a manner may modulate the level of response to viral dsRNA, especially in CNS cells. For example, such TLR3 form may constitute a negative regulator of signaling, as found for TLR9 [54], but this requires further investigation. TLR3 present in mammalian cells has a size of approximately 110 kDa; however, cleaved TLR3 molecules have been shown to remain associated and are also capable of binding the TLR3 ligand [55, 56]. Such TLR3 configuration may represent the primary form of the receptor, and it is possible that the cleavage is aimed at actuating the novel receptor attributes, other than separation of the two progeny fragments. Conclusions from previous studies on the role of TLR3 cleavage are ambiguous. Proteolytic processing of TLR7 or 9 by cathepsins is required for signaling; however, TLR3 cleavage may not determine the activation of the immune response [57]. The addition of the cathepsin inhibitor or mutation at the TLR3 cleavage site did not influence TLR3 response to poly(I:C) in 4 cell lines, although inhibition of cleavage decreased the abundance of the receptor to be degraded in lysosomes [46]. On the other hand, TLR3 cleavage was indispensable for the receptor activation in murine RAW cells [58]. Zhang et al. [59] linked mutation situated in the region of the TLR3 cleavage and critical for dsRNA binding (P554S) in a patient suffering from HSE with the loss of TLR3 function in CNS cells and increased penetrance of the disease through insufficient antiviral response. This highlights the importance of proper TLR3 cleavage and its possible influence on ligand recognition and activation of the signaling pathway.

Hrs and STAM are components of the ESCRT-0 transportation complex; however, they also function as separate proteins, e.g., Hrs bound in the membrane occurs partly as a monomer and partly as a form associated with STAM [50]. Hrs appears to be only partially involved in cooperation with STAM in C8-D1A cells not stimulated or stimulated with poly(I:C) (Figure 8(c)), and we did not observe any significant differences in the TLR3-mediated immune response level following STAM depletion (Figures 4(a)–4(c)). This indicates that after TLR3 activation in astrocytes, Hrs may interact with proteins from complexes other than ESCRT-0. ESCRT-0 subunits, alone or in combination with other proteins, may moonlight in manifold activities; e.g., Hrs in cooperation with the product of tumor susceptibility gene 101 (*TSG101*), an ESCRT-I subunit, leads to the endocytic downregulation of EGFR [51]. This protein is a tyrosine kinase responsible for the phosphorylation of Tyr858 of TLR3, a modification indispensable for the recruitment of TRIF

[36]. Silencing of Hrs, resulting in the reduced degradation of EGFR and concomitantly increased activatory influence on TLR3, could manifest in an increase of TLR3-mediated innate response to poly(I:C) and possibly viral dsRNA. Furthermore, we have demonstrated that TLR3 interacts with Hrs, which may have a direct influence on the fate of the receptor. Hrs may be involved in directing TLR3 N to the degradative pathway, as is the case with various cell membrane receptors. This, particularly, appears likely because IFNβ, IL-6, and CXCL8 secretion following knockdown of Hrs was higher compared to cells with intact Hrs. In the noncanonical ESCRT-0 pathway, which does not engage MVBs or lysosomes, Hrs has been implicated in targeting of ubiquitinated TLR9 and TLR7 to endosomes for ligand recognition. Furthermore, Hrs silencing blocked the nuclear transportation of NF-κB p65 and reduced the level of TNFα and IFNα secretion following TLR9 stimulation [27]. We performed a similar experiment to examine NF-κB activation in the astrocytes with the knockdown of Hrs. Following TLR3 stimulation, NF-κB exhibited reduced but not abolished transportation to the cell nucleus. However, we did not observe a significant influence of Hrs knockdown on the nuclear accumulation of IRF-3 or IRF-7, suggesting that Hrs neither is a key moderator nor participates in signaling steps leading to the intracellular transfer of these transcription factors. Furthermore, knockdown of Syk and Hrs in C8-D1A cells increased TLR3-dependent IFNβ, IL-6, and CXCL8 secretion following stimulation with poly(I:C). This suggests that Syk and Hrs participate in TLR3-mediated innate response to dsRNA; however, it is likely that Hrs potentially engages in the signaling events not related to TLR3 endosomal trafficking aimed at ligand detection, as in the case of TLR7 and TLR9. Syk may play a dual role in TLR4 activation by promoting the signaling through mediation of endocytosis or inhibiting signaling from the plasma membrane [60], similar to Hrs, which supports contradictory cellular events leading to degradation or recycling of numerous receptors. Following LPS sensing, ubiquitinated TLR4 interacts with Hrs on the way to degradation in lysosomes and it is possible that other cell surface TLRs are trafficked in the analogous manner [32]. It should be noted that although we were unable to acquire complete silencing of Syk, the knockdown achieved was adequate to affect Hrs phosphorylation, NF-κB nuclear translocation, or IFNβ, IL-6, and CXCL8 secretion. We speculate that deprivation of the cells of the vast majority of Syk is sufficient to prevent Hrs phosphorylation, which may indicate Syk as the key protein responsible for Hrs activation. Therefore, the shortage in Syk followed by lack of Hrs phosphorylation may be reflected in subsequent cellular events associated with TLR3 signaling.

Posttranslational modifications play important roles in the regulation of Hrs activity, and Hrs phosphorylation has been proven to correlate with EGFR degradation [33]. Interestingly, astrocytes exhibited phosphorylation of a small proportion of the cellular pool of Hrs (Figure 2(b)), which is consistent with the Hrs phosphorylation level observed downstream of EGFR activation by Stern et al. [33]. If Hrs was implicated in retaining of degradative transportation of TLR3, the depletion of Syk and Hrs would open the possibility of prolonged TLR3 recruitment in the signaling cycle. It is highly probable that following viral dsRNA-mediated stimulation of astrocytes, concurrent with endosomal trafficking, ligand recognition, and execution of the TLR3 signaling cascade, a process leading to ligand-induced degradation of the receptor is initiated with the aim of modulating and maintaining the proinflammatory response at an adequate level.

Indirect immunofluorescence analysis revealed that TLR3 and STAM exhibited distinct staining patterns at different time courses after poly(I:C) stimulation (Figures 7(a) and 7(b)). STAM was found to colocalize with ER, Golgi, and endosomal markers and participate in the reconstruction and restoration of the Golgi structure [28]. Owing to the VHS domain, STAM may interact with the Golgi-localizing proteins and participate in protein sorting at the *trans*-Golgi network [61, 62]. Thus, the distribution pattern of STAM observed after poly(I:C) stimulation may reflect its functions related to intracellular TLR3 trafficking; however, this requires further investigation. Another unique attribute of STAM is the diphosphorylated immune tyrosine activation motif (ITAM) [63], the distinctive sequence found in the cytoplasmic subunits of B and T cell receptors, as well as Fc receptors. Upon phosphorylation, ITAM serves as a ligand for SH2 domains of various cytoplasmic tyrosine kinases, e.g., Syk. Following docking at ITAM, kinase undergoes conformational changes, resulting in autophosphorylation of the Syk catalytic domain. Such an event increases Syk enzymatic activity and leads to propagation of downstream signaling [64, 65]. We used specific anti-Syk mouse (pY342) antibodies to confirm that conserved tyrosine Y-342 in the Syk SH-2 linker region was phosphorylated following TLR3 activation (Figure 2(a)). Mutation of this particular tyrosine residue alone was found to diminish Syk ability to interact with other proteins, while a concomitant mutation in Y-346 induced a significant reduction in FcεRI-mediated signaling [66]. Lin et al. [52] confirmed that stimulation with poly(I:C) led to the activation of Syk in bone marrow-derived macrophages (BMDM) and RAW.264.7 macrophages; however, phosphorylation of the kinase was detected 15 min after stimulation of the cells. We have shown that Syk undergoes rapid phosphorylation and associates with Hrs after poly(I:C) stimulation of astrocytes (Figures 2(a) and 2(b)); however, it cannot be precluded that such interaction occurs with the participation of other proteins. Further, studies are necessary to confirm whether STAM may associate with the phosphorylated SH-2 domain of the Syk *via* its ITAM region, although the ITAM-independent pathway may underlay Syk-Hrs interaction.

The possibilities where Syk may affect TLR responses are manifold; in this work, we addressed the ways in which Syk could influence TLR3 signaling and cytokine responses in cells of brain origin. Syk may play reverse roles in mediating TLR-dependent responses by opposingly regulating the ubiquitination of TRAF3 or TRAF6 [60]. Furthermore, Syk might inhibit MyD88-dependent production of proinflammatory cytokines and augment the TRIF-dependent expression of IFN-dependent genes. Despite the fact that Syk-mediated TRIF phosphorylation leads to TRIF

proteasomal degradation resulting in downregulation of TLR signaling [38], phosphorylation of this adaptor protein is critical for the activation of the type I IFN pathway [67]. Thus, the observed restriction of NF-κB nuclear localization in the absence of Syk (Figure 3(c)) appears to correspond with insufficient activatory influence on the TRIF phosphorylation [67]. Most recently, preclinical and clinical studies highlight pharmacological inhibitors of Syk as promising drug targets, due to their inhibitory influence on the inflammatory responses [52, 68, 69]. Nevertheless, some studies present contradictory findings—Syk deficient cells exhibit higher proinflammatory response than do wild-type cells [70, 71], and such a relationship has been pointed out for Syk-dependent inhibition of TLR signaling [38]. Our data distinguish Syk as the balancing component in TLR3-mediated immune response, intended to avoid unstrained production of inflammatory factors.

TLR3 expression may be modulated by proinflammatory molecules that are upregulated in various neurodegenerative disorders [72]. Recently, the essential role of astrocytes was highlighted in the course of such neurodegenerative diseases as multiple sclerosis (MS), amyotrophic lateral sclerosis (ALS), AD, Parkinson's disease (PD), and HIV-1 associated dementia (HAD) [73–77].

Importantly, recent reports explore and confirm the possible role of HSV-1 infection in the pathogenesis of the most common form of dementia—AD [78, 79]. Therapies targeting glial cells might benefit the cells affected by neurodegenerative disorders. There is good support for the hypothesis that Aβ secreted by cells may constitute an antimicrobial protein (AMP) and astrocytes may produce it as an essential defensive component of the innate immunity [80]. Furthermore, inflammatory agents that appear during both acute and chronic brain infections may upregulate amyloid precursor protein levels in both astrocytes of murine and human brain [81]. During H3N2 and H1N1 influenza A viruses (IAV) or HSV-1 infections, Aβ may play a protective role against these pathogens and constitute a host response to infection, e.g., reduce virus replication in neurons or prevent viral entry into the cells [82, 83]. On the other hand, HSE, and particularly recurrent or persistent HSV-1 infections in the brain, may be the determining factors that increase the risk of AD development. The extent to which HSV-1 infection may contribute to the deposition of Aβ in the brain was analyzed by Wozniak et al. [9]. In brains of people suffering from AD, HSV-1 nucleic acid was found in 90% of Aβ plaques, while over 70% of viral DNA was associated with the plaques. These data indicate HSV-1's presence in the brain as one of the initiating factors in the formation of Aβ plaques in the brain, as well as an important factor that may lead to the onset of AD. Knowledge regarding TLR3 biology in brain cells is significant since the receptor is crucial in combating HSV-1 infection. Results obtained in this work contribute to the understanding of TLR3 functioning in astrocytes.

A functional TLR3 reveals as an essential component of natural immunity to HSV-1 in the brain, while impaired innate immunity to HSV-1 may increase susceptibility to HSE in children and adults. Here, we point out Syk and Hrs as immune factors which influence TLR3 signaling that may affect inflammatory-mediated encephalitic responses during HSE. Details regarding how Syk and Hrs influence TLR3-mediated antiviral response call attention to novel elements which may require careful examination when analyzing the TLR3 activity in CNS, such as the role of post-translational modifications of these proteins, or contribution of TLR3 N-terminal form in mounting the effective antiviral defense. Precise regulation of the TLR3 transportation and degradation, most likely related to Syk and Hrs, is essential for maintaining the adequate level of an active receptor and generating an effective immune response.

5. Conclusions

Endosomal TLR3 undergoes cleavage upon poly(I:C) stimulation of murine astrocytes in a dose- and time-dependent manner. Stimulation of murine astrocytes with poly(I:C) upregulates the expression of Syk and Hrs in a time-dependent manner and additionally in a dose-dependent manner for Syk, while the expression of STAM is not affected. Distribution of TLR3 and STAM is altered, from a perinuclear location in nonstimulated cells to a much dispersed arrangement upon poly(I:C) stimulation of astrocytes. The increased expression of Syk appears to orchestrate its activation and eventual interaction with Hrs followed by tyrosine phosphorylation of Hrs, which in turn interacts with the N-terminal form of TLR3. Knockdown of TLR3, Syk, or Hrs followed by TLR3 stimulation of astrocytes leads to perturbations in nuclear translocation of NF-κB and IRF3, while IRF7 is not influenced. Moreover, Syk and Hrs knockdown results in the increase of IFNβ, IL-6, and CXCL8 secretion. These results suggest that Syk and Hrs have a regulatory role in signaling through TLR3 in murine astrocytes.

Data Availability

All data used to support the findings of this study are included within the article.

Conflicts of Interest

The authors declare that there is no conflict of interest regarding the publication of this paper.

Acknowledgments

We thank J. Struzik (Warsaw University of Life Sciences) for providing antibodies and help with the nuclear and cytoplasmic extraction experiments and C. A. Leifer (Cornell University, USA) for suggestions on the manuscript. We also thank R. A. Mielcarski for artwork and W. W. Mielcarski for assistance with the experiments. This work was supported by Ross University School of Veterinary Medicine Intramural Grant; Grants from National Science Centre, Poland: 5660/B/P01/2011/40 and 0152/B/P01/2011/40 to TNF and UMO-2016/23/N/NZ6/02499 to MBM; and Warsaw University of Life Sciences Intramural Grants for PhD Students:

505-10-023400-M00246-99 and 505-10-023400-N00166-99 to MBM.

References

[1] C. S. von Bartheld, J. Bahney, and S. Herculano-Houzel, "The search for true numbers of neurons and glial cells in the human brain: a review of 150 years of cell counting," *The Journal of Comparative Neurology*, vol. 524, no. 18, pp. 3865–3895, 2016.

[2] B. Liu, A. G. Teschemacher, and S. Kasparov, "Astroglia as a cellular target for neuroprotection and treatment of neuropsychiatric disorders," *Glia*, vol. 65, no. 8, pp. 1205–1226, 2017.

[3] A. Verkhratsky, R. Zorec, J. J. Rodriguez, and V. Parpura, "Pathobiology of neurodegeneration: the role for astroglia," *Opera Medica et Physiologica*, vol. 2, no. 1, pp. 13–22, 2016.

[4] N. Vardjan, M. Gabrijel, M. Potokar et al., "IFN-γ-induced increase in the mobility of MHC class II compartments in astrocytes depends on intermediate filaments," *Journal of Neuroinflammation*, vol. 9, no. 1, article 657, 2012.

[5] J. Ghiso and B. Frangione, "Amyloidosis and Alzheimer's disease," *Advanced Drug Delivery Reviews*, vol. 54, no. 12, pp. 1539–1551, 2002.

[6] G. R. Frost and Y.-M. Li, "The role of astrocytes in amyloid production and Alzheimer's disease," *Open Biology*, vol. 7, no. 12, 2017.

[7] M. Olabarria, H. N. Noristani, A. Verkhratsky, and J. J. Rodríguez, "Concomitant astroglial atrophy and astrogliosis in a triple transgenic animal model of Alzheimer's disease," *Glia*, vol. 58, no. 7, pp. 831–838, 2010.

[8] J. L. Zamanian, L. Xu, L. C. Foo et al., "Genomic analysis of reactive astrogliosis," *The Journal of Neuroscience*, vol. 32, no. 18, pp. 6391–6410, 2012.

[9] M. Wozniak, A. Mee, and R. Itzhaki, "Herpes simplex virus type 1 DNA is located within Alzheimer's disease amyloid plaques," *The Journal of Pathology*, vol. 217, no. 1, pp. 131–138, 2009.

[10] D. C. Peltier, A. Simms, J. R. Farmer, and D. J. Miller, "Human neuronal cells possess functional cytoplasmic and TLR-mediated innate immune pathways influenced by phosphatidylinositol-3 kinase signaling," *Journal of Immunology*, vol. 184, no. 12, pp. 7010–7021, 2010.

[11] R. Vontell, V. Supramaniam, C. Thornton et al., "Toll-like receptor 3 expression in glia and neurons alters in response to white matter injury in preterm infants," *Developmental Neuroscience*, vol. 35, no. 2-3, pp. 130–139, 2013.

[12] A. B. Salmina, Y. K. Komleva, O. L. Lopatina et al., "Astroglial control of neuroinflammation: TLR3-mediated dsRNA-sensing pathways are in the focus," *Reviews in the Neurosciences*, vol. 26, no. 2, pp. 143–159, 2015.

[13] M. Aschner, U. Sonnewald, and K. H. Tan, "Astrocyte modulation of neurotoxic injury," *Brain Pathology*, vol. 12, no. 4, pp. 475–481, 2002.

[14] S. S. Choi, H. J. Lee, I. Lim, J. Satoh, and S. U. Kim, "Human astrocytes: secretome profiles of cytokines and chemokines," *PLoS One*, vol. 9, no. 4, article e92325, 2014.

[15] M. L. Hanke and T. Kielian, "Toll-like receptors in health and disease in the brain: mechanisms and therapeutic potential," *Clinical Science (London, England)*, vol. 121, no. 9, pp. 367–387, 2011.

[16] G. M. McCarthy, C. R. Bridges, Y. A. Blednov, and R. A. Harris, "CNS cell-type localization and LPS response of TLR signaling pathways," *F1000Research*, vol. 6, article 1144, 2017.

[17] R. Gesuete, S. G. Kohama, and M. P. Stenzel-Poore, "Toll-like receptors and ischemic brain injury," *Journal of Neuropathology and Experimental Neurology*, vol. 73, no. 5, pp. 378–386, 2014.

[18] E. Okun, K. J. Griffioen, J. D. Lathia, S.-C. Tang, M. P. Mattson, and T. V. Arumugam, "Toll-like receptors in neurodegeneration," *Brain Research Reviews*, vol. 59, no. 2, pp. 278–292, 2009.

[19] H. K. Lim, M. Seppanen, T. Hautala et al., "TLR3 deficiency in herpes simplex encephalitis: high allelic heterogeneity and recurrence risk," *Neurology*, vol. 83, no. 21, pp. 1888–1897, 2014.

[20] N. Mørk, E. Kofod-Olsen, K. B. Sørensen et al., "Mutations in the TLR3 signaling pathway and beyond in adult patients with herpes simplex encephalitis," *Genes and Immunity*, vol. 16, no. 8, pp. 552–566, 2015.

[21] M. Sironi, A. M. Peri, R. Cagliani et al., "TLR3 mutations in adult patients with herpes simplex virus and varicella-zoster virus encephalitis," *The Journal of Infectious Diseases*, vol. 215, no. 9, pp. 1430–1434, 2017.

[22] M. B. Mielcarska, M. Bossowska-Nowicka, and F. N. Toka, "Functional failure of TLR3 and its signaling components contribute to herpes simplex encephalitis," *Journal of Neuroimmunology*, vol. 316, pp. 65–73, 2018.

[23] J. W. Gnann and R. J. Whitley, "Herpes simplex encephalitis: an update," *Current Infectious Disease Reports*, vol. 19, no. 3, article 13, 2017.

[24] C. K. Glass, K. Saijo, B. Winner, M. C. Marchetto, and F. H. Gage, "Mechanisms underlying inflammation in neurodegeneration," *Cell*, vol. 140, no. 6, pp. 918–934, 2010.

[25] B. L. Lee, J. E. Moon, J. H. Shu et al., "UNC93B1 mediates differential trafficking of endosomal TLRs," *eLife*, vol. 2, article e00291, 2013.

[26] B. L. Lee and G. M. Barton, "Trafficking of endosomal toll-like receptors," *Trends in Cell Biology*, vol. 24, no. 6, pp. 360–369, 2014.

[27] C.-Y. Chiang, A. Engel, A. M. Opaluch et al., "Cofactors required for TLR7- and TLR9-dependent innate immune responses," *Cell Host & Microbe*, vol. 11, no. 3, pp. 306–318, 2012.

[28] N. Rismanchi, R. Puertollano, and C. Blackstone, "STAM adaptor proteins interact with COPII complexes and function in ER-to-Golgi trafficking," *Traffic*, vol. 10, no. 2, pp. 201–217, 2009.

[29] Y. Amano, K. Yoshino, K. Kojima, and T. Takeshita, "A hydrophobic amino acid cluster inserted into the C-terminus of a recycling cell surface receptor functions as an endosomal sorting signal," *Biochemical and Biophysical Research Communications*, vol. 441, no. 1, pp. 164–168, 2013.

[30] L.-S. Chin, M. C. Raynor, X. Wei, H.-Q. Chen, and L. Li, "Hrs interacts with sorting nexin 1 and regulates degradation of epidermal growth factor receptor," *The Journal of Biological Chemistry*, vol. 276, no. 10, pp. 7069–7078, 2001.

[31] H. Takata, M. Kato, K. Denda, and N. Kitamura, "A hrs binding protein having a Src homology 3 domain is involved in intracellular degradation of growth factors and their receptors," *Genes to Cells*, vol. 5, no. 1, pp. 57–69, 2000.

[32] H. Husebye, Ø. Halaas, H. Stenmark et al., "Endocytic pathways regulate toll-like receptor 4 signaling and link innate and adaptive immunity," *The EMBO Journal*, vol. 25, no. 4, pp. 683–692, 2006.

[33] K. A. Stern, G. D. Visser Smit, T. L. Place, S. Winistorfer, R. C. Piper, and N. L. Lill, "Epidermal growth factor receptor fate is controlled by Hrs tyrosine phosphorylation sites that regulate Hrs degradation," *Molecular and Cellular Biology*, vol. 27, no. 3, pp. 888–898, 2007.

[34] L. Malerød, S. Stuffers, A. Brech, and H. Stenmark, "Vps22/EAP30 in ESCRT-II mediates endosomal sorting of growth factor and chemokine receptors destined for lysosomal degradation," *Traffic*, vol. 8, no. 11, pp. 1617–1629, 2007.

[35] K.-G. Lee, S. Xu, Z.-H. Kang et al., "Bruton's tyrosine kinase phosphorylates toll-like receptor 3 to initiate antiviral response," *Proceedings of the National Academy of Sciences*, vol. 109, no. 15, pp. 5791–5796, 2012.

[36] M. Yamashita, S. Chattopadhyay, V. Fensterl, P. Saikia, J. L. Wetzel, and G. C. Sen, "Epidermal growth factor receptor is essential for toll-like receptor 3 signaling," *Science Signaling*, vol. 5, no. 233, pp. ra50–ra50, 2012.

[37] T. Kawasaki and T. Kawai, "Toll-like receptor signaling pathways," *Frontiers in Immunology*, vol. 5, p. 461, 2014.

[38] C. Han, J. Jin, S. Xu, H. Liu, N. Li, and X. Cao, "Integrin CD11b negatively regulates TLR-triggered inflammatory responses by activating Syk and promoting degradation of MyD88 and TRIF via Cbl-b," *Nature Immunology*, vol. 11, no. 8, pp. 734–742, 2010.

[39] F. Gasparrini, R. Molfetta, L. Quatrini, L. Frati, A. Santoni, and R. Paolini, "Syk-dependent regulation of Hrs phosphorylation and ubiquitination upon FcεRI engagement: impact on Hrs membrane/cytosol localization," *European Journal of Immunology*, vol. 42, no. 10, pp. 2744–2753, 2012.

[40] F. Zhou, J. Hu, H. Ma, M. L. Harrison, and R. L. Geahlen, "Nucleocytoplasmic trafficking of the Syk protein tyrosine kinase," *Molecular and Cellular Biology*, vol. 26, no. 9, pp. 3478–3491, 2006.

[41] C. Raiborg, K. G. Bache, A. Mehlum, E. Stang, and H. Stenmark, "Hrs recruits clathrin to early endosomes," *The EMBO Journal*, vol. 20, no. 17, pp. 5008–5021, 2001.

[42] V. Sancho-Shimizu, R. Perez de Diego, E. Jouanguy, S.-Y. Zhang, and J.-L. Casanova, "Inborn errors of anti-viral interferon immunity in humans," *Current Opinion in Virology*, vol. 1, no. 6, pp. 487–496, 2011.

[43] R. I. Freshney, *Culture of Animal Cells : a Manual of Basic Technique*, Wiley-Liss, 1994.

[44] J. N. Leonard, R. Ghirlando, J. Askins et al., "The TLR3 signaling complex forms by cooperative receptor dimerization," *Proceedings of the National Academy of Sciences of the United States of America*, vol. 105, no. 1, pp. 258–263, 2008.

[45] A. Garcia-Cattaneo, F.-X. Gobert, M. Muller et al., "Cleavage of toll-like receptor 3 by cathepsins B and H is essential for signaling," *Proceedings of the National Academy of Sciences*, vol. 109, no. 23, pp. 9053–9058, 2012.

[46] R. Qi, D. Singh, and C. C. Kao, "Proteolytic processing regulates toll-like receptor 3 stability and endosomal localization," *The Journal of Biological Chemistry*, vol. 287, no. 39, pp. 32617–32629, 2012.

[47] Y. I. Miller, S.-H. Choi, P. Wiesner, and Y. S. Bae, "The SYK side of TLR4: signalling mechanisms in response to LPS and minimally oxidized LDL," *British Journal of Pharmacology*, vol. 167, no. 5, pp. 990–999, 2012.

[48] M. A. Sanjuan, N. Rao, K.-T. A. Lai et al., "CpG-induced tyrosine phosphorylation occurs via a TLR9-independent mechanism and is required for cytokine secretion," *The Journal of Cell Biology*, vol. 172, no. 7, pp. 1057–1068, 2006.

[49] Z. Luo, M. Ge, J. Chen et al., "HRS plays an important role for TLR7 signaling to orchestrate inflammation and innate immunity upon EV71 infection," *PLoS Pathogens*, vol. 13, no. 8, article e1006585, 2017.

[50] K. Kojima, Y. Amano, K. Yoshino, N. Tanaka, K. Sugamura, and T. Takeshita, "ESCRT-0 protein hepatocyte growth factor-regulated tyrosine kinase substrate (Hrs) is targeted to endosomes independently of signal-transducing adaptor molecule (STAM) and the complex formation with STAM promotes its endosomal dissociation," *The Journal of Biological Chemistry*, vol. 289, no. 48, pp. 33296–33310, 2014.

[51] Q. Lu, L. W. Hope, M. Brasch, C. Reinhard, and S. N. Cohen, "TSG101 interaction with HRS mediates endosomal trafficking and receptor down-regulation," *Proceedings of the National Academy of Sciences*, vol. 100, no. 13, pp. 7626–7631, 2003.

[52] Y.-C. Lin, D.-Y. Huang, C.-L. Chu, and W.-W. Lin, "Anti-inflammatory actions of Syk inhibitors in macrophages involve non-specific inhibition of toll-like receptors-mediated JNK signaling pathway," *Molecular Immunology*, vol. 47, no. 7-8, pp. 1569–1578, 2010.

[53] L. Cao, K. Yu, C. Banh et al., "Quantitative time-resolved phosphoproteomic analysis of mast cell signaling," *Journal of Immunology*, vol. 179, no. 9, pp. 5864–5876, 2007.

[54] A. Chockalingam, J. L. Cameron, J. C. Brooks, and C. A. Leifer, "Negative regulation of signaling by a soluble form of toll-like receptor 9," *European Journal of Immunology*, vol. 41, no. 8, pp. 2176–2184, 2011.

[55] F. Toscano, Y. Estornes, F. Virard et al., "Cleaved/associated TLR3 represents the primary form of the signaling receptor," *Journal of Immunology*, vol. 190, no. 2, pp. 764–773, 2013.

[56] Y. Murakami, R. Fukui, Y. Motoi et al., "Roles of the cleaved N-terminal TLR3 fragment and cell surface TLR3 in double-stranded RNA sensing," *Journal of Immunology*, vol. 193, no. 10, pp. 5208–5217, 2014.

[57] S. E. Ewald, B. L. Lee, L. Lau et al., "The ectodomain of toll-like receptor 9 is cleaved to generate a functional receptor," *Nature*, vol. 456, no. 7222, pp. 658–662, 2008.

[58] S. E. Ewald, A. Engel, J. Lee, M. Wang, M. Bogyo, and G. M. Barton, "Nucleic acid recognition by toll-like receptors is coupled to stepwise processing by cathepsins and asparagine endopeptidase," *The Journal of Experimental Medicine*, vol. 208, no. 4, pp. 643–651, 2011.

[59] S.-Y. Zhang, E. Jouanguy, S. Ugolini et al., "TLR3 deficiency in patients with herpes simplex encephalitis," *Science*, vol. 317, no. 5844, pp. 1522–1527, 2007.

[60] Y.-C. Lin, D.-Y. Huang, C.-L. Chu, Y.-L. Lin, and W.-W. Lin, "The tyrosine kinase Syk differentially regulates toll-like receptor signaling downstream of the adaptor molecules TRAF6 and TRAF3," *Science Signaling*, vol. 6, no. 289, pp. ra71–ra71, 2013.

[61] H. Takatsu, Y. Katoh, Y. Shiba, and K. Nakayama, "Golgi-localizing, gamma-adaptin ear homology domain, ADP-ribosylation factor-binding (GGA) proteins interact with acidic

dileucine sequences within the cytoplasmic domains of sorting receptors through their Vps27p/Hrs/STAM (VHS) domains," *The Journal of Biological Chemistry*, vol. 276, no. 30, pp. 28541–28545, 2001.

[62] O. Lohi, A. Poussu, Y. Mao, F. Quiocho, and V. P. Lehto, "VHS domain – a longshoreman of vesicle lines," *FEBS Letters*, vol. 513, no. 1, pp. 19–23, 2002.

[63] T. Takeshita, T. Arita, H. Asao et al., "Cloning of a novel signal-transducing adaptor molecule containing an SH3 domain and ITAM," *Biochemical and Biophysical Research Communications*, vol. 225, no. 3, pp. 1035–1039, 1996.

[64] R. P. Siraganian, R. O. de Castro, E. A. Barbu, and J. Zhang, "Mast cell signaling: the role of protein tyrosine kinase Syk, its activation and screening methods for new pathway participants," *FEBS Letters*, vol. 584, no. 24, pp. 4933–4940, 2010.

[65] R. O. de Castro, "Regulation and function of syk tyrosine kinase in mast cell signaling and beyond," *Journal of Signal Transduction*, vol. 2011, Article ID 507291, 9 pages, 2011.

[66] M. Simon, L. Vanes, R. L. Geahlen, and V. L. J. Tybulewicz, "Distinct roles for the linker region tyrosines of Syk in FcεRI signaling in primary mast cells," *The Journal of Biological Chemistry*, vol. 280, no. 6, pp. 4510–4517, 2005.

[67] S. Liu, X. Cai, J. Wu et al., "Phosphorylation of innate immune adaptor proteins MAVS, STING, and TRIF induces IRF3 activation," *Science*, vol. 347, no. 6227, article aaa2630, 2015.

[68] D. Liu and A. Mamorska-Dyga, "Syk inhibitors in clinical development for hematological malignancies," *Journal of Hematology & Oncology*, vol. 10, no. 1, article 145, 2017.

[69] P. Balsas, A. Esteve-Arenys, J. Roldán et al., "Activity of the novel BCR kinase inhibitor IQS019 in preclinical models of B-cell non-Hodgkin lymphoma," *Journal of Hematology & Oncology*, vol. 10, no. 1, article 80, 2017.

[70] C.-L. Chu, Y. L. Yu, K. Y. Shen, C. . A. Lowell, L. . L. Lanier, and J. . A. Hamerman, "Increased TLR responses in dendritic cells lacking the ITAM-containing adapters DAP12 and FcRγ," *European Journal of Immunology*, vol. 38, no. 1, pp. 166–173, 2008.

[71] J. A. Hamerman, N. K. Tchao, C. A. Lowell, and L. L. Lanier, "Enhanced toll-like receptor responses in the absence of signaling adaptor DAP12," *Nature Immunology*, vol. 6, no. 6, pp. 579–586, 2005.

[72] D. S. Arroyo, J. A. Soria, E. A. Gaviglio, M. C. Rodriguez--Galan, and P. Iribarren, "Toll-like receptors are key players in neurodegeneration," *International Immunopharmacology*, vol. 11, no. 10, pp. 1415–1421, 2011.

[73] G. Ponath, C. Park, and D. Pitt, "The role of astrocytes in multiple sclerosis," *Frontiers in Immunology*, vol. 9, p. 217, 2018.

[74] A. Kia, K. McAvoy, K. Krishnamurthy, D. Trotti, and P. Pasinelli, "Astrocytes expressing ALS-linked mutant FUS induce motor neuron death through release of tumor necrosis factor-alpha," *Glia*, vol. 66, no. 5, pp. 1016–1033, 2018.

[75] E. J. Goetzl, J. B. Schwartz, E. L. Abner, G. A. Jicha, and D. Kapogiannis, "High complement levels in astrocyte-derived exosomes of Alzheimer disease," *Annals of Neurology*, vol. 83, no. 3, pp. 544–552, 2018.

[76] H. D. E. Booth, W. D. Hirst, and R. Wade-Martins, "The role of astrocyte dysfunction in Parkinson's disease pathogenesis," *Trends in Neurosciences*, vol. 40, no. 6, pp. 358–370, 2017.

[77] L. R. Gray, S. G. Turville, T. L. Hitchen et al., "HIV-1 entry and trans-infection of astrocytes involves CD81 vesicles," *PLoS One*, vol. 9, no. 2, article e90620, 2014.

[78] A. S. Costa, S. Agostini, F. R. Guerini et al., "Modulation of immune responses to herpes simplex virus type 1 by IFNL3 and IRF7 polymorphisms: a study in Alzheimer's disease," *J. Alzheimer's Dis.*, vol. 60, no. 3, pp. 1055–1063, 2017.

[79] R. F. Itzhaki, "Herpes simplex virus type 1 and Alzheimer's disease: possible mechanisms and signposts," *The FASEB Journal*, vol. 31, no. 8, pp. 3216–3226, 2017.

[80] M. Zaiou, "Multifunctional antimicrobial peptides: therapeutic targets in several human diseases," *Journal of Molecular Medicine*, vol. 85, no. 4, pp. 317–329, 2007.

[81] B. Brugg, Y. L. Dubreuil, G. Huber, E. E. Wollman, N. Delhaye-Bouchaud, and J. Mariani, "Inflammatory processes induce beta-amyloid precursor protein changes in mouse brain," *Proceedings of the National Academy of Sciences of the United States of America*, vol. 92, no. 7, pp. 3032–3035, 1995.

[82] J. Miklossy, "Emerging roles of pathogens in Alzheimer disease," *Expert Reviews in Molecular Medicine*, vol. 13, article e30, 2011.

[83] K. Bourgade, H. Garneau, G. Giroux et al., "β-Amyloid peptides display protective activity against the human Alzheimer's disease-associated herpes simplex virus-1," *Biogerontology*, vol. 16, no. 1, pp. 85–98, 2015.

Hindawi
Oxidative Medicine and Cellular Longevity
Volume 2019, Article ID 2302835, 17 pages
https://doi.org/10.1155/2019/2302835

Research Article

Nitric Oxide Influences HSV-1-Induced Neuroinflammation

Joanna Cymerys,[1] Andrzej Kowalczyk,[2] Katarzyna Mikołajewicz,[2] Anna Słońska,[1] and Małgorzata Krzyżowska[2]

[1]*Department of Preclinical Sciences, Faculty of Veterinary Medicine, Warsaw University of Life Sciences, Ciszewskiego 8, 02-786 Warsaw, Poland*
[2]*PORT Polish Center for Technology Development, Stablowicka 147, 54-066 Wroclaw, Poland*

Correspondence should be addressed to Małgorzata Krzyżowska; krzyzowskam@yahoo.com

Received 14 September 2018; Revised 14 November 2018; Accepted 28 November 2018; Published 11 February 2019

Guest Editor: Agueda A. Rostagno

Herpes simplex virus type 1 (HSV-1) has the ability to replicate in neurons and glial cells and to produce encephalitis leading to neurodegeneration. Accumulated evidence suggests that nitric oxide (NO) is a key molecule in the pathogenesis of neurotropic virus infections. NO can exert both cytoprotective as well as cytotoxic effects in the central nervous system (CNS) depending on its concentration, time course exposure, and site of action. In this study, we used an *in vitro* model of HSV-1-infected primary neuronal and mixed glial cultures as well as an intranasal model of HSV-1 in BALB/c mice to elucidate the role of NO and nonapoptotic Fas signalling in neuroinflammation and neurodegeneration. We found that low, nontoxic concentration of NO decreased HSV-1 replication in neuronal cultures together with production of IFN-alpha and proinflammatory chemokines. However, in HSV-1-infected glial cultures, low concentrations of NO supported virus replication and production of IFN-alpha and proinflammatory chemokines. HSV-1-infected microglia downregulated Fas expression and upregulated its ligand, FasL. Fas signalling led to production of proinflammatory cytokines and chemokines as well as induced iNOS in uninfected bystander glial cells. On the contrary, NO reduced production of IFN-alpha and CXCL10 through nonapoptotic Fas signalling in HSV-1-infected neuronal cultures. Here, we also observed colocalization of NO production with the accumulation of β-amyloid peptide in HSV-1-infected neurons both in vitro and in vivo. Low levels of the NO donor increased accumulation of β-amyloid in uninfected primary neuronal cultures, while the NO inhibitor decreased its accumulation in HSV-1-infected neuronal cultures. This study shows for the first time the existence of a link between NO and Fas signalling during HSV-1-induced neuroinflammation and neurodegeneration.

1. Introduction

Herpes simplex virus type 1 (HSV-1) causes a contagious infection that affects approximately 60% to 95% of adults worldwide. HSV-1 is associated mainly with infections of the mouth, pharynx, face, eye, and central nervous system (CNS). The virus persists in the body by becoming latent in the cell bodies of nerves after the primary infection. People infected with HSV-1 can expect to have several (typically four or five) outbreaks (symptomatic recurrences) within a year. HSV-1 has the ability to replicate in neurons and glial cells and to produce acute focal, necrotizing encephalitis localized in the temporal and subfrontal regions of the brain [1, 2]. Herpes simplex encephalitis (HSE) predominantly affects children and the elderly, is one of the most common forms of viral encephalitis, and has remarkably poor outcomes despite the availability of good antiviral therapy [3–5].

Pathogen-induced neurodegeneration occurs by both direct effects on brain cells and indirect inflammatory and oxidative effects. Mounting evidence suggests that HSV-1 exposure to neuronal cells results in cellular production of β-amyloid proteins (Aβ). Mouse brains infected with HSV-1 showed increases in Aβ42 five days postintranasal infection compared to uninfected controls [6]. In HSV-1-infected human neuroblastoma cells, experimentally induced oxidative stress was found to significantly enhance the accumulation of intracellular Aβ and to inhibit Aβ secretion [7]. HSV-1 interactions with oxidative stress are significant

because oxidative damage is thought to occur early in the pathogenesis of Alzheimer disease (AD) [8].

Microglia and astroglia are consistently found surrounding amyloid plaques in AD brains [9]. Aβ deposition causes a microglial-mediated inflammatory response [10]. Proinflammatory molecules have been shown to be involved in pathways of neuronal apoptosis [11]. Aβ-stimulated microglia secrete TNF-α and glutamate in vitro, resulting in simultaneous activation of neuronal TNF-α and N-methyl-D-aspartate (NMDA) receptors and subsequent neuronal apoptosis [11]. Additional neurotoxic compounds produced by activated microglia include superoxide, hydrogen peroxide, and nitric oxide. Fas and other receptors from the tumor necrosis factor (TNF) receptor family upon interaction with their ligands (e.g., FasL) trigger the so-called death receptor pathway of apoptosis [12]. Fas is not expressed in the adult brain under physiological conditions, but it has been detected in the brains of patients with AD, in human malignant astrocytic brain tumors, during ischemic injury, in multiple sclerosis (MS), and in HIV encephalopathy (HIVE) [13, 14], while FasL expression during neuroinflammation is detected mainly on infiltrating myeloid cells or on the activated microglia [15, 16].

Nitric oxide (NO) is a signalling molecule synthesized from the amino acid L-arginine via enzymes called NO-synthases (NOS) [16]. There are three different kinds of NOS [16]. NOS is induced in a variety of experimental virus infections in rats and mice, including neuroviruses, such as Borna disease virus, herpes simplex virus type 1, and rabies virus [17–19]. Viral or synthetic dsRNA, also in conjunction with interferon gamma (IFN-γ), increases the expression and activity of NF-κB, which further induces iNOS expression [20].

Previous studies have shown that HSV-1 is susceptible to the effects of NO *in vivo* in mice and rats [19]. Despite its antiviral activity, NO is not always beneficial, as it can promote the pathogenesis of HSV-1 by damaging cells in host tissues [19]. In a prooxidant environment, NO reacts with superoxide anion to generate peroxynitrite (ONOO−), a highly reactive anion [21, 22]. Peroxynitrite has been shown to induce lipid peroxidation, as well as functional alterations to proteins through tyrosine nitration (nitrotyrosination) [21, 22]. These modifications are molecular markers of AD [21, 22].

It was suggested that increased expression of all NOS forms in astrocytes and neurons contributes to the synthesis of peroxynitrite which leads to generation of nitrotyrosine, which can be detected in blood and cerebrospinal fluid (CSF) of AD patients [21]. Also, aberrant expression of nNOS in cortical pyramidal cells colocalized with nitrotyrosine in the brains of AD patients and it correlated with the cognitive impairment [21, 22].

We have previously shown that the lack of the Fas-dependent pathway of apoptosis plays an important role in the elimination of the inflammation surrounding the HSV-2-infected sites and regulation of monocyte-induced inflammation during HSV infection [23]. Here, we hypothesize that both the NO and Fas/FasL pathways are involved in HSV-1 induced neuroinflammation and neurodegeneration during HSV-1 infection. The Fas/FasL pathway leads to increased levels of NO observed during both *in vitro* and *in vivo* HSV-1 infection, which in turn can contribute to Aβ aggregation.

2. Materials and Methods

2.1. Cell Lines and Virus. Murine astrocyte C8-D1A and African green monkey kidney (Vero) cell lines were purchased from the American Type Culture Collection (ATCC® CRL-2541™ and ATCC® CCL-81™, respectively). C8-D1A cells were grown in Dulbecco's modified essential medium (D-MEM), supplemented with 10% fetal bovine serum (FBS), 4 mM L-glutamine, 1 mM sodium pyruvate (Gibco by Thermo Fisher Scientific, Carlsbad, CA, USA), 5 g/l glucose, 100 U/ml penicillin, 100 μg/ml streptomycin, and 0.25 μg/ml amphotericin B (Thermo Fisher Scientific) in standard conditions. Vero cells were grown in Eagle's minimum essential medium, supplemented with 10% FBS, 100 U/ml penicillin, 100 μg/ml streptomycin, and 0.25 μg/ml amphotericin B (Thermo Fisher Scientific).

HSV-1 strain McKrae [24] was grown (PFU/ml) in African green monkey kidney (Vero) cells. Virus titers were determined by plaque assay on Vero cells.

2.2. Primary Neuronal Cultures and Mixed Glial Cultures. BALB/c mice were used to establish primary culture of murine neurons, as described before [25]. Neuronal cells were cultured in B-27 Neuron Plating Medium consisting of neurobasal medium, B-27 supplement, glutamine (200 mM), glutamate (10 mM), antibiotics (penicillin and streptomycin), 10% FBS, and horse serum (Thermo Fisher Scientific) in standard conditions. At day 3, 1 μM AraC (cytosine β-D-arabinofuranoside) for 24 hrs was added. Four days after plating, the medium was removed and replaced with Neuron Feeding Medium (B-27 Neuron Plating Medium without glutamate). In this medium, murine neurons were maintained for the next 6 days, prior to treatment.

Mixed glial cultures were obtained as described by Draheim et al. [26]. In brief, whole brains of neonatal BALB/c mice were taken and blood vessel and meninges were carefully removed. Then, the whole brains of five mice were pooled together and digested with 0.25% trypsin/Hanks' balanced salt solution for 10 minutes. Next, the homogenate was filtered through a 70 μm cell strainer (BD Biosciences) into a 50 ml conical tube. After rinsing the filter with PBS, the resulting cell suspension was centrifuged again at 300 g for 5 min at room temperature. The pellet was dissolved in Dulbecco's modified Eagle's/F12 medium with GlutaMAX (DMEM/F12) supplemented with 10% FBS, 100 units/ml penicillin, 100 μg/ml streptomycin (Thermo Fisher Scientific), and 5 ng/ml murine recombinant granulocyte and macrophage colony stimulating factor (GM-CSF) (Sigma-Aldrich, St. Luis, MO, USA). Medium was changed every 72 h, and the mixed glial cells were used for experiments after two weeks of culture. The cultures consisted of 40% CD11b+ cells and 60% GFAP+ cells as assessed by flow cytometry (details below).

Both neuronal and mixed glial cultures were infected with HSV-1 at MOI = 1 for 24 h and subjected to treatment with the NO donor—sodium nitroprusside (SNP) (1000, 500, 100, 50, and 10 μM)—and the inhibitor of iNOS—aminoguanidine (AMG, 50 μM).

2.3. Intranasal HSV-1 Infection. Six- to 10-week-old male mice were anesthetized with isoflurane (Geulincx), and 10^6 PFU (plaque-forming units) of the purified HSV-1 contained in 10 μl was inhaled by the mice. The control mice inhaled PBS. The mouse colonies and all of the experimental procedures were performed according to the institutional animal care and use guidelines. From 24 h before infection up to 5 days of infection, mice received aminoguanidine sulphate (100 mg/kg body weight, intraperitoneally) (Sigma-Aldrich) dissolved in physiological saline. Five days later, mice of both treated groups were sacrificed and their trigeminal ganglia as well as brains were collected for further assays. The brains were fixed in 4% paraformaldehyde (PFA) in PBS, then saturated with 30% sucrose, frozen in liquid nitrogen, and used to prepare cryostat sections.

2.4. Virus Titration. Total DNA was isolated from trigeminal ganglia and brains preserved in RNA later (Thermo Fisher Scientific, MA, USA) using RNA/DNA Extracol kit (EURx, Gdansk, Poland). HSV-1 was detected using a HSV-1 probe labeled with FAM in a real-time PCR instrument Stratagene MX4000 Real-Time qPCR System (Agilent Technologies, USA) as described by Namvar et al. [27] and Orłowski et al. [28]. A plasmid vector pCR 2.1 containing an envelope glycoprotein (gB) gene fragment was constructed and purified by the Institute of Biochemistry and Biophysics Polish Academy of Sciences (Warsaw, Poland). Standard curve analysis was based on Ct values and serial of 10-fold dilutions of the plasmid standard with an initial concentration of 2.62×10^6 HSV-1 genome copy numbers per reaction. A standard curve was included in each PCR run. The amplification efficiency (E) was calculated from the standard curves, using the formula $E = 10(-1/a) - 1$, where a is the slope. Data are expressed as the HSV-1 copy number per ng of the total DNA in the tissue.

2.5. Flow Cytometry Analysis. Cell suspensions prepared from cell cultures by the use of trypsin were pretreated with the Fc receptor block rat anti-CD16/32 antibody (2.4G2) (BD Biosciences, Franklin Lakes, NJ, USA) according to the manufacturer's protocol. Astrocytes were detected by anti-GFAP-FITC or APC-conjugated antibody (GA5, eBioscience), and microglia were stained with rat anti-CD11b-APC (M1/70, BD Biosciences). For detection of Fas and FasL, cells were washed in 1% FBS/PBS, and then, FITC-conjugated hamster anti-mouse Fas antibody (Jo2, BD Biosciences) and PE-conjugated hamster anti-mouse FasL antibody were used (MFL3, BD Biosciences). For all staining, rat IgG2a, rat IgG2b, and hamster IgG1 isotype antibodies conjugated with appropriate fluorochromes were used (BD Biosciences). Apoptosis in single cell suspensions was detected using Annexin V- APC Apoptosis detection kit (BD Biosciences), according to the manufacturer's protocol. The annexin V+ and propidium iodide (-) cells were scored as apoptotic, while annexin V+/propidium iodide (+) cells as secondary necrotic and annexin V (-)/propidium iodide (+) cells as necrotic. Apoptotic/secondary-, apoptotic/necrotic CD11b+-, or GFAP+-positive cells were detected by prestaining with anti-CD11b-FITC (M1/70, BD Biosciences) and anti-GFAP-FITC (GA5, eBioscience) antibodies. Intracellular antigens were detected using Cytofix/Cytoperm fixation/permeabilization kit (BD Biosciences) according to the manufacturer's protocol and by using anti-iNOS-PE antibody (CXNFT, eBioscience). The stained cell suspensions were analyzed in FACS Calibur for the percentage of positively stained cells or the mean fluorescence intensity.

2.6. Immunofluorescent Staining and Microscopy Analysis. Primary murine neurons or mixed glial cultures seeded on glass coverslips in a 6-well plate were infected with HSV-1. At 24 h p.i. (hour post infection), neuronal cells were washed twice in PBS (Sigma-Aldrich) and fixed in 3.7% paraformaldehyde/PBS (Sigma-Aldrich) for 10 min at room temperature (RT), and then, permeabilization with 0.5% Triton X-100 (Sigma-Aldrich) solution in PBS was performed. Before staining, slides with cell cultures or brain cryosections were blocked with PBS containing 1% bovine serum albumin (BSA) and 0.5% saponin (Sigma-Aldrich) for 30 min at RT. For immunophenotypic characterization and identification of iNOS, Fas, FasL, and Aβ, slides were stained by means of immunofluorescence with appropriate antibodies: anti-CD11b-APC (M1/70, BD Biosciences) and anti-GFAP-APC (GA5, eBioscience), anti-Fas-APC (Jo2, BD Biosciences), biotinylated anti-FasL (MFL3, BD Biosciences), anti-iNOS-PE (CXNFT, eBioscience), anti-NeuN-biotin (A60, Sigma), and anti-β-Amyloid (NAB228; Thermo Fisher Scientific) antibodies (dilution 1 : 100, overnight). After several washes with PBS, slides were incubated with secondary antibodies: Alexa 647 goat anti-mouse IgG (dilution 1 : 1000, 1 h, RT) and Streptavidin-Alexa 647 (dilution 1 : 200, 1 h, RT). The presence of viral antigen was detected by using rabbit mAb anti-HSV (dilution 1 : 250, 1 h, RT) and anti-rabbit FITC (dilution 1 : 200, 1 h, 37°C). Slides were mounted in ProLong Gold Antifade Reagent (Thermo Fisher Scientific) with DAPI. Noninfected cell cultures or uninfected brains served as negative control. Images were acquired using Leica SP8 resonant scanning confocal system (Leica Microsystem, Wetzlar, Germany). Stacks of confocal 8-bit images with a pixel size of 0.186 μm and a 0.5 μm Z step were acquired using 40x oil immersion objective (NA 1.30).

2.7. Western Blot Analysis. Cultured neuronal cells prepared as described before were first washed with ice-cold PBS and lysed in N-PER Neuronal Protein Extraction Reagent (Thermo Fisher Scientific) containing protease and phosphatase inhibitors (Halt Phosphatase Inhibitor Cocktail and Halt Protease Inhibitor Cocktail; Thermo Fisher Scientific), for 20 min on ice. The lysates were clarified by centrifugation for 15 min at 4°C. Quantitation of the protein content in lysates was performed with Micro BCA Protein Assay Kit (Thermo Fisher Scientific) and spectrophotometry on an Epoch BioTek spectrophotometer. Samples containing

20 μg of protein were incubated with Laemmli sample buffer containing β-ME (Bio-Rad; Hercules, CA, USA) for 5 min at 95°C. Subsequently, the samples and protein markers were electrophoresed on a 10% polyacrylamide Bis-Tris Plus gel with MES running buffer and transferred onto a PVDF membrane. The membrane was blocked with 5% BSA in TBST and incubated overnight with primary mAb Aβ (NAB228; Thermo Fisher Scientific). After several washes in 0.1% Tris-buffered saline (TBS) Tween 20, blots were incubated with HRP-conjugated secondary antibodies for 1 h at RT and developed using enhanced chemiluminescence (Clarity Western ECL Substrate; Bio-Rad). The protein bands were visualized by ChemiDoc™ MP Imaging System (Bio-Rad).

2.8. Quantitative Reverse Transcriptase-Polymerase Chain Reaction for Cytokines and Chemokines. Total RNA was isolated from cells using Universal RNA Purification Kit (Eurx). Transcripts of IFN-α, CXCL9, CXCL10, TNF-α, and GADPH were quantified using TaqMan® Gene Expression Assays (Thermo Fisher Scientific). All PCR reactions were carried out with QuantiFast Probe RT-PCR Kit (QIAGEN, Hilden, Germany) using a real-time PCR instrument Stratagene MX4000 Real-Time qPCR System (Agilent Technologies) according to the manufacturer's protocol. The $2^{-\Delta\Delta Ct}$ method was used in calculating the relative ratio to control uninfected tissue.

2.9. Statistical Methods. Data are presented as the mean ± standard error of the mean (SEM) from at least three independent experiments. Data were analyzed using a two-tailed paired Student's *t*-test (normal distribution) or with nonparametric Kruskal-Wallis, and Wilcoxon tests were applied using BioStat 2009 software. In every analysis, values of $p \leq 0.05$ were considered significant.

3. Results

3.1. Influence of NO upon HSV-1 Replication Depends on the Cell and Organ Type. To ascertain the susceptibility of HSV-1 replication in cell cultures to NO, sodium nitroprusside (SNP) was used as an exogenous NO donor at the concentration range of 1000-50 μM and aminoguanidine sulphate (AMG) at the concentration of 50 μM was used as an inhibitor of inducible nitric oxide synthase (iNOS). The SNP concentration ≤ 100 μM and AMG concentration ≤ 50 μM have been shown in the literature as nontoxic to neuronal cultures, while for glial cells, toxic doses of SNP are ≥ 1000 μM [29, 30]. As indicated in Figure 1(a), the whole range of SNP concentrations inhibited HSV-1 replication in primary neuron cultures, while inhibition of iNOS caused no significant upregulation of HSV-1 replication ($p \leq 0.01$) (Figure 1(a)).

The primary glial culture consisting of microglia and astrocytes showed a dose-dependent effect of NO upon HSV-1 replication (Figure 1(b)). Concentrations of SNP $\geq$ 500 μM caused a significant inhibition of HSV-1 replication ($p \leq 0.01$) (Figure 1(b)), while SNP concentrations $\leq$ 100 μM significantly stimulated HSV-1 replication ($p \leq 0.05$) (Figure 1(b)). The astrocyte C8-D1A cell line showed a similar effect: SNP at ≤ 100 μM led to the significant upregulation of HSV-1 replication ($p \leq 0.05$) (Figure 1(c)), while 1000 μM SNP inhibited HSV-1 replication ($p = 0.045$). AMG had no effect upon HSV-1 replication in C8-1A astrocytes, while it significantly inhibited HSV-1 replication in mixed glial cells ($p = 0.02$) (Figure 1(b)). Furthermore, AMG showed different effects upon HSV-1 replication in the mouse model of neuroinfection (Figure 1(d)). At day 5 post infection (p.i.), HSV-1 DNA copies in mice treated with AMG were significantly higher in trigeminal ganglia (TG) in comparison to those in untreated mice ($p \leq 0.01$) (Figure 1(d)). However, treatment with AMG led to significantly lower HSV-1 titers in the whole brain tissue ($p \leq 0.01$) (Figure 1(d)).

3.2. Nitric Oxide Protects Infected Microglial Cells from Cell Death. The main sources of NO in HSV-1-infected primary neuronal and glial cell cultures were microglial cells and only a small proportion of astrocytes (Figures 2(a) and 2(b)). Flow cytometric analysis of mixed glial cultures for the percentage of iNOS+ cells showed that $23 \pm 1.5\%$ of CD11b+ were positive for iNOS, while $1.9 \pm 0.54\%$ of GFAP+ astrocyte cells were positive for iNOS (Figure 2(c)). In the brains of HSV-1-infected mice, HSV-1-positive cells were detected in the cerebellum, brain stem, midbrain, and tissue lining the lateral ventricles. Not only CD11b+-positive cells surrounding HSV-1-infected sites were positive for iNOS (Figure 3) but also single GFAP+ astrocytes positive for iNOS were found (Figure 3). The increased staining for iNOS was not associated with HSV-1 staining or staining for neurons (NeuN+) (Figure 3).

Infected neuronal cultures showed no apoptosis upon HSV-1 infection (data not shown), while primary glial cells, consisting of astrocytes and microglia, showed upregulation of apoptosis and secondary necrosis (Figure 4(a)). Upon HSV-1 infection, only CD11b+ microglial cells show significant increase in apoptosis and secondary necrosis induction ($p \leq 0.05$) (Figure 4(a)). Interestingly, while the nitric oxide donor caused increase in apoptosis induction in control, uninfected cells ($p \leq 0.05$) (Figure 4(a)), it protected HSV-1-infected microglial cells from secondary necrosis ($p \leq 0.05$) (Figure 4(a)). Both infected and uninfected neuronal cultures are not susceptible to Fas-induced apoptosis by cytotoxic recombinant sFasL (data not shown). Similarly, uninfected and infected mixed glial cultures also did not respond by apoptosis to stimulation of Fas receptor by sFasL (data not shown). Fas stimulation led to significant upregulation of iNOS expression not only in HSV-1-infected glial cells but also in uninfected cells from infected and control mixed glial cultures (Figure 4(b)).

3.3. Nitric Oxide Influences Production of Cytokines and Chemokines. To determine how NO can influence local inflammation during HSV-1, we measured expression levels of selected cytokines and chemokines in primary neuronal and mixed glial cultures at 24 p.i. We found that while no expression of cytokines or chemokines was detected in uninfected neuronal cultures, HSV-1 infection upregulated mRNA expression levels for IFN-alpha, TNF-alpha, CXCL9, and CXCL10 (Table 1). The NO donor—SNP—significantly

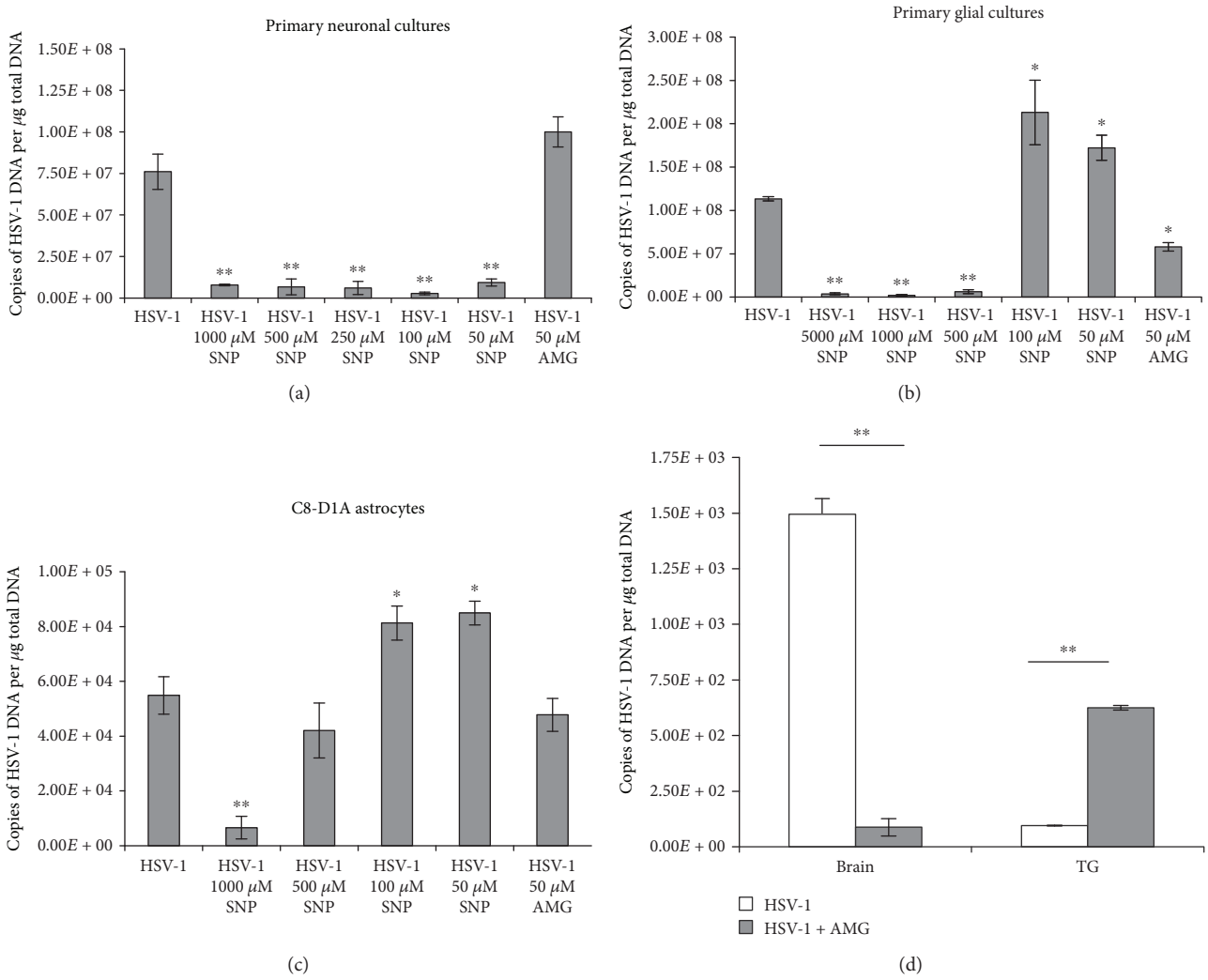

Figure 1: Nitric oxide influences HSV-1 replication. (a) Primary neuronal cultures and (b) primary glial cultures and (c) C8-D1A astrocyte cell line were subjected to treatment with the NO donor (SNP) or the inhibitor of iNOS (AMG) for 24 h and harvested for determination of HSV-1 DNA copies by PCR. (d) Numbers of HSV-1 DNA copies in the trigeminal ganglia (TG) and brains obtained at day 5 post intranasal infection with HSV-1 with or without treatment with AMG (100 mg/kg) were assessed by PCR. Means are expressed as mean ± SEM for $n = 7$; *significant differences with $p \leq 0.05$, while **$p \leq 0.01$ in comparison to infected controls.

downregulated expression of IFN-alpha, TNF-alpha, and CXCL10 in HSV-1-infected neuronal culture ($p \leq 0.05$) (Table 1). Addition of sFasL to uninfected neuronal cultures led to upregulation of TNF-alpha and CXCL10 expression (Table 1). Furthermore, sFasL significantly induced expression of CXCL10 and reduced expression of TNF-alpha in HSV-1-infected cultures ($p \leq 0.05$), while when coadded with the NO donor, it downregulated TNF-alpha and CXCL10 expression and upregulated CXCL9 expression ($p \leq 0.05$) (Table 1). Upon HSV-1 infection, mixed glial cultures upregulated INF-alpha, TNF-alpha, CXCL9, and CXCL10 mRNA expression levels ($p \leq 0.01$) (Table 2). The NO donor significantly upregulated mRNA expression levels for TNF-alpha, while it downregulated mRNA expression levels for IFN-alpha, CXCL9, and CXCL10 in HSV-1-infected mixed glial cultures ($p \leq 0.05$) (Table 2). AMG significantly upregulated INF-alpha expression in comparison to HSV-1-infected cultures ($p = 0.002$) (Table 2). Addition of sFasL in uninfected mixed glial cultures led to upregulation of TNF-alpha, IFN-alpha, and CXCL9 expression levels ($p \leq 0.05$) (Table 2).

However, sFasL downregulated TNF-alpha expression in HSV-1-infected glial cultures ($p = 0.45$) (Table 2). On the contrary, sFasL significantly upregulated CXC9 and CXCL10 expression levels in HSV-1-infected glial cultures ($p \leq 0.05$) (Table 2). Coaddition of sFasL and the NO donor significantly downregulated TNF-alpha, CXCL9, and CXCL10 mRNA expression levels ($p \leq 0.05$) (Table 2).

3.4. Fas and FasL Expression Can Be Regulated by Nitric Oxide. HSV-1 infection of mixed glial primary cultures led to significant downregulation of Fas expression on microglial cells ($p \leq 0.05$) (Figure 5(a)) in comparison to uninfected cells, while it had no influence upon Fas expression on astrocytes ($p \geq 0.05$) (Figure 5(a)). The NO donor—SNP—significantly downregulated Fas expression both on infected

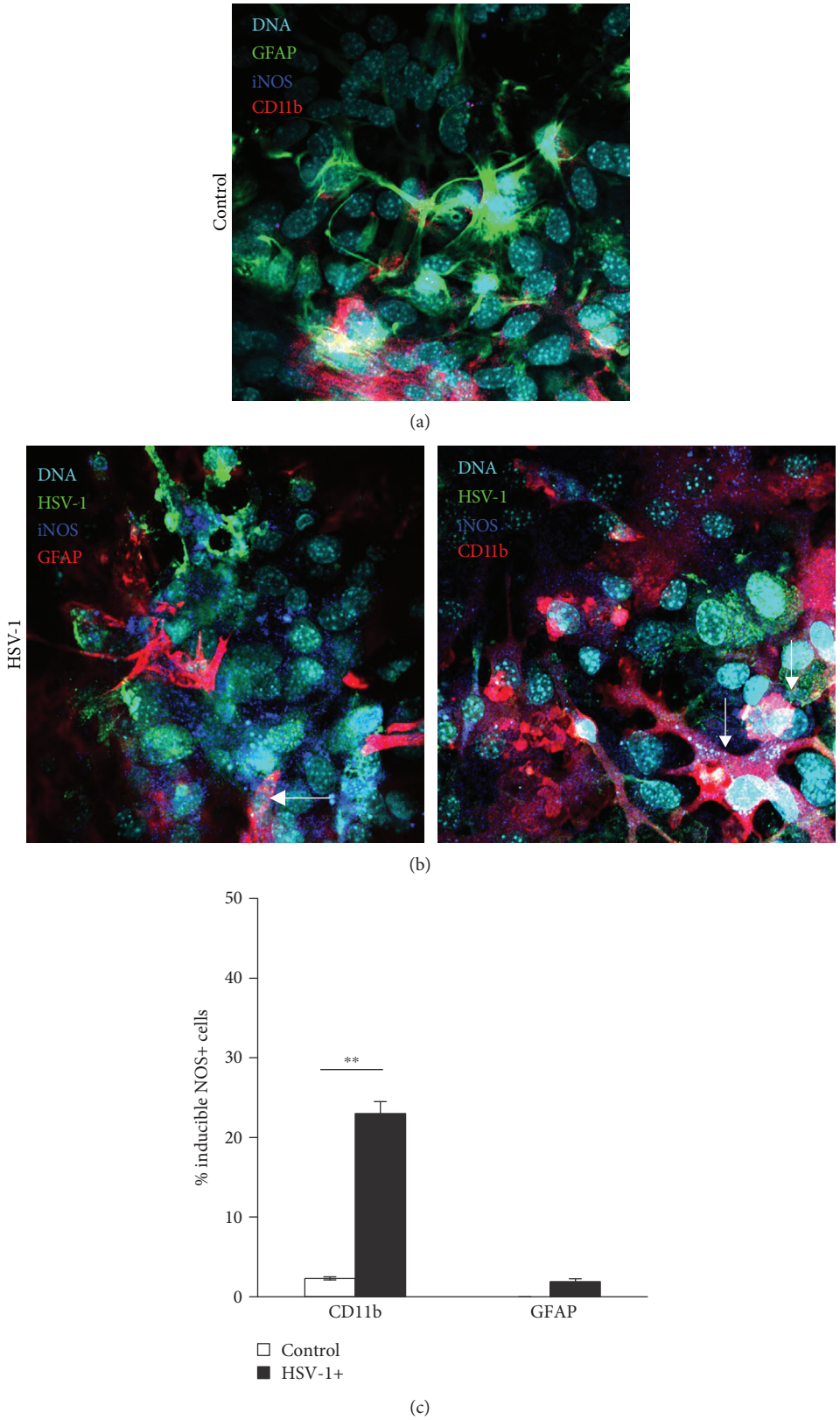

Figure 2: Cells positive for iNOS in HSV-1-infected mixed cultures. Representative confocal images of mixed glial cultures uninfected (a) or HSV-1 infected (b) at 24 h p.i. and stained for HSV-1, astrocytes (GFAP+), microglia (CD11b+), and iNOS (inducible NOS). Nuclei were counterstained with DAPI. (c) Percentage of CD11b+ and GFAP+ cells positive for iNOS accessed by flow cytometry in HSV-1-infected and control uninfected mixed glial cultures. Means are expressed as mean ± SEM for $n = 3$; *significant differences with $p \leq 0.05$, while $^{**}p \leq 0.01$.

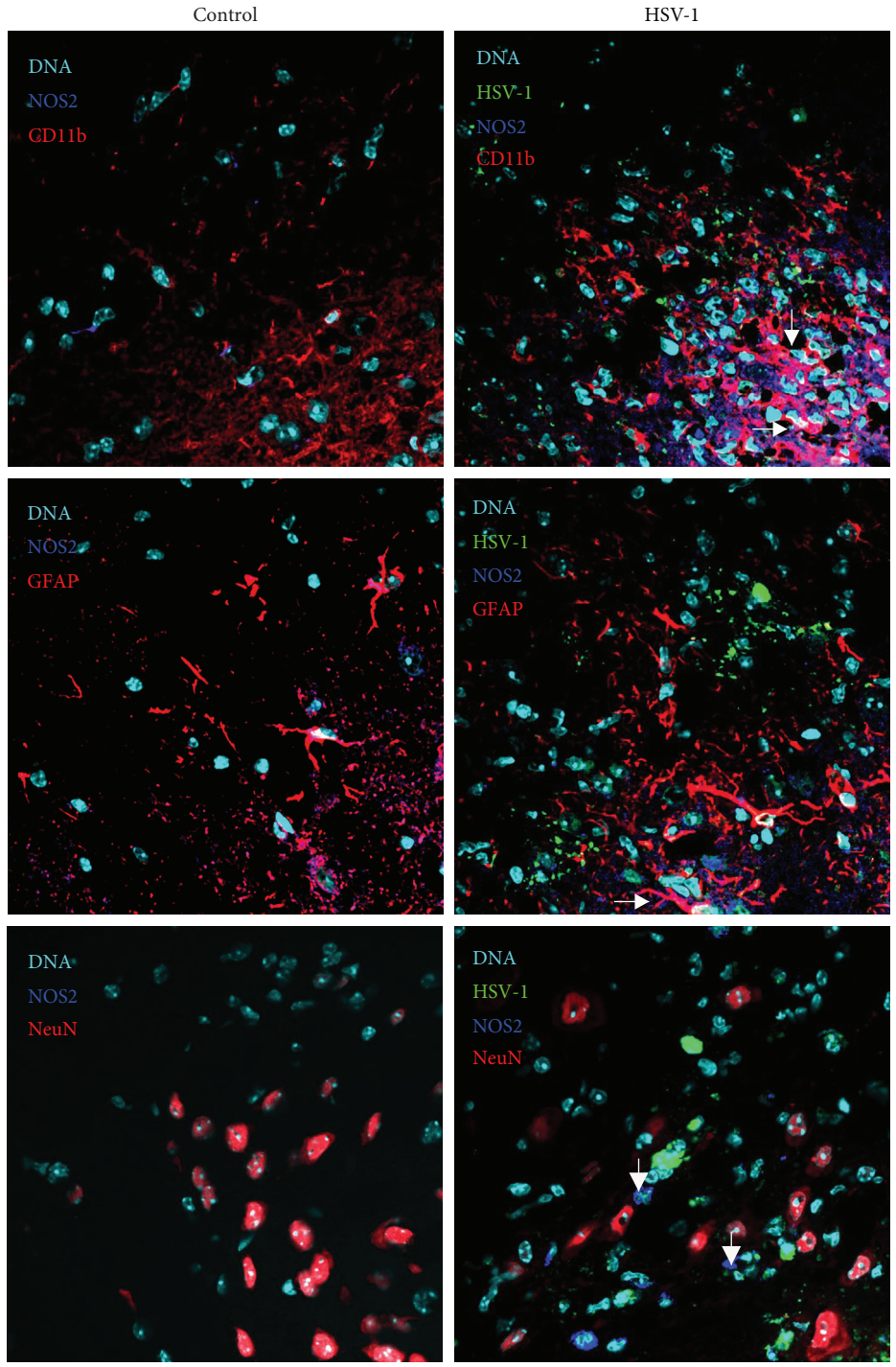

Figure 3: Microglia are the main source of iNOS in HSV-1-infected brains. Representative confocal images of brain stems obtained at day 5 p.i. with HSV-1. Neurons were identified as NeuN+-positive cells, while astrocytes as GFAP+ and microglia as CD11b+ and costained for iNOS and HSV-1. Nuclei were counterstained with DAPI.

astrocytes and microglial cells ($p \leq 0.05$) (Figure 5(a)) in comparison to uninfected control ($p \leq 0.05$) (Figure 5(a)). AMG added to HSV-1-infected primary glial cultures upregulated Fas expression to the levels observed in control, uninfected cells (Figure 5(a)). SNP significantly increased FasL expression on microglial and astrocyte cells from uninfected primary cell cultures ($p \leq 0.05$) (Figure 5(b)). HSV-1 infection led to significant upregulation of FasL expression only on microglia, while either SNP or AMG had no influence upon FasL expression in HSV-1-infected mixed glial cultures (Figure 5(b)). In HSV-1-infected mixed glial cultures, FasL-positive cells were identified as surrounding the infected cells, but also on infected cells. No Fas expression was detected on infected glial cells (Figure 5(c)).

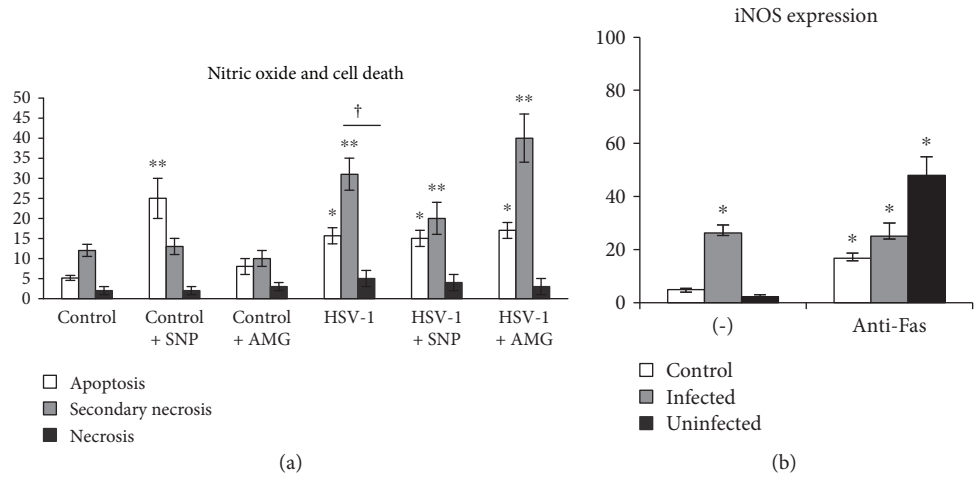

Figure 4: Nitric oxide protects microglia from cell death, while Fas signalling stimulates iNOS expression. (a) Percentage of apoptotic (annexin V+/propidium iodide -), secondary necrotic (annexin V+/propidium iodide+), and necrotic (annexin V-/propidium iodide+) CD11b+ cells in mixed glial cultures subjected to HSV-1 infection and treatment with the NO donor (SNP, 100 μM) and the inhibitor of iNOS (AMG, 50 μM) for 24 h. (b) Percentage of iNOS+ cells in mixed glial cultures infected with HSV-1 for 24 h. Means are expressed as mean ± SEM for $n = 3$; *significant differences with $p \leq 0.05$, while $^{**}p \leq 0.01$ in comparison to uninfected control, † represents a significant difference with $p \leq 0.05$ in comparison to HSV-1-infected cells.

Table 1: Cytokine and chemokine expression in neuronal primary cultures.

	TNF-alpha	IFN-alpha	CXCL9	CXCL10
Control + NO donor	n.d.	n.d.	n.d.	n.d.
Control + iNOS inhibitor	n.d.	n.d.	n.d.	n.d.
sFasL	3.37 ± 0.8	n.d.	n.d.	52.22 ± 6.7
HSV-1	30.225 ± 5.1	24.25 ± 4.5	0.29 ± 0.2	109.13 ± 21.3
HSV − 1 + NO donor	10.69 ± 3.4*	2.78 ± 0.9*	n.d.	17.26±5.6**
HSV − 1 + iNOS inhibitor	n.d.	n.d.	n.d.	n.d.
HSV − 1 + sFasL	8.59 ± 1.11*	n.d.	n.d.	137.93 ± 3.1*
HSV − 1 + NO donor + sFasL	3.86±0.9**	n.d.	3.1* ± 0.5	53.2 ± 3.33*

Cytokine and chemokine expression changes in the neuronal cultures at 24 h p.i. with HSV-1. Neuronal cultures were subjected to treatment with the NO donor—SNP (100 μM)—and the inhibitor of iNOS—AMG (50 μM)—and sFasL (0.1 μg/ml). mRNA levels of IFN-alpha, TNF-alpha, CXCL9, and CXCL10 are shown as expression relative to control on the basis of the $2^{-\Delta\Delta Ct}$ method. mRNA levels were counted from three PCR reactions for each sample. $^{*}p \leq 0.05$ and $^{**}p \leq 0.01$ versus HSV-1-infected control. n.d. means not detected.

Table 2: Cytokine and chemokine expression in mixed glial primary cultures.

	TNF-alpha	IFN-alpha	CXCL9	CXCL10
Control + NO donor	0.71 ± 0.03	0.45 ± 0.01	0.94 ± 0.02	1.27 ± 0.34
Control + iNOS inhibitor	1.01 ± 0.02	1.1 ± 0.45	0.17 ± 0.04	1.1 ± 0.03
sFasL	8.88 ± 1.89†	4.5 ± 0.7†	45.2 ± 0.54††	n.d.
HSV-1	86 ± 9.1††	7422 ± 892††	152 ± 29††	424 ± 39††
HSV − 1 + NO donor	189±35**	1247±299**	95 ± 23*	146±49**
HSV − 1 + iNOS inhibitor	79 ± 12	10401±501**	294±51**	215±61**
HSV − 1 + sFasL	43 ± 5*	5673 ± 1329	445±91**	552 ± 59**
HSV − 1 + NO donor + sFasL	49 ± 6.6*	6427 ± 987	110 ± 23*	150±45**

Cytokine and chemokine expression changes in the mixed glial cultures at 24 h p.i. with HSV-1. Mixed glial cultures were subjected to treatment with the NO donor—SNP (100 μM)—or the inhibitor of iNOS—AMG (50 μM). mRNA levels of IFN-alpha, TNF-alpha, CXCL9, and CXCL10 are shown as expression relative to control on the basis of the $2^{-\Delta\Delta Ct}$ method. mRNA levels were counted from three PCR reactions for each sample. $^{*}p \leq 0.05$ and $^{**}p \leq 0.01$ versus HSV-1-infected control and $^{\dagger}p \leq 0.05$ and $^{\dagger\dagger}p \leq 0.01$ versus uninfected control. n.d. means not detected.

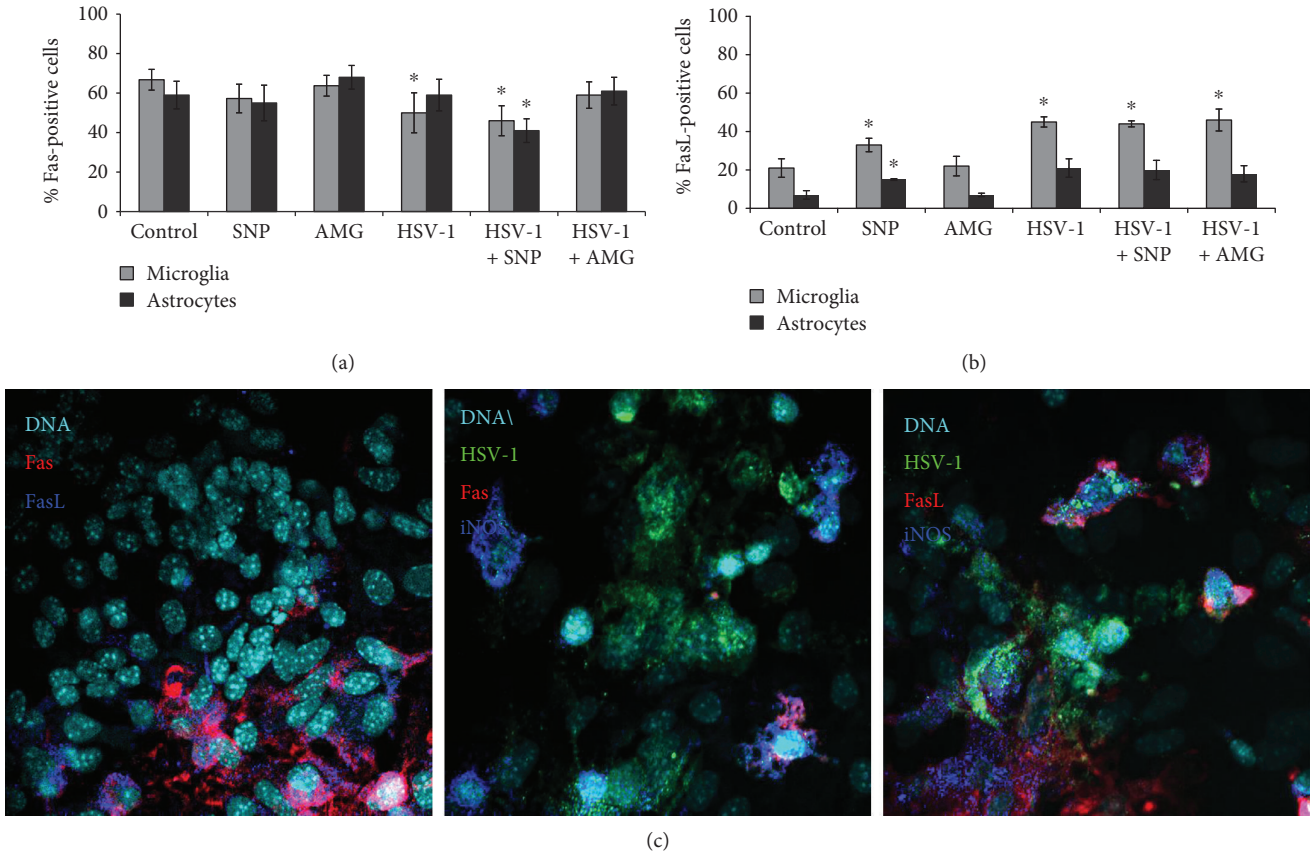

Figure 5: Nitric oxide regulates Fas/FasL expression on glial cells. Percentage of Fas-positive (a) and FasL-positive (b) microglial (CD11b+) and astrocyte (GFAP+) cells in mixed glial cultures subjected to HSV-1 infection and treatment with the NO donor (SNP 100 μM) and the inhibitor of iNOS (AMG 50 μM) for 24 h. (c) Representative confocal images of mixed glial cultures infected with HSV-1 for 24 h and stained for Fas, FasL, iNOS, and HSV-1. Means are expressed as mean ± SEM for $n = 3$; *significant differences with $p \leq 0.05$, while **$p \leq 0.01$ in comparison to uninfected control.

In the brains of HSV-1-infected BALB/c mice, FasL-positive cells were identified mostly as infected and uninfected CD11b+ cells surrounding HSV-1-infected sites, while only single FasL-positive GFAP+ cells were identified within the infected sites (Figure 6). Fas expression was detected in uninfected controls, while very little or no Fas expression was detected in HSV-1-infected brains (Figure 6). While we could detect cells positive for Fas expression in the uninfected control animals around neuronal cells, the infected area showed decreased Fas expression on the surrounding cells (Figure 6).

3.5. Nitric Oxide Production during HSV-1 Infection Adds to Aβ Accumulation. We performed tests to determine whether HSV-1 infection and NO production modulate amyloid precursor protein (APP) proteolysis processing into Aβ. It has been previously shown that HSV-1 causes the accumulation of intracellular Aβ in human neuroblastoma cells [6]. As a first step, the Aβ presence in cultured neurons and in the brains of HSV-1-infected mice was examined by immunofluorescence (Figures 7(a) and 7(b)). Intracellular or extracellular Aβ was barely detectable in uninfected cells. In contrast, HSV-1 infection induced a strong elevation of Aβ at 24 h p.i., both in neuronal culture and in the brains of HSV-1-infected mice (Figures 7(a) and 7(b)). Aβ was accumulated extracellularly around the HSV-1-infected neurons in the brains of HSV-1-infected mice at 5 d p.i. within the midbrain, brain stem, and hypothalamus (Figure 7(a)). Aβ also colocalized with HSV-1 antigens (Figures 7(a) and 7(b)). In primary neuronal cultures, Aβ was found mostly in the perikaryons of infected cells but also colocalized with HSV-1 antigens within processes (Figure 7(b)). In addition, we demonstrated colocalization of iNOS-positive cells at HSV-1-infected sites with accumulated Aβ (Figure 7(a)).

To confirm that not only HSV-1 infection but also NO production led to significant upregulation of Aβ levels, we incubated cultured neurons with the NO donor—SNP (100 μM)—or the inhibitor of iNOS—AMG (50 μM). Using Western blot analysis, we found that the NO donor significantly upregulated Aβ levels in both noninfected (positive control with NO donor) and HSV-1-infected neurons, in comparison to negative control (without NO donor) (Figures 7(c) and 7(d)). Furthermore, treatment with the inhibitor of iNOS caused downregulation of Aβ levels in infected neurons (Figures 7(c) and 7(d)).

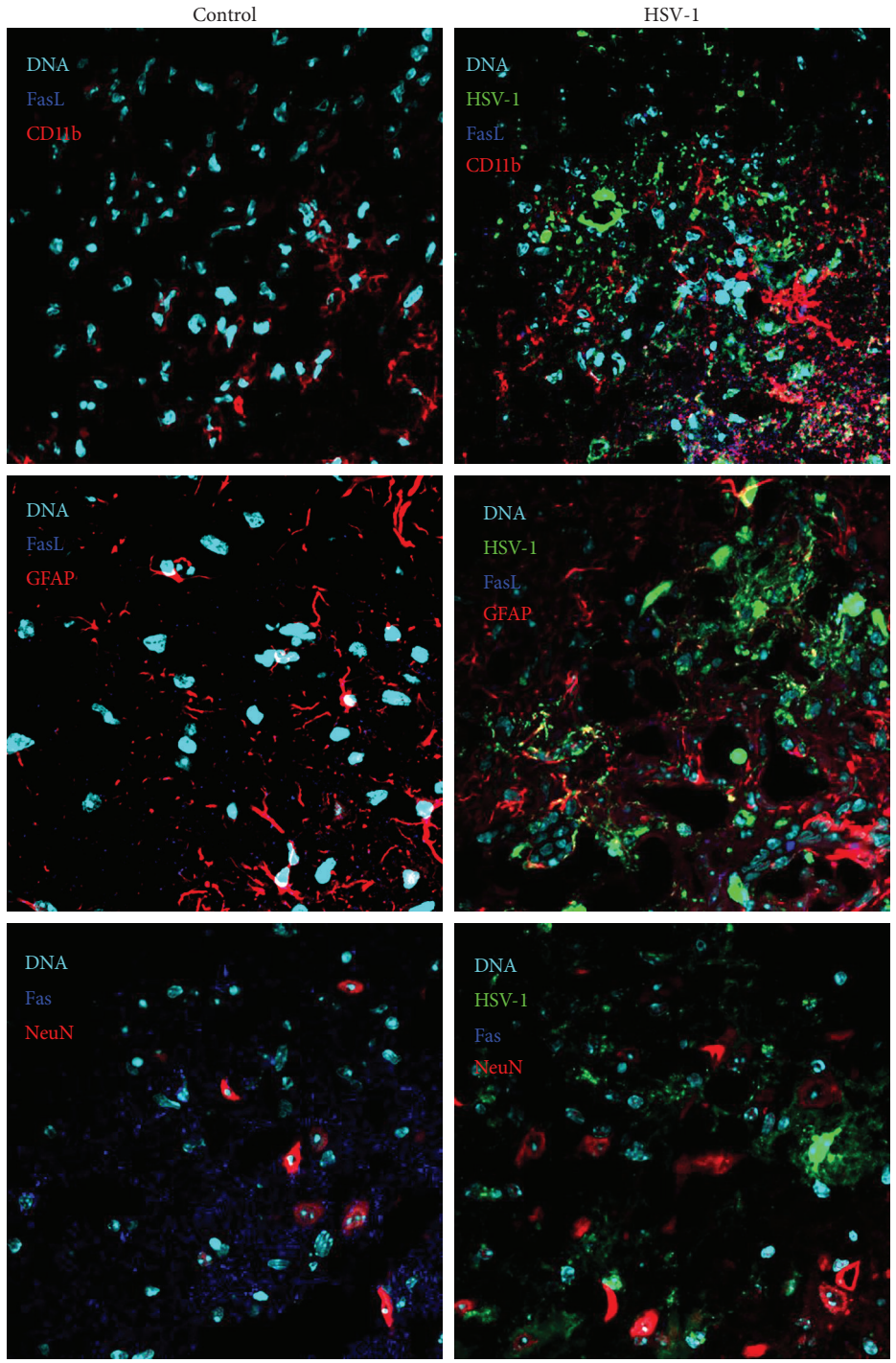

Figure 6: Microglia are the main source of FasL in HSV-1-infected brains. Representative confocal images of the brains obtained at day 5 p.i. with HSV-1. Tissue sections from brain stems were stained for microglia (CD11b+), astrocytes (GFAP+), neurons (NeuN), Fas, and FasL. Nuclei were counterstained with DAPI.

4. Discussion

There is a growing body of evidence that nitric oxide (NO), a ubiquitous gaseous cellular messenger, plays significant roles in a variety of neurobiological processes. Several functions of this regulatory molecule have been identified in the nervous system, such as vasodilatation, neurotransmission, and host defence mechanisms [31, 32]. However, NO can exert both cytoprotective and cytotoxic effects in the central nervous system (CNS) [33, 34], depending on its concentration, time course exposure, and presence/absence of ROS at particular levels and cells. NO is a neuroprotectant at low levels, while it might behave as a toxicant at higher concentrations [35]. Overproduction of NO is caused by inducible NO synthase

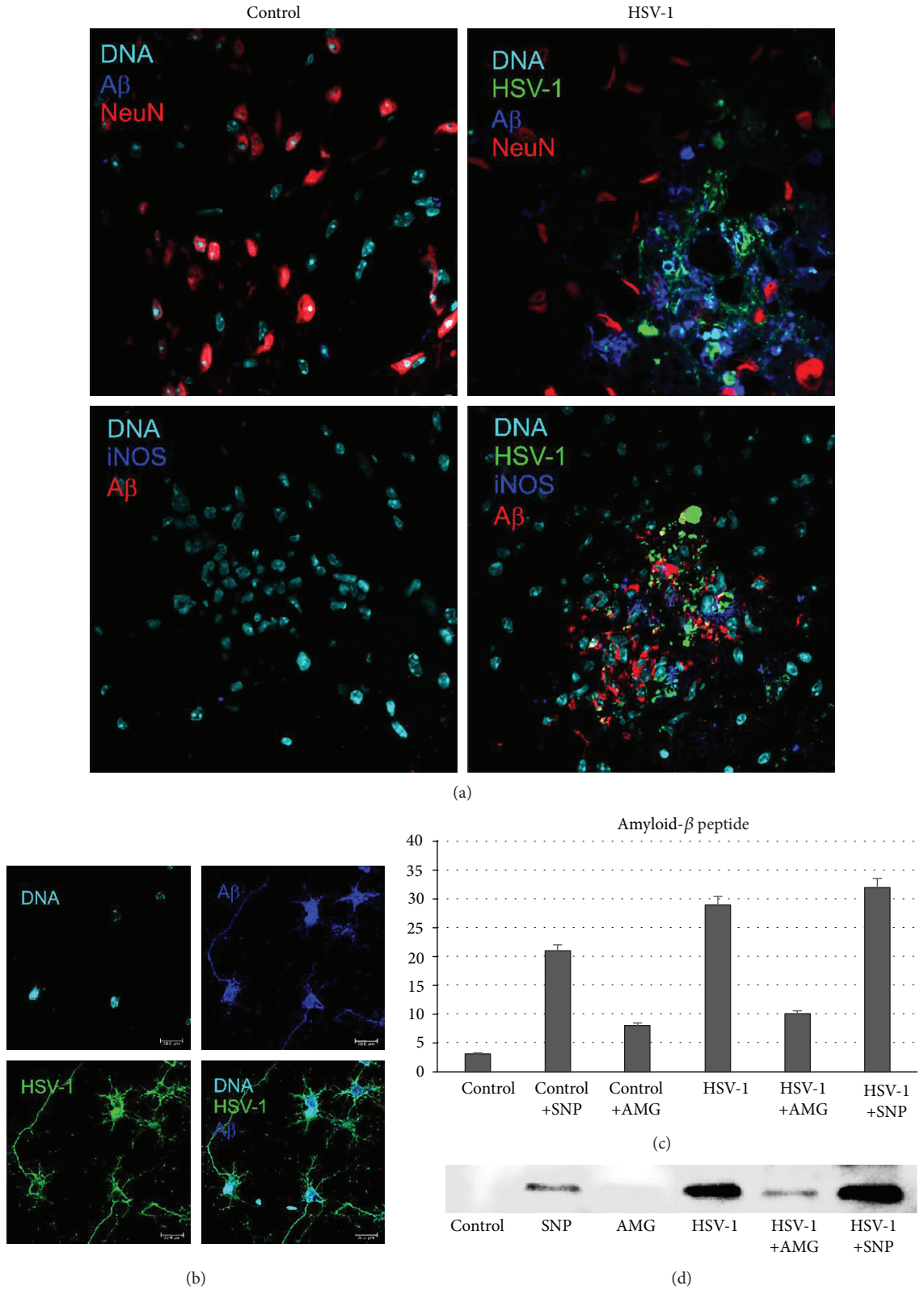

Figure 7: Nitric oxide production during HSV-1 infection adds to Aβ accumulation. (a) Representative confocal images of brains obtained at day 5 p.i. with HSV-1, with the hypothalamus and midbrains stained for HSV-1, Aβ, NeuN (neuronal marker), and iNOS. (b) Neuronal culture positive for Aβ and HSV-1. (c, d) Western blot analysis of Aβ in HSV-1-infected and control uninfected neuronal cultures subjected to treatment with the NO donor SNP (100 μM) or the inhibitor of iNOS AMG (50 μM) for 24 h. Means are expressed as the mean densitometric value ± SEM for $n = 3$. *Significant differences with $p \leq 0.05$. Nuclei were counterstained with DAPI.

(iNOS), which is usually expressed by inflammatory phagocytic cells and other types of cells (e.g., epithelial and glial cells), and it has a defence function against bacteria, fungi, and parasites [36]. iNOS produces a much larger amounts of NO for a longer time than the other two constitutive enzymes, neuronal NOS and endothelial NOS [37].

NOS is induced in a variety of experimental virus infections in rats and mice, including Borna disease virus, herpes simplex virus type 1, and rabies virus, and in human diseases caused by human immunodeficiency virus-1 (HIV-1) and hepatitis B virus (HBV) [17, 18, 38, 39]. Furthermore, its induction in virus infection can be mediated indirectly by proinflammatory cytokines such as interferon-γ (IFN-γ) [40] and directly, by virus components, for example, an envelope glycoprotein of HIV, gp41, triggers iNOS expression in human astrocytes and murine cortical brain cells in culture [41]. Evidence suggests that localized production of NO early during HSV brain infection may be responsible for decreased neuronal infection [42, 43]. In this study, we found that antiviral effects of NO actually depended upon the type of HSV-1-infected cells and the concentration of the NO donor. In primary neuronal cultures, NO caused significant reduction of HSV-1 replication irrespectively of the used concentration, while in astrocytes, the NO donor supported HSV-1 replication if used at $\leq 100\,\mu$M, while at higher concentrations, it blocked HSV-1 replication. Inhibition of iNOS activity in HSV-1-infected BALB/c mice led to upregulation of virus replication in trigeminal ganglia, but it had an opposite effect upon the brain infection. The results obtained here for trigeminal ganglia are consistent with papers published by Gamba et al. and Benencia et al., showing that the iNOS inhibitor, aminoguanidine, increased HSV-1 replication upon ocular and intranasal infection outside the CNS, respectively [42, 43]. The main sources of NO in HSV-infected trigeminal ganglia are dendritic cells (DCs) and monocytes/macrophages (Mo/Mϕ), which, together with type I IFNs, are essential for the early immune response against HSV [44]. Therefore, we may conclude that high levels of NO produced by macrophages and dendritic cells can block early stages of HSV infection in the peripheral nervous system, while low concentrations of NO actually provide advantageous effect for HSV replication in astrocytes. This may explain why the iNOS inhibitor—AMG—blocked replication of the virus in the brain later during infection.

There are reports showing that treatment of infected animals with the nonselective NOS inhibitor L-NMMA resulted in significantly improved survival rates, despite no decrease in viral titers [19, 45]. Similarly, experimental inhibition of NO during neuronal infection with West Nile virus (WNV) attenuated disease and prolonged survival [46]. During WNV encephalitis, more than 70% of the inflammatory monocyte-derived macrophages in the WNV-infected brain produced NO. Importantly, whereas inhibition of NO with AMG during the entire course of infection had no effect on the disease outcome, late inhibition resulted in enhanced survival of WNV-infected mice [46].

The main sources of NO in the brain during herpes encephalitis are microglia, as shown by Marques et al. [47]. In this study, we identified microglia and only a small portion of astrocytes *in vitro* as the main sources of NO in HSV-1-infected primary mixed glial cultures. Similarly, the brains of HSV-1-infected BALB/c mice indicated microglia as the main NO producers, rather than astrocytes, as shown previously [47].

Upon HSV-1 infection, microglia undergo activation, which is necessary for host defence, and are the source of proinflammatory cytokines and chemokines, such as tumor necrosis factor- (TNF-) α, interleukin- (IL-) 1β, CXCL10 [48], and NO [47]. However, the activated state of this cell type has also been linked to neurotoxicity, neurodegeneration, and chronic neuroinflammation in several disorders including Alzheimer's disease, Parkinson's disease, amyotrophic lateral sclerosis, and HIV-associated dementia [9, 10, 15]. Here, we found that NO influenced production of proinflammatory cytokines by primary neuronal cultures and mixed glial cultures.

In neuronal cultures, infection with HSV-1 upregulated IFN-alpha, TNF-alpha, CXCL9, and CXCL10, while addition of NO downregulated all tested cytokines and chemokines. Upon stress, neurons can release multiple cytokines and chemokines: interleukin 3 (IL-3), TNF-alpha, CXCL9, VEGF, L-selectin, IL-4, GM-CSF, IL-10, IL-1Ra, MIP, and CCL20 [49]. CXC-type chemokines, including CXCL9 and CXCL10, are potent chemoattractants for activated T cells, NK cells, monocytes, dendritic cells, and B cells [49, 50], while type I interferons (IFN-alpha and IFN-beta) are important in limiting viral replication and spread *in vitro*, but also *in vivo* at the periphery during initial HSV infection and virus reactivation [51]. Therefore, while NO produced by microglial cells helps to reduce viral replication in the infected neurons but not in astrocytes, it also downregulates cytokines important for antiviral response in the neuronal microenvironment. At the same time, NO may induce production of inflammatory TNF-alpha cytokine in the local site of HSV-1 infection. Therefore, prolonged or strong local production of NO may further add to HSV-1 local spread and further pathology by limiting the specific antiviral immune response. It has been previously suggested that NO affects the polarized Th1/Th2 response by a suppressive effect on Th1 subpopulations [52].

Upon HSV-1 infection, microglial cells undergo an abortive infection and induce a burst of proinflammatory cytokine and chemokine production. Following the HSV-1 infection, microglia also undergo a cell death—apoptosis and necrosis, while HSV-1-infected astrocytes suppress apoptosis. Here, we found that the NO donor at low levels protected HSV-1-infected microglia from secondary necrosis but it had no influence upon apoptosis. Taking into account that secondary necrotic cells are actually apoptotic cells, which did not undergo phagocytosis in vitro and microglia undergo abortive infection, we may conclude that NO protected microglia in HSV-1-infected glial cultures from early apoptosis following the virus entry.

Antiapoptotic actions of low levels of NO are numerous, ranging from an immediate interference with proapoptotic signalling cascades to long-lasting effects based on expression of cell protective proteins and the ability

of NO to block caspases by S-nitrosylation/S-nitrosation [53]. Thus, we may conclude that NO exerts a double-edged role during HSV-1 infection. While it inhibits HSV-1 replication in neurons, NO contributes to microglia- and astroglia-induced chronic neuroinflammation and virus replication.

The extrinsic apoptotic pathway is initiated by ligand binding to the cell surface death receptor (tumor necrosis factor receptor) superfamily (e.g., Fas/CD95, tumor necrosis factor, and tumor necrosis factor-related apoptosis-inducing ligand- (TRAIL-) R1 and TRAIL-R2) [54]. However, emerging evidence accumulates on Fas as a mediator of apoptosis-independent processes including proliferation, angiogenesis, fibrosis, and inflammation. Cullen et al. observed that Fas-induced apoptosis of HeLa cells was associated with the production of an array of cytokines and chemokines, including IL-6, IL-8, CXCL1, MCP-1, and GM-CSF. Fas-induced production of MCP-1 and IL-8 promoted chemotaxis of phagocytes toward apoptotic cells, suggesting that these factors serve as "find-me" signals [55]. Furthermore, Fas/FasL death receptors activate apoptosis-independent inflammatory or proliferative signalling via the prototypic proinflammatory transcription factor NF-κB or the mitogen-activated protein kinase (MAPK) family of kinases [56]. Krzyzowska et al. have previously shown that the Fas/FasL-dependent apoptotic pathway was a crucial mechanism for elimination of the inflammatory cells present in the HSV-2-infected sites within the vaginal epithelium during herpes genitalis [57]. Furthermore, Fas/FasL-dependent apoptosis of monocytes led to development of the local chemokine and cytokine milieu, necessary for mounting proper antiviral response [23, 57]. HSV-2-infected monocytes upregulated FasL during the whole tested period of HSV-2 infection, but Fas expression was elevated only early during infection to later decrease [57].

Here, we found that upon HSV-1 infection, both microglia and astrocytes were resistant to Fas-induced apoptosis. In addition, stimulation of Fas through soluble FasL led to significant upregulation of TNF-alpha and CXCL10 in uninfected and CXCL10 in HSV-1-infected neuronal cultures, while coaddition of the NO donor and sFasL reduced TNF-alpha and CXCL10 to the levels observed in untreated infected cultures. Only for CXCL9, coaddition of sFasL and the NO donor to HSV-1-infected culture showed a cumulative effect of a high expression level. The results obtained for CXCL9 follow those obtained previously for HSV-2-infected monocytes [57], which after Fas-stimulation upregulated both CXCL9 and TNF-alpha [57]. Similarly, as for HSV-2-infected mouse monocytes [57], HSV-1-infected microglia downregulate Fas expression and upregulate its ligand, FasL. Production of cytokines and chemokines together with NO through the Fas/FasL pathway has a primary role not only in reduction of replication and in attraction of cytotoxic T cells but also in reduction of inflammation. However, HSV-1 infection disturbs this natural antiviral mechanism—lack of Fas—or NO-induced cell death of microglia leads to excessive NO production and inflammatory reaction. Therefore, depending on the concentration, time course, and place, Fas/FasL together with NO can regulate a delicate balance between protection from HSV-1 neuroinfection and neuroinflammation (Figure 8).

Previously published studies have shown that both acute and latent HSV-1 brain infections are associated with oxidative damage [7, 9]. Recently, it has been shown that HSV infection-induced formation of reactive nitrogen and reactive oxygen species (RNS and ROS) leads to damage within the virus-infected brain. Ball [58] pointed out that the brain regions most frequently involved in herpes encephalitis are also the earliest and most severely involved targets of the neurodegenerative alterations of Alzheimer's disease (AD). A large prospective population-based study also showed that the risk of AD is increased in elderly subjects with positive titers of anti-HSV-1 IgM antibodies, which are markers of primary or reactivated HSV-1 infection [59]. One of the most widely accepted hypotheses on the molecular pathogenesis of AD focuses on the accumulation and aggregation of two proteins: Aβ, in the form of extracellular plaques, and hyperphosphorylated tau, as intracellular neurofibrillary tangles [11]. The accumulation of Aβ peptides in the extracellular spaces gives rise to the aggregates (plaques) that disrupt cell signalling, trigger inflammatory immune responses, and cause oxidative stress [60, 61]. Links between HSV-1 and AD include the discovery that the viral DNA is located very specifically within AD plaques [62] and that the main component of plaques, Aβ, accumulates in HSV-1-infected cell cultures [7] and in the brains of HSV1-infected mice [6]. Furthermore, Aβ is characterized by some degrees of sequence homology with HSV-1 glycoprotein B, so it may act as a seed for Aβ deposition in amyloid plaques [63]. Bourgade et al. showed that Aβ inhibited HSV-1 replication in fibroblast and epithelial and neuronal cell lines when added 2 h prior to or concomitantly with virus challenge, but not when added 2 or 6 h after virus challenge [64]. Aβ peptides also displayed antiviral activities against the enveloped influenza A virus [65]. Therefore, Aβ peptides can represent a novel class of antimicrobial peptides that protect against neurotropic virus infections such as HSV-1. It has been also suggested that antiviral treatments may open an antiviral approach for clinical therapy of AD [66].

Here, we also observed accumulation of Aβ both in HSV-1-infected neurons and in the extracellular space surrounding HSV-1-infected neurons *in vivo*. Furthermore, we also found that the NO donor increased accumulation of Aβ in uninfected primary neuronal cultures, while the iNOS inhibitor decreased its accumulation in HSV-1-infected neuronal cultures (Figure 8). The HSV-1-infected sites were surrounded by iNOS-positive CD11b cells. Several studies have suggested that NO modulates the processing of amyloid precursor protein (APP) and alters Aβ production [8, 9, 21]. Cai et al. [9] using human SH-SY5Y neuroblastoma cells stably transfected with wild-type APPwt695 demonstrated that low (physiological) levels of NO given in the form of sodium nitroprusside can inhibit the amyloidogenic processing of APP, whereas extra-high (pathological) concentrations of NO favor the amyloidogenic pathway of APP processing. Inflammatory and immune responses in the neuronal tissue involve increased iNOS activity in microglia and astrocytes, which further generates high levels of NO and peroxynitrite

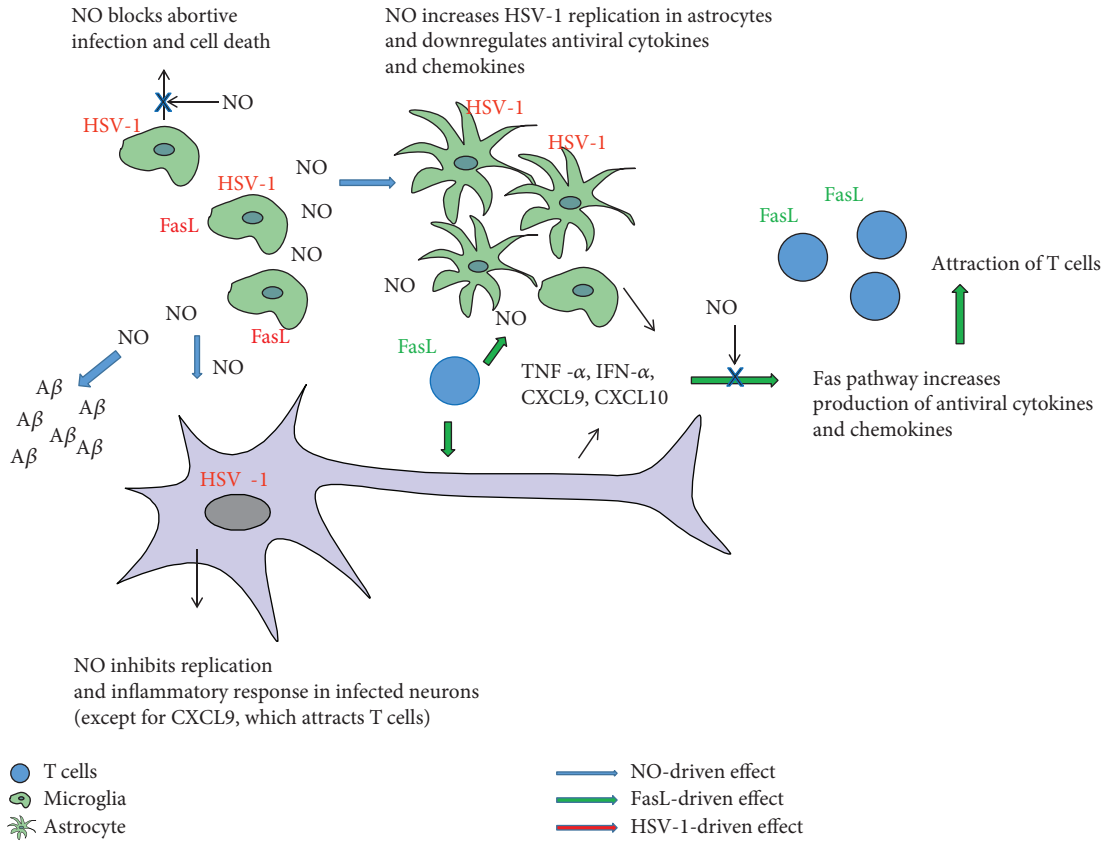

Figure 8: Schematic drawing depicting relations between HSV-1 infection, NO production, and the Fas/FasL pathway.

through the NO/superoxide pathway. Removal of iNOS in transgenic AD mice or the use of iNOS inhibitors to block NO production has been shown to protect against Aβ-induced neurotoxicity [67]. Accumulation of misfolded proteins such as Aβ is known to induce phosphorylation of eukaryotic initiation factor-2 (eIF2 α) [67]. Genetic and environmental risks for AD may influence modulation of the eIF2 α phosphorylation pathway. eIF2 α phosphorylation suppresses general protein synthesis, but it also induces translational activation of β-site APP cleaving enzyme 1 (BACE1), responsible for Aβ production [68]. NO can upstream induce and downstream mediate the kinases that phosphorylate eIF2α. Therefore, production of NO can indirectly add to activation of BACE1, responsible for development of amyloid plaques. In addition to being an upstream regulator of protein kinase R (PKR), NO production is regulated downstream by PKR [69]. It was also found that PKR activation was required for dsRNA-induced NF-κB activation and iNOS expression in U373 MG astroglial cells [70].

5. Conclusion

This study may provide further evidence to clarify the molecular roles of NO and NO-related signalling during herpes simplex-induced neuroinflammation and neurodegeneration. It also indicates for the first time the existence of a link between Fas signalling due to neuroinflammation and nitrosative stress during HSV-1 infection. Further studies can contribute to finding of the potential molecular targets for a treatment of virus-induced neurodegeneration and Aβ accumulation.

Data Availability

The data used to support the findings of this study are available from the corresponding author upon request.

Conflicts of Interest

The authors declare no conflict of interest.

Acknowledgments

This work was supported by the Polish National Science Centre grant no. 2015/18/M/NZ6/00414.

References

[1] B. Roizman and D. M. Knipe, "Herpes simplex viruses and their replication," in *In Fields Virology*, D. M. Knipe, P. M. Howley, and D. E. Griffen, Eds., pp. 2399–2459, Lippincott Williams, Philadelphia, PA, USA, 4th edition, 2001.

[2] J. Booss and J. H. Kim, "Biopsy histopathology in herpes simplex encephalitis and in encephalitis of undefined etiology," *The Yale Journal of Biology and Medicine*, vol. 57, no. 5, pp. 751–755, 1984.

[3] M. Sabah, J. Mulcahy, and A. Zeman, "Herpes simplex encephalitis," *BMJ*, vol. 344, article e3166, 2012.

[4] S. Miura, T. Kurita, K. Noda, M. Ayabe, H. Aizawa, and T. Taniwaki, "Symmetrical brainstem encephalitis caused by herpes simplex virus," *Journal of Clinical Neuroscience*, vol. 16, no. 4, pp. 589-590, 2009.

[5] R. J. Whitley, S. J. Soong, C. Linneman Jr., C. Liu, G. Pazin, and C. A. Alford, "Herpes simplex encephalitis. Clinical assessment," *JAMA*, vol. 247, no. 3, pp. 317–320, 1982.

[6] M. A. Wozniak, R. F. Itzhaki, S. J. Shipley, and C. B. Dobson, "Herpes simplex virus infection causes cellular β amyloid accumulation and secretase up-regulation," *Neuroscience Letters*, vol. 429, no. 2-3, pp. 95–100, 2007.

[7] S. Santana, I. Sastre, M. Recuero, M. J. Bullido, and J. Aldudo, "Oxidative stress enhances neurodegeneration markers induced by herpes simplex virus type 1 infection in human neuroblastoma cells," *PLoS One*, vol. 8, no. 10, article e75842, 2013.

[8] D. J. Bonda, X. Wang, G. Perry et al., "Oxidative stress in Alzheimer disease: a possibility for prevention," *Neuropharmacology*, vol. 59, no. 4-5, pp. 290–294, 2010.

[9] Z. Cai, M. D. Hussain, and L. J. Yan, "Microglia, neuroinflammation, and beta-amyloid protein in Alzheimer's disease," *The International Journal of Neuroscience*, vol. 124, no. 5, pp. 307–321, 2013.

[10] T. Wyss-Coray and J. Rogers, "Inflammation in Alzheimer disease–a brief review of the basic science and clinical literature," *Cold Spring Harbor Perspectives in Medicine*, vol. 2, no. 1, article a006346, 2012.

[11] G. Ho, R. Drego, E. Hakimian, and E. Masliah, "Mechanisms of cell signaling and inflammation in Alzheimer's disease," *Current Drug Targets Inflammation and Allergy*, vol. 4, no. 2, pp. 247–256, 2005.

[12] M. Ehrenschwender and H. Wajant, "The role of FasL and Fas in health and disease," *Advances in Experimental Medicine and Biology*, vol. 647, pp. 64–93, 2009.

[13] P. Dowling, G. Shang, S. Raval, J. Menonna, S. Cook, and W. Husar, "Involvement of the CD95 (APO-1/Fas) receptor/ligand system in multiple sclerosis brain," *The Journal of Experimental Medicine*, vol. 184, no. 4, pp. 1513–1518, 1996.

[14] I. Elovaara, F. Sabri, F. Gray, I. Alafuzoff, and F. Chiodi, "Upregulated expression of Fas and Fas ligand in brain through the spectrum of HIV-1 infection," *Acta Neuropathologica*, vol. 98, no. 4, pp. 355–362, 1999.

[15] M. L. Block, L. Zecca, and J. S. Hong, "Microglia-mediated neurotoxicity: uncovering the molecular mechanisms," *Nature Reviews. Neuroscience*, vol. 8, no. 1, pp. 57–69, 2007.

[16] E. U. Uehara, B. d. S. Shida, and C. A. de Brito, "Role of nitric oxide in immune responses against viruses: beyond microbicidal activity," *Inflammation Research*, vol. 64, no. 11, pp. 845–852, 2015.

[17] Y. M. Zheng, M. K. Schäfer, E. Weihe et al., "Severity of neurological signs and degree of inflammatory lesions in the brains of rats with Borna disease correlate with the induction of nitric oxide synthase," *Journal of Virology*, vol. 67, no. 10, pp. 5786–5791, 1993.

[18] S. Fujii, T. Akaike, and H. Maeda, "Role of nitric oxide in pathogenesis of herpes simplex virus encephalitis in rats," *Virology*, vol. 256, no. 2, pp. 203–212, 1999.

[19] T. Akaike, S. Fujii, A. Kato et al., "Viral mutation accelerated by nitric oxide production during infection *in vivo*," *The FASEB Journal*, vol. 14, no. 10, pp. 1447–1454, 2000.

[20] K. Uetani, S. D. der, M. Zamanian-Daryoush et al., "Central role of double-stranded RNA-activated protein kinase in microbial induction of nitric oxide synthase," *Journal of Immunology*, vol. 165, no. 2, pp. 988–996, 2000.

[21] T. Malinski, "Nitric oxide and nitroxidative stress in Alzheimer's disease," *Journal of Alzheimer's Disease*, vol. 11, no. 2, pp. 207–218, 2007.

[22] M. Virarkar, L. Alappat, P. G. Bradford, and A. B. Awad, "L-arginine and nitric oxide in CNS function and neurodegenerative diseases," *Critical Reviews in Food Science and Nutrition*, vol. 53, no. 11, pp. 1157–1167, 2013.

[23] M. Krzyzowska, P. Baska, A. Grochowska, P. Orlowski, Z. Nowak, and A. Winnicka, "Fas/FasL pathway participates in resolution of mucosal inflammatory response early during HSV-2 infection," *Immunobiology*, vol. 219, no. 1, pp. 64–77, 2014.

[24] P. Seth, W. E. Rawls, R. Duff, F. Rapp, E. Adam, and J. L. Melnick, "Antigenic differences between isolates of herpesvirus type 2," *Intervirology*, vol. 3, no. 1-2, pp. 1–14, 1974.

[25] J. Cymerys, T. Dzieciatkowski, A. Słońska et al., "Equine herpesvirus type 1 (EHV-1) replication in primary murine neurons culture," *Polish Journal of Veterinary Sciences*, vol. 13, no. 4, pp. 701–708, 2010.

[26] H. J. Draheim, M. Prinz, J. R. Weber, T. Weiser, H. Kettenmann, and U. K. Hanisch, "Induction of potassium channels in mouse brain microglia: cells acquire responsiveness to pneumococcal cell wall components during late development," *Neuroscience*, vol. 89, no. 4, pp. 1379–1390, 1999.

[27] L. Namvar, S. Olofsson, T. Bergstrom, and M. Lindh, "Detection and typing of herpes simplex virus (HSV) in mucocutaneous samples by TaqMan PCR targeting a gB segment homologous for HSV types 1 and 2," *Journal of Clinical Microbiology*, vol. 43, no. 5, pp. 2058–2064, 2005.

[28] P. Orłowski, A. Kowalczyk, E. Tomaszewska et al., "Antiviral activity of tannic acid modified silver nanoparticles: potential to activate immune response in herpes genitalis," *Viruses*, vol. 10, no. 10, 2018.

[29] L. Wang and Z. A. Zhu, "Nitric oxide show its survival role by NO-PKC pathway through cGMP-dependent or independent on the culture of cerebella granular neurons," *Neuroscience Letters*, vol. 583, pp. 165–169, 2014.

[30] M. A. Salykina, E. G. Sorokina, I. A. Krasilnikova, V. P. Reutov, and V. G. Pinelis, "Effects of selective inhibitors of neuronal and inducible NO-synthase on ATP content and survival of cultured rat cerebellar neurons during hyperstimulation of glutamate receptors," *Bulletin of Experimental Biology and Medicine*, vol. 155, no. 1, pp. 40–43, 2013.

[31] E. Džoljić, I. Grbatinić, and V. Kostić, "Why is nitric oxide important for our brain?," *Functional Neurology*, vol. 30, no. 3, pp. 159–163, 2015.

[32] E. E. Benarroch, "Nitric oxide a pleiotropic signal in the nervous system," *Neurology*, vol. 77, no. 16, pp. 1568–1576, 2011.

[33] Z. S. Katusic and S. A. Austin, "Endothelial nitric oxide: protector of a healthy mind," *European Heart Journal*, vol. 35, no. 14, pp. 888–894, 2014.

[34] V. Calabrese, C. Cornelius, E. Rizzarelli, J. B. Owen, A. T. Dinkova-Kostova, and D. A. Butterfield, "Nitric oxide in cell

survival: a janus molecule," *Antioxidants & Redox Signaling*, vol. 11, no. 11, pp. 2717–2739, 2009.

[35] G. C. Brown, "Nitric oxide and neuronal death," *Nitric Oxide*, vol. 23, no. 3, pp. 153–165, 2010.

[36] D. J. Stuehr and O. W. Griffith, "Mammalian nitric oxide synthases," *Advances in Enzymology and Related Areas of Molecular Biology*, vol. 65, pp. 287–346, 1992.

[37] C. Nathan, "Inducible nitric oxide synthase: what difference does it make?," *The Journal of Clinical Investigation*, vol. 100, no. 10, pp. 2417–2423, 1997.

[38] M. I. Bukrinsky, H. S. Nottet, H. Schmidtmayerova et al., "Regulation of nitric oxide synthase activity in human immunodeficiency virus type 1 (HIV-1)-infected monocytes: implications for HIV- associated neurological disease," *The Journal of Experimental Medicine*, vol. 181, no. 2, pp. 735–745, 1995.

[39] P. L. Majano, C. García-Monzón, M. López-Cabrera et al., "Inducible nitric oxide synthase expression in chronic viral hepatitis. Evidence for a virus-induced gene upregulation," *The Journal of Clinical Investigation*, vol. 101, no. 7, pp. 1343–1352, 1998.

[40] G. Karupiah, Q. Xie, R. Buller, C. Nathan, C. Duarte, and J. MacMicking, "Inhibition of viral replication by interferon-gamma-induced nitric oxide synthase," *Science*, vol. 261, no. 5127, pp. 1445–1448, 1993.

[41] K. Hori, P. R. Burd, K. Furuke, J. Kutza, K. A. Weih, and K. A. Clouse, "Human immunodeficiency virus-1–infected macrophages induce inducible nitric oxide synthase and nitric oxide (NO) production in astrocytes: astrocytic NO as a possible mediator of neural damage in acquired immunodeficiency syndrome," *Journal of Immunology*, vol. 93, pp. 1843–1850, 1999.

[42] G. Gamba, H. Cavalieri, M. C. Courreges, E. J. Massouh, and F. Benencia, "Early inhibition of nitric oxide production increases HSV-1 intranasal infection," *Journal of Medical Virology*, vol. 73, no. 2, pp. 313–322, 2004.

[43] F. Benencia, M. C. Courrèges, G. Gamba, H. Cavalieri, and E. J. Massouh, "Effect of aminoguanidine, a nitric oxide synthase inhibitor, on ocular infection with herpes simplex virus in Balb/c mice," *Investigative Ophthalmology & Visual Science*, vol. 42, no. 6, pp. 1277–1284, 2001.

[44] N. Lucinda, M. M. Figueiredo, N. L. Pessoa et al., "Dendritic cells, macrophages, NK and $CD8^+$ T lymphocytes play pivotal roles in controlling HSV-1 in the trigeminal ganglia by producing IL1-beta, iNOS and granzyme B," *Virology Journal*, vol. 14, no. 1, p. 37, 2017.

[45] H. Adler, J. L. Beland, N. C. Del-Pan et al., "Suppression of herpes simplex virus type 1 (HSV-1)-induced pneumonia in mice by inhibition of inducible nitric oxide synthase (iNOS, NOS2)," *The Journal of Experimental Medicine*, vol. 185, no. 9, pp. 1533–1540, 1997.

[46] D. R. Getts, R. L. Terry, M. T. Getts et al., "Targeted blockade in lethal West Nile virus encephalitis indicates a crucial role for very late antigen (VLA)-4-dependent recruitment of nitric oxide-producing macrophages," *Journal of Neuroinflammation*, vol. 9, no. 1, p. 246, 2012.

[47] C. P. Marques, M. C. J. Cheeran, J. M. Palmquist, S. Hu, and J. R. Lokensgard, "Microglia are the major cellular source of inducible nitric oxide synthase during experimental herpes encephalitis," *Journal of Neurovirology*, vol. 14, no. 3, pp. 229–238, 2008.

[48] J. R. Lokensgard, S. Hu, W. Sheng et al., "Robust expression of TNF-α, IL-1β, RANTES, and IP-10 by human microglial cells during nonproductive infection with herpes simplex virus," *Journal of Neurovirology*, vol. 7, no. 3, pp. 208–219, 2001.

[49] J. H. Dufour, M. Dziejman, M. T. Liu, J. H. Leung, T. E. Lane, and A. D. Luster, "IFN-γ-inducible protein 10 (IP-10; CXCL10)-deficient mice reveal a role for IP-10 in effector T cell generation and trafficking," *Journal of Immunology*, vol. 168, no. 7, pp. 3195–3204, 2002.

[50] M. K. Park, D. Amichay, P. Love et al., "The CXC chemokine murine monokine induced by IFN-γ (CXC chemokine ligand 9) is made by APCs, targets lymphocytes including activated B cells, and supports antibody responses to a bacterial pathogen in vivo," *Journal of Immunology*, vol. 169, no. 3, pp. 1433–1443, 2002.

[51] R. L. Hendricks, P. C. Weber, J. L. Taylor, A. Koumbis, T. M. Tumpey, and J. C. Glorioso, "Endogenously produced interferon α protects mice from herpes simplex virus type 1 corneal disease," *The Journal of General Virology*, vol. 72, no. 7, pp. 1601–1610, 1991.

[52] X. Q. Wei, I. G. Charles, A. Smith et al., "Altered immune responses in mice lacking inducible nitric oxide synthase," *Nature*, vol. 375, no. 6530, pp. 408–411, 1995.

[53] B. Brüne, A. von Knethen, and K. B. Sandau, "Nitric oxide and its role in apoptosis," *European Journal of Pharmacology*, vol. 351, no. 3, pp. 261–272, 1998.

[54] L. Galluzzi, M. C. Maiuri, I. Vitale et al., "Cell death modalities: classification and pathophysiological implications," *Cell Death and Differentiation*, vol. 14, no. 7, pp. 1237–1243, 2007.

[55] S. P. Cullen, C. M. Henry, C. J. Kearney et al., "Fas/CD95-induced chemokines can serve as "find-me" signals for apoptotic cells," *Molecular Cell*, vol. 49, no. 6, pp. 1034–1048, 2013.

[56] H. Wajant, K. Pfizenmaier, and P. Scheurich, "Non-apoptotic Fas signaling," *Cytokine & Growth Factor Reviews*, vol. 14, no. 1, pp. 53–66, 2003.

[57] M. Krzyzowska, P. Baska, P. Orlowski et al., "HSV-2 regulates monocyte inflammatory response via the Fas/FasL pathway," *PLoS One*, vol. 8, no. 7, article e70308, 2013.

[58] M. J. Ball, "Limbic predilection in Alzheimer dementia: is reactivated herpesvirus involved?," *The Canadian Journal of Neurological Sciences*, vol. 9, no. 3, pp. 303–306, 1982.

[59] L. Letenneur, K. Pérès, H. Fleury et al., "Seropositivity to herpes simplex virus antibodies and risk of Alzheimer's disease: a population-based cohort study," *PLoS One*, vol. 3, no. 11, article e3637, 2008.

[60] D. A. Butterfield, J. Drake, C. Pocernich, and A. Castegna, "Evidence of oxidative damage in Alzheimer's disease brain: central role for amyloid β-peptide," *Trends in Molecular Medicine*, vol. 7, no. 12, pp. 548–554, 2001.

[61] A. Reynolds, C. Laurie, R. Lee Mosley, and H. E. Gendelman, "Oxidative stress and the pathogenesis of neurodegenerative disorders," *International Review of Neurobiology*, vol. 82, pp. 297–325, 2007.

[62] M. A. Wozniak, A. Mee, and R. Itzhaki, "Herpes simplex virus type 1 DNA is located within Alzheimer's disease amyloid plaques," *The Journal of Pathology*, vol. 217, no. 1, pp. 131–138, 2009.

[63] D. H. Cribbs, B. Y. Azizeh, C. W. Cotman, and F. M. LaFerla, "Fibril Formation and Neurotoxicity by a Herpes Simplex Virus Glycoprotein B Fragment with Homology to the

Alzheimer's Aβ Peptide," *Biochemistry*, vol. 39, no. 20, pp. 5988–5994, 2000.

[64] K. Bourgade, H. Garneau, G. Giroux et al., "β-Amyloid peptides display protective activity against the human Alzheimer's disease-associated herpes simplex virus-1," *Biogerontology*, vol. 16, no. 1, pp. 85–98, 2015.

[65] M. R. White, R. Kandel, S. Tripathi et al., "Alzheimer's associated β-amyloid protein inhibits influenza A virus and modulates viral interactions with phagocytes," *PLoS One*, vol. 9, no. 7, article e101364, 2014.

[66] R. F. Itzhaki and M. A. Wozniak, "Could antivirals be used to treat Alzheimer's disease?," *Future Microbiology*, vol. 7, no. 3, pp. 307–309, 2012.

[67] C. Nathan, N. Calingasan, J. Nezezon et al., "Protection from Alzheimer's-like disease in the mouse by genetic ablation of inducible nitric oxide synthase," *The Journal of Experimental Medicine*, vol. 202, no. 9, pp. 1163–1169, 2005.

[68] R. C. C. Chang, A. K. Y. Wong, H.-K. Ng, and J. Hugon, "Phosphorylation of eukaryotic initiation factor-2α (eIF2α) is associated with neuronal degeneration in Alzheimer's disease," *Neuroreport*, vol. 13, no. 18, pp. 2429–2432, 2002.

[69] T. O'Connor, K. R. Sadleir, E. Maus et al., "Phosphorylation of the translation initiation factor eIF2α increases BACE1 levels and promotes amyloidogenesis," *Neuron*, vol. 60, no. 6, pp. 988–1009, 2008.

[70] C. J. Auch, R. N. Saha, F. G. Sheikh, X. Liu, B. L. Jacobs, and K. Pahan, "Role of protein kinase R in double-stranded RNA-induced expression of nitric oxide synthase in human astroglia," *FEBS Letters*, vol. 563, no. 1-3, pp. 223–228, 2004.